BRIDGE EVALUATION UTILIZING STRUCTURAL HEALTH MONITORING DATA

by

Hadi T. Al-Khateeb

A dissertation submitted to the Faculty of the University of Delaware in partial fulfillment of the requirements for the degree of Doctor of Philosophy in Civil Engineering

Summer 2016

BRIDGE EVALUATION UTILIZING STRUCTURAL HEALTH MONITORING DATA

by

Hadi T. Al-Khateeb

Approved: _____
Harry W. Shenton III, Ph.D.
Chair of the Department of Civil and Environmental Engineering

Approved: _____
Babatunde A. Ogunnaike, Ph.D.
Dean of the College of Engineering

Approved: _____
Ann L. Ardis, Ph.D.
Senior Vice Provost for Graduate and Professional Education

I certify that I have read this dissertation and that in my opinion it meets the academic and professional standard required by the University as a dissertation for the degree of Doctor of Philosophy.

Signed: _____

Michael J. Chajes, Ph.D.
Professor in charge of dissertation

I certify that I have read this dissertation and that in my opinion it meets the academic and professional standard required by the University as a dissertation for the degree of Doctor of Philosophy.

Signed: _____

Harry W. Shenton III, Ph.D.
Professor in charge of dissertation

I certify that I have read this dissertation and that in my opinion it meets the academic and professional standard required by the University as a dissertation for the degree of Doctor of Philosophy.

Signed: _____

Dennis R. Mertz, Ph.D.
Member of dissertation committee

I certify that I have read this dissertation and that in my opinion it meets the academic and professional standard required by the University as a dissertation for the degree of Doctor of Philosophy.

Signed: _____

Michael H. Santare, Ph.D.
Member of dissertation committee

ACKNOWLEDGMENTS

In the name of Allah, the Most Beneficent, the Most Merciful

First and foremost, praises and thanks to Almighty Allah, for His showers of blessings and guidance throughout my research work. Alhamdulillah, thank you Allah for giving me the patience and the strength to complete this thesis.

I would like to express the sincere gratitude and highest appreciation to my primary advisers Prof. Michael Chajes and Prof. Harry "Tripp" Shenton for helping me in every step in this work and providing invaluable guidance throughout this research. I am extremely grateful having been offered this research opportunity. It was a great privilege and honor to work and study under their guidance. I would not be able to finish this thesis without their insightful and knowledgeable advice. I cannot imagine having better advisers and mentors for my Ph.D study.

In addition to my advisers, I am extremely thankful to Prof. Dennis Mertz for his continuous support and help during my Ph.D research. Many thanks are extended to the rest of the committee members as well. Also, I would like to extend my sincerest thanks to those who helped me including the graduate students and staff in the Department of Civil and Environmental Engineering at University of Delaware.

Last but not the least a special recognition goes to my family and friends for their support and encouragement throughout the Ph.D and my life in general. Words cannot express my gratitude for their continuous emotional support. To my lovely wife, Dear Amani, without your love and encouragement, I would not be able to write this thesis. To our future baby "Jawad," we cannot wait to see you.

DEDICATION

I dedicate my dissertation to my loving father, Turki Al-Khateeb and in memory of my late mother, Amneh Al-Omari. Both of your love, patience, sacrifice, support, and unconditional help have had a great influence on my life. Your words have always been a source of motivation and inspiration. Dad, I pray for Allah always to keep you healthy and blessed in this life. Mom, you are greatly missed and will always be remembered, I will always pray for Allah to shower you with mercy and forgiveness. I am glad that Allah has chosen you as father and mother for me in this life. Thank you both very much for everything that you have done for me and for my brothers and sisters in this life.

TABLE OF CONTENTS

LIST OF TABLES xii
LIST OF FIGURES xiv
ABSTRACT xix

Chapter

1 INTRODUCTION 1

1.1 Introduction 1
1.2 Problem Description 2
1.3 Primary Objectives 2
1.4 Methodology 3
1.5 Outline of Dissertation 5

2 BRIDGE DESCRIPTION 9

2.1 Location 9
2.2 Background 10
2.3 Bridge Details 11

2.3.1 Edge Girder 14
2.3.2 Transverse Floor Beams 15
2.3.3 Pylons 16
2.3.4 Stay Cables 17

3 STRUCTURAL HEALTH MONITORING SYSTEM 18

3.1 System Overview 18
3.2 Sensors 19

3.2.1 Strain and Temperature Sensors 21

3.3 Data Acquisition System 24

4 ANALYTICAL MODEL 27

4.1 2-D SAP2000 Model 28
4.2 Three-Dimensional CSiBridge Model with Shell Elements 30

4.2.1 Geometry of the Bridge 31
4.2.2 Element Types 33
4.2.2.1 Beam Elements 33
4.2.2.1.1 Edge girders 34
4.2.2.1.2 Pylons 36
4.2.2.1.3 Floor Beams 36
4.2.2.2 Shell Elements 37
4.2.2.3 Cable Element 39
4.2.3 Material Properties 42
4.2.3.1 Concrete 42
4.2.3.2 High Strength Steel Wire 42
4.2.4 Boundary Condition and Bearing Stiffness 43
4.2.5 Analysis and Preliminary Results 45
4.3 Three-Dimensional CSiBridge Beam Element Model 47
5 MODEL VALIDATION WITH LOAD TESTS AND DESIGN MODEL 50
5.1 Load Tests 50
5.1.1 Loading 51
5.1.2 Passes 53
5.1.3 Results 54
5.2 Extracted Design Loads 59
5.2.1 Design Model versus UD Model 61
5.3 Load Tests Results vs. Model 63
5.3.1 Adjustments to FE Design Model 64
5.4 Conclusions 74
6 EDGE GIRDER CONVENTIONAL RATING 76
6.1 Contribution of this Chapter 76
6.2 Introduction 76
6.3 Service I Limit State 80

6.4 Service III Limit State 81
6.5 Strength I Limit State 83

6.5.1 Moment and Axial Capacities 84
6.5.2 Rating Using Interaction Diagram 84
6.5.3 Inventory and Operating 86

6.5.3.1 Flexural Ratings 87
6.5.3.2 Axial Ratings 87
6.5.3.3 Shear Ratings 88

6.6 Summary 88

7 RELIABILITY ANALYSIS BASED ON DESIGN LOADS 90

7.1 Background 90
7.2 Introduction 92
7.3 Statistical Parameters for Design Loads and Resistance 93
7.4 Reliability Method 97
7.5 Monte Carlo Simulation 100
7.6 Results 101

7.6.1 Strength I Limit State 102
7.6.2 Service III Limit State 103
7.6.3 Service I Limit State 104

7.7 Discussion and Conclusion 105

8 COMPUTING CONTINUOUS RATING FACTORS USING CONTINUOUS STRUCTURAL HEALTH MONITORING DATA 107

8.1 Introduction 107
8.2 Literature Review 108
8.3 Contribution of this Chapter 111
8.4 Methodology of Extracting Structural Forces and Stresses from SHM Data 112
8.5 Data Collection for Rating Purposes 121

8.5.1 Protocols for Data Collection 122

8.5.1.1 Low Frequency Data Collection Protocol 123
8.5.1.2 High Frequency Data Collection Protocol 125

8.5.1.2.1 Signal Processing 126

8.6 Updated Rating Equations with SHM Forces and Stresses 128

8.6.1 Low Frequency Rating Method 128
8.6.2 High Frequency Rating Method 129
8.6.3 Service I and Service III Limit States 129
8.6.4 Strength I Limit State 131

8.6.4.1 Flexural 131
8.6.4.2 Axial 132

8.7 Example Applying the Low Frequency Rating Method 133
8.8 Example Applying the High Frequency Rating Method 135
8.9 Automated Matlab Code and Data Analysis 138

8.9.1 Low Frequency Protocol 139
8.9.2 High Frequency Protocol 141
8.9.3 Combined Low Frequency and High Frequency Results 143

8.10 Example Showing Strain Comparison with Rating Factor 145
8.11 Summary 148
8.12 Conclusions 150

9 RELIABILITY ANALYSIS BASED ON STRUCTURAL HEALTH MONITORING DATA 157

9.1 Background 157
9.2 Literature Review 158
9.3 Contribution 161
9.4 Reliability Method 162
9.5 General Framework 167
9.6 Load Effects Statistical Models 170

9.6.1 Dead Load Statistical Model 171
9.6.2 Live Load Statistical Model 172

9.6.2.1 Weigh-In-Motion Data 173

9.6.2.1.1 Weigh-In-Motion Data Processing 175
9.6.2.1.2 Weigh-In-Motion Data Scrubbing 177
9.6.2.1.3 Results of Weigh-In-Motion Data Scrubbing 179

9.6.2.2 Trucks Simulation in 3D CSiBridge Model 181
9.6.2.3 Final Live Load Model 182

9.6.3 Environmental Statistical Model 185
9.6.3.1 Sample of Collected Data 186
9.6.3.2 Delaware Environmental Observing System (DEOS) Data 187
9.6.3.3 Correlation and Regression Analysis 192
9.6.3.4 Final Environmental Model 196
9.7 Resistance Statistical Model 200
9.8 Reliability Analysis in Matlab Code 201
9.9 Analysis Results 202
9.10 Discussion and Conclusions 206
10 CONCLUSIONS 211
10.1 Research Overview 211
10.2 Principal Contributions, Findings, and Conclusions 211
10.3 Future Work 217
REFERENCES 219
Appendix
A DESIGN, LEGAL, AND PERMIT TRUCKS CONFIGURATIONS 222
A.1 Load Rating Manual Truck Configurations 222
B LOAD RATING 227
B.1 Extracted live and Dead Load Stresses with Calculated Rating Factors for Service I and Service III Limit States 228
B.2 Extracted live and Dead Load Forces with the Calculated Rating Factors for Strength I Inventory Limit State 232
B.3 Extracted live and Dead Load Forces with the Calculated Rating Factors for Strength I Operating Limit State 236
B.4 Extracted live and Dead Load Shear Forces with the Calculated Rating Factors for Strength I Inventory and Operating 240
C RELIABILITY ANALYSIS BASED ON DESIGN INFORMATION 245
C.1 Matlab Code for Reliability Analysis Based on Design Information 245
D CONTINUOUS RATING FACTORS USING STRUCTURAL HEALTH MONITORING DATA 247

D.1 Low Frequency Rating Factor Report 247
D.2 High Frequency Rating Factor Report 259
D.3 Combined Rating Factor Report..... 271

E RELIABILITY ANALYSIS BASED ON STRUCTURAL HEALTH MONITORING DATA 283

E.1 Matlab Code for Reliability Analysis Using SHM Data Applied on Service III Limit State 283

LIST OF TABLES

Table 4.1. Pylon Section Properties 36

Table 4.2. Section Properties of Floor Beams 37

Table 4.3. Cable Section Names and Cross Sectional Areas 41

Table 4.4. Bearing Types and Restraint Direction 44

Table 4.5. Modeled Bearing Stiffness 45

Table 5.1. Truck Weights Used In Load Tests 52

Table 5.2. Maximum Responses from Four Truck Passes in all Load Tests 57

Table 5.3. Maximum Responses from Six Truck Passes in all Load Tests 58

Table 6.1. Limit States and Load Factors for Load Rating (AASHTO 2011) 79

Table 7.1. Bias Factors and Coefficient of Variation for Dead Load (Kulicki et al. 2007) 95

Table 7.2. Bias Factors and Coefficients of Variation for Live Load (Kulicki et al. 2007) 96

Table 7.3. Bias Factors and Coefficient of Variation for Resistance (Kulicki et al. 2007) 97

Table 8.1. Sample of Calculated Low Frequency Rating Factors and LRFR Conventional Rating Factors at the Center of Mid-span Location Sensors (S-W7 & S-W8) 134

Table 8.2. Example One Recorded and Analyzed Data. 136

Table 8.3. Sample of Calculated High Frequency Rating Factors and ISRF at the Center of Mid-span Location Sensors (S-W7 & S-W8) 137

Table 8.4. Comparison between High Frequency Ratings and Design Ratings 151

Table 8.5. Comparison between Low Frequency Ratings and Design Ratings 153

Table 9.1. WIM Data Record Format (fhwa.dot.gov 2013) 176

Table 9.2. Correlation Coefficients and Regression Model Slopes between measured Strain and Temperature 196

Table 9.3. Parameters Estimation for Cumulative Distribution Function 198

Table 9.4. Calculated Parameters for The CDF At Sensor SE-22 199

Table B.1. Rating Factors for Service I and Service III 228

Table B.2. Rating Factors for Strength I-Flexural Inventory 232

Table B.3. Rating Factors for Strength I-Flexural Operating 236

Table B.4. Rating Factors for Strength I-Shear Inventory and Operating 240

LIST OF FIGURES

Figure 2.1. Location of the Indian River Inlet Bridge (IRIB) 9

Figure 2.2. Bathymetry Contour Plot Showing Scour Pits near the Piers of the Steel Girder Bridge. 10

Figure 2.3. Elevation View of the Indian River Inlet Bridge 12

Figure 2.4. Indian River Inlet Bridge Deck Cross-Section View of Cable Supported Spans 14

Figure 2.5. Edge Girder Cross Section with the Effective Flange Width (AECOM 2012a) 15

Figure 2.6. Pylon Configurations and Dimensions (A) at Foundation Level and (B) at Anchoring Level 16

Figure 2.7. Stay Cable Numbering 17

Figure 3.1. General Elevation View Showing Sensor Layout on the Bridge 20

Figure 3.2. Sensor Layout on the Indian River Inlet Bridge 21

Figure 3.3. Micron-Optics os3600 Strain Sensor with Mounting Brackets 22

Figure 3.4. Photograph of Strain Sensor Anchored to Rebar in Pylon 22

Figure 3.5. Edge Girder Strain Sensor Detail 24

Figure 3.6. Photograph Showing Control Cabinet 26

Figure 4.1. 2-D SAP2000 Model of the IRIB 29

Figure 4.2. 3-D CSiBridge Model with Shell Elements for the IRIB 31

Figure 4.3. 3-D CSiBridge Actual Nodal locations 32

Figure 4.4. Global and Local Coordinate Systems for Frame Element 33

Figure 4.5. Modeled Edge Girder Section 35

Figure 4.6. Shell Element Geometry and Node Locations (Abell 2012) 38

Figure 4.7. Boundary Conditions and Bearing Locations 43

Figure 4.8. 3-D CSiBridge Beam Element Model for the IRIB 48

Figure 5.1. Conventional Ten Wheel Dump Truck 52

Figure 5.2. Sample of Dump Truck Axles Spacing 53

Figure 5.3. Truck Configuration for Side by Side Passes. 54

Figure 5.4. Four Truck Pass in All Load Tests @ SW-8 55

Figure 5.5. Four Trucks Pass in All Load Tests @ SW-22 56

Figure 5.6. Sample of Designer Rating Factors Tables Submitted to DelDOT (AECOM 2012a) 60

Figure 5.7. Maximum Envelops Stresses of UD Model Vs. Designer Model. 63

Figure 5.8. Concrete Compressive Strength from 56-day Cylinders 65

Figure 5.9. First Load Test, Four Trucks, West Girder 67

Figure 5.10. Second Load Test, Four Trucks, West Girder 68

Figure 5.11. Third Load Test, Four Trucks, West Girder 68

Figure 5.12. Fourth Load Test, Four Trucks, West Girder 69

Figure 5.13. First Load Test, Four Trucks, East Girder 69

Figure 5.14. Second Load Test, Four Trucks, East Girder 70

Figure 5.15. Third Load Test, Four Trucks, East Girder 70

Figure 5.16. Fourth Load Test, Four Trucks, East Girder 71

Figure 5.17. Second Load Test, Six Trucks, West Girder 71

Figure 5.18. Third Load Test, Six Trucks, West Girder 72

Figure 5.19. Fourth Load Test, Six Trucks, West Girder 72

Figure 5.20. Second Load Test, Six Trucks, East Girder 73

Figure 5.21. Third Load Test, Six Trucks, East Girder 73

Figure 5.22. Fourth Load Test, Six Trucks, East Girder 74

Figure 6.1. Sample Calculation for RF for Member WG278 Using Service I (ksf) 80

Figure 6.2. Comparison between Designer RF and Calculated UD RF for Service I .. 81

Figure 6.3. Sample Calculation for RF for Member WG281 Using Service III (ksf) .. 82

Figure 6.4. Comparison between Designer RF and Calculated UD RF for Service III 83

Figure 6.5. Steps to Extract Axial and Moment Capacities Using an Interaction Diagram 86

Figure 6.6. Sample Calculation of Inventory Moment (k-ft) RF for Member WG281 87

Figure 6.7. Sample Calculation of Operating Moment (k-ft) RF for Member WG281 87

Figure 6.8. Sample Calculation of Inventory Axial (kips) RF for Member WG281 ... 87

Figure 6.9. Sample Calculation of Operating Axial (kips) RF for Member WG281 ... 88

Figure 6.10. Sample Calculation of Inventory Shear (kips) RF for Member WG177 . 88

Figure 6.11. Sample Calculation of Operating Shear (kips) RF for Member WG196. 88

Figure 7.1. Graphical Presentation of Reliability Analysis Using Normal Distributions (Nowak & Collins 2013) 98

Figure 7.2. Reliability Indices Along Edge Girder for Strength I- Flexure 103

Figure 7.3. Reliability Indices Along Edge Girder for Service III-Flexural Tension 104

Figure 7.4. Reliability Indices Along Edge Girder for Service I-Flexural Compression 105

Figure 8.1. Measured Strain from a Top and Bottom Sensors for a Simple Beam Subjected to Different Load Cases 114

Figure 8.2. Strain Distribution Along the Cross Section for the Superposition Case 115

Figure 8.3-A. A Year Sample of the Low Frequency Data for Sensor SW_22 123

Figure 8.3-B. A Week Sample of the Low Frequency Data for Sensor SW_22 124

Figure 8.4. Sample of High Frequency Signal for Sensor SW_7 and Signal Processing Shows Long and Short Terms Signals 127

Figure 8.5. Sample of High Frequency Signal for Sensor SW_8 and Signal Processing Shows Long and Short Terms Signals 128

Figure 8.6. Sample of Low Frequency Rating Factors for S-W7 and S-W8..... 140

Figure 8.7. Sample of High Frequency Rating Factors Report for S-W7 and S-W8 . 142

Figure 8.8. Sample of the Final Plot in the High and Low Frequency Rating Factors Report for S-W7 and S-W8 144

Figure 8.9. Maximum Peak Strains Recorded by Sensor S-E6 147

Figure 8.10. High Frequency Rating Factors 148

Figure 9.1. Framework for Reliability Analysis Based on SHM 168

Figure 9.2. Automatic Traffic Recorder (ATR) Locations in Delaware Including Two WIM Stations of Interest 174

Figure 9.3. Example of WIM "White File" Data 175

Figure 9.4. Gross Vehicle Weight for Filtered Weigh-In-Motion Data 180

Figure 9.5. Total Length of Vehicles for Filtered Weigh-In-Motion Data 180

Figure 9.6. Total Number of Axles for Filtered Weigh-In-Motion Data 181

Figure 9.7. Final Strain Distribution Obtained By WIM Data and Log-normal Distribution Parameters for Member 10 184

Figure 9.8. Final Strain Distribution Obtained By WIM Data and Log-normal Distribution Parameters for Member 89 at Mid-span location..... 184

Figure 9.9. Final Strain Distribution Obtained By WIM Data and Log-normal Distribution Parameters for Member 149 at Controlling Location 185

Figure 9.10. Sample of Low Frequency Strain Data for Sensor SW-22 187

Figure 9.11. DE-LSS DEOS Station Location Compared to the IRIB Location 188

Figure 9.12. Sample of DEOS Table Shows Minimum, Maximum, and Average Temperature with Wind Speed for January 1, 2013..... 189

Figure 9.13. Average Daily Temperature and Wind Speed for June 2012 to June 2014 at DE-LSS station..... 190

Figure 9.14. Daily and Seasonal Temperature Fluctuations (2010 to 2014)..... 191

Figure 9.15. Maximum Daily Wind Speed (2010 to 2014)..... 192

Figure 9.16. Regression Model for Sensor SE-22 with all Measured Data Between March 7, 2014 to May 7, 2014 193

Figure 9.17. Comparison Between Measured Temperature at sensor SE-22 and Recorded Temperature by DEOS System at DE-LSS Station 195

Figure 9.18. Empirical and Theoretical Probability Distribution Function and Cumulative Distribution Function For Temperature Fluctuations 198

Figure 9.19. Reliability Indices Based on Design and SHM Data Along West Edge Girder for Strength I-Flexural 205

Figure 9.20. Reliability Indices Based on Design and SHM Data Along West Edge Girder for Service III..... 205

Figure 9.21. Reliability Indices Based on Design and SHM Data Along West Edge Girder for Service I..... 206

Figure A.1. Rating Truck Axle Configurations and Wheel Weights for Design 223

Figure A.2. Rating Truck Axle Configurations and Wheel Weights for Legal Loads224

Figure A.3. Rating Truck Axle Configurations and Wheel Weights for Legal Loads225

Figure A.4. Rating Truck Axle Configurations and Wheel Weights for Permit Loads 226

ABSTRACT

The safety and serviceability of bridges is of paramount concern for bridge owners and for the traveling public. As our bridge infrastructure continues to age, there is a growing need for new methods and technologies that can enable transportation agencies to better evaluate their bridges to ensure their structural safety and to optimize their maintenance and inspection procedures. Following the collapse of the I-35 Bridge in Minnesota in 2007, the Federal Highway Administration (FHWA) began requiring a bridge load rating for all bridges in the United States. According to the American Society of Civil Engineers, one out of every nine bridges in the United States is classified as structurally deficient and is in urgent need of repair. The required maintenance of these and other bridges is very expensive. In fact, the FHWA estimates that it would cost nine billion dollars per year more than what is currently being spent on bridge maintenance to repair and maintain our deficient bridges. Structural Health Monitoring (SHM) is a technique that has been evolving and has been used in recent years to measure the loading environment and response of bridges in order to assess serviceability and safety. There are several examples around the world that have demonstrated the benefits of SHM using both short- and long-term monitoring. However, transportation agencies still lack the ability to directly implement SHM data into their maintenance and decision making processes. More specifically, transportation agencies are generally not capable of implementing the existing complex methods for using short- or long-term SHM data for bridge evaluation.

The primary objective of this study was to develop new methods for utilizing SHM data that are analogous to more traditional methods and can be easily implemented by transportation agencies to better evaluate their bridges to achieve optimal maintenance and effective decision making. In developing the new methods, two approaches were taken.

The first approach, referred to as the Continuous Rating Factor-Structural Health Monitoring method, uses SHM data to compute continuous rating factors. This approach applies SHM data directly into the Load Resistance Factor Rating (LRFR) equations to produce continuous rating factors for specific bridge components. To do this, the continuously recorded SHM data is converted into structural forces and/or stresses and incorporated directly into conventional rating equations to calculate continuously rating factors over time. More specifically, this new approach converts the measured strain and temperature data to live loads, thermal loads, prestressing losses, i.e. to yield accurate site-specific rating factors for various critical bridge components.

The second approach, referred to as the Reliability Analysis-Structural Health Monitoring method, uses a reliability analysis framework combined with SHM data. In this approach loads and resistances were expressed as Probability Distribution Functions (PDF), where loads and resistances are treated as random variables. The concept of estimating the probability of failure or probability of exceedance is utilized and expressed as a reliability index for a specific bridge component. The reliability analysis was conducted first using design loads and then using long-term SHM data. The analyses were performed using Monte Carlo simulation and Rackwitz-Fiessler method and considered a variety of limit states. In the first type of analysis (using

design information), the resistance model, dead load model, and live load model used in the reliability analysis were based solely on design information. In this analysis, the same statistical parameters used to develop the load effects and resistances in the AASHTO LRFD calibration were applied. In the second type of analysis (using SHM data), the load effects consisted of dead, live, and thermal loads. A live load statistical model was created based on data from Weigh-In-Motion (WIM) stations close to the location of the IRIB and a 3-D finite element model. The thermal load statistical model was created based on data from Delaware Environmental Observing System (DEOS) and correlation analysis between measured SHM strain and temperature data from the IRIB. In both cases, reliability indices for the west edge girder were computed along the bridge for various limit states.

In order to demonstrate the two methods, the Indian River Inlet Bridge (IRIB), a prestressed concrete cable-stayed bridge located in Sussex County Delaware, was used as a study case. The research showed that the two methods can serve as possible evaluation approaches for bridges that have SHM systems. Both methods are successful in taking huge amounts of SHM data and translating them into simple and well understood evaluation parameters (ratings and reliability indices).

The primary findings from results given by the continuous rating factor method were (1) SHM data can be used to directly compute bridge load ratings, (2) the developed technique provides results that can be easily understood and utilized by transportation agencies, and (3) the ratings show that thermal effects can have a significant effect on load ratings for long-span bridges. The primary findings from results given by the reliability method based on SHM data were (1) the method can be used to determine whether or not the monitored bridge meets the design code

standards in terms of reliability by allowing a comparison of the target reliability indices to indices computed based on SHM data, (2) the developed reliability-based methodology using SHM data can be applied to other bridges, (3) the developed method shows promise for enabling SHM data to be directly incorporated into the maintenance, inspection, and decision making processes, and (4) the work suggests how reliability analysis results can be integrated with bridge field inspection results.

Chapter 1

INTRODUCTION

1.1 Introduction

The safety and serviceability of bridges is of paramount concern for bridge owners and for the traveling public. As our bridge infrastructure continues to age, there is a growing need for new methods and technologies that can enable transportation agencies to better evaluate their bridges to ensure their structural safety and to optimize their maintenance and inspection procedures. Following the collapse of the I-35 Bridge in Minnesota in 2007, the Federal Highway Administration (FHWA) began requiring a bridge load rating for all bridges in the United States. According to the American Society of Civil Engineers, one out of every nine bridges in the United States is classified as structurally deficient and is in urgent need of repair (ASCE 2013). The required maintenance of these and other bridges is very expensive. In fact, the FHWA estimates that it would cost nine billion dollars per year more than what is currently being spent on bridge maintenance to repair and maintain our deficient bridges (ASCE 2013). Therefore, there is an urgent need for new methods and technologies that can help transportation agencies to evaluate bridges in a better way to ensure their structural safety and to optimize the maintenance and inspection procedures.

One potential method/technology involves Structural Health Monitoring (SHM). In general, SHM is defined as the process of implementing a damage identification strategy for aerospace, civil and mechanical engineering infrastructure

(Farrar & Worden 2007). SHM has been used in recent years to measure the loading environment and response of bridges to assess serviceability and safety while tracking the symptoms of operational incidents and potential damage (Xu & Xia 2012). There are many examples that have shown the benefits of collecting and utilizing both short- and long-term SHM monitoring data.

1.2 Problem Description

As a result of the revolution in new information technologies and advanced sensing systems, and the investments in infrastructure due to its impact on the economy, the number of bridges using SHM systems has been increasing in recent years and is expected to continue to grow. Large amounts of data are collected and reported by the SHM systems. Despite the fact that the collected data has vital information about the health of the monitored bridges, transportation agencies lack a direct method for incorporating the monitored data into the maintenance and decision making processes. Transportation agencies need well defined methods for translating the large quantities of short- and long-term SHM data into simple and understandable measures of bridge health.

1.3 Primary Objectives

The primary objective of this research was to develop new methods and approaches, based on SHM data that transportation agencies can use to better evaluate their bridges and to achieve optimal maintenance and effective decision making. Two main methods are proposed in this study. The first method leads to continuous rating factors based on SHM data. This approach depends on the direct use of monitored SHM data in Load Resistance Factor Rating (LRFR) equations to produce continuous

rating factors for bridge components. The second method involves the use of SHM data in traditional reliability analysis. The main goal of this work is to establish new techniques by which transportation agencies can use SHM data to ensure the structural safety of their bridges and guide their future maintenance and decision making procedure.

1.4 Methodology

Transportation agencies evaluate their structures in two ways; (1) through visual inspection which depends on the inspector's judgment and experience, and (2) through the application of Load and Resistance Factor Ratings (LRFR). The rating factor for a bridge, according to the Load Resistance Factor Design (LRFD) specifications, does not change with time unless damage to a bridge, or section loss to its components, occurs. The accuracy of the current evaluation methods depend on the accuracy of visual inspection and the subsequent evaluation and characterization of damage/section loss. To improve the accuracy of bridge evaluations, a new rating method that combines the standard approach of evaluating structures with the information from SHM systems, is needed. The first method presented in this study results in continuous rating factors based on SHM data. In this approach, the data from a continuous SHM system is converted into structural forces and combined with the conventional rating equations to calculate continuous rating factors over time. The new approach takes into consideration the available SHM data which includes live loads, thermal loads, prestressing losses, and more to yield accurate rating factors for bridge components. The developed method was applied to the Indian River Inlet Bridge (IRIB), a prestressed concrete bridge that has a robust SHM system. The continuous rating factor approach was performed on all applicable limit states for the

prestressed concrete bridge. The new approach demonstrated the effect of thermal loads on bridge load rating factors for long-span bridges, and it showed a direct use of SHM data in bridge load rating.

The second method presented in this study is reliability analysis. In this approach, loads and resistances are expressed as Probability Distribution Functions (PDF), where loads and resistances are treated as random variables. The concept of estimating the probability of failure or probability of exceedance is presented and expressed using reliability indices for bridge components. The reliability analysis is conducted in two stages, first using design loads and next based on long-term monitored SHM data. The analysis is performed on various limit states using Monte Carlo simulation and the Rackwitz-Fiessler method. In one case, the resistance model, dead load model, and live load models are considered based on design information in the reliability analysis. In this case, the same statistical parameters used for the load effects and the resistances in the AASHTO LRFD calibration are also used to perform this analysis. In the second type of reliability analysis, the load effects consisted of dead, live, and thermal loads in which the live load statistical model is created based on monitored data from Weigh-In-Motion (WIM) stations close to the location of the IRIB and a 3-D finite element model. The thermal load statistical model is created based on data from Delaware Environmental Observing System (DEOS) and correlation analysis between measured strain and temperature data on the IRIB. Reliability indices for the west edge girder are estimated along the bridge for various limit states. The main goal of this approach is to establish a new technique by which transportation agencies can utilize SHM data to ensure the structural safety of their

bridges. This approach can help transportation agencies guide their maintenance and decision making procedure.

1.5 Outline of Dissertation

The following presents a chapter by chapter outline of the contents of this dissertation.

Chapter 1 presents a general introduction to the topic. The motivation for the work is described and an overview of the primary objectives of this study is presented. Also, the general methodology used in the study is outlined and summarized.

Chapter 2 presents a short description of the Indian River Inlet Bridge (IRIB), which was used as a study case in this research. It presents the bridge location, bridge geometry, structural components, structural properties, and material properties according to the as-built plans.

Chapter 3 presents the Structural Health Monitoring (SHM) system that was installed on the IRIB. It presents an overview of the system including the data acquisition system and data collection protocols, and presents a summary of the types and locations of the sensors that were installed on the IRIB.

Chapter 4 presents the finite element models that were developed for the IRIB. These include a 2-D SAP2000 model, a 3-D CSiBridge shell element model, and a 3-D CSiBridge beam element model. The material types, sectional properties, and boundary conditions of each model are also discussed in this chapter.

Chapter 5 presents a summary of the four diagnostic load tests that have been conducted on the IRIB. Of primary interest are the maximum measured strains in the main edge girders caused by four and six side-by-side truck passes. The approach of extracting the design structural forces from the files submitted by the designer is also

presented, as are comparisons between the measured load test response and the results of finite element analyses. Finally, a comparison between results from the developed finite element model, and results reported by the designer, is shown.

Chapter 6 presents the conventional load rating process for the west edge girder of the IRIB. Conventional rating calculations were computed based on the applicable limit states and compared to rating factors developed by the designer. The main contribution of this chapter is to provide Delaware Department of Transportation (DelDOT) with the structural forces and stresses that were used in the rating process, and to show samples calculation for future ratings.

Chapter 7 presents the background for reliability analysis by discussing the AASHTO LRFD calibration and the methodology involved in using design loads in a reliability analysis. The chapter presents an overview of the statistical parameters used for the code calibration. The chapter presents the Monte Carlo simulations that were conducted using statistical models for load effects and resistances to estimate the reliability indices, considering various applicable limit states, along the west edge girder of the IRIB.

Chapter 8 presents an approach for computing continuous load ratings using SHM data. The chapter shows how monitored strain and temperature measurements were converted into structural forces and stresses. The method for converting SHM data into structural forces and stresses and the mechanics behind that conversion is described. The chapter also presents an overview of the data collection protocols and samples of the collected data. Load and Resistance Factor Rating (LRFR) equations were adapted to incorporate the structural forces and stresses obtained from the SHM data. Two methods of rating, each based on a different data collection protocol, were

developed. A low frequency rating method is presented that uses loads and resistances from the design information and adds a new term of SHM forces or stresses to the nominator portion of the LRFR equation. A high frequency rating method is presented that uses all of the structural forces and stresses computed in the low frequency method except the live load effects that are obtained directly from the high frequency data. Finally, the chapter presents examples to help the reader understand the new approaches and to highlight the output of the new rating methods compared to conventional rating methods.

Chapter 9 presents a method for conducting reliability analysis based on SHM data. The chapter provides a literature review of work done related to reliability analysis based on SHM data. The general concept of reliability analysis and reliability indices based on probability distribution functions is discussed. The general framework that was followed in this study is described and explained. The statistical parameters for the load effects (dead loads, live loads, and thermal loads) and for the resistance are presented. In the method presented, the same statistical parameters used for the AASHTO code calibration were used for the dead load and resistance models. The live load statistical model was based on Weigh-In-Motion (WIM) data that, after filtering, was applied to a 3-D finite element model. The thermal load statistical model was created based on data from Delaware Environmental Observing System (DEOS) and correlation analysis between measured strain and temperature data on the IRIB. Reliability indices for the west edge girder were estimated along the bridge for various limit states using the Rackwitz-Fiessler procedure. The results of the reliability analysis are presented and compared to the reliability indices found based on design

information. Conclusions and recommendations are drawn based on the reliability indices values.

Chapter 10 provides a synopsis of the research conducted in this study. Conclusions and recommendations are presented in this chapter and limitations of the methodology and potential future work are outlined.

Chapter 2

BRIDGE DESCRIPTION

2.1 Location

The Charles W. Cullen Bridge, also known as the Indian River Inlet Bridge (IRIB), crosses the Indian River Inlet between the Indian River Bay and the Atlantic Ocean. The bridge services Delaware Route 1 (DE1) and it is located in Sussex County in Delaware between Rehoboth Beach and Bethany Beach, see Figure 2.1.

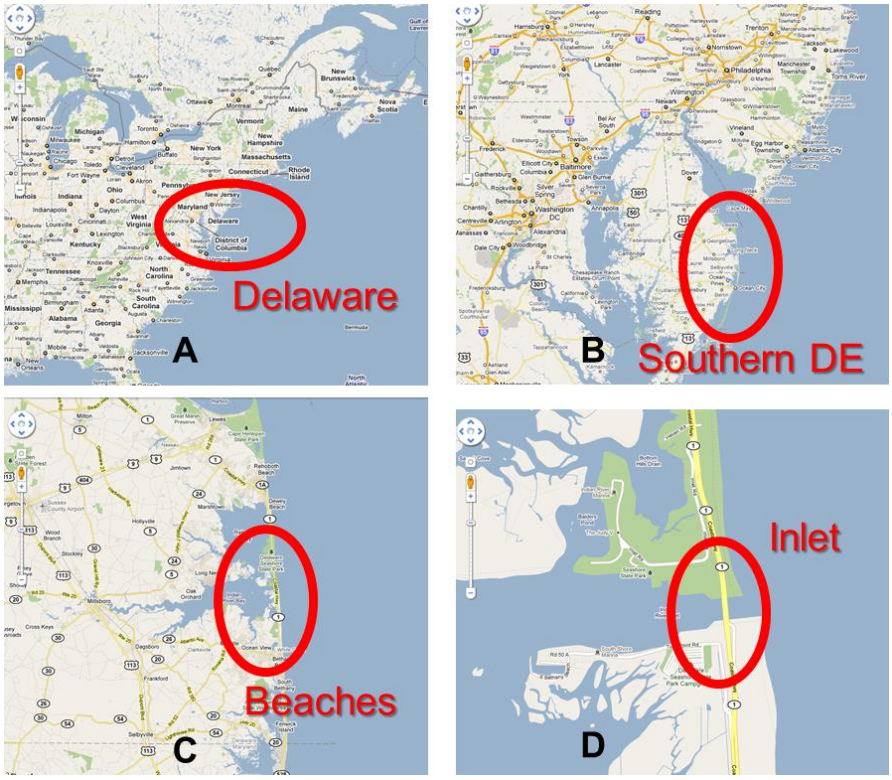

Figure 2.1. Location of the Indian River Inlet Bridge (IRIB)

2.2 Background

The current bridge is the fifth in the series of bridges built to cross the inlet. The first bridge built over the Indian River Inlet was a timber bridge, it was built in 1934. It lasted only four years and was replaced by a concrete and steel swing bridge in 1938. This bridge was destroyed by ice and tides in 1948. Another concrete and steel swing bridge was rebuilt and finished in 1952. This last bridge was closed in 1962 due to severe storm damage. After that, a steel girder bridge was built in 1965. An identical twin span was built in 1976 to handle the increase in traffic on DE 1. This bridge suffered from a serious scour problem at the main supporting piers, which were located in the inlet channel, and it was rated as structurally deficient in 1989. See Figure 2.2.

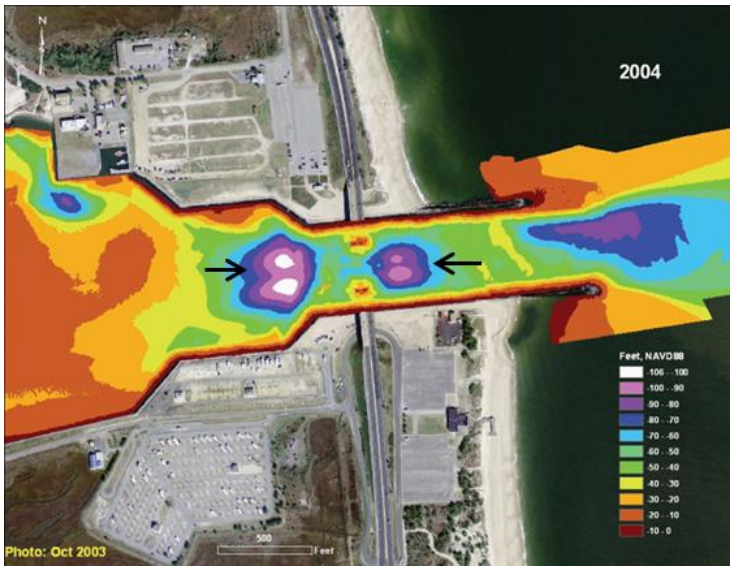

Figure 2.2. Bathymetry Contour Plot Showing Scour Pits near the Piers of the Steel Girder Bridge.

A reinforced concrete arch span bridge was designed to replace the steel girder bridge, which would have been the longest arch bridge of its type in the world if it was built; however, construction bids to build the arch bridge were well over the available budget. The Delaware Department of Transportation (DelDOT) requested bids for a design-build project for the new bridge in 2006.

The new bridge is a cable-stayed bridge, which was built at a cost of $150 million. DelDOT awarded the design-build contract to the joint venture team of Skanska/AECOM. The work started on the bridge in August, 2008. The south bound lanes of the bridge were opened to traffic in January, 2012 and the bridge was opened to full traffic in May, 2012.

2.3 Bridge Details

The new bridge is a concrete harped cable-stayed design that consists of a cable-stayed bridge with four-approach spans at each end. Each unit of the approach spans consists of four 106 feet-3 inch long sections for a total length of 425 feet. Prestressed concrete bulb tee girders with a depth of 70 inches were used to support an 8.5 inches thick concrete deck in all approach spans.

The cable-stayed bridge has a total length of 1,750 feet and consists of four pylon towers with 152 stays supporting the three spans: the southern back span is 400 feet; the main span is 950 feet; and the northern back span is 400 feet. See Figure 2.3. Each of these spans consists of cast-in-place concrete edge girders with both precast and cast-in-place concrete transverse floor beams, and a cast-in-place concrete deck. The 152 cables are distributed so that there are 19 cables on each side of the four pylons connecting to the edge girder.

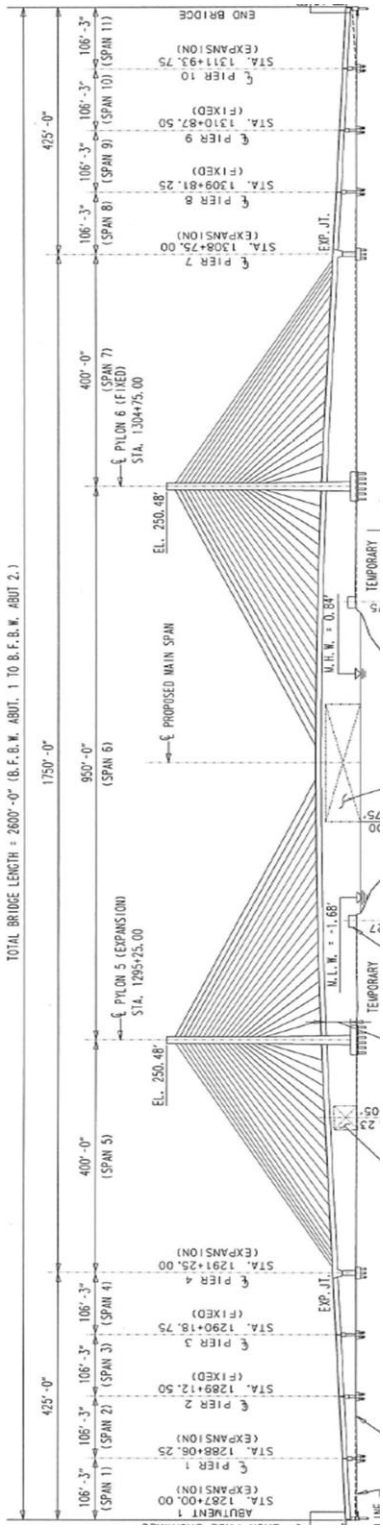

Figure 2.3. Elevation View of the Indian River Inlet Bridge

The bridge is fixed at the northern pylon and is free to expand at the south pylon and the abutments. A more detailed description of the bridge design and construction can be found in (Nelson 2012).

The total width of the bridge is 106 feet and 2 inches; the bridge carries four lanes of traffic, two lanes of traffic in each direction, and a 12 feet wide pedestrian walk way on the east side of the bridge, which shifts the centerline of the roadway toward the west side. The 8 ½ inch thick deck was cast-in-place and includes 1-5/8 inches of latex modified concrete as a wearing surface. See Figure 2.4 for the general cross-section and lane positions.

The construction of the main cable bridge was performed in two stages. The portions of the deck over land were constructed on falsework, which was faster and more economical than using a form traveller. In this region the floorbeams were precast pretensioned I sections that tapered in depth from the center to their ends. The second region, over water, was constructed in 24 foot sections using a form traveller. Cast-in-place floor beams were used in this region. Post-tensioning was used in the entire bridge, except the deck portion over land; post-tensioning was used in edge girders, cast-in-place floorbeams, and the connection of precast floor beams to the edge girders.

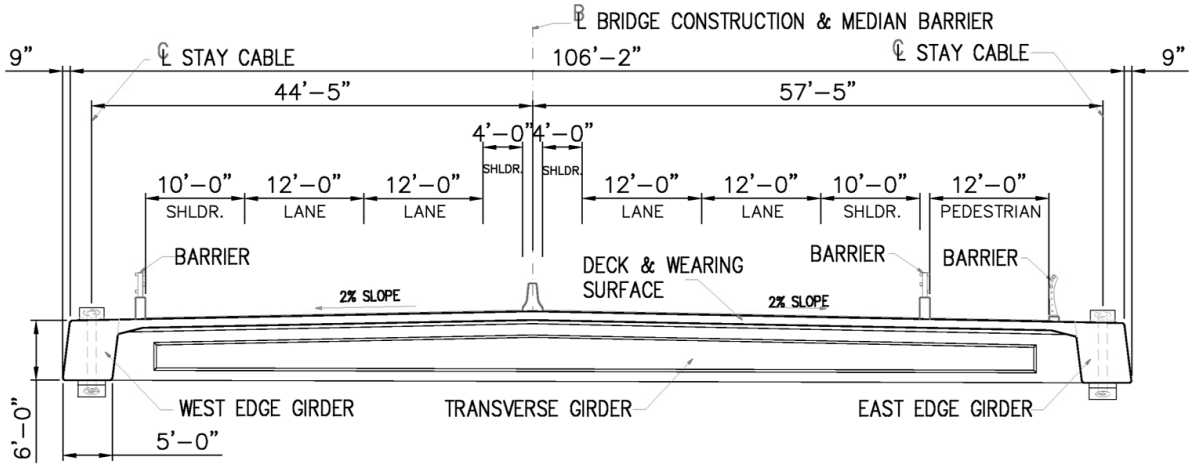

Figure 2.4. Indian River Inlet Bridge Deck Cross-Section View of Cable Supported Spans

2.3.1 Edge Girder

The edge girders resemble oblique rectangle shapes; they are 6 feet tall and 5 feet wide. They are continuous cast-in-place prestressed sections with a design concrete compressive strength of 6,500 psi. A set of data collected from concrete cylinder breaks at 56 days shows a wide range of the concrete compressive strength used in the edge girder. The maximum, average, and minimum concrete compressive strength recorded from that data are 14200, 8200, and 5500 psi, respectively.

In order for the designer to determine the effective flange width of the edge girder, they have used the influence lines from a SAP2000 model to determine the notional span length. Figures 4.6.2.6.2-1 and 4.6.2.6.2-2 of the ASHTO LRFD code were used to determine the approximate effective flange width that was used in designing the edge girder. Figure 2.5 is taken from the Load Rating Calculations for Edge Girder submitted by AECOM to DelDOT (AECOM 2012a). It illustrates the cross sections and the section properties used for designing the edge girder.

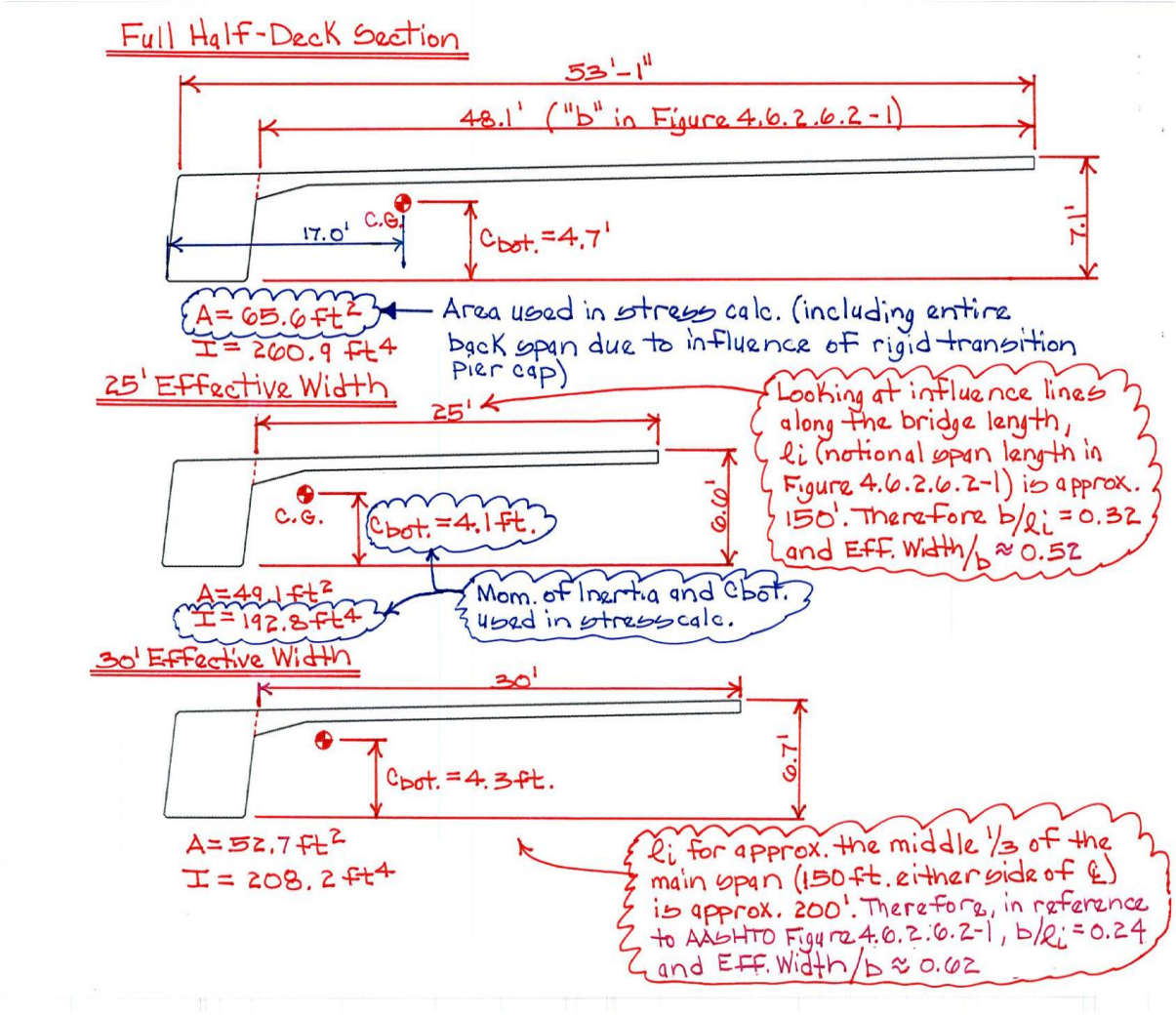

Figure 2.5. Edge Girder Cross Section with the Effective Flange Width (AECOM 2012a)

2.3.2 Transverse Floor Beams

The bridge has a combination of precast and cast-in-place floor beams. The floor beams are spaced 12 feet in general. They are precast pretensioned I sections in the region of the falsework construction. However, in the region over the water where the traveler form was used, they were cast with the deck and the edge girder, and post-tensioned together to create a monolithic superstructure.

2.3.3 Pylons

There are two cast-in-place twin pylons, each of which reaches a height of 248 feet high above the ground level. Each pylon is composed of two slightly tapered concrete boxes, 16 feet by 11 feet at the foundation level, that transition to one concrete box at the road deck level. In the stay cable anchorage portion the dimension is 12 feet by 11 feet and the cables are anchored to steel boxes contained within the pylons. See Figure 2.6.

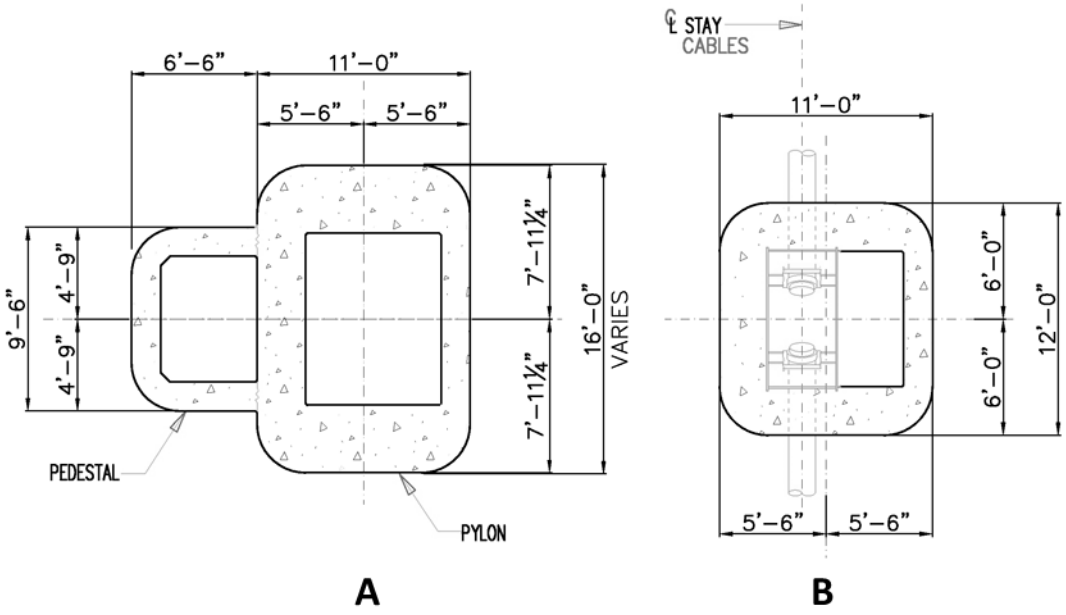

Figure 2.6. Pylon Configurations and Dimensions (A) at Foundation Level and (B) at Anchoring Level

The twin pylons are connected only by a grade beam at the base. Using an aerodynamically efficient cross section and by minimizing the eccentricity of the stay plane with respect to the centroid of the cross section, designers were able to eliminate

the conventional strut between pylons typically seen above deck level in bridges of this type. The pylons are supported on a 10-foot thick spread footing that is supported by three foot diameter prestressed concrete piles ranging from 42 to 49 piles.

2.3.4 Stay Cables

There are 152 stay cables; 19 stays are anchored on each side of the pylons. The stay cables are anchored every 24 feet to the edge girder center and the underside of the transverse floor beams. The stay cables are composed of 0.62 inch diameter, seven wire strands, in bundles of 19 to 61. The strands are waxed and encapsulated in high-density polyethylene sheathing. The stays are protected by a high density polyethylene (HDPE) pipe for corrosion protection. The pipe has a raised helical strake to minimize the potential for wind-rain induced vibrations. See Figure 2.7.

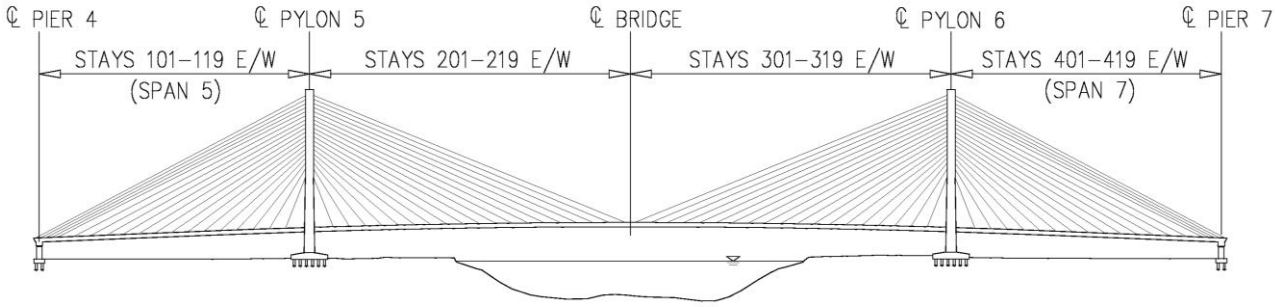

Figure 2.7. Stay Cable Numbering

Chapter 3

STRUCTURAL HEALTH MONITORING SYSTEM

3.1 System Overview

The Center for Innovative Bridge Engineering (CIBrE) at University of Delaware proposed the idea of a permanent long-term Structural Health Monitoring (SHM) system for the new Indian River Inlet Bridge. The Delaware Department of Transportation (DelDOT) ranks as one of the more progressive DOT's today in the use of technology: as DelDOT saw the value of having such a monitoring system on the bridge, they decided to make it an integral element of the design-build project.

The CIBrE at University of Delaware was awarded the contract of designing and installing the long-term SHM system on the bridge. Since the bridge was a design-build project, the CIBrE worked very closely with the contractor, designer, and the owner to accomplish the work without causing any delays in the construction process.

The SHM system aims to help the Delaware Department of Transportation (DelDOT) to better maintain and operate the bridge through its service life. The SHM system was designed to provide quantitative data at key locations on the structure to help assess and evaluate the condition of the bridge through its service life.

Researchers at the University of Delaware had two options for the SHM system, a conventional analog type system or a more innovative fiber-optic based sensor system. After comparing the advantages and the disadvantages of both systems, the fiber-optic system was selected.

The fiber-optic sensors were supplied by Cleveland Electric Laboratories (CEL) and Chandler Monitoring Systems (CMS). CMS also supplied two Micron Optics model SM 130 interrogators for acquiring the data. For more details about the SHM system see (Shenton et al. 2016).

3.2 Sensors

The total number of sensors installed on the bridge is 129. The SHM system was designed to monitor various types of structural responses. They include:

- 70 strain and temperature sensors, located in the edge girders, pylons, and deck.
- 27 accelerometers, mounted at the pylons, stay cables, and deck.
- 9 tiltmeters, located along the east edge girder.
- 3 displacement gauges, at the expansion joints and at the south east pylon.
- 16 chloride sensors, 10 are fiber optic sensors, and 6 are conventional analog type.
- 2 anemometers, one at the deck level, and the other at the north east pylon.

Figures 3.1 and 3.2 show the sensor layout on an elevation view of the bridge and on a perspective illustration.

The research in this report focuses on the strain and temperature sensors in the edge girders, for more details about the other sensors and the SHM system, see (Shenton et al. 2016).

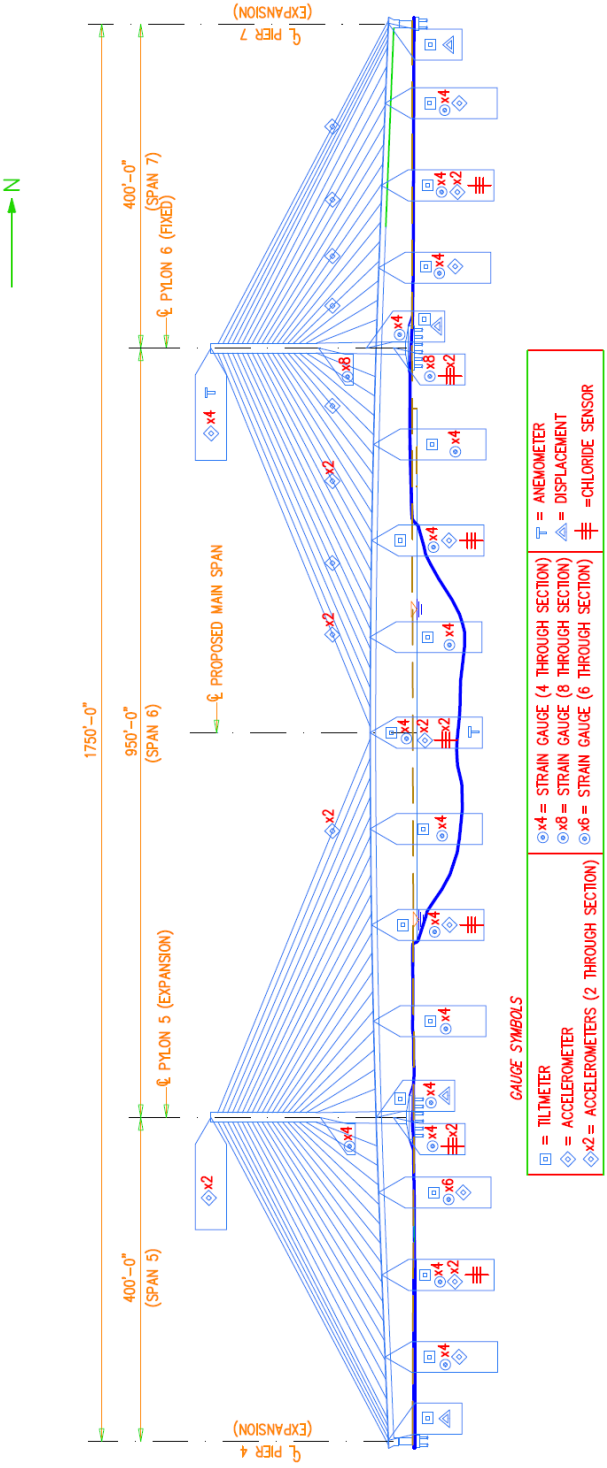

Figure 3.1. General Elevation View Showing Sensor Layout on the Bridge

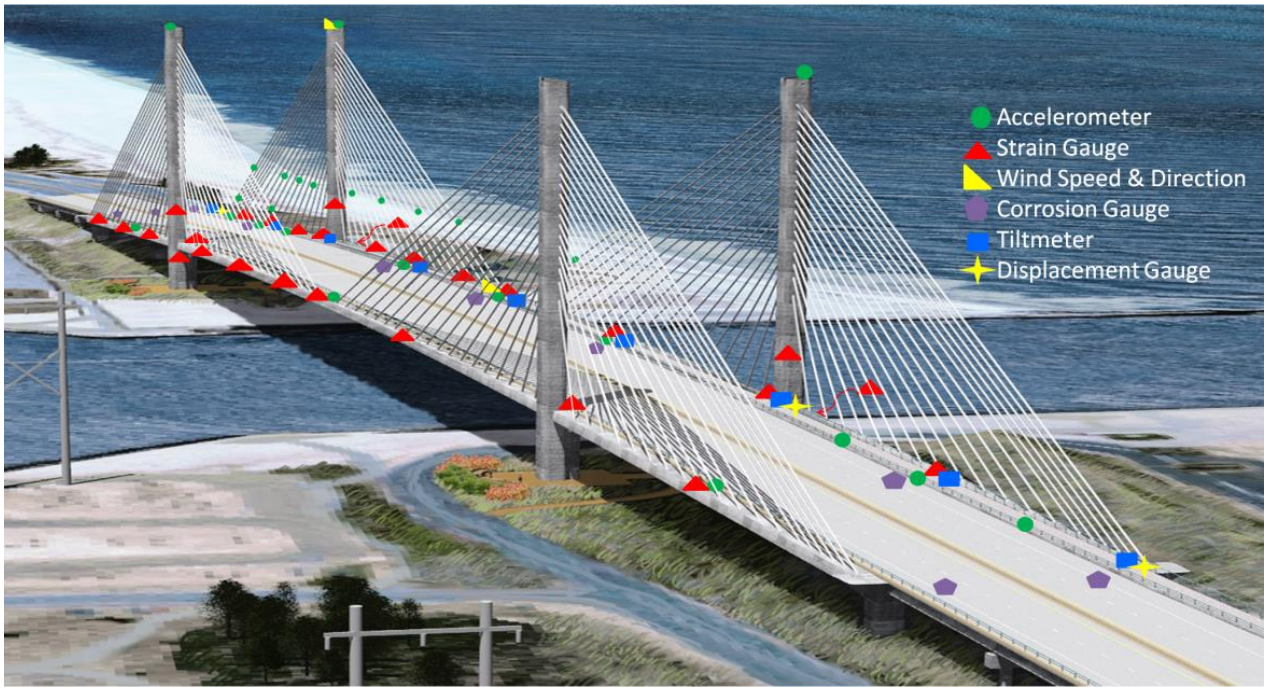

Figure 3.2. Sensor Layout on the Indian River Inlet Bridge

3.2.1 Strain and Temperature Sensors

There are 70 strain and temperature sensors throughout the bridge. All of them are Micron Optics os3600 strain sensors. The sensors have a gage length of 9.8 inches, a range of +/- 2500 με, and a sensitivity of 1.2 pm/με.

The os3600 is based on Fiber Bragg Grating (FBG) technology; it measures average strain over the length of the gage, while providing active temperature compensation. Each of the gage ends has a mounting bracket, that is clamped to a steel rebar and embedded in the concrete. Figures 3.3 and 3.4 show the os3600 sensors with the mounting brackets and an example of the sensor mounted to a pylon rebar, respectively.

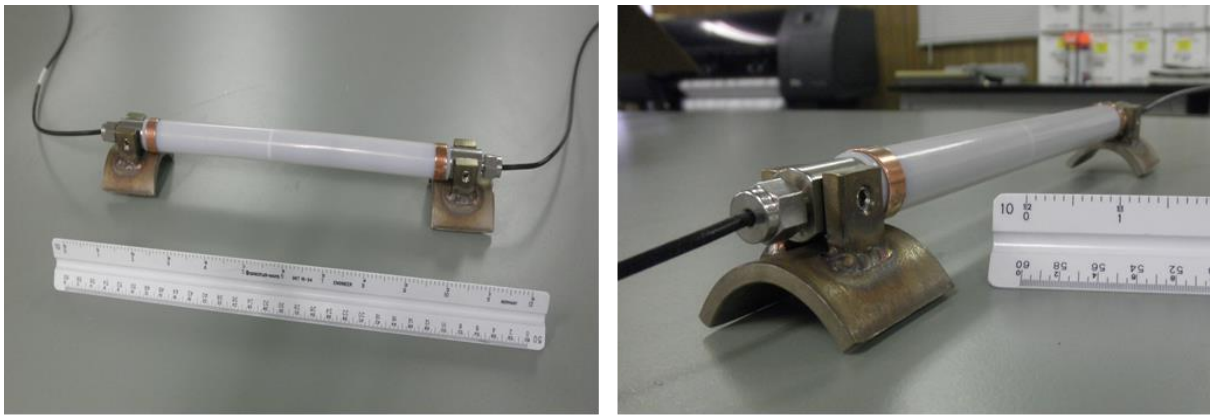

Figure 3.3. Micron-Optics os3600 Strain Sensor with Mounting Brackets

Figure 3.4. Photograph of Strain Sensor Anchored to Rebar in Pylon

A strain sensor delivers the total strain from the FBG's response, corrected for thermally induced changes in the gage optics. Equation 3.1 is used to calculate the total strain. It accounts for the change in refractive index and thermal expansion of glass for both the strain sensing and gage temperature compensation gratings.

$$\epsilon_{Total} = 10^6 \left[\frac{\left(\frac{\Delta\lambda}{\lambda_\circ}\right)_{strain} - \left(\frac{\Delta\lambda}{\lambda_\circ}\right)_{Temp}}{F_G} \right] + \left[\frac{\left(\frac{\Delta\lambda}{\lambda_\circ}\right)_{Temp}}{S_T} * CTE_{Temp} \right] \quad Equation 3.1$$

Where,

- $\Delta\lambda$= Wavelength shift, nm
- $\lambda_\circ$= Nominal wavelength, nm
- F_G= Gage factor, factory value
- S_T= Temperature sensitivity, pm/^{o}C
- CTE_{Temp}= Coefficient of thermal expansion for the temperature FBG mount, µm/m-^{o}C

The strain is measured in the east and west edge girders at 11 different locations along the length of the bridge. The longitudinal positions correspond to approximately 1/8 points on the main span and back spans. At each position, the strain is measured at four unique locations; at the top and bottom of both the east and west edge girders. Therefore, the edge girder strain is measured at 44 unique locations. At any given edge girder location the strain is measured in the longitudinal direction of the bridge at approximately 5 inches from the top and bottom of the girder, as shown in Figure 3.5. The strain is measured in the pylons at 24 different locations. The pylon sensors are placed in groups of 4 at different elevations, measuring the vertical strain

in each wall of the pylon. Also, strain is measured at two locations in the deck. In both cases the strain is measured in the direction transverse to the travel direction.

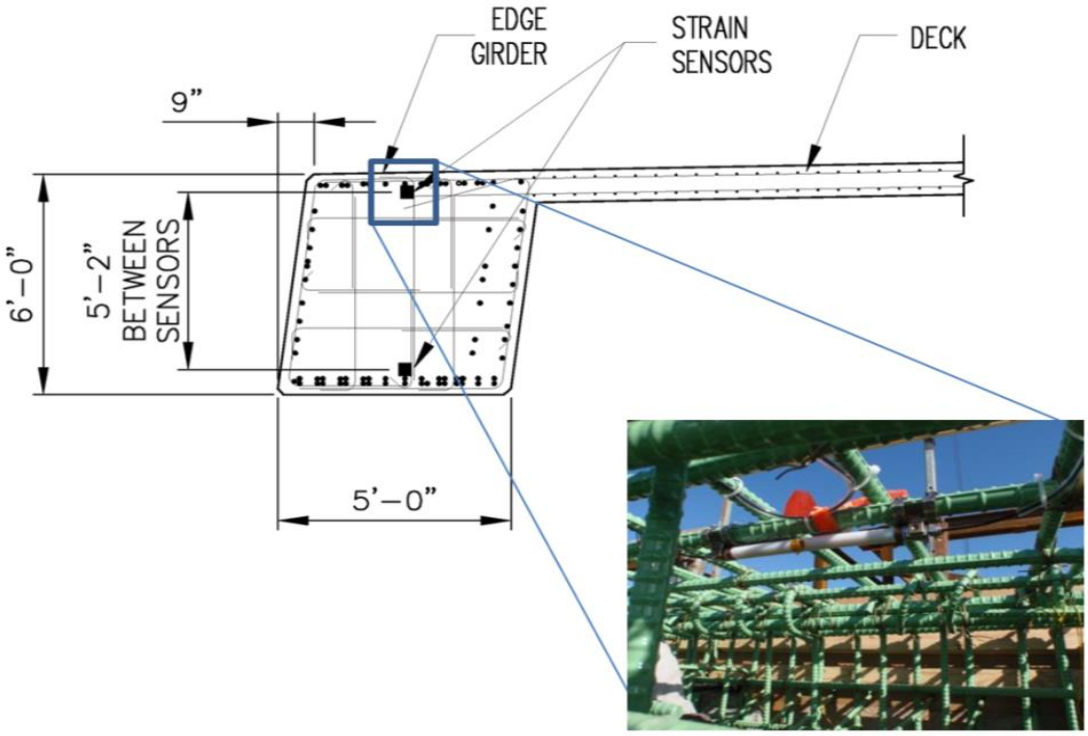

Figure 3.5. Edge Girder Strain Sensor Detail

3.3 Data Acquisition System

The heart of the fiber-optic system is a pair of Micro Optics SM130 Interrogators. Each interrogator has 4-channels, but a 16 channel multiplexer is connected to each which increases the effective number of main fibers of the system to 32. Interrogator “A” can sample at a maximum rate of 500 Hz; it is normally set to run at a rate of 125 Hz and handles all of the sensors except the accelerometers and a few strain sensors. Interrogator “B” can sample at a maximum rate of 1000 Hz, it is

normally set to run at a rate of 250 Hz and handles all of the accelerometers and the few remaining strain sensors.

The back end control software for the system is Micro Optic's "Enlight" software. This is where all of the fundamental control parameters for the system are set and the sensor parameters are stored. On the front end is running Cleveland Electric Labs/Chandler Monitoring Systems, "Intellioptics" software. This is a GUI program that provides overall control and database management of the SHM system. Figure 3.6 shows the control cabinet in the communications hut underneath the bridge where all of the fibers terminate, the interrogators are located, as well as the control computers. The communications structure has internet capabilities allowing the data acquisition system to be remotely accessed using a secure internet connection. Using this internet connection, the data can be downloaded and accessed at any time by researchers at the Center for Innovative Bridge Engineering at University of Delaware.

The data is recorded according to two different protocols; the low and high frequency protocol. In the low frequency protocol, one data point is being saved every 10 minutes from each sensor, making a frequency of 1/600 Hz. The goal behind the saved low frequency data is to study the long term load effects on the bridge. However, the high frequency protocol is intended to capture loads affect the bridge in a shorter period of time, such as live loads, in which the frequency is set to 25 Hz. The high frequency data is being recorded from all strain sensors in the edge girders (44 locations). More details about the data collection protocols and samples of the collected data are presented in Chapter 8 in this report.

Figure 3.6. Photograph Showing Control Cabinet

Chapter 4

ANALYTICAL MODEL

In the last several decades cable-stayed bridges have become very popular due to their special features. Most of that popularity is attributed to their appealing aesthetics, structural efficiency, ease of construction, and the economic efficiency of cable-stayed bridges over other types of bridges. Those aforementioned advantages have made the number of cable-stayed bridges worldwide increase.

A cable-stayed bridge has a more complicated behavior than other conventional types of bridges. The combination of axial forces and moments make the structural analysis of this type of bridge not an easy task. Elastic theory and deflection theory were the most commonly used theories for static analysis of cable-stayed bridges (Hu et al. 2006).

After the invention of the Finite Element (FE) method and the evolution of computer technology, analysis of cable-stayed bridges has become more accurate. The FE method can be used to analyze the static and the dynamic behavior of cable-stayed bridges.

For the purposes of this research, three live load FE analytical models were created for the IRIB, a two dimensional (2-D) SAP2000 model, a three dimensional (3-D) CSiBridge model with shell elements, and a 3-D CSiBridge beam element model. These models will be discussed and described in this chapter.

4.1 2-D SAP2000 Model

The need for a FE model came across after the goal of developing a baseline for the IRIB behavior. The designer company has refused to give the models used for designing the IRIB. The researchers at the CIBrE at University of Delaware decided to start with 2-D live load FE model.

Marquez (2013) created the first 2-D model of the IRIB using STAAD Pro, while a graduate student in the department of civil and environmental engineering at University of Delaware. The west side of the bridge carries slightly more load than the east side due to the presence of the pedestrian walkway on the east side, therefore, the west side was modeled in the 2-D model.

Using the same assumptions that Marquez (2013) used to develop the 2-D STAAD model, a 2-D SAP2000 beam element model was first developed by the author, with the intention of expanding it in the future to a 3-D model. SAP2000 version 15.1.0 was used to develop the 2-D model. SAP2000 is an integrated commercial FE software package developed and maintained by Computers & Structures Inc., (CSI). SAP2000 is a general purpose FE program for structural analysis and design which has strong capabilities for bridges. This is the reason SAP2000 was selected as the program of choice for this study.

Section properties, material types, geometry, and boundary conditions were obtained from the final as-built drawings submitted to DelDOT by the designer. The same element types used in the STAAD model were used in the SAP2000 model, with the exception of the element used to model the stays; SAP2000 has a cable element in its library that allows for modeling the stays more easily and more accurately.

The 2-D SAP2000 model has 154 frame elements, 301 nodes, and 76 cable elements. Nodes are created at certain locations to define the global geometry of the

west side of the bridge as reported in the as-built drawings. Nodes are created at the centroid of cross-sections and positioned at the intersections of elements and/or when there is a significant change in the section properties of the two connected elements. Cables span between the centroid of the edge girder cross-section and the centroid of the pylon cross-section. The origin of the model is located at the left (south) end of the bridge and level with the base of the pylons. The model was created in the X-Z plane at Y=0, the coordinates (X,Y,Z) of the first node at the left expansion joint are (0,0,35.27) ft. Figure 4.1 illustrates an overview of the 2-D SAP2000 beam element model and the positive coordinates directions from its origin.

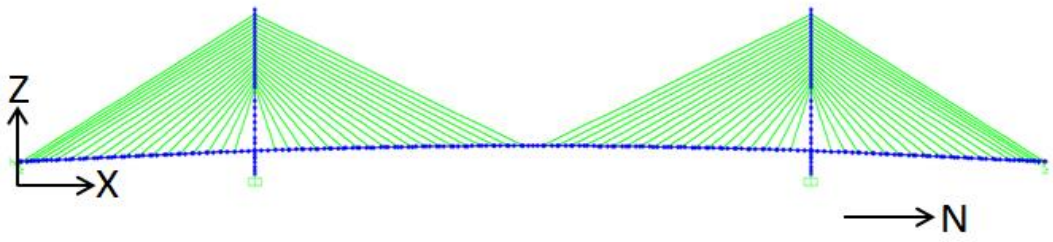

Figure 4.1. 2-D SAP2000 Model of the IRIB

The 2-D SAP2000 beam element model has three types of members: frame elements, cable elements and joint springs, which are used to represent the expansion bearings. The frame element has six degrees of freedom at each joint: translational displacements in X, Y, and Z directions and rotational displacements about the X, Y, and Z directions. All section properties for the edge girder and the pylon sections were calculated and verified through the section wizard in STAAD software and also

confirmed through hand calculation. For more details about the general 2-D modeling see Marquez (2013).

The 2-D SAP2000 and the 2-D STAAD models give results very close to each other, but overestimate the response of the bridge in general when compared to the measured data (this will be discussed in more detail in Chapter 5). Also, since the 2-D model has some limitations in modeling the actual structure (it cannot represent the moving trucks on the bridge in a real way), it was decided to take one further step and create a 3-D model to study the global behavior of the bridge, and to improve the results of the FE modeling.

Two 3-D CSiBridge models were developed for the IRIB, one using shell elements to represent the bridge deck, and another that uses beam elements to represent the composite effect of the deck and edge girder together. The two models will be described in the following sections.

4.2 Three-Dimensional CSiBridge Model with Shell Elements

A 3-D FE model was established by using the FE software CSiBridge version 15.1.0. CSiBridge is an integrated commercial FE software package developed and maintained by Computers & Structures Inc., (CSI). The CSiBridge software is a newer version of the SAP2000 software and was developed specifically for bridges. It offers several advantages over SAP2000, such as extracting moving load analysis results automatically and provides built-in cross-sections of AASHTO girders.

The global geometry of the bridge, section properties, and boundary conditions were once again obtained from the final as-built drawings submitted to DelDOT by the designer. In addition to the three types of members used in the 2-D SAP2000 model, shell elements were used to model the deck.

Due to the complexities and variations of cable stayed bridges in general, many assumptions were made for geometry, element types, materials, boundary conditions, and section properties in the process of developing the 3-D model for the IRIB. In addition to these assumptions used in the 2-D SAP2000 model, other new assumptions related to 3-D modelling are made. The following sections will discuss these assumptions and give more details about the bridge. Figure 4.2 shows an overview of the 3-D CSiBridge model.

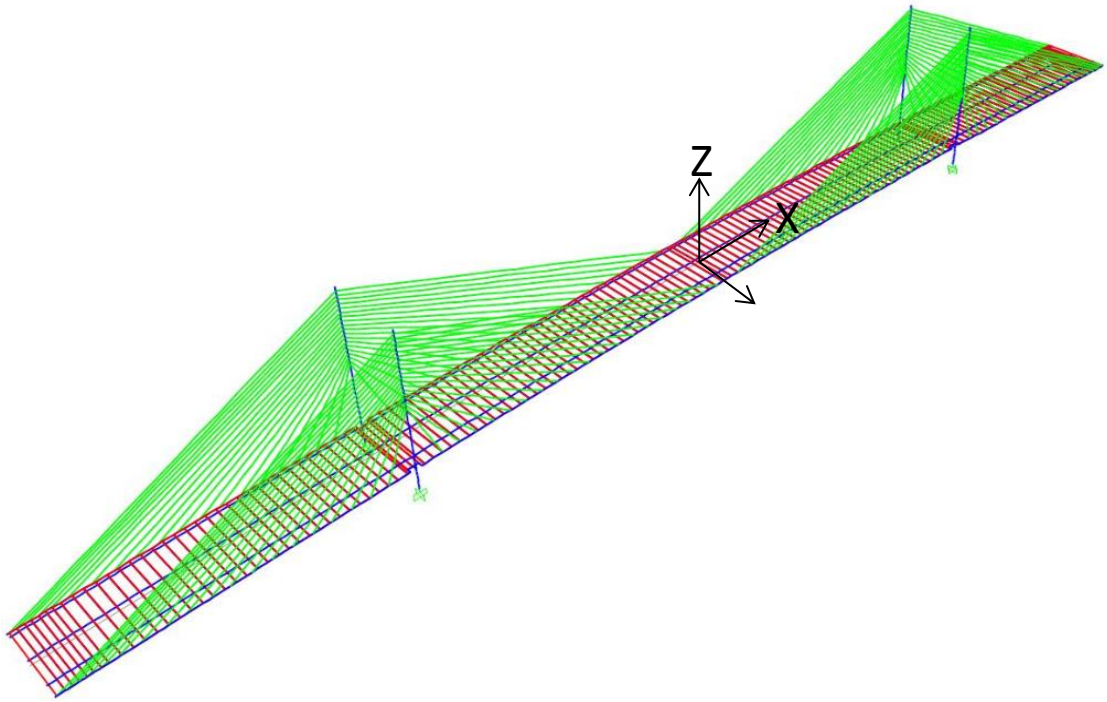

Figure 4.2. 3-D CSiBridge Model with Shell Elements for the IRIB

4.2.1 Geometry of the Bridge

In order to develop the global geometry of the bridge reported in the as-built drawings, the structural members are discretized into structural nodes. Nodes are

created at the centroid of cross-sections and positioned at the intersections of elements and/or when there is a significant change in the section properties of the two connected elements. Cables span between the centroid of the edge girder cross-section and the centroid of the pylon cross-section; the floor beams span between the east and the west edge girder cross-sections.

There are 622 nodes in the model. Each of these nodes is enabled in all six degrees-of-freedom. See Figure 4.3 for a representative layout of the nodes and the general positive global X-Y-Z coordinate system. In addition to the global coordinate system, each member in the model has its own local 1-2-3 coordinate system. The origin of this model is defined at the center of the middle span. Figure 4.3 shows the general layout of the nodes with its origin point and the positive coordinates directions.

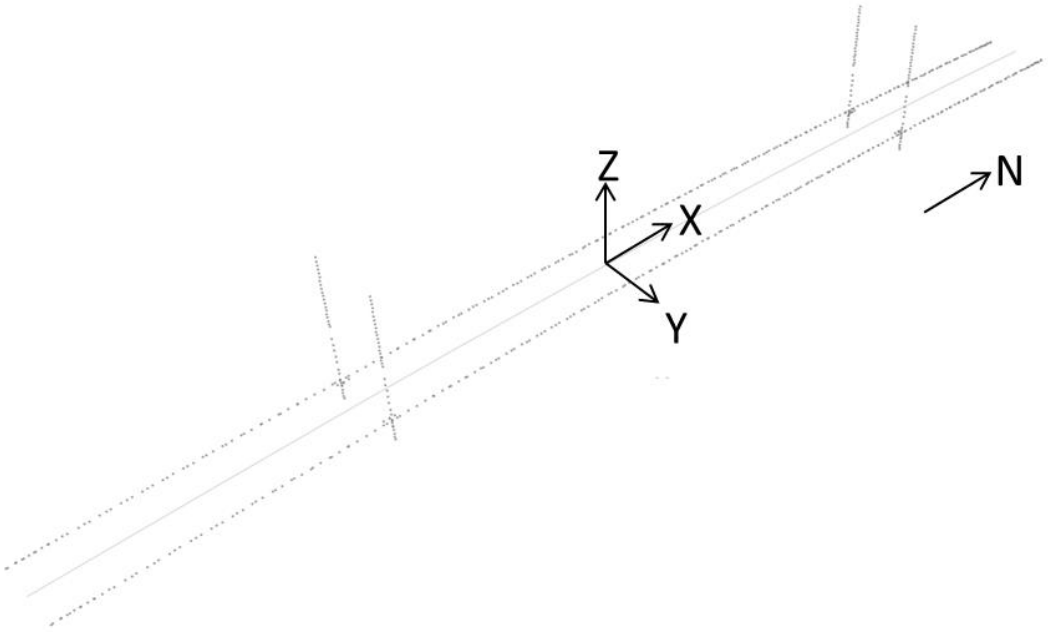

Figure 4.3. 3-D CSiBridge Actual Nodal locations

4.2.2 Element Types

There are four types of structural members used in the first 3-D CSiBridge model: beam elements, shell elements, cable elements, and joint springs which are used to represent the expansion bearings. The theoretical background of each of these structural members will be briefly described below.

4.2.2.1 Beam Elements

A beam element is usually defined as a straight frame element in the CSiBridge software. A straight frame is a uniaxial 3-D elastic element that carries tension, compression, torsion, and bending. It has six degrees of freedom at each joint: translational displacements in X, Y, and Z directions and rotations about the X, Y, and Z directions.

The frame element is modeled as a straight line between two joints. The geometry of the straight frame is defined by the coordinates of the two joints at the ends of each frame. Figure 4.4 illustrates the global (X-Y-Z) coordinate system, the local (1-2-3) coordinate system, geometry, and node locations for the frame element.

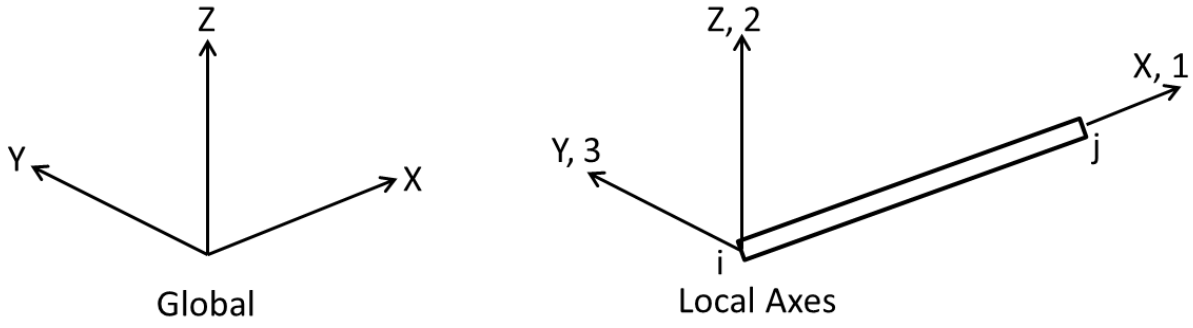

Figure 4.4. Global and Local Coordinate Systems for Frame Element

Each frame element can be assigned to a material property that can be predefined independently in the material section. In addition to the material properties, there are six cross-section properties that need to be defined for the frame element to generate the stiffness matrix of the element. These are: cross-sectional area, moment of inertia about the 3 axis (bending in 1-2 plane), moment of inertia about the 2 axis (bending in 1-3 plane), torsional constant, shear area in the 1-2 plane, and shear area 1-3 plane.

CSiBridge gives the user a wide range of shape types to choose from for the frame element. Selection of the shape type will determine if the six section properties are specified directly, computed from the user provided section dimensions, or read from a specified property database file. The frame elements in this model were selected as general shapes: section properties were calculated by section wizard in STAAD and confirmed with AUTOCAD, and then entered manually for each frame element.

The total number of frame elements in the model is 767. All of the edge girder members, pylons members, and floor beam members are modeled as straight frame elements. The two nodes assigned at the ends of the frame determine its length. More details about the section properties will be described and listed in the subsections below.

4.2.2.1.1 Edge girders

The edge girders have a uniform cross-section along the bridge. There are 476 frames named as edge girder in the model. These elements span between stay cable anchorages and they are discretized at the floor beams connections. The six section properties for the edge girder are as follows:

- Cross-sectional area , A= 30.25 ft^2
- Torsional constant, J=125 ft^4
- Moment of inertia about the 3 axis, I3-3 = 92.3 ft^4
- Moment of Inertia about the 2 axis, I2-2= 64.62 ft^4
- Shear area in 2 direction, AS-2= 25 ft^2
- Shear area in 3 direction, AS-3=24.5 ft^2

Figure 4.5 illustrates the modeled edge girder section and shows the local axes.

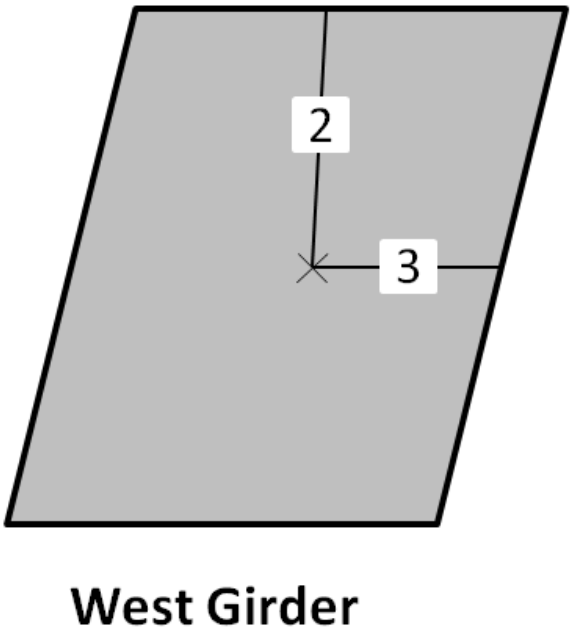

Figure 4.5. Modeled Edge Girder Section

4.2.2.1.2 Pylons

The four pylons are represented using a total of 140 frame elements. Each pylon consists of 35 members, which are categorized into fifteen different sections. The discretization process was done based on any major change in the pylon cross-section geometry and/or to create nodes at locations where the stays connect to the pylons. A general shape type was selected for all pylon sections; the six section properties for each section are displayed in Table 4.1 with the start and end elevation for each section. Figure 2.6 shows some of the modeled sections.

Table 4.1. Pylon Section Properties

Section	Elevation (ft)		Six Section Properties for Pylons					
	Start	End	A (ft^2)	J (ft^4)	I 3-3 (ft^4)	I 2-2 (ft^4)	AS-2 (ft^2)	AS-3 (ft^2)
Pylon 1	14	19	133.8	4630	3281	3218	61	31
Pylon 2	19	24	133.0	4565	3179	3201	31	60
Pylon 3	24	30	132.2	4500	3079	3185	59	31
Pylon 4	30	36	119.4	4000	2972	2727	0	0
Pylon 5	36	38	131.0	4401	2933	3159	32	58
Pylon 6	38	43	162.7	4982	2952	4106	73	76
Pylon 7	43	48	102.8	2813	2443	1266	48	53
Pylon 8	48	58	101.6	2725	2307	1242	47	53
Pylon 9	58	66	100.4	2637	2176	1218	46	54
Pylon 10	66	78	84.8	2366	1795	1120	43	37
Pylon 11	78	88	82.8	2229	1623	1081	41	38
Pylon 12	88	98	81.6	2147	1525	1057	40	38
Pylon 13	98	109	80.0	2038	1400	1026	39	38
Pylon 14	109	118	78.4	1930	1281	995	37	38
Pylon 15	118	248	77.6	1877	1224	979	36	39

4.2.2.1.3 Floor Beams

There are 151 floor beams in the IRIB; each was modeled using a single frame element that spans between the two edge girders. Some are pre-cast and the others are cast in place. They have different cross-sections and their depth varies in the

transverse direction to account for the cambering in the deck. There are three different named cross sections in the model, cast in place floor beams at the ballast area (FB-B-CIP), cast in place floor beams (FB-CIP), and precast floor beams (FB-PC). Table 4.2 shows the section properties for the modeled floor beams sections.

Table 4.2. Section Properties of Floor Beams

Section	Six Section Properties for Floor Beams					
	A (ft^2)	J (ft^4)	I 3-3 (ft^4)	I 2-2 (ft^4)	AS-2 (ft^2)	AS-3 (ft^2)
FB-B-CIP	7.3	1.0	38.7	7.7	2.7	5.1
FB-CIP	5.8	1.5	19.4	0.4	4.8	4.8
FB-PC	6.6	1.8	24.9	0.6	5.1	5.8

4.2.2.2 Shell Elements

Shell elements are three dimensional members. They are used to model three dimensional area objects in a plane. They are three or four node objects, and each shell element has its own local coordinate axes. The shell elements used in this model are quadrilateral shells and are defined by four nodes (j1, j2, j3, and j4). Each of these nodes is enabled in all six degrees-of-freedom. See Figure 4.6 for geometry and local axes direction.

CSiBridge allows the user to define area elements as membrane, plate, or shell elements. Based on the purpose of design you can define the area object as pure membrane, pure plate, or shell, which combines the membrane and the plate behavior. For a pure membrane behavior only the in-plane forces and the normal moment can be supported. For the pure plate behavior only the bending moments and the transverse shear force can be supported. The shell behavior combines the membrane and the plate behavior; all forces and moments can be supported. Also the software gives the option

to model the area objects as thick or thin formulations, that gives the designer the option to count for the transverse shear deformation or not, respectively.

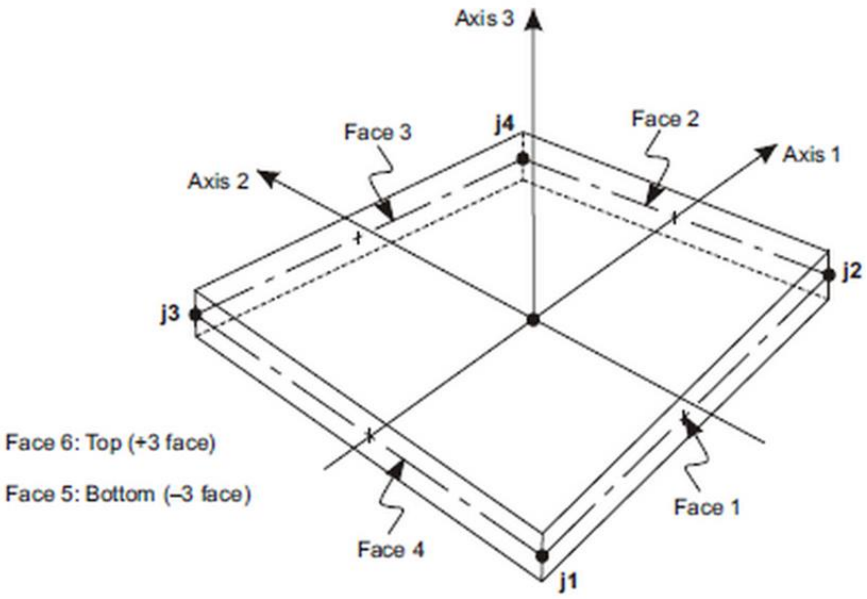

Figure 4.6. Shell Element Geometry and Node Locations (Abell 2012)

There are 156 shell elements used in this model, each shell element has four nodes; two of them are located on the west edge girder element and the other two nodes are located on the parallel east edge girder element, making the shell span in the transverse direction of the bridge. Each shell element is subdivided into 6 feet by 6 feet smaller shell elements during analysis. The deck has a uniform thickness of 8.5 inches along the bridge, except at the pylon locations, where the deck is 10.5 inches thick. Therefore, there are two deck sections in the model named as deck and deck-pylon section.

In order to determine whether shear deformation needs to be considered, a preliminary analysis was carried out by comparing the results of a moving load analysis with shear deformation included (thick element), to when it was not (thin element). The analysis showed that considering the shear deformation is significant, therefore thick shell elements were used in the model. After entering the thickness of the shell element, the section properties are calculated automatically by the software.

4.2.2.3 Cable Element

Stays are modeled as cable elements in this model. The geometry for a cable element is defined by two nodes connected by a curve. The cable element has three degrees of freedom at each node; translational in the X, Y, and Z directions. The rotations about the same axes are not supported at the nodes. Cable elements in general are tension only members, i.e., they do not carry any compression force.

Similar to other elements, each cable has a local coordinate system (1-2-3) that can be used to define loads acting on the element. Cable elements can be defined by cross sectional properties and material. The cable sections are always assumed to be circular and they can be specified by the cross sectional area or the diameter of the cable. Material can be defined independently and be assigned later to the cable element.

There are 152 cable elements in this model. Each of these cables is assigned to a different name and different cross sectional properties based on the as-built drawings. Also, each cable is assigned to the appropriate initial tension force reported in the as-built drawings. See Figure 2.7 for cable numbering.

The cross sectional area of each cable was calculated based on multiplying the number of strands in each stay by the average area per strand of 0.2325 in^2. Table 4.3 shows the section names and the associated areas used in the models.

Table 4.3. Cable Section Names and Cross Sectional Areas

Cable Section	Area (ft^2)	Cable Section	Area (ft^2)	Cable Section	Area (ft^2)	Cable Section	Area (ft^2)
101E	0.0307	201E	0.0307	301E	0.0307	401E	0.0307
101W	0.0307	201W	0.0307	301W	0.0307	401W	0.0307
102E	0.0371	202E	0.0355	302E	0.0339	402E	0.0339
102W	0.0371	202W	0.0355	302W	0.0339	402W	0.0339
103E	0.0371	203E	0.0355	303E	0.0355	403E	0.0355
103W	0.0371	203W	0.0355	303W	0.0355	403W	0.0355
104E	0.0388	204E	0.0388	304E	0.0371	404E	0.0388
104W	0.0388	204W	0.0388	304W	0.0371	404W	0.0388
105E	0.0452	205E	0.042	305E	0.0404	405E	0.0436
105W	0.0452	205W	0.042	305W	0.0404	405W	0.0436
106E	0.0484	206E	0.0452	306E	0.0436	406E	0.0468
106W	0.0484	206W	0.0452	306W	0.0436	406W	0.0468
107E	0.0517	207E	0.0468	307E	0.0452	407E	0.0517
107W	0.0517	207W	0.0468	307W	0.0452	407W	0.0517
108E	0.0549	208E	0.0501	308E	0.0484	408E	0.0533
108W	0.0549	208W	0.0501	308W	0.0484	408W	0.0533
109E	0.0581	209E	0.0565	309E	0.0533	409E	0.0565
109W	0.0581	209W	0.0565	309W	0.0533	409W	0.0565
110E	0.0597	210E	0.0597	310E	0.0565	410E	0.0581
110W	0.0597	210W	0.0597	310W	0.0565	410W	0.0581
111E	0.0581	211E	0.0614	311E	0.0614	411E	0.0581
111W	0.0581	211W	0.0614	311W	0.0614	411W	0.0581
112E	0.0597	212E	0.063	312E	0.063	412E	0.0597
112W	0.0597	212W	0.063	312W	0.063	412W	0.0597
113E	0.0662	213E	0.0662	313E	0.0662	413E	0.063
113W	0.0662	213W	0.0662	313W	0.0662	413W	0.063
114E	0.0694	214E	0.0678	314E	0.0662	414E	0.0614
114W	0.0694	214W	0.0678	314W	0.0662	414W	0.0614
115E	0.0727	215E	0.0678	315E	0.0678	415E	0.0678
115W	0.0727	215W	0.0678	315W	0.0678	415W	0.0678
116E	0.0775	216E	0.0694	316E	0.0694	416E	0.071
116W	0.0775	216W	0.0694	316W	0.0694	416W	0.071
117E	0.084	217E	0.071	317E	0.071	417E	0.0775
117W	0.084	217W	0.071	317W	0.071	417W	0.0775
118E	0.0872	218E	0.0727	318E	0.0727	418E	0.084
118W	0.0872	218W	0.0727	318W	0.0727	418W	0.084
119E	0.0888	219E	0.0759	319E	0.0743	419E	0.0856
119W	0.0888	219W	0.0759	319W	0.0743	419W	0.0856

4.2.3 Material Properties

The materials used in this model are concrete and high strength steel for the stays. Properties and design information will be briefly discussed below.

4.2.3.1 Concrete

The majority of the superstructure and the pylons of the IRIB were designed for a low permeability concrete with a 28-day minimum compressive strength of 6500 psi. Only the center section of the main span was designed for 7000 psi compressive strength. Cylinders were cast and tested throughout construction to determine the actual concrete strength. The results showed wide variability and an average concrete strength of 8200 psi.

Three different concrete materials were defined for the model, 6500 psi, 7000 psi, and 8200 psi, named as Concrete-6.5, Concrete-7.0, and Concrete-8.2, respectively. In addition to the compressive strength property, the modulus of elasticity is calculated based on equation 4.1 and entered in the material section property.

$$E = 57{,}000 * \sqrt{fc'} \quad Equation\ 4.1$$

Where,

- E = modulus of elasticity, psi
- fc' = compressive strength of concrete, psi

4.2.3.2 High Strength Steel Wire

The IRIB stays are seven wires, low relaxation strand, conforming to ASTM A416 grade 270 steel. All the cables are assigned to a material property of 270 ksi

strength wire strand with a modulus of elasticity of 29,000 ksi. The material is named "A416Gr270" in the model.

4.2.4 Boundary Condition and Bearing Stiffness

The IRIB is designed to expand and contract at both ends. Also, it is designed to have an expansion boundary condition at Pylon 5, and a fixed boundary condition at Pylon 6. Figure 4.7 illustrates these locations.

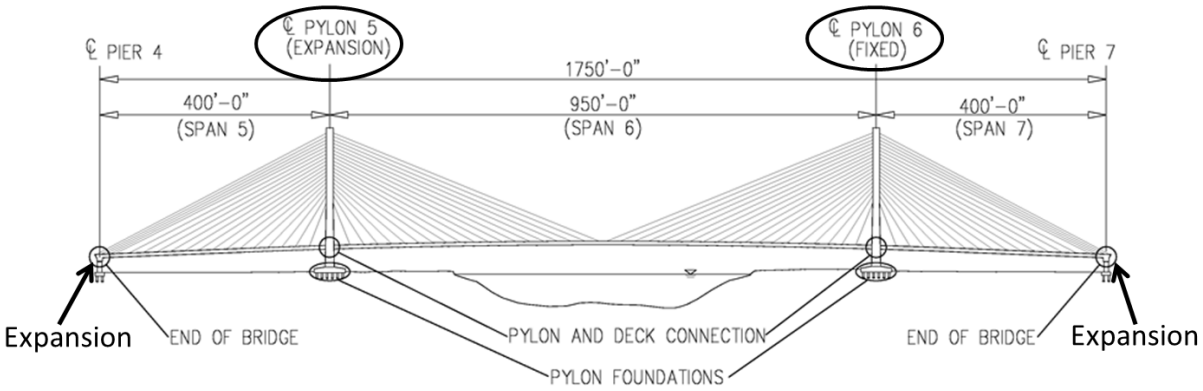

Figure 4.7. Boundary Conditions and Bearing Locations

There are different types of bearings used on the IRIB. The bearings at Pier 4 and Pier 7 are disc bearings with uplift restraint. The edge girders and the pylons are connected through bearings. Only vertical and transverse bearings are used at Pylon 5, while Pylon 6 has vertical, longitudinal, and transverse bearings. Table 4.4 summarizes all bearings with their direction of restraint.

Table 4.4. Bearing Types and Restraint Direction

Location	Name	Bearing Type	Restrained Direction
Ends of the Bridge	Vertical	Uni-Direction Disc Bearing with Uplift Restraint	Vertical, Transverse, and Transverse Rotational
Pylon 5	Vertical	Elastomeric Bearing with PTFE sliding plate	Vertical
	Transverse	Elastomeric Bearing	Transverse
Pylon 6	Longitudinal	Elastomeric Bearing with PTFE sliding plate	Longitudinaland Vertical
	Vertical	Elastomeric Bearing	Vertical, Transverse, Longitudinal, and Rotational
	Transverse	Elastomeric Bearing	Transverse

CSiBridge gives the user the ability to assign any node restraints in any or all displacement and rotational directions, and to model a support condition with a spring of specified stiffness. The foundation of the pylons are setting on deep piles, therefore the bottom of the pylons are modeled as fixed supports restrained in all translational and rotational directions. Joint springs are used to model the bearings at the ends of the bridge.

The connection between the edge girders and the pylons was a special challenge in developing the FE model. CSiBridge gives the user the ability to define such connections in link members. A link member can be defined as a fully rigid link that restrains all translational and rotational directions or as partially rigid link that requires the user to specify the required translational and rotational stiffness. Two partially rigid link members are used to model these connections. The connection between Pylon 5 and the edge girder is modeled with a vertical link member named "Pylon5-Plinth". It is defined to provide stiffness in the vertical, longitudinal, and transverse directions and release all rotational directions. The connection between Pylon 6 and the edge girder is modeled as a vertical link member named "Pylon6-Plinth", that provides stiffness in all rotational and displacement directions. Some of

the stiffness values were submitted by the design companies, and the others were calculated by the author and the previous master's degree student (Marquez 2013). Table 4 shows the named link members and the associated stiffness values.

Table 4.5. Modeled Bearing Stiffness

Location	Bearing Name	Stiffness					
		(kip/ft)			(kip.ft/degree)		
		U1 (X)	U2 (Y)	U3 (Z)	R1 (X)	R2 (Y)	R3 (Z)
End	Springs	48	89,724	71,832	96	268.74	96
Pylon 5	Pylon 5-plinth	48	48	46,833	released	released	released
Pylon 6	Pylon 6-Plinth	86,503	63,989	43,251	18,858	54	54

4.2.5 Analysis and Preliminary Results

In order to perform a moving load analysis on this model, the four traffic lanes were defined in the same locations indicated in the as-built drawings. Sensor locations and especially strain sensors in the edge girders are the locations of interest for this study. To obtain the results from this model at the sensors locations, section cuts have to be created at those locations.

A section cut is a quadrilateral three-dimensional plane, that is defined with four points in the three dimensional space, and a summation point about which all the structural member forces will be summed. The goal of using the section cut is to obtain the full composite behavior of all elements included in the section cut plane. Therefore, section cuts were created in the global YZ plane perpendicular to global X direction as shown in Figure 4.3 at all sensor locations for the east and the west edge girders. Each section cut included 25 ft effective width of the deck (Y direction) and the edge girder as used by the designer.

The process of creating the section cuts is time and effort consuming. In order to find the structural forces from a section cut, the coordinates of the centroids of each section cut must be calculated. For IRIB with its complicated geometry, this was time-consuming and required significant effort. Furthermore, to test the sensitivity of the results due to a change in the coordinates in the centroid points, a study was carried out that showed that any small changes in the calculated centroid could lead to a significant difference in the resulting structural forces. Therefore, considerable time and effort was needed to calculate the exact locations of the centroids.

In order to obtain accurate results from FE programs in general, meshing for big elements has to be performed during the analysis. A convergence study was done with different mesh sizes for a moving load to determine the required mesh size needed for the analysis. The best model was selected due to a convergence in the results and the lowest time needed for analysis. The best model was achieved by meshing the plate elements to 6 feet by 6 feet elements, the edge girders to 3 feet long elements, the floor beams to 6 feet long elements, and the pylons to 3 feet long elements. The computation time required for conducting a four truck live load analysis is about 80 hours, and the size of the result files are about 80 Gigabytes. A coarser meshing than the previous mentioned takes less analysis time, but it will not produce accurate results (less than 2% difference).

To date, the CIBrE at UD has conducted four load tests on the bridge; each load test has many static and dynamic passes. More details about the load tests and a comparison between the measured data and the FE models will be discussed in detail in Chapter 5. In order to establish a moving load analysis, CSiBridge creates influence lines at each node, after that it multiplies the loads from the trucks by the influence

lines to obtain the structural forces. Therefore, the live load analysis is very time and effort consuming. Also, this model gives results at the section cut locations only. The need for another FE model that requires less analysis time and less effort, and yields continuous results along the edge girders was obvious. A new three-dimensional model was developed with CSiBridge using the bridge wizard menu. This new model is described and discussed in the next section.

4.3 Three-Dimensional CSiBridge Beam Element Model

Most of the nodes in the 3-D shell model are in the shell elements; therefore, to reduce the computation time and the size of the output files, the shell elements have to be removed and replaced with other structural members. To this end, a new 3-D CSiBridge beam element model was developed in which the shell element and edge girder were removed and replaced with a single edge girder element that has the effect of a composite edge girder/deck member.

In order to determine the effective width (the tributary width of the deck that should be included when conducting the edge girder analysis) that yields the best results, a comparison study was done with different effective widths and the results compared to measured load test data. After comparing the computed results to the load test data, as explained in Chapter 5, the design effective width yielded the closest results to the measured data; therefore, the decision was made to use the same effective width as used in the design (see Figure 2.5 for more details about the design cross-section). The new model was created with the bridge wizard menu. It was defined as a conventional bridge cross-section, and then it was modified to match the IRIB cross-section. The bridge wizard menu allows the user to obtain the composite behavior forces and stresses along the superstructure, therefore, eliminating the need

for creating section cuts to perform the live load analysis and thereby reducing the computation time.

The same assumptions, geometry, materials, and boundary conditions that were used in the shell element model are also used in this beam element model. The new model has 453 nodes, 590 frame elements, and 152 cables. The main difference from the shell element model is the edge girder section; it includes section properties for the edge girder and a part of the deck. See Figure 4.8 for a full three-dimensional view with the lanes indicated.

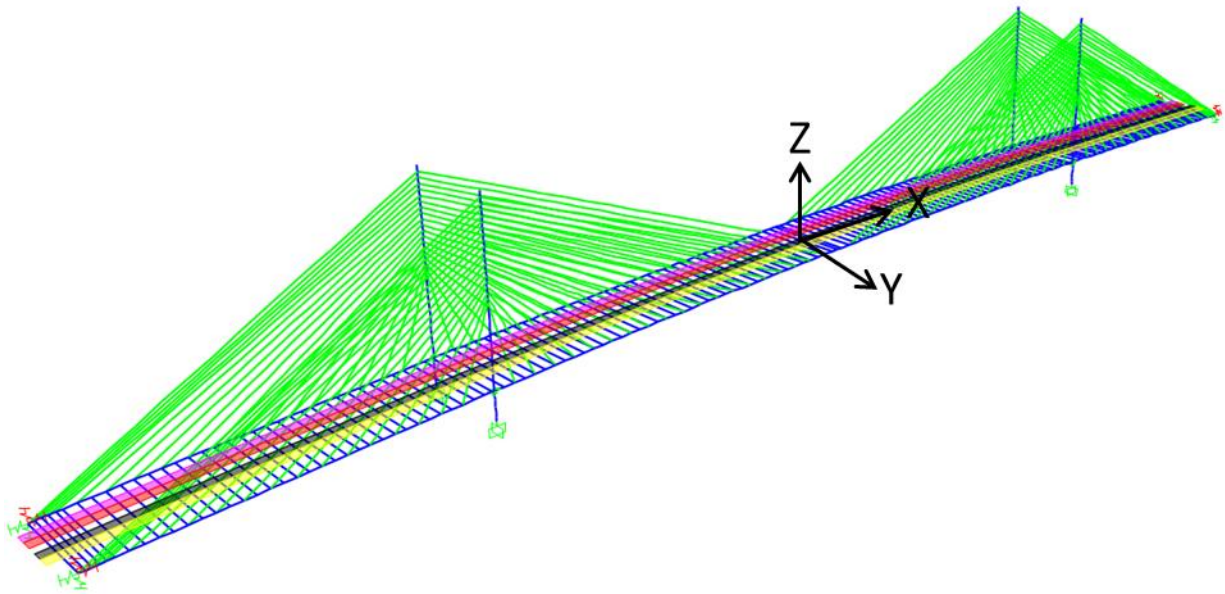

Figure 4.8. 3-D CSiBridge Beam Element Model for the IRIB

Live load analysis results can be obtained with this model in 10 to 12 minutes, and it provides continuous results along the edge girder. However, for other types of

analyses such as dynamic and wind load analyses, when the locations of the assembled joint masses have a great influence on the analysis results, the shell element model is more accurate to use since it has a larger number of nodes.

The new model has shown a very good comparison to the design model and also a good comparison to the measured data during the load tests. More details about these comparisons will be shown in the next chapter. Another comparison was done between the shell element model and the beam element model showing close results between the two models. The shell element model will be used for other research purposes in the future. The 3-D CSiBridge beam element model is adapted and will be used for the research purposes in this dissertation.

Chapter 5

MODEL VALIDATION WITH LOAD TESTS AND DESIGN MODEL

This chapter presents a short summary of the first four load tests conducted on the IRIB. It shows results for strain sensors in the west and east edge girder for the selected passes (four and six side-by-side trucks). The design dead and live loads were extracted from the load rating calculation manual that AECOM submitted to DelDOT. The adapted finite element (FE) model that was presented in Chapter 4 was compared to the extracted live loads. The FE model showed a good comparison to the AECOM model. Also, the FE model was compared to the measured data during the load tests; the model yielded good results using the values of the tested concrete compressive strength from the 56-day cylinder breaks.

5.1 Load Tests

The Center for Innovative for Bridge Engineering (CIBrE) at UD has conducted four live load tests on the IRIB on April 30, 2012, November 28, 2012, May 9, 2013, and May 7, 2014. The primary purpose of the load tests was to establish the baseline bridge performance for live loads. Also, to confirm that the Structural Health Monitoring (SHM) system installed on the IRIB was functioning properly.

Live load tests were performed by driving trucks with known axle spacing and weights across the bridge. During the load passes, data is collected from all sensors by the SHM system. All of the tests were performed at night time to minimize traffic

disruption and to minimize the effects of thermal variations and radiant heating due to the sunshine.

Multiple passes were performed as part of each load test. Passes varied by the number of trucks included in the pass and also by the travelling lanes that the truck(s) were positioned in. The number of trucks included in the pass and travel lanes used were selected based on the purpose of the pass. While the permanent SHM system collected data from all sensors during the passes, this research will focus only on the strain sensors in the west and east edge girders. For more information about the load tests and the data collected see Shenton et al., (2016).

5.1.1 Loading

Fully loaded 10 wheel dump trucks were used in all load tests. Six trucks side-by-side were used in the last three load tests to develop a maximum strain response, while only four trucks side-by side were used in the first load test. The truck axles were weighed offsite by DelDOT, and the weights were confirmed onsite with portable truck scales. Figure 5.1 shows a typical type of dump truck used in the load tests.

Figure 5.1. Conventional Ten Wheel Dump Truck

The average weight for each truck was about 64 kips. There were slight differences in the truck weights and axle spacing from test to test. Table 5.1 shows a comparison of the truck weights used in each load test.

Table 5.1. Truck Weights Used In Load Tests

Truck Weights (lbs.)							
Load Test	**Pass #**	**Lane 1**	**Lane 2**	**Lane 3**	**Lane 4**	**Total Weight**	**Average**
#1	11 (4a)	63150	63400	63650	63500	253700	63425
#2	21 (4a)	62350	62700	63150	61200	249400	62350
#3	13 or 14	59200	59250	60850	61050	240350	60088
#4	13 or 14	63950	62350	64000	63950	254250	63563

While the weights were close to each other, they will be normalized when comparing load tests results. Also, axles spacings were measured at the site prior to each load test. While all trucks had similar axle spacings, the variation will also be considered when comparing experimental results using FE model. A sample of truck axle spacings is presented in Figure 5.2.

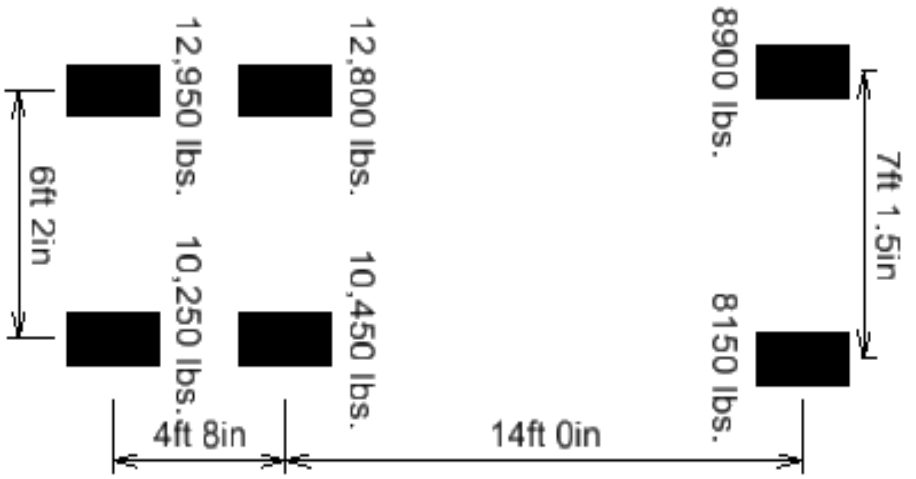

Figure 5.2. Sample of Dump Truck Axles Spacing

5.1.2 Passes

Several passes were conducted in each load test. Most of the passes were quasi-static, in which the trucks traveled across the bridge at roughly 5 to 10 mph to eliminate dynamic effects. A few passes were dynamic, in which the trucks passed at a high speed, such as 50 mph. Some of these passes were performed with single trucks while others utilized side-by-side trucks to achieve a maximum response. The single truck passes were used to establish the relationship between the east and the west girder sensors, and to study the experimental effective width. The side-by-side passes were performed with four and six trucks and were used to produce the maximum responses from the sensors. In the four trucks pass, trucks were placed in the four traffic lanes, while in the six truck pass the extra two trucks were placed in the east and west shoulders. Figure 5.3 illustrates the location of the four and six side-by-side truck passes.

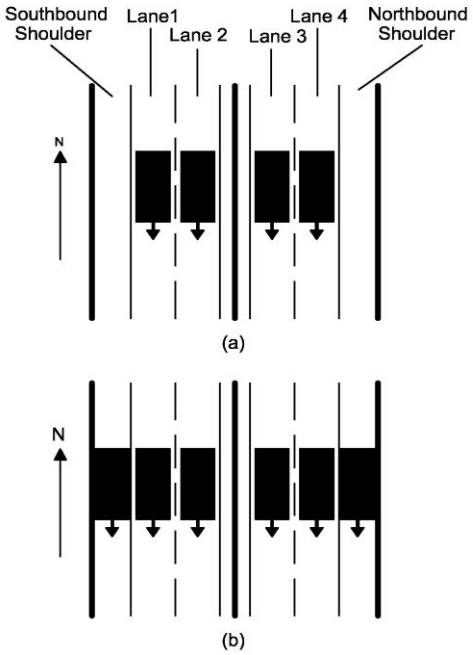

Figure 5.3. Truck Configuration for Side by Side Passes.

5.1.3 Results

This section presents the response recorded by strain gauges in the west and east edge girders due to four and six side-by-side truck passes and compares the results from the different load tests.

It should be noted that data collected from SHM system will have some noise related to the sensitivity of the sensors. In order to obtain the actual strain responses from the load test data, the signals must be processed to eliminate the noise, which in this case varies between +/- 3 microstrain for the strain gauges in the edge girders. The moving average method is used eliminate the noise from all the collected data during the load tests. Also, the initial strain reading for some of the load test data is not the same, therefore some of these signals are shifted up or down to make the initial points match.

The SHM system records strain time history signals for all strain sensors. Figures 5.4 and 5.5 illustrate samples of the strain signals for four truck passes in the four load tests before truck weights normalization. SW-8 is a strain gauge located at the bottom of the west edge girder at the main mid-span where thermal effects have their biggest influence as will be explained later in Chapter 8. SW-22 is a strain gauge located at the bottom of the west edge girder; this gauge is 5 feet away from the controlling rating location reported by AECOM.

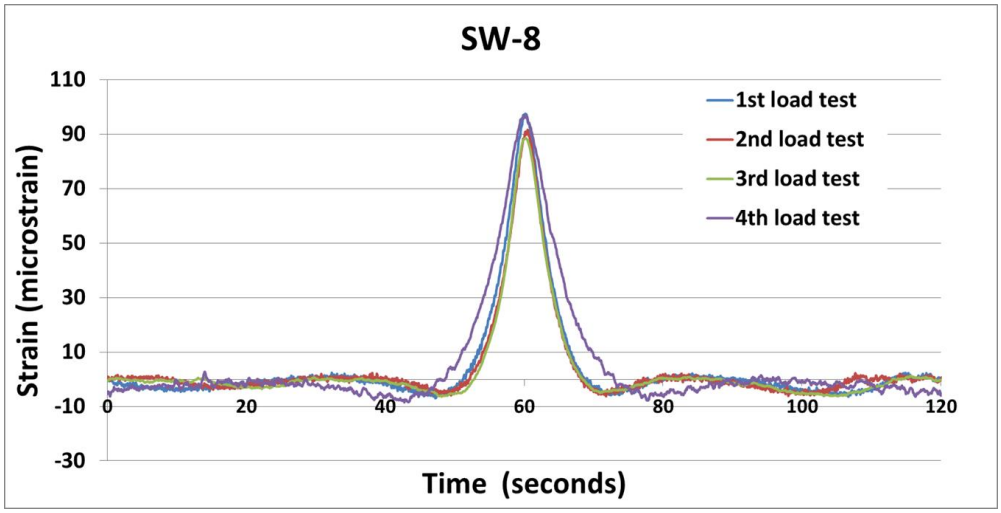

Figure 5.4. Four Truck Pass in All Load Tests @ SW-8

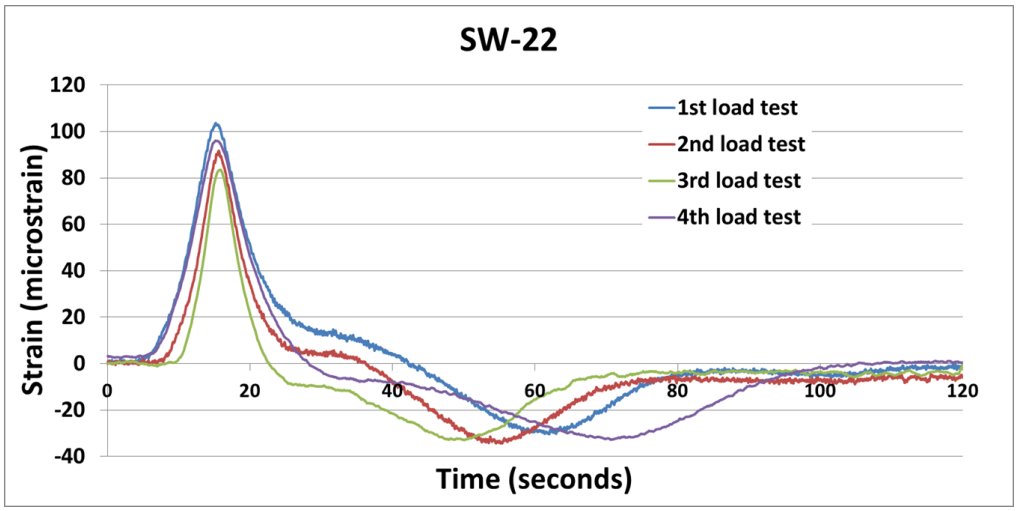

Figure 5.5. Four Trucks Pass in All Load Tests @ SW-22

It is clear from the figures that large positive peaks represent the time when the four trucks are above the strain gauge locations and thus create positive bending with tension in the bottom of the edge girder. Similarly when the trucks are away from the strain gauge location, measured strains are small. Also, negative bending at location SW-22 was developed when the trucks were on the main span. The high peaks in the previous figures represent the maximum response from the strain gauges during each pass. These peak values will be used when FE models of the bridge are evaluated and also when in-service live load response is analyzed. Also, the time history strain signal represents the influence lines for strain change at the sensor location. Tables 5.2 and 5.3 show the maximum responses recorded from four and six truck passes in all load tests from all strain gauges in the west and east edge girders. The west sensors are indicated with name SW (number), the S meaning strain, the W meaning west and the number indicates the location of the gauge on the edge girder. The number also indicates if the gauge is at the top or the bottom of the edge girder: odd numbers

indicating the gauge is at the top, and even numbers indicating that the gauge is at the bottom of the edge girder. The east sensors are indicated by SE (number) and they follow the same location and numbering convention as the west sensors.

Table 5.2. Maximum Responses from Four Truck Passes in all Load Tests

Sensor	Load Tests # 1	Load Tests # 2	Load Tests # 3	Load Tests # 4	Sensor	Load Tests # 1	Load Tests # 2	Load Tests # 3	Load Tests # 4
SW1	-20.3	-19.3	-15.9	-18	**SE1**	-13.2	-14.1	NaN	NaN
SW2	85.4	83.9	72.7	88.8	**SE2**	58.3	58.9	NaN	NaN
SW3	-17.7	-17.714	-16.2	-17	**SE3**	-0.9	-2.2	-14	-23
SW4	23.3	23.3	21	24	**SE4**	5.6	6.2	20.7	15
SW5	-23.5	-22.8	-16.7	-20	**SE5**	-16.6	-16.4	-11.8	-14
SW6	87.3	82.1	77.2	81.3	**SE6**	64.4	62.2	61.5	65
SW7	-26.9	-25.8	-22.9	-24	**SE7**	-21.9	-20.9	-18.3	-21
SW8	97.4	90.8	88.2	97.8	**SE8**	85.5	78.6	75.3	81.2
SW9	-24.9	-24.1	-20	-22	**SE9**	-20.1	-21	-14.8	-28
SW10	90.3	85.8	77.8	87	**SE10**	72.9	72.2	65.7	NaN
SW11	-23.1	-22.4	-18.6	-22.5	**SE11**	-16.1	-15.8	-14.8	-16
SW12	67.9	65.3	56.5	66	**SE12**	54	53.3	46	51.2
SW13	-27.4	-25.1	-21.1	-24.5	**SE13**	-20.1	-21.3	-18.3	-20.5
SW14	54.7	56	45.5	54	**SE14**	45.9	48.4	38.8	44.7
SW15	-20.5	-20.47	NaN	NaN	**SE15**	-15.7	-17	-14.6	-16
SW16	23.3	23.3	NaN	NaN	**SE16**	21	21.3	17.2	20
SW17	-17.6	-20.1	NaN	-20	**SE17**	-15.4	-15.1	NaN	-13
SW18	40.5	42.5	NaN	42	**SE18**	40.5	40.3	NaN	39.4
SW19	-19.3	-20	-17.3	NaN	**SE19**	-14.1	-14.6	-13.9	NaN
SW20	84.3	76.4	69.7	NaN	**SE20**	65.4	63.2	58.4	NaN
SW21	-44.6	-40.1	-37.2	-38.5	**SE21**	-33.3	-30.9	-28.8	-30
SW22	102.1	91.1	85.4	97	**SE22**	89.1	80.5	74.5	82.3

Positive sign strain indicates tension, while negative strain indicates compression.

Table 5.3. Maximum Responses from Six Truck Passes in all Load Tests

Sensor	Load Tests # 2	Load Tests # 3	Load Tests # 4	Sensor	Load Tests # 2	Load Tests # 3	Load Tests # 4
SW1	-30.8	-25.5	-28	**SE1**	-21.9	NaN	NaN
SW2	128.8	117.6	133.3	**SE2**	85.7	NaN	NaN
SW3	-26	-24.9	-27	**SE3**	-2	-29.4	-29
SW4	38.4	34.6	35	**SE4**	7.9	20.8	22
SW5	-34.1	-29.2	-32	**SE5**	-22.5	-18.4	-20.5
SW6	126.7	112.7	124	**SE6**	92.6	89	94.5
SW7	-41.1	-35.6	-39	**SE7**	-29.8	-25.8	-29
SW8	138.1	137.7	153	**SE8**	115.3	111.9	120
SW9	-35.4	-30.8	-35	**SE9**	-28.6	-22.5	-23
SW10	132.2	124.7	135	**SE10**	107.8	97.9	NaN
SW11	-34.9	-30.6	-33.5	**SE11**	-22.9	-19.3	-22.5
SW12	97.8	91.3	100	**SE12**	80.1	68.7	76
SW13	-39.9	-33.9	-34	**SE13**	-32	-25.7	-29.5
SW14	82.5	71.9	81.5	**SE14**	71.4	56.3	65.3
SW15	-30.1	NaN	-30	**SE15**	-23	-21.7	-23
SW16	38.4	34.6	35	**SE16**	29	26	30
SW17	-28.8	NaN	-32	**SE17**	-21.9	NaN	-18
SW18	65.2	NaN	64.5	**SE18**	57.7	NaN	57
SW19	-26.8	-25.5	NaN	**SE19**	-21.1	-18.5	NaN
SW20	116.4	108.5	NaN	**SE20**	95.1	84.1	NaN
SW21	-59.2	-55.1	-59	**SE21**	-47.2	-39.7	-44.5
SW22	149	141.6	155.2	**SE22**	128.8	116.1	126.5

Note that from the previous tables that the west edge girder sensors are measuring larger strain readings when compared to the east girder readings, and that is due to the existence of the pedestrian walk way on the east side of the bridge as mentioned in previous chapters. Also, note that no six side-by-side trucks were used for load test one. The “NaN” readings indicate that the sensor/s was out of service during that specific load test.

Before comparing the developed FE model to the measured responses from load tests, the author wanted to ensure the accuracy of the developed FE model by comparing it

to the designer's (AECOM) model. However, AECOM did not provide DelDOT with their design models, but the author was able to extract the design loads from the design information and use them to conduct the comparison between the developed FE model and the extracted design values.

5.2 Extracted Design Loads

The design firm, AECOM, submitted comprehensive design information to DelDOT during and after the construction of the IRIB. AECOM also submitted a load rating manual (AECOM 2012), which included rating procedures and rating factors for different components of the bridge. In addition to the rating manual, AECOM provided DelDOT with load rating calculations specifically for the edge girder. In the load rating calculations, AECOM rated the edge girder using four limit states: Service I, Service III, Strength I, and Service III Principal Tension Stress (AECOM 2012a).

Different loads were used to rate the edge girder: design loads, legal loads, and permit loads. Appendix A.1 illustrates the various axle configurations and loads. In the load rating calculation file, AECOM submitted tables that included the stresses for Service I and Service III limit states for the different kinds of loads along the west edge girder. Figure 5.6 shows a sample table for the design HL-93 design load.

Member Number	Y-Coordinate (feet)	Station along P.G.L. (feet)	HL-93 Live Load — HL-93 - 4 Lanes SERVICE III Combination (*with* DL Day 10,000) — *Maximum* Force Envelope			*Minimum* Force Envelope		
			Top (ksf)	Bottom (ksf)	Rating Factor	Top (ksf)	Bottom (ksf)	Rating Factor
WG270	714.00	1307+14.00	-277.9	-80.9	1.76	-148.4	-326.3	5.54
WG271	714.00	1307+14.00	-265.7	-106.7	1.95	-137.7	-349.5	5.32
WG272	726.00	1307+26.00	-294.1	-60.1	1.61	-156.2	-319.3	5.15
WG273	726.00	1307+26.00	-330.1	-40.5	1.47	-189.9	-304.2	5.93
WG274	738.00	1307+38.00	-335.3	-31.9	1.39	-183.8	-314.3	5.28
WG275	738.00	1307+38.00	-324.4	-54.7	1.53	-174.5	-334.4	5.14
WG276	750.00	1307+50.00	-346.4	-18.8	1.31	-190.0	-309.1	5.06
WG277	750.00	1307+50.00	-366.9	-7.6	1.24	-209.6	-300.2	5.50
WG278	762.00	1307+62.00	-365.3	-10.2	1.25	-202.7	-311.5	5.12
WG279	762.00	1307+62.00	-341.1	-20.2	1.31	-180.0	-318.7	4.76
WG280	774.00	1307+74.00	-354.6	2.0	1.19	-193.6	-296.5	4.84
WG281	774.00	1307+74.00	-355.7	4.5	1.17	-195.2	-293.2	4.98
WG282	786.00	1307+86.00	-345.6	-12.0	1.27	-188.5	-304.1	4.87
WG283	786.00	1307+86.00	-321.7	-21.1	1.33	-166.1	-310.6	4.50
WG284	798.00	1307+98.00	-326.0	-14.0	1.31	-179.3	-288.9	4.79
WG285	798.00	1307+98.00	-326.2	-13.7	1.31	-181.7	-283.7	5.02

Figure 5.6. Sample of Designer Rating Factors Tables Submitted to DelDOT (AECOM 2012a)

Service I and Service III are defined in the AASHTO specifications by the following two equations.

$$Service\ I = 1.0\ (DL + DW) + 1.0(LL + IM) \quad Equation\ 5.1$$

$$Service\ III = 1.0\ (DL + DW) + 0.8(LL + IM) \quad Equation\ 5.2$$

Where,

- DL : Dead load stresses
- DW : Wearing surface stresses
- LL : Live load stresses
- IM : Dynamic impact factor
- Service I : Stress limit state equation based on a limiting value of 60 percent of the concrete compressive strength (f'c)

- Service III : Stress limit state equation based on a limiting value of $3\sqrt{f'c}$ psi

Using the load rating calculation file submitted to DelDOT (which was in a pdf format), the values were exported into an excel file. The total stresses from Service I and Service III were reported in the submitted calculation file. By subtracting the two equations and solving for the unknown loads, the design live and dead loads used in the design and the rating of the IRIB were extracted. The extracted design loads were used later on as a comparison to the developed FE model and needed to rerate the edge girder of the bridge and for the reliability analysis as explained in the following chapters. Appendix A.2 presents the extracted design dead and live loads.

5.2.1 Design Model versus UD Model

The FE model presented in Chapter 4 was first compared to the results from the AECOM model. The stresses and forces that AECOM used in the design were obtained by the method described in the previous section. The design model was built according to the as-built drawings, and using the section and material properties used in the design. The extracted design stresses included stresses from the HL-93 design live load, legal loads, and permit loads. Moving load analysis was conducted by simulating the previous cases in the FE model. The maximum envelops for axial forces and moments were obtained from the moving load analysis. Utilizing the section properties for the design effective width, and the design material, the model forces were used to calculate the stresses at the top and bottom of the west edge girder for different live load cases. Equation 5.3 was used to calculate the stresses utilizing the obtained axial forces and moments applied on the design section.

$$\sigma = \frac{M * C}{I} + \frac{P}{A} \quad Equation\ 5.3$$

Where,

- σ= Calculated stress
- M= Maximum envelop moment from the FE model
- C= Distance from top surface to neutral axis when calculating top surface stresses, or distance from bottom surface to neutral axis when calculating bottom surface stresses
- I= Moment of inertia for the design section
- P= Maximum envelop axial force from the FE model
- A= Area for the design section

Using equation 5.3 and the structural forces obtained from the FE model, stresses were computed and compared to the extracted design stresses for different live load cases. Figure 5.7 shows a comparison between the developed FE model and AECOM model for a S-335 legal load truck described in Appendix A.1.

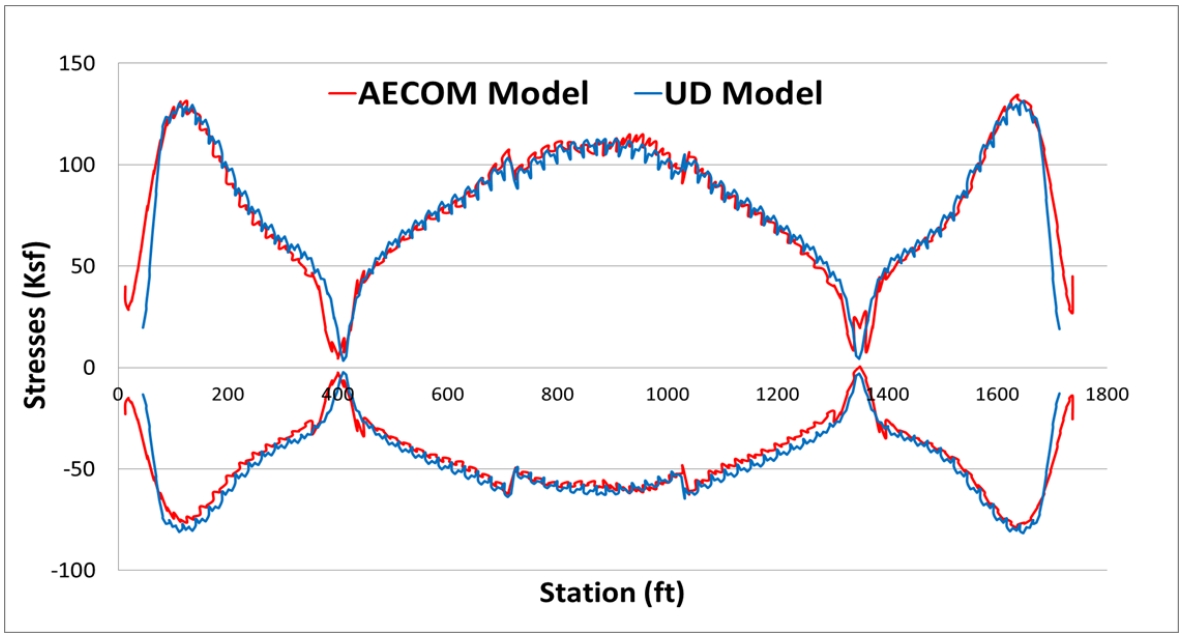

Figure 5.7. Maximum Envelops Stresses of UD Model Vs. Designer Model.

The lines in the positive portion of figure 5.7 represent the maximum positive tensile envelop stress in the bottom of the west edge girder, while the negative portion represent the maximum negative compressive envelop stress in the top of the west edge girder. The FE model yields very similar results to AECOM model. These results suggest that the developed FE model is valid. Finally, the extracted design loads will be used later in rating the edge girder and for reliability analysis purposes. The developed FE model will be given to DelDOT to be used for further aspects such as computation of rating factors for permit vehicles.

5.3 Load Tests Results vs. Model

Ten wheel dump trucks were used in all load tests. Even though the trucks were similar, as mentioned earlier there were some differences in axle spacing and

axle loads. These differences were considered when simulating the trucks in the model. All load trucks used in the load tests are simulated in CSiBridge with the exact axles spacing and axle's weights as reported for the test.

A moving load analysis was performed for several passes in each load test. Moving load analyses create influence lines at each node of the refined mesh during the analysis. Structural forces (e.g. moments, axial forces, shear, and torsion etc.) are reported at each node. The maximum envelop forces and stresses can be obtained from the CSiBridge software by selecting the "Show Bridge Superstructure Forces/Stresses" icon on the display menu.

In this analysis, only moments and axial forces are obtained from the FE model, and then stresses at the top and bottom of the edge girder are calculated using the design section properties and using equation 5.3. In order to be able to compare the results to the measured data, equation 4.1 is used to convert the stresses into strains.

5.3.1 Adjustments to FE Design Model

Some properties of the as built bridge vary from the design. Most significantly is the in place concrete strength. Since the FE model should represent the as-built bridge, parametric studies were conducted to achieve the "best" model. The parameter found to have the most significant effect on the computed results was concrete strength, which also has an indirect effect on the stiffness.

The majority of the superstructure was designed using a low permeability concrete with a 28-days compressive strength of 6500 psi. Only the center part of the main span was designed with a 7000 psi compressive strength. The 56-day cylinder break data collected during the construction of the bridge have shown a wide variability in concrete strength. The average compressive strength for the cylinders

was 8400 psi, with a maximum and minimum concrete compressive strength of 14,200 psi and 5,500 psi respectively. Figure 5.8 shows a histogram of the concrete compressive strength from the 56-day cylinder tests.

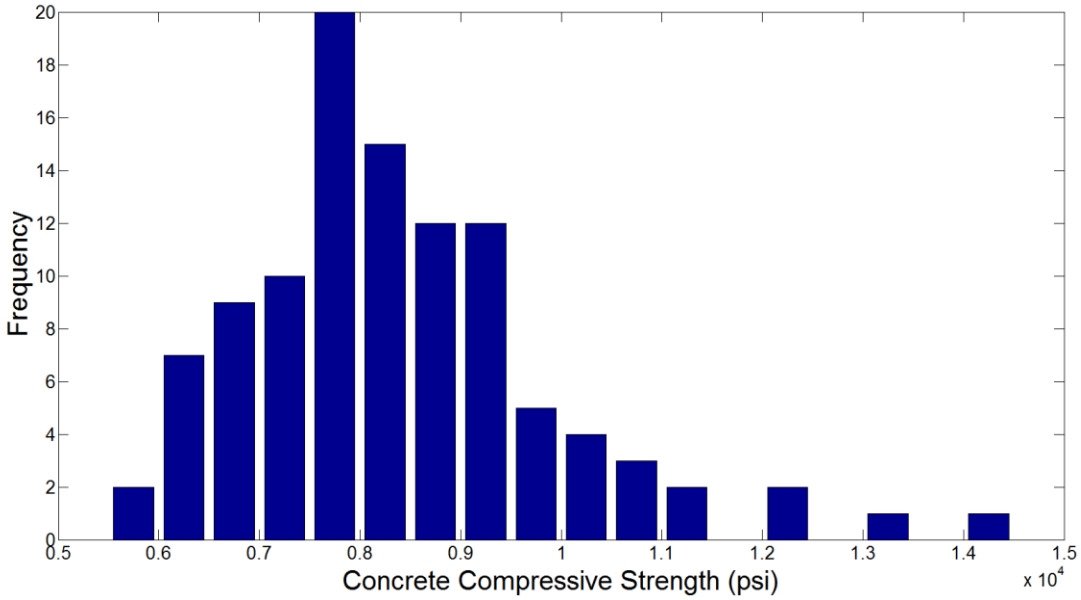

Figure 5.8. Concrete Compressive Strength from 56-day Cylinders

In order to investigate the effect of concrete strength on the model, the bridge was modeled with concrete having the minimum (5,500 psi), average (8,400 psi), and maximum (14,200 psi) strengths as found from the 56-day cylinder tests. The most useful passes to investigate are those that create the maximum live load response on the bridge (i.e. the four and six truck side-by-side passes).

The following figures (5.9 through 5.22) show a comparison of the measured data from the strain sensors in the west and the east edge girders collected from the

four and the six truck side-by-side passes with the FE model. Analyses were performed for each pass using the three different concrete strengths.

The three lines (red, orange, and green) located in the positive portion in each figure represent the maximum positive tensile envelope strain in the bottom of the edge girder using the minimum, the average, and the maximum concrete compressive strength during the associated pass from the model. The three lines (red, orange, and green) located in the negative portion in each figure represent the minimum negative compressive envelope strain in the top of the edge girder using the minimum, the average, and the maximum concrete compressive strength during the associated pass from the model.

The measured data is represented by the blue circles. The circles in the positive portion of each figure represent the maximum measured strain from the bottom sensors during the associated pass. The circles in the negative portion of each figure represent the synchronized measured strain from the top sensors during the associated pass.

The circles are arranged from the left to right to match the numbering of sensors on the bridge from south to north. For example in figure 5.9 the top circle on the left represents sensor SW-2, followed by SW-4, then SW-6, and until the last senor SW-22. The bottom circles represent the measured data in the top sensors, starting from SW-1 and going through SW-21. If the circle lies on the zero axis, that means the sensor data was lost during that load test or the sensor was out of service at that time.

The FE model using the average concrete compressive strength yielded good results for the actual bridge behavior along the west edge girder in most of the load

tests. Due to the complicated geometry at the pylon location areas and the complication in modelling the connection between the pylons and edge girders as explained in Chapter 4, the model does not show good results there; however the overall behavior is reasonable and acceptable.

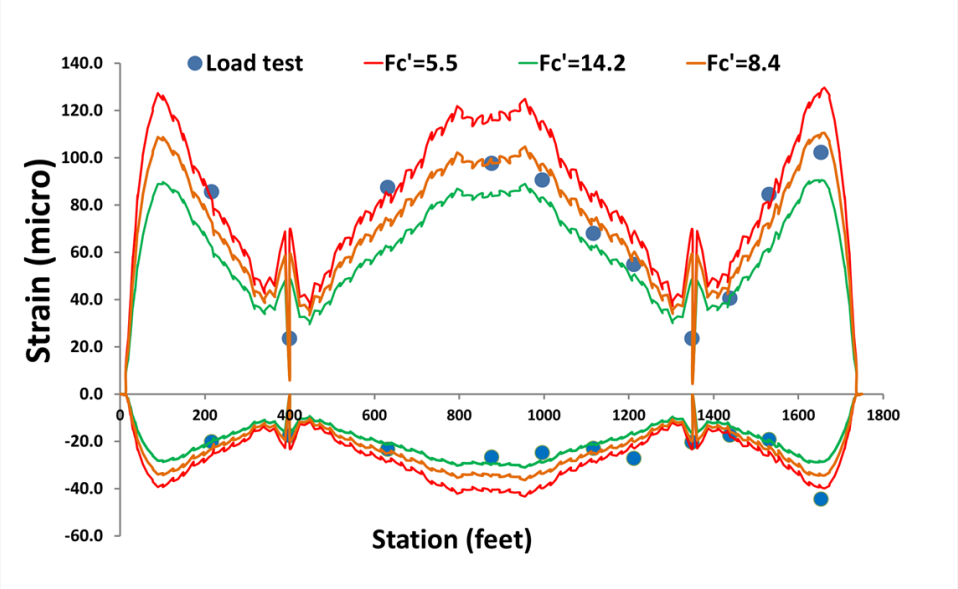

Figure 5.9. First Load Test, Four Trucks, West Girder

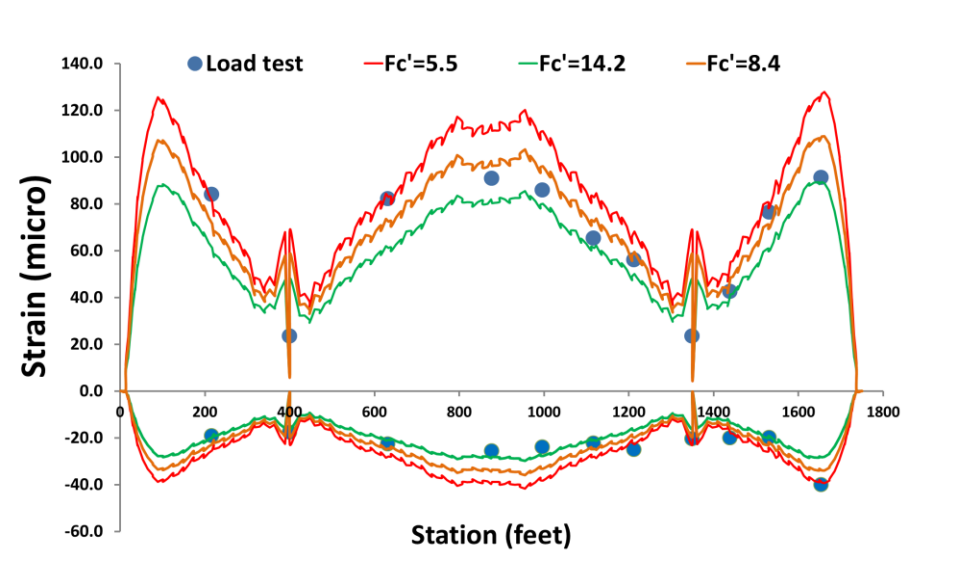

Figure 5.10. Second Load Test, Four Trucks, West Girder

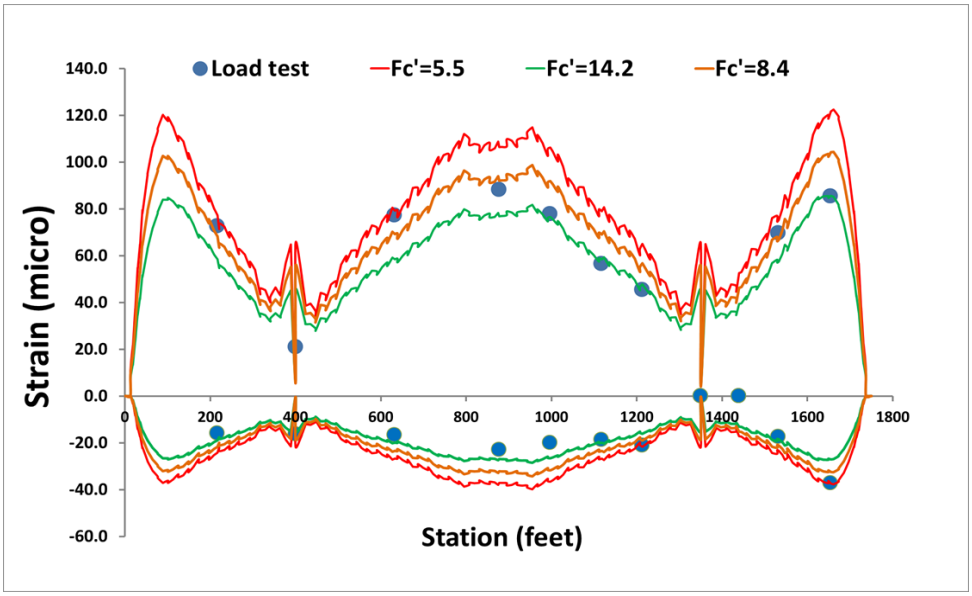

Figure 5.11. Third Load Test, Four Trucks, West Girder

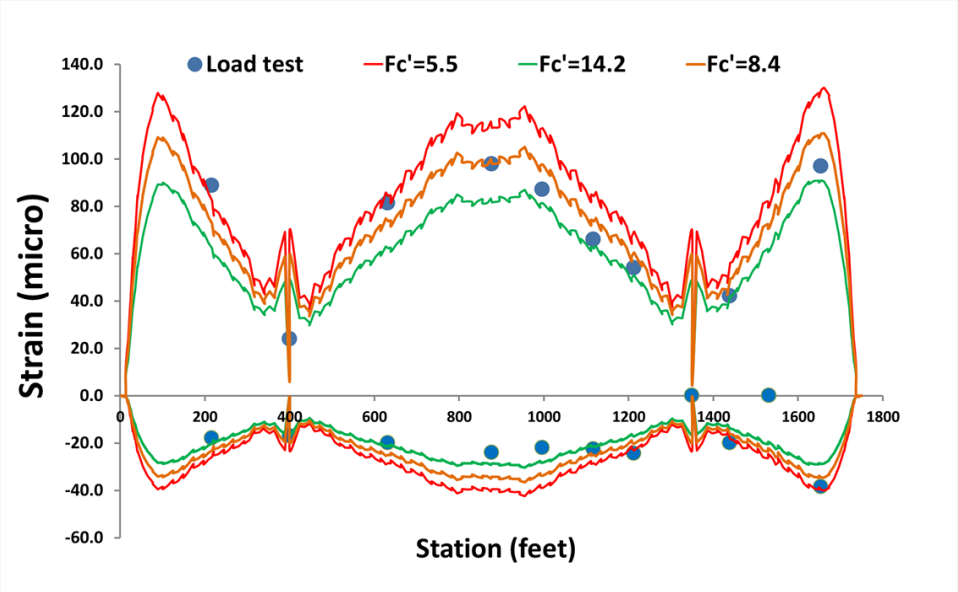

Figure 5.12. Fourth Load Test, Four Trucks, West Girder

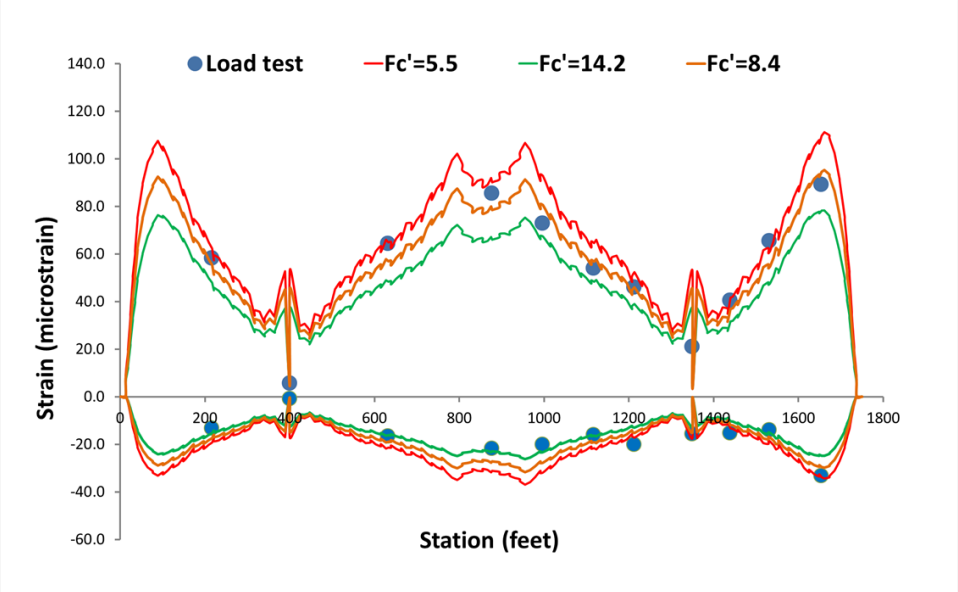

Figure 5.13. First Load Test, Four Trucks, East Girder

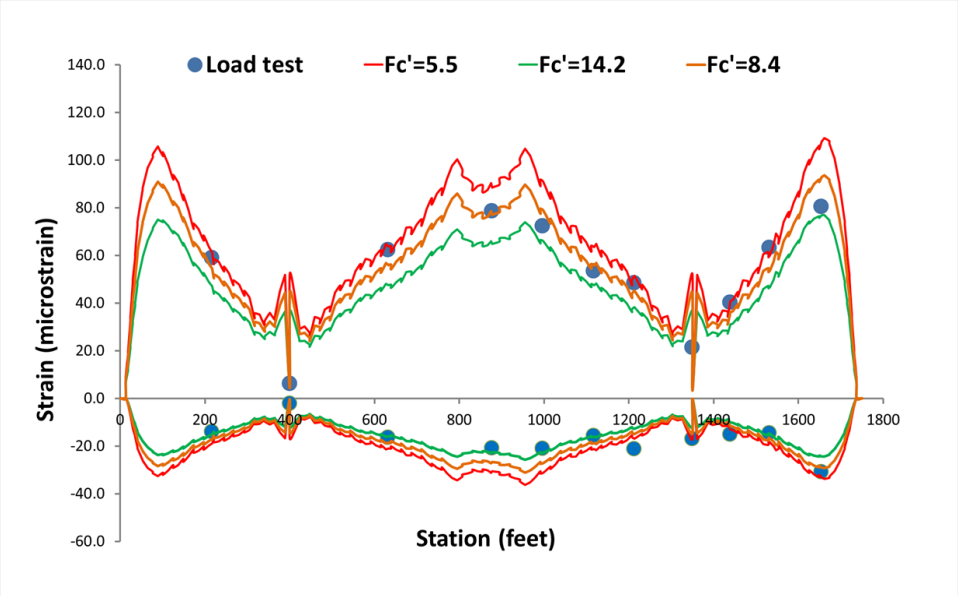

Figure 5.14. Second Load Test, Four Trucks, East Girder

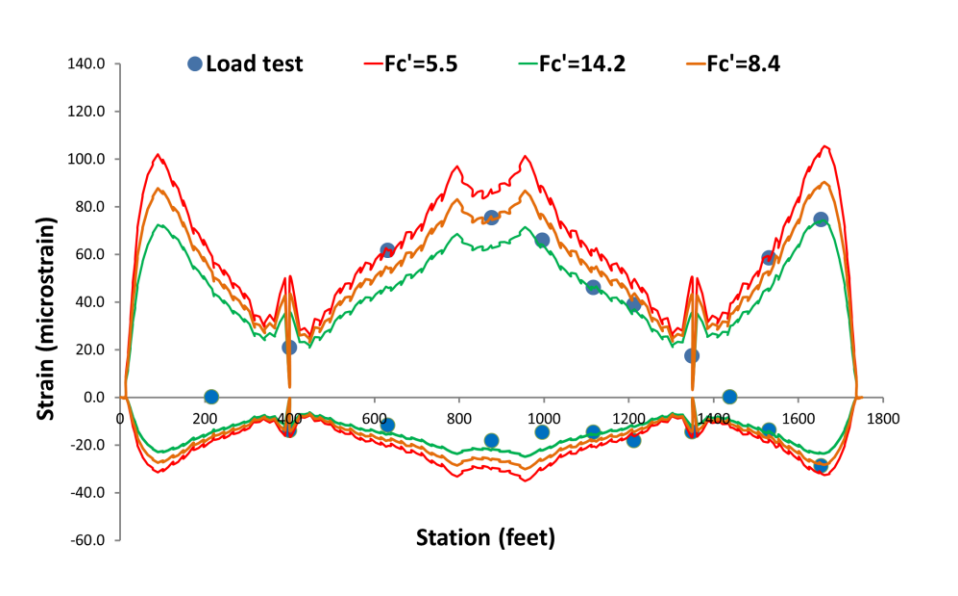

Figure 5.15. Third Load Test, Four Trucks, East Girder

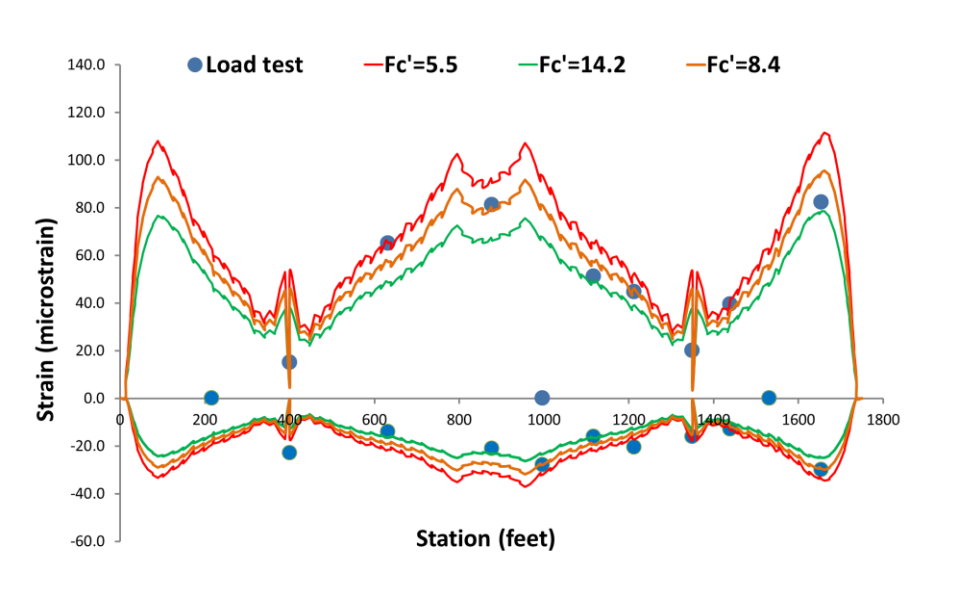

Figure 5.16. Fourth Load Test, Four Trucks, East Girder

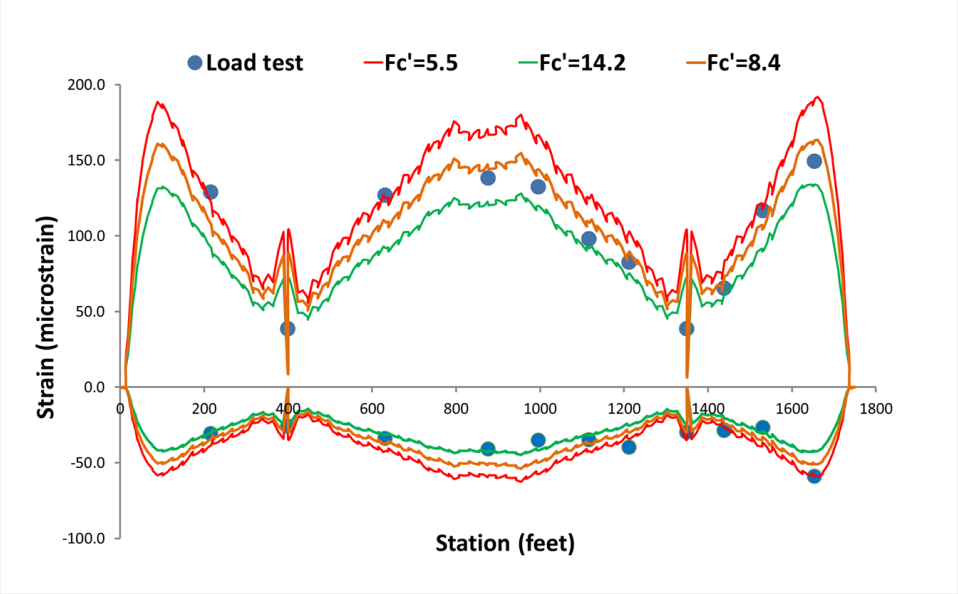

Figure 5.17. Second Load Test, Six Trucks, West Girder

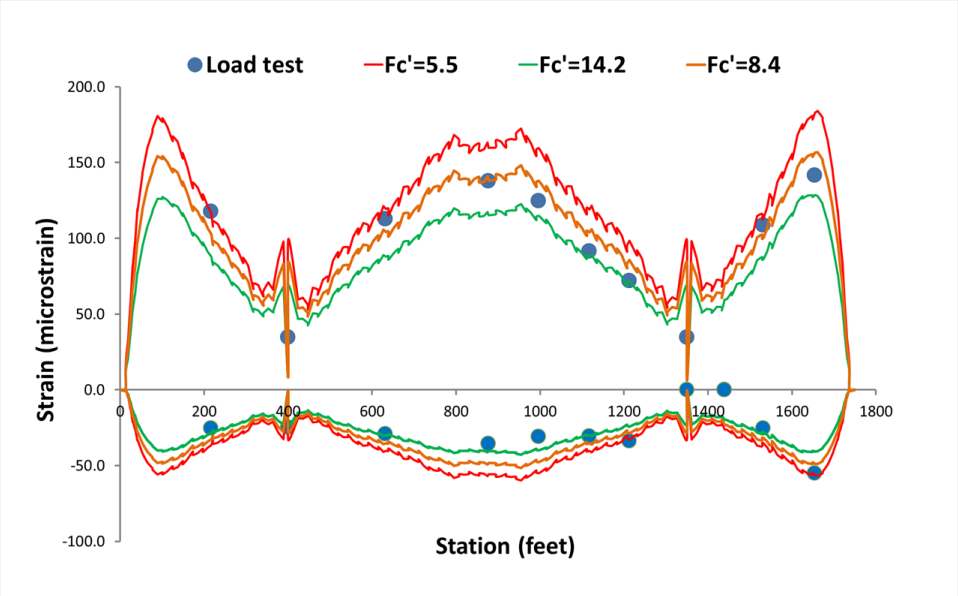

Figure 5.18. Third Load Test, Six Trucks, West Girder

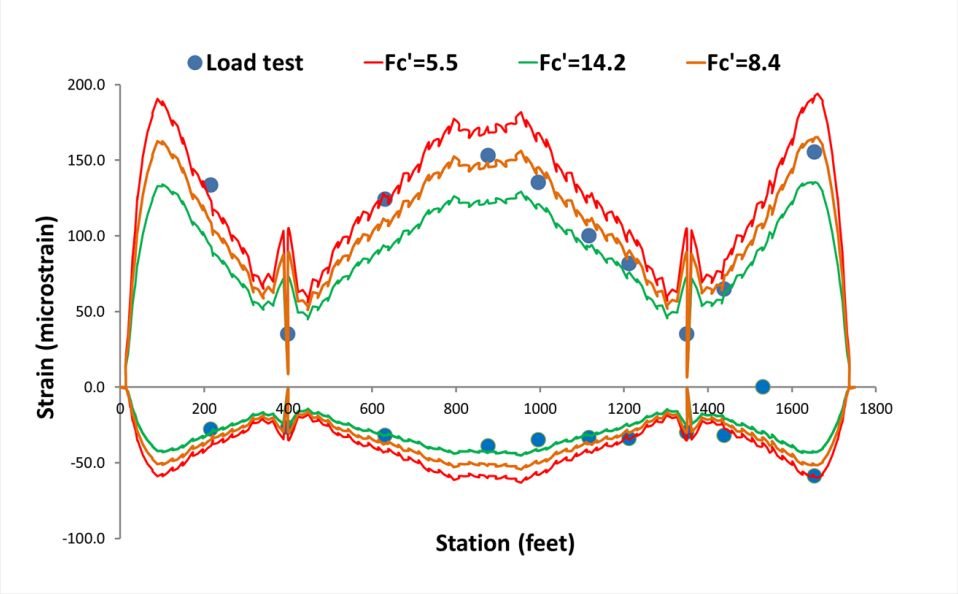

Figure 5.19. Fourth Load Test, Six Trucks, West Girder

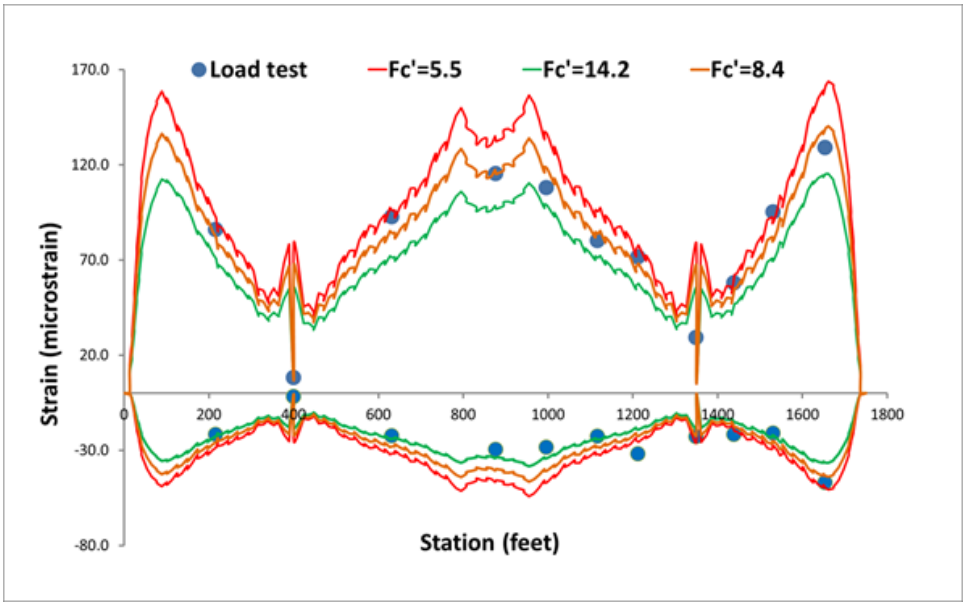

Figure 5.20. Second Load Test, Six Trucks, East Girder

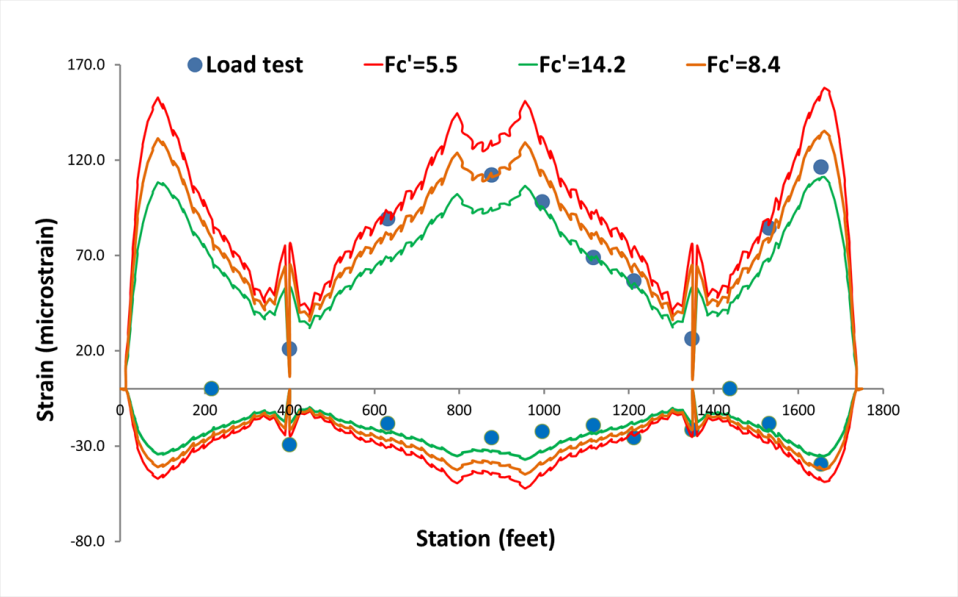

Figure 5.21. Third Load Test, Six Trucks, East Girder

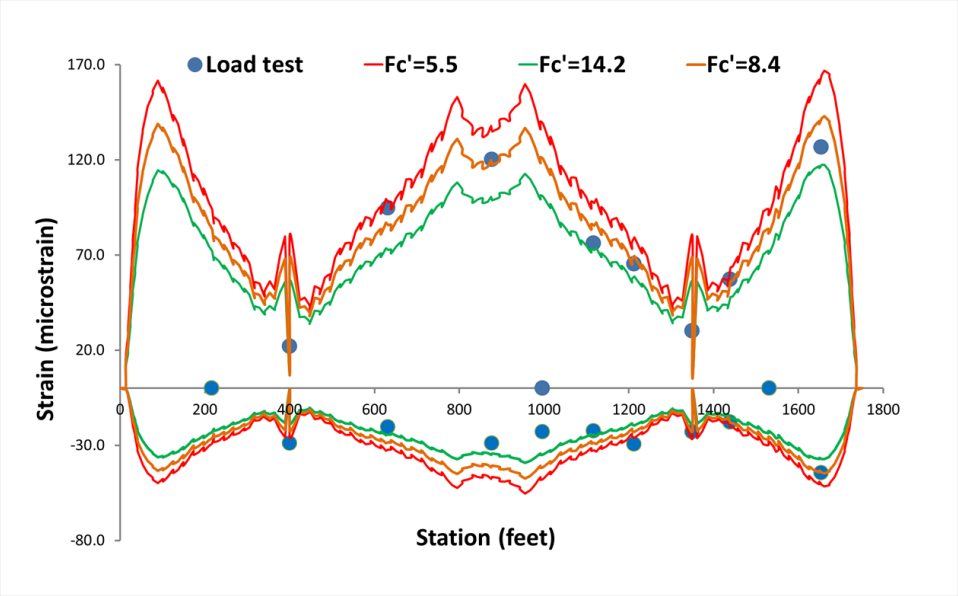

Figure 5.22. Fourth Load Test, Six Trucks, East Girder

5.4 Conclusions

To date, four diagnostic load tests have been conducted on the IRIB utilizing fully loaded 10-wheel dump trucks. The main purpose of load tests was to establish the baseline bridge performance for live loads and to confirm that the SHM system at the IRIB was functioning properly. In this chapter selected tests results were used to establish the accuracy of the FE model.

There are different types of uncertainties that can cause the differences in the results between the measured data and the model such as material properties, effective width, modelling errors, boundary conditions, etc. Some of those uncertainties were studied through parametric studies, however it turned out that the concrete compressive strength had the biggest influence among other variables. Therefore, three models using the tested minimum, average, and maximum 56-day cylinder break

results were created to explain the differences between the measured strain and the FE model.

The FE model that was developed showed good comparison to the AECOM design model, and also to the measured load tests data. Parametric studies showed that concrete compressive strength has a local effect on the results. Therefore, it is hard to specify one value of concrete compressive strength that produces accurate results for all locations along the edge girders. However, the results from using the average tested concrete compressive strength (8,400 psi) looked reasonable. The model with the average tested concrete compressive strength was adopted and used for future research purposes as explained in Chapter 9. The model yielded good results for the actual bridge behavior along the west edge girder in most of the quasi-static passes conducted in all load tests. Due to the complicated geometry at the pylons location areas and the complication in modelling the connection between the pylons and edge girders as explained in Chapter 4, the model does not show good results there; however the overall behavior is reasonable and acceptable.

Chapter 6

EDGE GIRDER CONVENTIONAL RATING

6.1 Contribution of this Chapter

The rating manual and the calculation files that AECOM submitted to DelDOT included rating factor values and stress values for Service I and Service III limit states and structural forces (moment and axial) for Strength I limit state. These stress and structural force values cannot be used directly to calculate the rating factor values. Section 5.2 showed how dead load and live load stresses were extracted from the calculation files by comparing the limit state values. Once the dead and live load stresses and structural forces were extracted, the calculation of rating factors along the edge girder for all applicable limit states is possible.

This chapter focuses only on the rating of the edge girder. The main contribution of this chapter is to compute the extracted structural forces values and show sample calculations for determining rating factor values for different limit states. These values and calculations can be used in the future for rerating the bridge. The extracted structural forces will also be used to rate the bridge directly using SHM data as will be presented in Chapter 9.

6.2 Introduction

The process of determining the live load carrying capacity of a bridge is called a load rating. This process includes two tasks; visual inspection and applying Load Resistance Factor Rating (LRFR) criteria. The visual inspection is usually performed

by a qualified inspector. The inspection process includes scrutinizing all components of the bridge and looking for any structural defects that could reduce the structural capacity of these components. Once the visual inspection is done, a National Bridge Inventory (NBI) report is produced by the inspector/s. The NBI report contains general information about the bridge and the results of the inspection, that will be used to estimate a condition factor used later in the LRFR process. The load rating process is completed by applying the LRFR rating equation for each component of the bridge subjected to individual force effects (i.e., axial force, flexure, or shear).

The Federal Highway Administration (FHWA) requires an LRFR rating factor be computed for all in-service bridges. Modern bridges are designed according to the Load Resistance Factor Design (LRFD) specifications. A HL-93 live load is used as the Design Live Load in the LRFD specifications. The Manual for Bridge Evaluation (MBE) states that bridges that have been designed and checked with the HL-93 loading may not require load rating calculations until changes (section loss, damage, etc.) occur to specific bridge components and reduce their rating below the design load level. Guidance for general rating procedures for conventional bridge types is available in the MBE. However, complex bridges such as suspension bridges and cable-stayed bridges may require special analysis methods and procedures.

The IRIB was designed according to the LRFD specifications and rated according to the LRFR method. Since the IRIB is a complex bridge, the designer rated each structural element of the bridge separately in order to determine the rating factor for the entire bridge. The designer submitted a rating manual (AECOM 2012a) to DelDOT that contains procedures and summarizes the rating factors that were determined for the IRIB components. The components rated in this manual are:

Transverse Precast and Cast-In-Place Floor Beams, Pylon Pier Tables, Ballast Beams, Transition Pier Caps, Edge Girders, and Cable Stays. All elements were rated for flexure, axial, shear and principal stresses except the stays cables which were rated only for axial stresses.

The designer used design, legal, and permit live loads in rating the bridge components. The design live load used was the HL-93 load, which consists of HS-20 truck, lane loads (0.64 kip/feet), tandem loads, and two trucks back to back for the negative regions. The legal loads include Delaware specific trucks, S220, S335, S437, T435, and T540 along with a lane load. The permit loads include four different crane configurations: AC2, AC3, AC4, and AC5 along with a lane load. The axle configurations and loads for the design, legal, and permit Loads are shown in Appendix A.1. A combination of four trucks was used for all service limit states and a combination of six trucks was used for strength limit states.

The lowest rating factor for all of the components of the bridge is the controlling rating factor for the whole bridge. For the IRIB, the west edge girder has the lowest rating factor among all of the bridge components. Since the load rating process follows the design criteria, so the load rating should be carried out at each applicable design limit state.

According to the MBE prestressed concrete bridges are rated for four limit states. The IRIB is a prestressed concrete bridge, and therefore it was rated for Service I, Service III, Strength I, and Strength II limit states. Table 6A.4.2.2-1 (AASHTO 2011) from the MBE shows limit states and load factors for different types of bridges. In addition to the aforementioned limit states, the designer rated the bridge for Service III Principal Tension stress limit state.

Table 6.1. Limit States and Load Factors for Load Rating (AASHTO 2011)

Bridge Type	Limit State*	Dead Load γ_{DC}	Dead Load γ_{DW}	Design Load		Legal Load	Permit Load
				Inventory	Operating		
				γ_{LL}	γ_{LL}	γ_{LL}	γ_{LL}
Steel	Strength I	1.25	1.50	1.75	1.35	Tables 6A.4.4.2.3a-1 and 6A.4.4.2.3b-1	—
	Strength II	1.25	1.50	—	—	—	Table 6A.4.5.4.2a-1
	Service II	1.00	1.00	1.30	1.00	1.30	1.00
	Fatigue	0.00	0.00	0.75	—	—	—
Reinforced Concrete	Strength I	1.25	1.50	1.75	1.35	Tables 6A.4.4.2.3a-1 and 6A.4.4.2.3b-1	—
	Strength II	1.25	1.50	—	—	—	Table 6A.4.5.4.2a-1
	Service I	1.00	1.00	—	—	—	1.00
Prestressed Concrete	Strength I	1.25	1.50	1.75	1.35	Tables 6A.4.4.2.3a-1 and 6A.4.4.2.3b-1	—
	Strength II	1.25	1.50	—	—	—	Table 6A.4.5.4.2a-1
	Service III	1.00	1.00	0.80	—	1.00	—
	Service I	1.00	1.00	—	—	—	1.00
Wood	Strength I	1.25	1.50	1.75	1.35	Tables 6A.4.4.2.3a-1 and 6A.4.4.2.3b-1	—
	Strength II	1.25	1.50	—	—	—	Table 6A.4.5.4.2a-1

The conventional rating equation used for rating the edge girder can be given by Equation 6.1.

$$RF = \frac{C - (\gamma_{DC})(DC) - (\gamma_{DW})(DW) \pm (\gamma_P)(P)}{(\gamma_{LL})(LL + IM)} \quad Equation\ 6.1$$

Where,

- RF = Rating factor
- C = Capacity
- (γ_{DC}) DC = Factored dead load effects
- (γ_{DW}) DW = Factored wearing surface effects
- (γ_P) P = Permanent loads effects
- (γ_{LL}) (LL+IM) = Factored live load effects with dynamic load allowance

6.3 Service I Limit State

The Service I limit state requires that the compression flexural stresses in the edge girder should not exceed a certain level of stress given by a percentage of the design concrete compressive strength ($f'c$). The Service I limit state rating equation used is based on a limiting value of 60 percent of $f'c$. The Service I limit state was used to check the allowable service stresses produced by the flexural compression forces in the edge girder. The rating factor values were obtained along the top and the bottom of the edge girder using the design, legal, and permit live loads.

A sample calculation for the controlling rating factor for the design load case (HL-93) for member WG278 (located at 1637 ft right to pier 4 at the west edge girder as shown in Figure 4.7) is shown in the Figure 6.1.

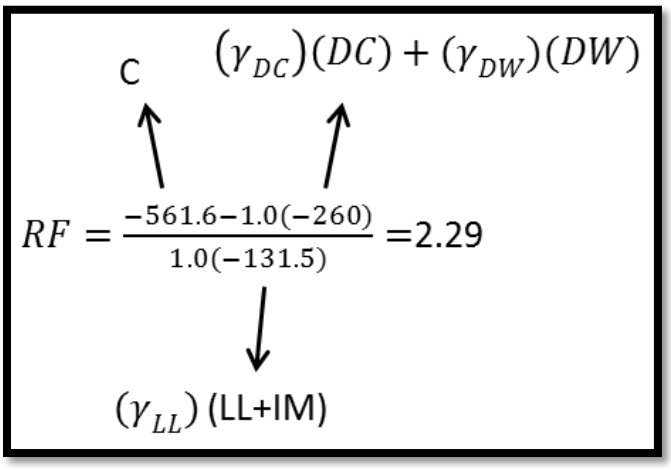

Figure 6.1. Sample Calculation for RF for Member WG278 Using Service I (ksf)

Figure 6.2 shows a comparison between the designer rating factors and the calculated rating factors by UD. As one can see the values are nearly identical. Dead load and live load stresses can be seen in Appendix B.1.

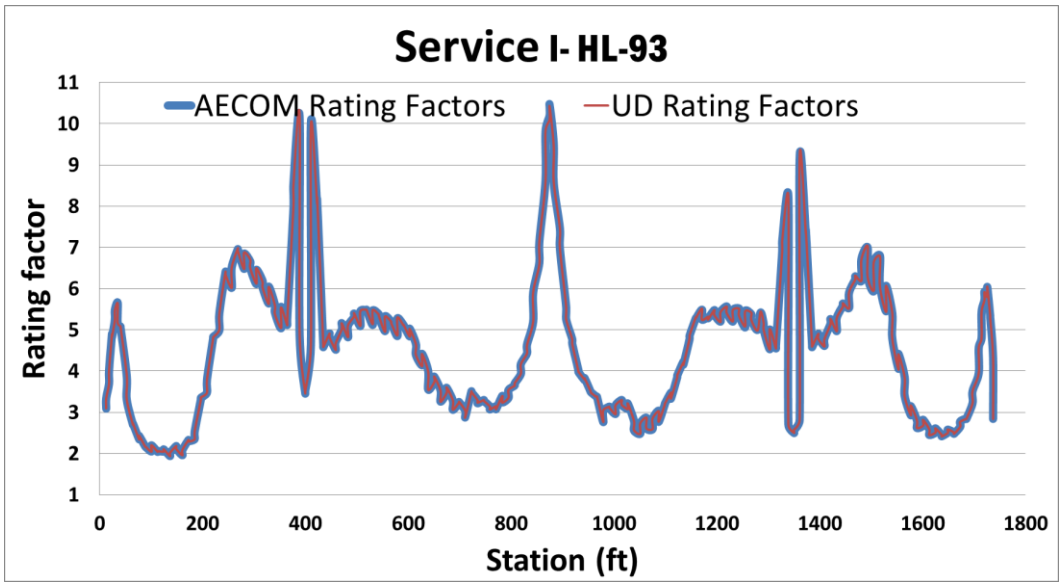

Figure 6.2. Comparison between Designer RF and Calculated UD RF for Service I

6.4 Service III Limit State

The Service III limit state requires that the tension flexural stresses in the edge girder should not exceed a certain level of stress given by a percentage of the design concrete compressive strength ($f'c$). The Service III limit state rating equation used is based on a limiting value of $3\sqrt{f'c}$ psi. The Service III limit state was used to check the allowable service stresses produced by the flexural tension forces in the edge girder. The rating factor values were obtained along the top and the bottom of the edge girder using the design, legal, and permit live loads.

A sample calculation for the controlling rating factor for the design load case (HL-93) for member WG281 (located at 1,649 ft right to pier 4 at the west edge girder as shown in Figure 4.7) is shown in the Figure 6.3.

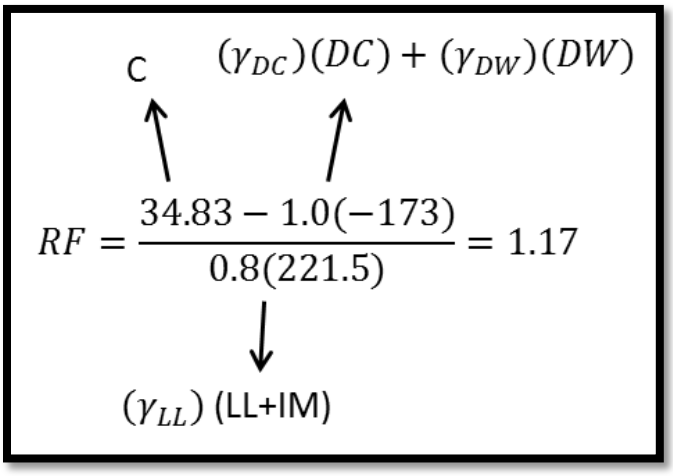

Figure 6.3. Sample Calculation for RF for Member WG281 Using Service III (ksf)

Figure 6.4 shows a comparison between the designer rating factors and the calculated rating factors by UD. As one can see, the values are nearly identical. Dead load and live load stresses can be seen in Appendix B.2.

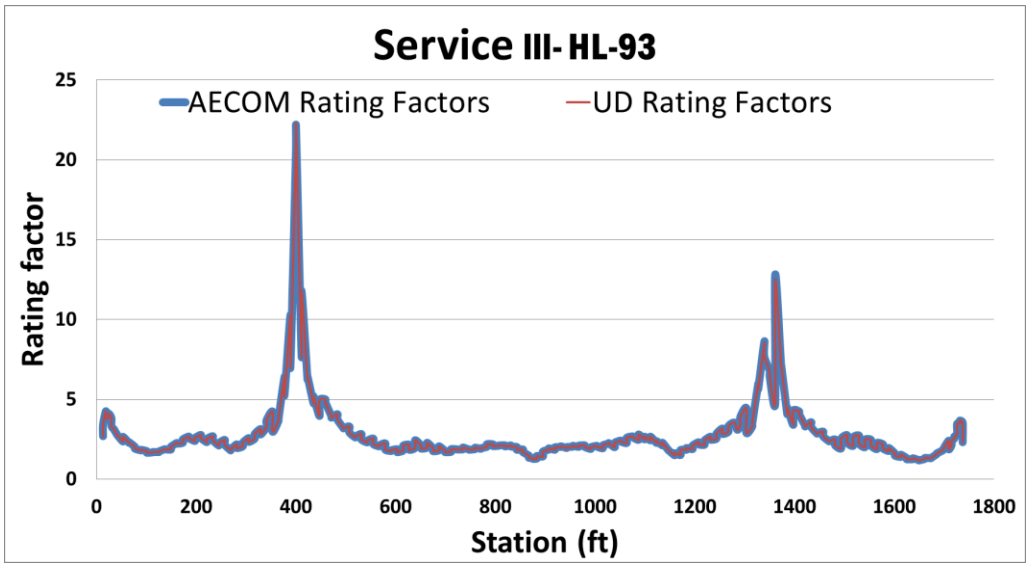

Figure 6.4. Comparison between Designer RF and Calculated UD RF for Service III

6.5 Strength I Limit State

The Strength I limit state was used to rate the bridge for flexure, axial, and shear forces produced by six fully loaded lanes of the design load (HL-93). The capacity used in the rating equation is determined by the LRFD code, which is expressed by the section's nominal resistance multiplied by three reduction factors; $C = \varphi_c \varphi_s \varphi R_n$. The $\varphi_c$is the condition factor based on the NBI report results. Since this IRIB is a new bridge; the condition factor is 1.0. The φ_s is a redundancy factor. Since the IRIB has two main edge girders, the redundancy factor is 1.0. The φ factor is an LRFD resistance factor. The value depends on the material and the load type. The nominal resistance follows the type of structural force being rated. For example, if the section is being rated for flexure, then R_n becomes the moment capacity of the section extracted from the interaction diagram.

6.5.1 Moment and Axial Capacities

In the load rating calculation file for the edge girder that AECOM submitted to DelDOT, sections of the west edge girder were divided into fifteen different sections based on the span location and based on the number of tendons in the adjacent deck section. AECOM reported an interaction diagram for each of these sections. They also submitted tables that included the maximum and minimum envelop results from the Strength I limit state produced by six fully loaded lanes of the design load. Due to the complexities of load rating with an interaction diagram for moment and axial force, the designer rated only the governing location from the Service III limit state and only using the design load (AECOM 2012)

The interaction diagrams were exported into excel sheets. A Matlab code was developed to obtain the capacities for all sections using the exported interaction diagrams and the Strength I limit state values reported in the tables. By doing this, moment and axial force capacities became available along the west edge girder. These capacities were used to calculate the rating factors for axial and flexure according to Strength I limit state. All obtained section flexural and axial capacities can be seen in Appendix B.3.

6.5.2 Rating Using Interaction Diagram

The capacity of any section subjected to both axial forces and bending moments can be determined by using an interaction diagram. AASHTO LRFD Specifications require using the strain compatibility method to obtain an interaction diagram. The capacity of any beam-column element depends on the combination of dead and live load axial forces and moments. Due to the non-linear behavior, determination of the accurate capacity is complicated.

The following procedure is used to determine the capacity and rate a section subjected to both axial forces and bending moments. The procedure is addressed in Load Rating of Complex Bridges (Morcous et al. 2010).

1. Develop the interaction diagram using as-built drawings or using as-inspected section properties, as shown in Figure 6.5.

2. Locate point A that represents the factored dead load moment and axial force.

3. Using the factored live load moment and axial force for live load rating, compute the live load eccentricity e_1.

4. Continue from Point A on a line with slope equal to the live load eccentricity to the intersection of the interaction diagram curve at point B.

5. Determine the moment and axial capacities from the diagram (i.e., the abscissa and ordinate values of point B).

6. Calculate the moment and axial rating factors.

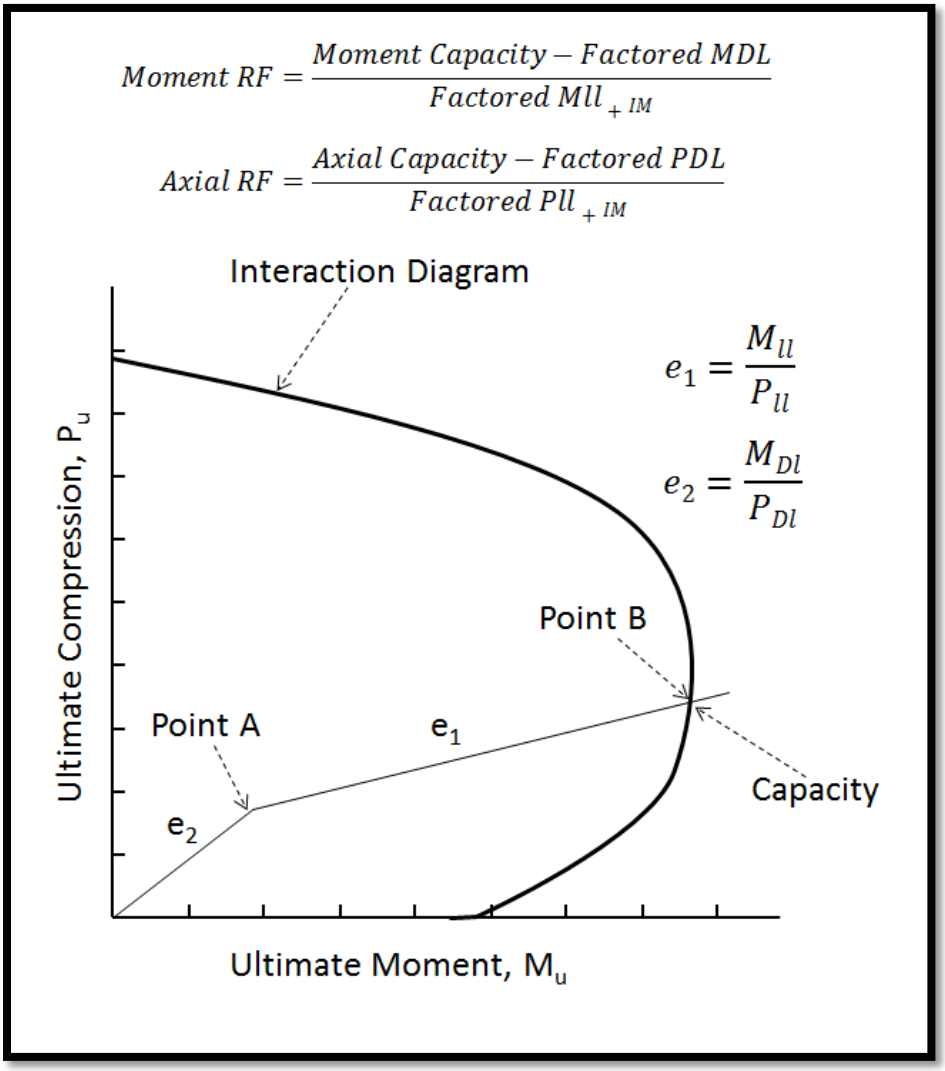

Figure 6.5. Steps to Extract Axial and Moment Capacities Using an Interaction Diagram

6.5.3 Inventory and Operating

The Strength I limit state includes two rating levels, inventory and operating. The inventory level is the lower of the two ratings, and is defined by AASHTO as the live load that can safely carried by the bridge for an indefinite period of time (assuming no deterioration). The operating rating is defined as the absolute maximum

permissible live load that can be placed on the bridge under any circumstances (note that both levels are assuming live loads in multiple lanes).

Flexural, axial, and shear rating factors for inventory and operating levels are obtained along the edge girder. The load factors in Table 6.1 were used in the rating equation. All forces and capacities were used in the rating calculations and rating factors can be seen in Appendix B.3 and B.4. Sample rating calculations for inventory and operating levels for flexural, axial and shear are shown in the following sections.

6.5.3.1 Flexural Ratings

$$Moment\ RF_{Inv} = \frac{Moment\ Capacity - Factored\ M_{DL}}{Factored\ M_{ll_{+IM}}} = \frac{32500 - 3340.4}{24759.6} = 1.18$$

Figure 6.6. Sample Calculation of Inventory Moment (k-ft) RF for Member WG281

$$Moment\ RF_{Opr} = \frac{Moment\ Capacity - Factored\ M_{DL}}{Factored\ M_{ll_{+IM}}} = \frac{32500 - 3340.4}{13806.6} = 2.11$$

Figure 6.7. Sample Calculation of Operating Moment (k-ft) RF for Member WG281

6.5.3.2 Axial Ratings

$$Axial\ RF_{Inv} = \frac{Axial\ Capacity - Factored\ P_{DL}}{Factored\ P_{ll_{+IM}}} = \frac{-5160 - (-6222.7)}{667.7} = 1.59$$

Figure 6.8. Sample Calculation of Inventory Axial (kips) RF for Member WG281

$$Axial\ RF_{Opr} = \frac{Axial\ Capacity - Factored\ P_{DL}}{Factored\ P_{ll_{+IM}}} = \frac{-5160-(-6222.7)}{367.2} = 2.89$$

Figure 6.9. Sample Calculation of Operating Axial (kips) RF for Member WG281

6.5.3.3 Shear Ratings

The shear capacities were also extracted from the tables in the AECOM calculation files. Shear rating factors for inventory and operating levels were calculated along the edge girder. Sample of calculations are presented in the following figures for members WG177 and WG196, they are located at 1039 ft and at 1159 ft, respectively right to pier 4 at the west edge girder as shown in Figure 4.7

$$\text{Shear } RF_{Inv} = \frac{Shear\ Capacity\ (\varphi V_n) - Factored\ V_{DL}}{Factored\ V_{ll_{+IM}}} = \frac{1159.4-494.1}{231.6} = 2.87$$

Figure 6.10. Sample Calculation of Inventory Shear (kips) RF for Member WG177

$$\text{Shear } RF_{Opr} = \frac{Shear\ Capacity\ (\varphi V_n) - Factored\ V_{DL}}{Factored\ V_{ll_{+IM}}} = \frac{1741.5-454.2}{275.9} = 4.67$$

Figure 6.11. Sample Calculation of Operating Shear (kips) RF for Member WG196

6.6 Summary

Service I and Service III limit states values submitted by AECOM were separated into dead load and live load stresses. These values were in turn used to compute rating factors for the edge girder for Service I and Service III limit states for

different live load cases. It was shown that the calculated rating factors are nearly identical to the designer's rating factors. The Strength I limit state values were also separated into dead and live axial loads and moments. Furthermore, the interaction diagrams were exported and used by a Matlab code to determine the axial and moment ultimate capacities along the edge girder. Due to the complexity of the load rating using interaction diagrams, the designer has rated the controlling location only for Strength I limit state. However, since all capacities were obtained by an automated Matlab code, rating factors for Strength I limit state along the edge girder were computed. The designer rating factors are very close to the calculated rating factors.

Sample calculations were presented in this chapter for each limit state and each case. In addition to the rating factors, all stresses and forces used to produce these rating factors are in Appendix B.2, B.3, and B.4. These extracted live load stresses, dead load stresses, live load forces, dead load forces, and section capacities will be used directly to obtain rating factors based on SHM data as will be presented in Chapter 9.

Chapter 7

RELIABILITY ANALYSIS BASED ON DESIGN LOADS

In this chapter, a reliability analysis based on design loads was performed for the west edge girder of the IRIB for a variety of limit states. The statistical parameters used in the NCHRP Projects 12-33 and 20-7/186 (Nowak 1999; Kulicki et al. 2007) for calibrating the AASHTO Bridge Specifications were used in this analysis. Monte Carlo simulation was used to perform the analysis and obtain the reliability indices along the west edge girder. The aim of the analysis was to check the IRIB design values to see if they achieve a target reliability index that is consistent with the NCHRP Report. Furthermore, performing reliability analysis based on the design loads proved to be a useful first step before performing a reliability analysis based on SHM data since such an analysis is more complicated, as illustrated in Chapter 9. Also, the reliability analysis based on design loads was used as a reference for comparing the reliability analysis based on the SHM data.

7.1 Background

Bridge design philosophies have developed and improved throughout the past decades. Prior to 1970, Allowable Stress Design (ASD) was the only design philosophy in use. The Allowable Stress Design method applies a factor of safety to a limiting stress value to achieve an allowable stress. The ASD method specifies that the maximum stress for a component computed based on service loads not exceed the allowable stress. The biggest disadvantage of the ASD method is that it treats all loads

with an equal statistical variability. Also, it doesn't consider the probability of simultaneous occurrence of higher than expected loads and a lower than expected resistance (State of California Department of Transportation/Division of Engineering Services 2015).

Beginning in early 1970, a new design philosophy referred to as Load Factor Design (LFD) was introduced. The LFD method considers that live loads have more variability than dead loads. In addition to the reduction factors that are applied to an elements resistance, the LFD method applies safety factors to dead and live loads. Although the LFD method incorporates different variability between live loads and dead loads, the load factors and resistance factors were not calibrated based on statistical studies that take in consideration the variability of design parameters (State of California Department of Transportation/Division of Engineering Services 2015).

In 1988 the National Cooperative Highway Research Program (NCHRP) initiated Project 12-33,"Development of a Comprehensive Bridge Specification and Commentary" to develop a Load and Resistance Factor comprehensive (LRFD) design code with statistically calibrated load and resistance factors. The resulting AASHTO code was published in 1994, titled the LRFD Bridge Design Specifications. NCHRP Report 368 (Nowak 1999), developed as part of that project, had the objective of developing and calibrating of load and resistance factors. NCHRP Report 368 was completed prior to the final selection of load and resistance factors in the AASHTO LRFD Bridge Design Specifications. NCHRP 368 report provides background information and calibration procedures used in developing the LRFD Specifications. In 2007, the calibration of load and resistance factors was updated through NCHRP

20-7/186 project. The updated load and resistance factors are the ones found in the current AASHTO LRFD 2014 specifications.

The LRFD code is calibrated to provide a consistent and uniform safety level for different types of bridges. The calibration process is based on a probability approach. A representative sample of structures, including non-composite steel girders, composite steel girders, reinforced concrete T-beams, and prestressed concrete girders was used to conduct the calibration. NCHRP Reports 368 and 20-7/186 (Nowak 1999; Kulicki et al. 2007) describe the calibration procedure based on the selected sample of bridges and provide information about the reliability calculation process.

The structural performance is measured in terms of probability of failures and expressed as reliability indices. A uniform level of safety is achieved by using a single target reliability index. The load and resistance factors were calibrated to achieve that target reliability index. As a result, bridges designed using the LRFD Specifications have a consistent and uniform level of safety.

7.2 Introduction

A reliability index is a useful measure of structural performance. The AASHTO LRFD Bridge Specifications were calibrated based on a target reliability index of 3.5 for the strength limit state. In other words, a 3.5 reliability index represents $2*10^{-4}$ probability of failure. Since the loads and resistance factors were obtained to ensure the target reliability index, bridges designed using the LRFD code should produce a consistent level of safety that is consistent with a target reliability index of 3.5.

The IRIB was designed according to the AASHTO LRFD Bridge Specifications. As explained in Chapter 6, design values were extracted from the design information submitted to DelDOT. The information extracted included dead and live load stresses, dead and live load axial forces and moments. Section capacities were also computed using the submitted interaction diagrams.

Using this information, a reliability analysis based on design loads was performed for the IRIB for a variety of limit states. The statistical parameters used in the NCHRP Reports were used for the IRIB reliability analysis. The aim of the analysis was to check the IRIB design values to see if they achieve a target reliability index that is consistent with the NCHRP Report. Performing reliability analysis based on the design loads proved to be a useful first step before performing a reliability analysis based on SHM data since such an analysis is more complicated as illustrated in Chapter 9. Furthermore, the reliability analysis based on design loads was used as a reference for comparing the reliability analysis based on the SHM data.

7.3 Statistical Parameters for Design Loads and Resistance

In order to measure reliability as a probability of failure, loads and resistance have to be expressed as Probability Distribution Functions (PDF), where loads and resistance are treated as random variables. The type of the PDF and the associated parameter(s) determine the shape of the PDF.

The total load effect (Q) is defined as a summation of the load components: dead, live, and dynamic loads. The statistical parameters of the total load effects are determined by the statistical parameters of each load component. The load models from the available data, surveys, and other observations at that time were used in the code calibration (Nowak 1999). Each of these loads is treated as having a normal

distribution (Gaussian distribution). A normal distribution is a continuous PDF with two related parameters; mean (μ), and standard deviation (σ). The mean of Q is a sum of the mean values of the components, $\mu_Q = \mu_{DL} + \mu_{LL+IM}$, where $\mu_{DL}$is mean of dead load, μ_{LL+IM} is mean of live load and impact, and μ_Q is the mean of the combined loads.

The mean value for each load component is calculated using bias factors (ratio of mean to nominal) multiplied by the nominal design value, $\mu_{DL}=\lambda_{DL}$ x (nominal design value). Since each of the load components is assumed to be normally distributed, the variance of Q, is the summation of the individual load components, $\sigma_Q^2 = \sigma_{DL}^2 + \sigma_{LL+IM}^2$, where σ_{DL}^2 is dead load variance, σ_{LL+IM}^2 is live load and impact variance, and σ_Q^2 is load effects variance. The standard deviation of the load effects (σ_Q) is equal to the square root of the variance (σ_Q^2). The coefficient of variation of the load effects (V_Q) is defined as the ratio of the standard deviation (σ) to the mean value (μ), $V_Q = {}^{\sigma_Q}/_{\mu_Q}$.

For the code calibration, four subcomponents were considered for the dead load effect. Each of these components is assumed to be normally distributed, so the final dead load effect is considered to be normally distributed. The four dead load subcomponents as indicated in the NCHRP Report are:

- DL_1: weight of factory made element
- DL_2: weight of cast-in-place concrete
- DL_3: weight of wearing surface
- DL_4: weight of miscellaneous items

According to the NCHRP Report 20-7/186, the bias factor for DL_1 and DL_2 were provided by the Ontario Ministry of Transportation based on survey data collected

during the calibration of the Ontario Highway Bridge Design Code (OHBDC 1979). The coefficient of variation for the DL_1 and DL_2 were taken from the NBS Report 577 (Kulicki et al. 2007). For DL_3, the bias factor and coefficient of variation were calculated from survey data provided by the Ontario Ministry of Transportation (Kulicki et al. 2007). Table 7.1 presents the bias factor and coefficients of variation for the dead load subcomponents.

Table 7.1. Bias Factors and Coefficient of Variation for Dead Load (Kulicki et al. 2007)

Dead Load Component	Bias Factor	Coefficient of Variation
Factory made members, DL_1	1.03	0.08
Cast-in-place, DL_2	1.05	0.10
Wearing surface, DL_3	1.0	0.25
Miscellaneous, DL_4	1.03 ~ 1.05	0.08 ~ 0.10

For the code calibration, the live load model was created using the Ontario truck survey (Kulicki et al. 2007). The total number of trucks considered in the survey was 9,250 trucks, these trucks were considered representative of two weeks traffic at an Average Daily Truck Traffic (ADTT) of 1,000. The maximum positive moment, shear, and negative moment were obtained based on influence line analysis for span lengths ranging from 10 feet to 200 feet. Multiple presence was considered through the correlation between trucks in the same lane and/or the parallel traffic lanes. In the NCHRP 368 Report an ADTT of 1,000 was used for calibrating the live load factor. The calibration yielded a live load factor of 1.7. In the NCHRP 20-7/186 project an ADTT of 5,000 was used in the calibration of the LRFD code. The latest calibration

led to an increase in the live load factor to 1.75 (Kulicki et al. 2007). Table 7.2 presents the bias factors and coefficients of variation for live load used in calibrating the LRFD code.

Table 7.2. Bias Factors and Coefficients of Variation for Live Load (Kulicki et al. 2007)

Moment or Shear	Number of Loaded Lanes	Bias Factor ADTT = 1000	Bias Factor ADTT = 5000	Coefficient of Variation
+ moment	1	1.23-1.36	1.26-1.38	0.12
	2	1.08-1.15	1.10-1.20	0.12
shear	1	1.17-1.28	1.21-1.32	0.12
	2	1.04-1.14	1.08-1.18	0.12
- moment	1	1.20-1.33	1.23-1.36	0.12
	2	1.10-1.22	1.14-1.26	0.12

In terms of the resistance factor, three uncertainties with Gaussian distribution were considered; material factor (M), fabrication factor (F), and the professional factor (P). The resistance factor (R) is calculated as the product of the three factors with the nominal resistance (R_n), $R = M \cdot F \cdot P \cdot R_n$. The mean value can be expressed as $\mu_R = \mu_M \cdot \mu_F \cdot \mu_P \cdot R$, and the coefficient of variation as the square root of the summation of the variances, $V_R = \sqrt{V_M^2 + V_F^2 + V_P^2}$. The result of the product of normal random variables will produce lognormal random variables. The final resistance model used for the code calibration has a lognormal distribution. Table 7.3 presents the statistical parameters for the resistance components.

Table 7.3. Bias Factors and Coefficient of Variation for Resistance (Kulicki et al. 2007)

Type of Structure	Material and Fabrication Factors, F M		Professional Factor, P		Resistance, R	
	λ	V	λ	V	λ	V
Noncomposite steel girders						
Moment (compact)	1.095	0.075	1.02	0.06	1.12	0.10
Moment (noncom.)	1.085	0.075	1.03	0.06	1.12	0.10
Shear	1.12	0.08	1.02	0.07	1.14	0.105
Composite steel girders						
Moment	1.07	0.08	1.05	0.06	1.12	0.10
Shear	1.12	0.08	1.02	0.07	1.14	0.105
Reinforced concrete						
Moment	1.12	0.12	1.02	0.06	1.14	0.13
Shear w/steel	1.13	0.12	1.075	0.10	1.20	0.155
Shear no steel	1.165	0.135	1.20	0.10	1.40	0.17
Prestressed concrete						
Moment	1.04	0.045	1.01	0.06	1.05	0.075
Shear w/steel	1.07	0.10	1.075	0.10	1.15	0.14

7.4 Reliability Method

A reliability index represents a probability of failure. In order to explain the concept of reliability index and probability of failure in a simple way, let us assume that the load effects (Q) and the resistance model (R) are both normally distributed functions. The limit state function Z is $Z = R - Q$. If the load effects and the resistance are normally distributed functions, then Z is a normal distribution function with a mean value of $\mu_Z = \mu_R - \mu_Q$, and variance of $V_Z^2 = V_R^2 + V_Q^2$. The negative area of the resulting distribution represents the probability of failure. Figure 7.1 illustrates a graphical representation of the probability of failure.

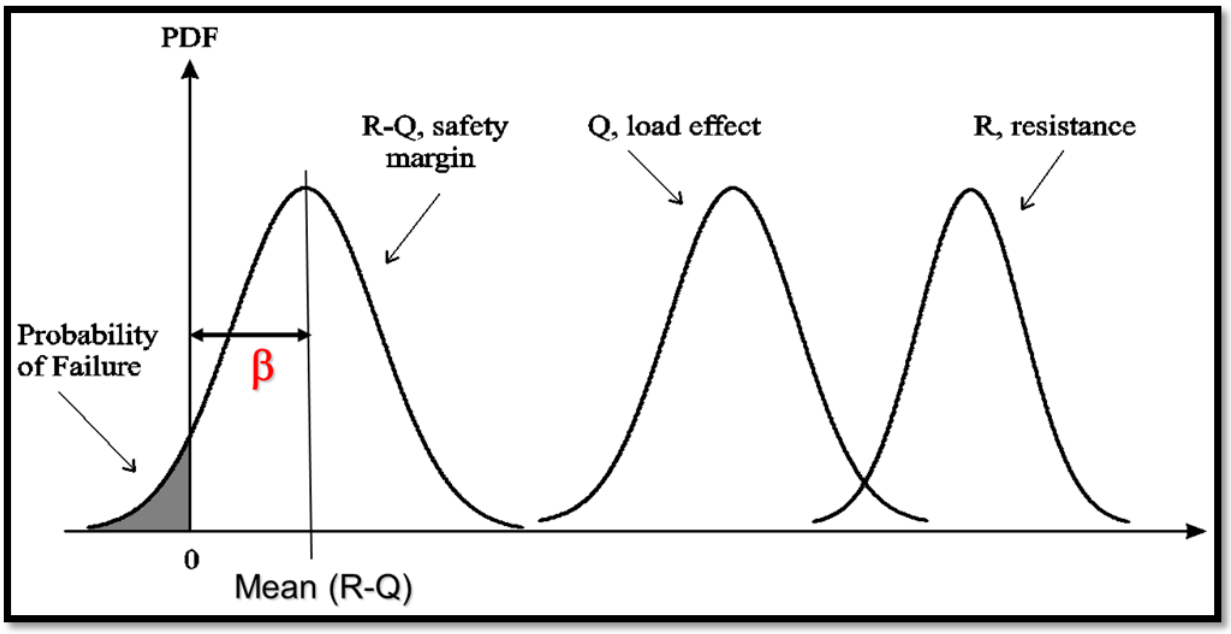

Figure 7.1. Graphical Presentation of Reliability Analysis Using Normal Distributions (Nowak & Collins 2013)

Then reliability index can be calculated based on a closed form solution as given by Equation 7.1.

$$\beta = \frac{\mu_R - \mu_Q}{\sqrt{\sigma_R^2 - \sigma_Q^2}} \quad Equation\ 7.1$$

Where,

- β : Reliability index
- μ_R: Mean resistance
- μ_Q: Mean load effects
- σ^2_R: Variance of resistance

- σ^2_Q: Variance of load effects

In general, the reliability index can be calculated by Equation 7.2

$$\beta = \varphi^{-1}(P_f) \quad Equation\ 7.2$$

Where,

- φ^{-1}: Inverse of the standard normal distribution function
- P_f : Probability of failure (shaded area)

In practice, calculating the reliability index based on a closed form solution can be done only in two cases. If both Q and R are normal random variables, the solution can be found using Equation 7.1. If both Q and R are lognormal random variables, the reliability index can be calculated as shown in Equation 7.3.

$$\beta = \frac{Ln\left[\mu_{R/}\mu_Q \sqrt{\frac{1+V_Q^2}{1+V_R^2}}\right]}{\sqrt{Ln\left[(1+V_Q^2)(1+V_R^2)\right]}} \quad Equation\ 7.3$$

Where,

- V_R : Coefficient of variation of the resistance
- V_Q : Coefficient of variation of the load effect

However, in all other cases, the available procedures produce only approximate results (Kulicki et al. 2007).

Similar to the LRFD code, for the IRIB reliability analysis based on design values, the load effects were assumed to be normally distributed, and the resistance assumed to have a lognormal distribution. The bias factors for dead load, live load, and resistance are taken from the tables shown in this chapter. A bias factor of 1.05 and coefficient of variation of 0.1 were used for the dead load. A bias factor of 1.08

and a coefficient of variation of 0.12 were used for the live load. Bias factor and coefficient of variation were used from Table 7.3 for prestressed concrete (Moment) to represent the resistance model. A bias factor of 1.05 and a coefficient of variation of 0.075 were used for the resistance factor. Since the load effects are normally distributed, and the resistance has lognormal distribution, neither closed form solution is valid. Therefore, Monte Carlo simulation was used to perform the analysis.

7.5 Monte Carlo Simulation

Monte Carlo simulation is a powerful tool that can be used to determine the numerical failure rate (Nowak & Collins 2013). Typically, the quantity of measured data is inadequate to estimate the reliability indices. However, Monte Carlo simulation utilizes the generated random variables to extrapolate the Cumulative Distribution Function (CDF) for each random variable. Once the CDF plots are extrapolated, reliability indices can be estimated for the established limit state (Allen et al. 2005).

MS Excel was used to perform Monte Carlo simulations in the development of the NCHRP Report 20-7/186. The NORMSINV command was used to calculate the inverse standard normal distribution function. A Matlab code using the same concepts explained was used to estimate the reliability indices along the edge girder. A sufficient number of iterations were assured by inspecting the number of failures at each location. In order to check the validity of the developed Matlab code the same example used in the NCHRP Report 20-7/186 was evaluated. The results found were consistent with the NCHRP Report example.

7.6 Results

The reliability analysis was performed using Monte Carlo simulation and extrapolation to obtain the reliability indices along the edge girder of the IRIB. Probability Distribution Functions (PDF) are generated using the extracted design information and bias factors and coefficient of variations. Random values are generated from these distributions randomly and applied in the limit state function. After conducting that for a sufficient number of iterations, the probability of failure can be calculated as presented earlier in this chapter. The design information was extracted from the designer reports as explained in Chapter 5. Appendices A.2 to A.3 show the extracted design values. Probability distribution functions were created along the west edge girder using the bias factor and coefficient of variation for the design loads and the resistance model. Values were generated randomly from each of these distributions and applied in the limit state function. The reliability index (**β**) is calculated based on probability of failure that is calculated by dividing the number of failures by the number of iterations (generated values from distributions). The analysis was performed using a developed Matlab code (Appendix B.1). Service I, Service III, and Strength I limit states were used to estimate the reliability indices along the west edge girder.

Since the LRFD code was calibrated for the Strength I limit state, the focus in this chapter will be to compare the calculated β factors from the analysis with the target reliability index (β_T). Since the code was calibrated for only the Strength I limit state, the β factors from the other limit states cannot be compared to β_T, but their results will be used as a reference for reliability analysis based on the SHM data in later chapters.

7.6.1 Strength I Limit State

Normal distributions with bias factors of 1.05, 1.08 and coefficients of variation of 0.1, 0.12 were used at each of the 160 members that represents the edge girder in the FE model for dead and live loads effects, respectively. A lognormal distribution with bias factor of a 1.05 and a coefficient of variation of 0.075 was used for section capacities along the edge girder.

The reliability analysis was performed using positive moments. The analysis was carried out for 10^7 cycles using the developed Matlab code. Results are presented in Figure 7.2; the red circles represent the reliability indices at the center of each member of the 160 members that represent the edge girder in the FE model. The missing results in the figure are a result of not having capacities at those locations. The lowest reliability index from the Strength I-Flexural limit state is 3.57 at a location of 1650 ft. This is very close to the expected target reliability from the code, and it occurs at the location that controls the load rating according to the designer.

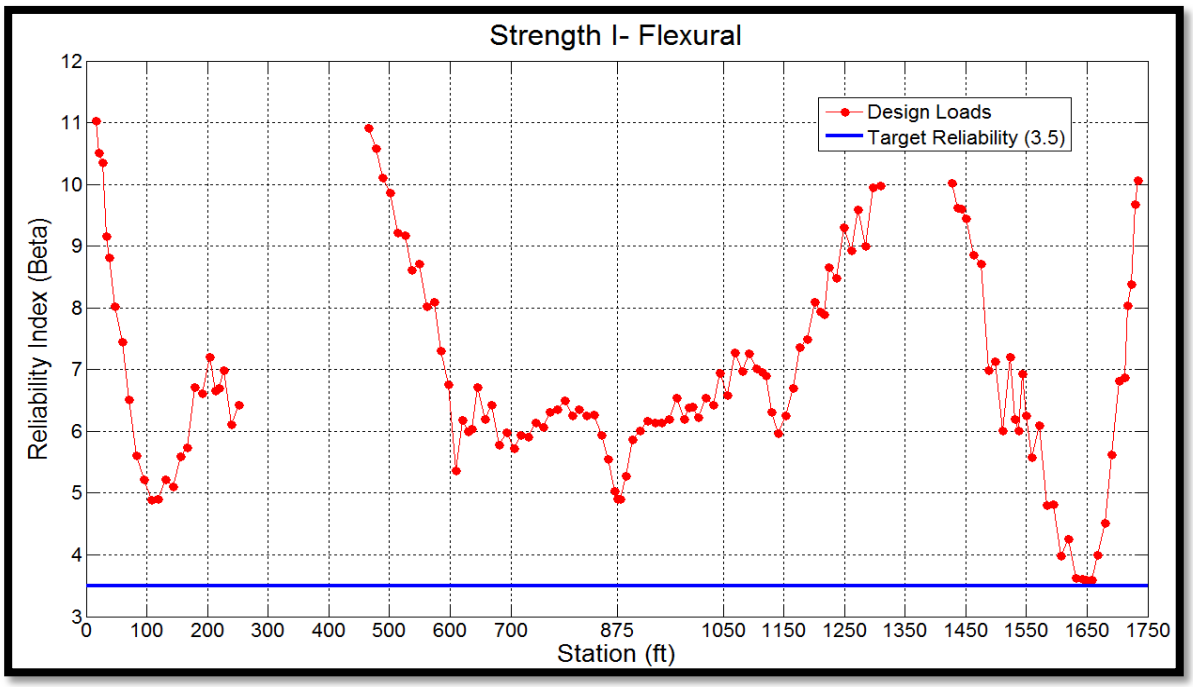

Figure 7.2. Reliability Indices Along Edge Girder for Strength I- Flexure

7.6.2 Service III Limit State

Since the Service III limit state involves ensuring that the flexural tensile stresses do not exceed a defined value of allowable stress ($3\sqrt{f'c}$ psi), a reliability analysis was performed based on computed flexural tension stresses. The analysis was carried out for 10^7 cycles using the developed Matlab code. Results are presented in Figure 7.3; the red circles represent the reliability indices at the center of each member of the 160 members that represent the edge girder in the FE model. The lowest reliability index from the Service III limit state is 0.77 at a location of 1650 ft. This occurs at the location that controls the load rating according to the designer.

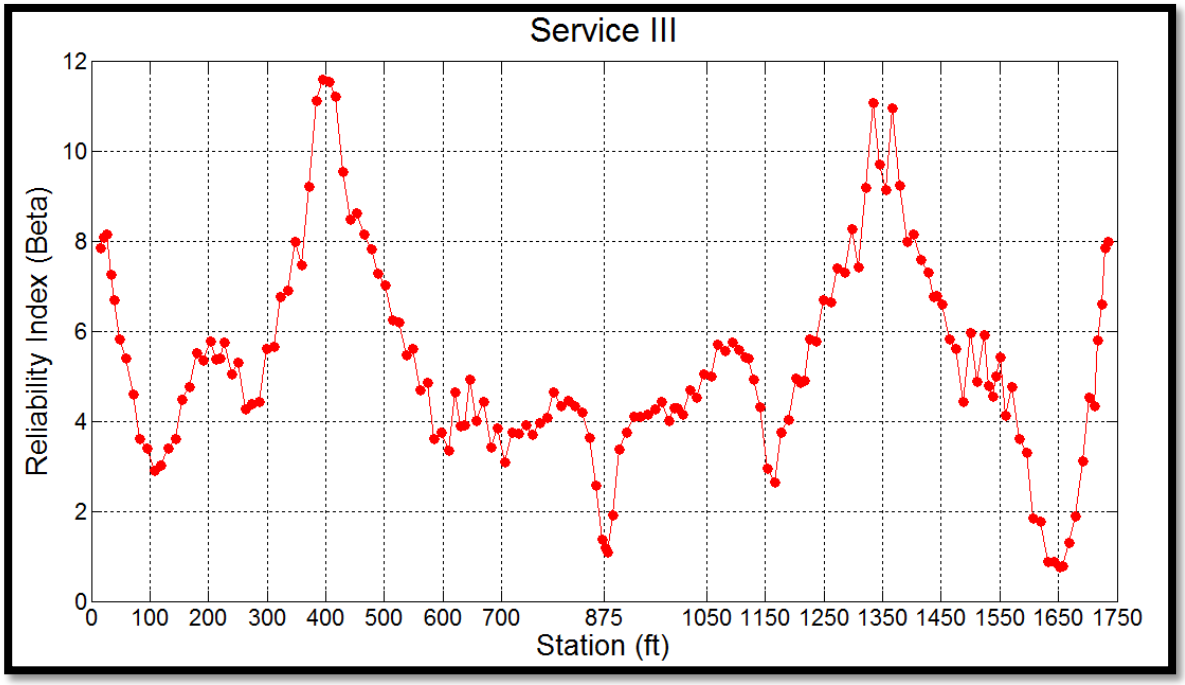

Figure 7.3. Reliability Indices Along Edge Girder for Service III-Flexural Tension

7.6.3 Service I Limit State

Since the Service I limit state involves ensuring that the flexural compression stresses do not exceed a defined value of allowable stress (60 percent of $f'c$), a reliability analysis was performed based on computed flexural compression stresses. The analysis was carried out for 10^7 cycles using the developed Matlab code. Results are presented in Figure 7.4; the red circles represent the reliability indices at the center of each member of the 160 members that represent the edge girder in the FE model. The lowest reliability index from the Service I limit state is 2.23 at a location of 155 ft.

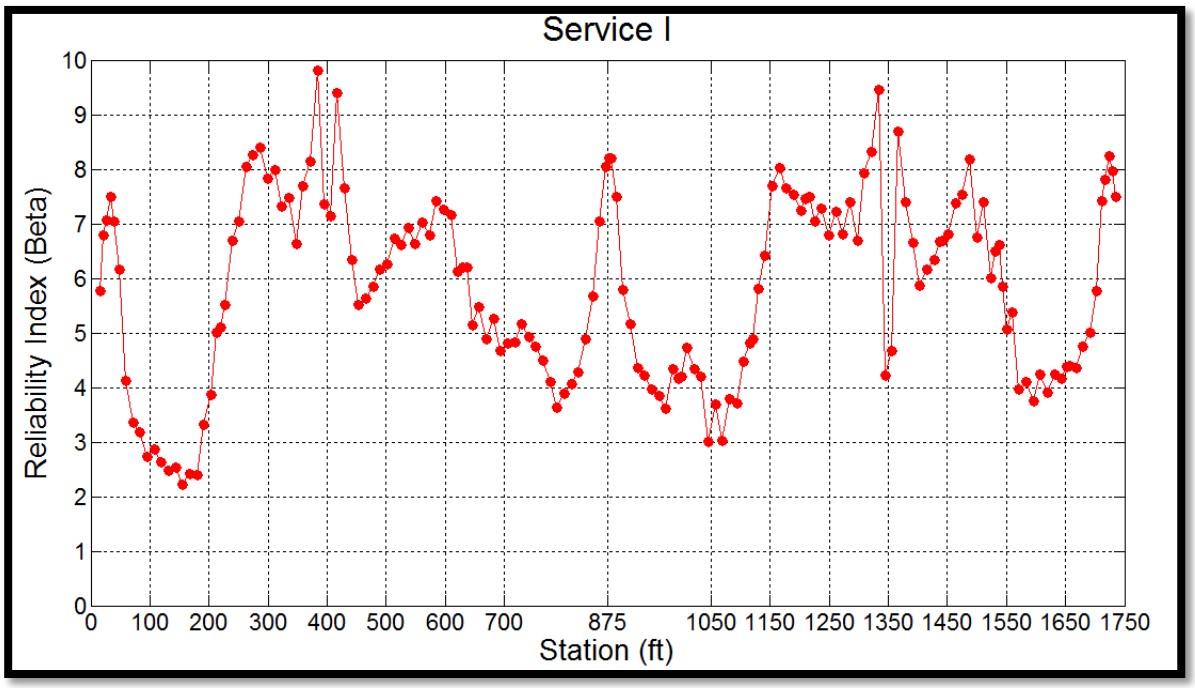

Figure 7.4. Reliability Indices Along Edge Girder for Service I-Flexural Compression

7.7 Discussion and Conclusion

Bridges designed according to the AASHTO LRFD code are intended to achieve a consistent level of safety. That level of safety is related to a probability of failure, which is represented by a target reliability index. The code was calibrated for the strength limit state and a target reliability (β_T =3.5). Therefore, performing reliability analysis on the design load effects (dead and live loads) and resistance should achieve at least the target reliability (β_T =3.5).

To evaluate the IRIB in terms of reliability, design values were used and a Monte Carlo Simulation was conducted. The results of the reliability analysis for Strength I limit state (Figure 7.2) showed that reliability index of 3.57 at the controlling rating location of the bridge. The results are consistent with the LRFD

code requirements. The code was not calibrated for the service limit states; therefore results cannot be compared to the target reliability. However, in discussion with Professor Andrzej S. Nowak, an expert in reliability analysis for bridges, he mentioned that the reliability indices for service limit states should be at least greater than zero (A. S. Nowak, personal communication, October 27, 2014). The results (Figures 7.3 and 7.4) show reliability indices greater than zero.

The IRIB is a new bridge and the results are expected to achieve the code requirements for all limit states. However, the main goal behind the reliability analysis is to obtain the reliability indices based on design loads and to later compare those results to the reliability indices based on SHM data (Chapter 9). The reliability indices obtained in this chapter will be used as a lower limit for the reliability indices obtained by SHM data (Chapter 9).

Chapter 8

COMPUTING CONTINUOUS RATING FACTORS USING CONTINUOUS STRUCTURAL HEALTH MONITORING DATA

8.1 Introduction

The process of determining the live load carrying capacity of a bridge is defined as load rating. This process includes determining section capacity, and any loads that affect the bridge, such as dead load, live load, etc. and enter them into the rating equation to obtain a factor called a "rating factor." The rating factor determines the bridge's live load carrying capacity relative to the applied live load effects.

The AASHTO code has established limit state functions for designing bridges. A limit state is defined as a condition of a structure beyond which it no longer fulfills the relevant design criteria. The AASHTO code defines the various design limit states and their associated load combinations in Table 3.4.1-1(AASHTO 2011). The safety factors applied to the loads come from studies of reliability and/or experience or empirical studies. Therefore, there are uncertainties in the estimation of the design loads. Structural health monitoring techniques can help define the actual load effects on bridges and reduce that uncertainty between the design loads and the actual loads.

One of the important loads that effects bridges, especially long span bridges is thermal load. Thermal loads can have a major effect and must be taken into account during the design and evaluation process (Zhou & Yi 2013). Indeed, the AASHTO code requires designing for thermal loads. The strength limit state, which is the common controlling limit state for designing bridges among other limit states, takes

into consideration thermal effects due to uniform and gradient temperature variations in the design process. In general, based on the bridge location, the code provides the designer with a maximum rise and a minimum fall in temperature that the bridge needs to be designed for. While thermal effects usually do not control the design of conventional bridges, even for these typical structures, temperature variations are used for designing the movements of the bearings at the expansion joints.

According to the AASHTO code, thermal effects should be considered for designing and rating long span bridges. The IRIB was designed for a 35^{o}F temperature rise, and a 45^{o}F temperature fall. The design temperatures were also used to account for the bearing movements at the expansion joints.

This chapter presents a new approach for obtaining rating factors using continuous structural health monitoring data. The continuously collected strain data from strain sensors in the west and east edge girders of the IRIB bridge includes the effects of thermal loads, live loads, prestressed losses, and concrete creep and shrinkage. The strain data is converted to continuous structural forces and stresses, and then used in the rating equations to obtain continuous rating factors based for the IRIB for various limit states.

8.2 Literature Review

According to the AASHTO LRFR code (AASHTO 2011), the rating factor for all limit states shall be determined according to the following formula:

$$RF = \frac{C-\gamma_{DC}DC-\gamma_{DW}DW-\gamma_{EL}(P+EL)-\gamma_{FR}FR-\gamma_{CR}(TU+CR+SH)-\gamma_{TG}TG}{\gamma_{LL}(LL+IM)} \quad Equation\ 8.1$$

Where,

- C =Capacity

- DC= Dead load of structural components
- DW= Dead load of superimposed loads
- P= Permeant effects other than dead load
- EL= Permeant effects of erection forces
- FR= Forces from fixed bearings
- TU= Uniform temperature effects from fixed bearings or frame action
- CR= Creep
- SH= Shrinkage
- TG= Thermal gradient
- LL= Live load
- IM= Dynamic load allowance
- γ= Load factors for the associated effects

In addition to the common major loads (live load and dead load) that are included in the conventional rating equation (Equation 6.1), the extended equation takes into consideration the effects of uniform and gradient temperature changes, concrete creep and shrinkage, prestressed losses, and forces from fixed bearings. In general, when rating conventional bridges, uniform and gradient temperature effects are ignored due to their small effects compared to the live and dead loads. In fact, the AASHTO Manual for Condition Evaluation of Bridges (MCEB) states that the thermal effects should not be considered in calculating load ratings except for long span bridges and concrete arches (AASHTO 2011). Also, the AASHTO MCEB states that environmental loads shall be included only at the operating level.

The Federal Highway Administration (FHWA) requires an LRFR rating factor greater than 1.0 for all applicable limit states. From the time of design, a bridge's rating factor (LRFR at design using HL-93 as a live load) does not change over time until changes occur in bridge components (i.e. section loss, damage, prestressed losses, etc.)

Research conducted (Lai 2013) on the thermal effects on load rating of reinforced concrete arch bridges shows that the eccentricity (moment to axial force ratio), which is used to extract the section capacity from an interaction diagram for a beam-column element, is an important factor effecting load ratings of reinforced concrete arch bridges. Lai's research showed that the eccentricity value could be affected by thermal loads, and because of the non-linearity of the interaction diagram, the eccentricity ratio could play a significant role in changing the rating factor calculation for the strength limit state. However, Lai obtained structural forces from limited temperature measurements applied to a finite element model. Also, Lai focused on calculating rating factors for the strength limit state.

In general, designers use finite element models to estimate thermal load effects; only a few have tried to utilize actual measurements of structural strains and stresses caused by thermal loads. Also, most of the prior research is based on non-continuous strain readings and/or temperature measurements applied to finite element models. Furthermore, developing a model that represents the actual behavior of a bridge is not an easy task due to the complexity in modeling boundary conditions and the various assumptions that need to be made during the modeling process.

8.3 Contribution of this Chapter

This chapter presents a new approach for obtaining rating factors based on continuous SHM data. This rating process includes measuring the effects of live loads, thermal loads, prestressing losses, and using the measurements to obtain rating factors at the sensor locations. While it is known that the thermal effects were considered in designing the bearings and the expansion joints of the IRIB, it is not clear whether or not thermal effects were used in the rating process. In Chapter 6, the decomposition of limit state values submitted by the designer into dead loads and live load effects was described. The loads were then used to rate the bridge at the design level for different limit states. This produced values that were nearly identical to the submitted design rating factors (indicating that thermal effects were not included).

The AASHTO Manual for Condition Evaluation of Bridges states that the environmental loads shall be included for the operating level. This chapter shows how continuous rating factors at the sensor locations can be computed by using the continuous measured data. More specifically, measured strain and temperature data in the west and east edge girders of the IRIB are used to produce continuous rating factors for different limit states.

This chapter also presents a new approach of presenting SHM data to transportation agencies. The IRIB SHM system has been in service since May 2012. A huge amount of continuous data has been recorded since that time. The continuous rating factor is an easy approach for presenting the continuous SHM data to DelDOT; the approach converts monitored strain and temperature values to simple rating factors that bridge engineers can easily understand. This allows the bridge owner to develop a comprehensive understanding of the effects on the bridge of live loads or thermal loads. Furthermore, the author shows an approach to estimate the actual forces and

stresses caused by the short term loads such as live loads and long term loads such as uniform and gradient temperature, prestressing losses, from SHM data and use them in the rating equation.

8.4 Methodology of Extracting Structural Forces and Stresses from SHM Data

Strain is measured in the east and west edge girders of the IRIB at 11 different locations along the length of the bridge. The longitudinal positions approximately correspond to the 1/8 points of the main span and back spans. At each location, strain is measured at four unique locations; the top and bottom of both the east and west edge girders. Therefore, the edge girder strain is measured at 44 unique locations. At any given edge girder location the strain is measured in the longitudinal direction of the bridge at approximately 5 inches from the top and bottom of the girder as shown in Figure 3.5. The strain is computed based on a change in the wave length of the strain and temperature of the fiber bragg gratings. Equation 8.2 and 8.3 show strain and relative temperature calculation in the SHM system, respectively.

$$\epsilon_{Total} = 10^6 \left[\frac{\left(\frac{\Delta\lambda}{\lambda_\circ}\right)_{strain} - \left(\frac{\Delta\lambda}{\lambda_\circ}\right)_{Temp}}{F_G} \right] + \left[\frac{\left(\frac{\Delta\lambda}{\lambda_\circ}\right)_{Temp}}{S_T} * CTE_{Temp} \right] \quad Equation\ 8.2$$

Where,

- $\Delta\lambda$= Wavelength shift, nm
- $\lambda_\circ$= Nominal wavelength, nm
- F_G= Gage factor, factory value
- S_T= Temperature sensitivity, pm/^{o}C
- CTE_{Temp}= Coefficient of thermal expansion for the temperature FBG mount, µm/m-^{o}C

$$\Delta T_{subst} = \frac{(\Delta\lambda/\lambda_o)_{Temp}}{S_T} \quad Equation\ 8.3$$

Where,

- ΔT_{subst}= Change in temperature of the substrate, ^{o}C

The strain calculated in Equation 8.2 represents the total strain and is a combination of mechanical and thermal strains. Figure 8.1, which illustrates a simple beam case with a rectangular cross-section subjected to different load cases, is used to explain the physical meaning of the total strain and its components. The strain obtained for each case shown is explained separately. The combination of these simple cases can be used to better understand the components of the total strain and its physical meaning.

We will first assume that the simply supported beam has a rectangular cross section with a top and bottom Fiber Bragg Grating (FBG) strain sensors at the surface level. The section depth is h, the distance from the top sensor to the neutral axis is c', and the distance from the bottom surface to the neutral axis is c. See Figure 8.2.

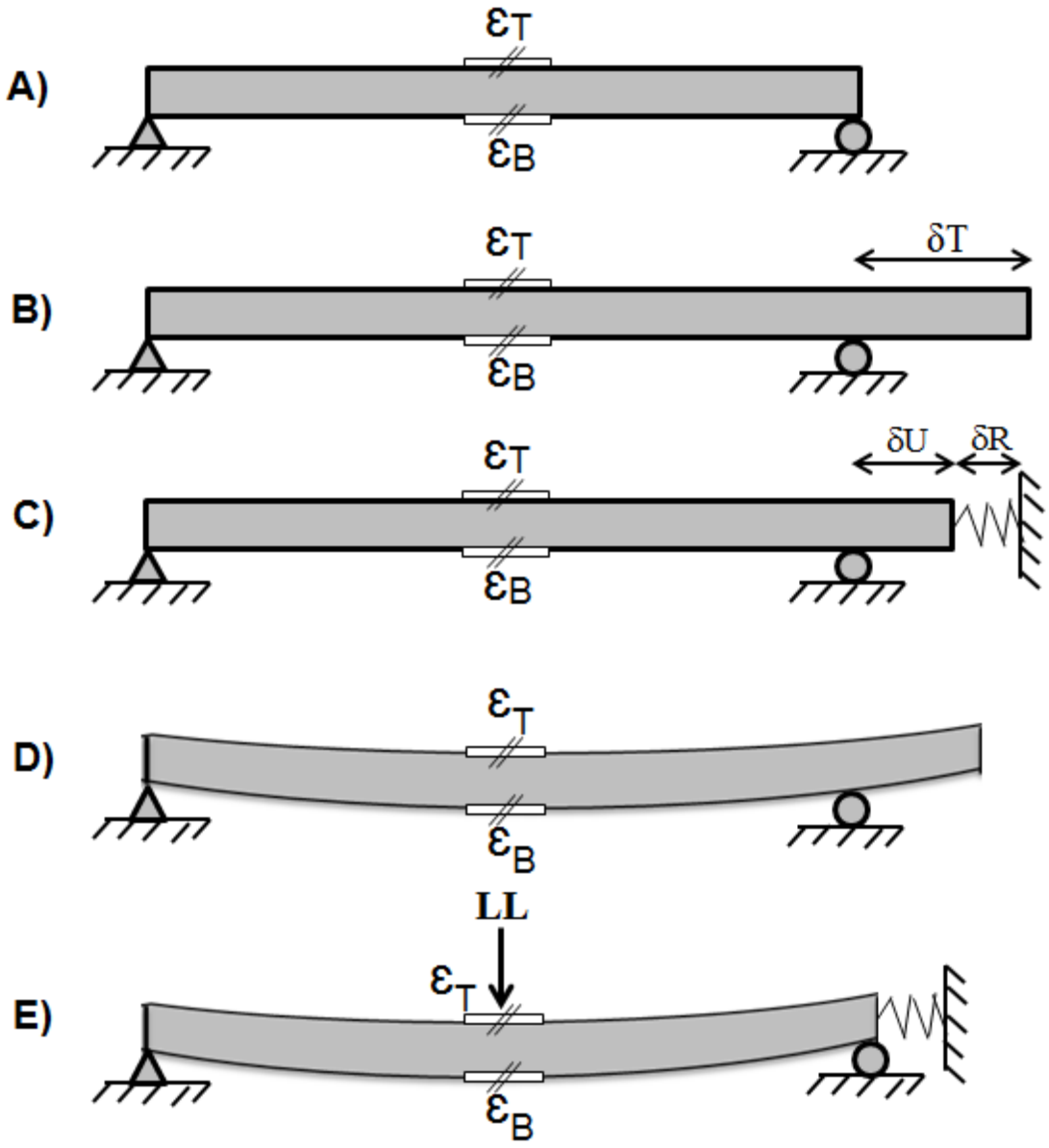

Figure 8.1. Measured Strain from a Top and Bottom Sensors for a Simple Beam Subjected to Different Load Cases

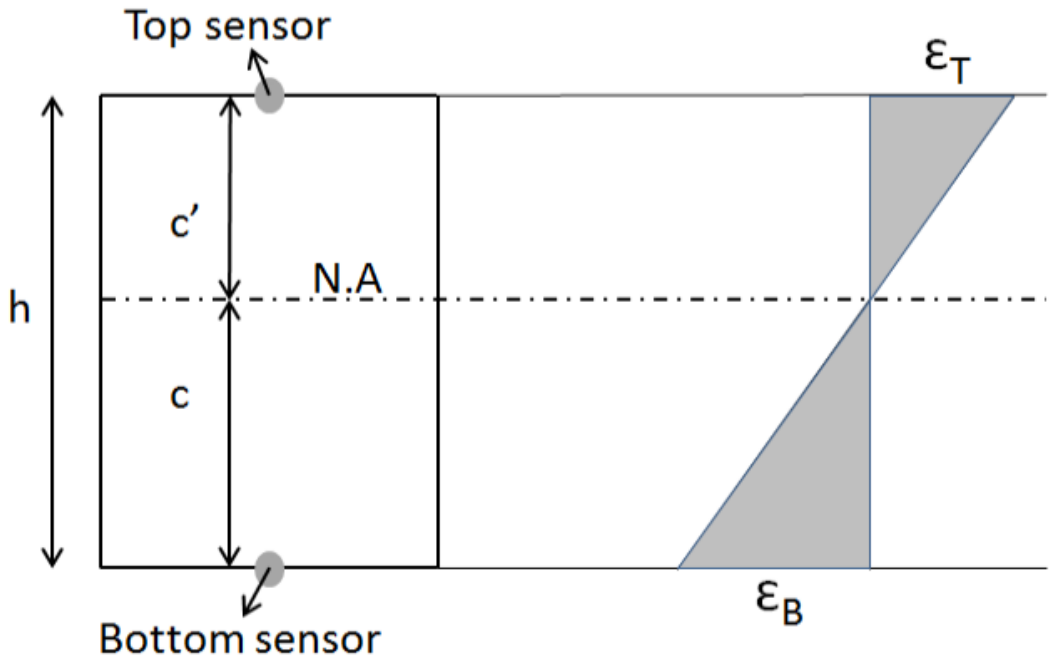

Figure 8.2. Strain Distribution Along the Cross Section for the Superposition Case

Case A: represents a simply supported beam, with a hinge at the left end and a roller at the right end. The beam is not subjected to any temperature change or any applied loads. This will lead to zero strain and temperature at both sensors.

$\Delta T_T = \Delta T_B = 0$ $\varepsilon_T = \varepsilon_B = 0$

Where,

- ε_T and ε_B = Strain readings at the top and the bottom sensors, respectively
- ΔT_T and ΔT_B = Relative temperature readings at the top and bottom sensors, respectively

Case B: represents the same beam subjected to a positive uniform change in temperature. Since the beam is free to expand, no stress is developed in the beam. The

beam will expand to the right side. Due to the uniform change in temperature, the measured top strain is equal to the measured bottom strain and that is equal to the change in length over the original length.

$\Delta T_T = \Delta T_B > 0$ $\varepsilon_T = \varepsilon_B = \delta T/L > 0$

Where,

- δT= Change in length
- L= Original length

Case C: A boundary condition represented by a horizontal spring is applied to the right side. The beam is subjected to a positive uniform change in temperature. As a result, a mechanical strain and a thermal induced strain are developed. The mechanical strain is a result of the developed axial force (P) as a result of the boundary condition.

$Ks > 0$ $\Delta T_T = \Delta T_B > 0$

Where,

- Ks= Spring stiffness

$\varepsilon_{Total} = \varepsilon_T = \varepsilon_B = \delta U/L > 0$

$\varepsilon_{Total} = \varepsilon_{mechanical} + \varepsilon_{thermal}$

$\delta U/L = (-Ks*\delta U/EA) + \alpha*\Delta T$

$P = Ks*\delta U$

Where,

- δU= Unrestricted change in length
- E= modulus of elasticity of the beam material
- A= Area of the cross section
- α= Coefficient of thermal expansion of the beam material

- ΔT= Change in temperature for top or bottom sensor (Uniform temperature)

The first part of the equation represents the mechanical strain. This strain would not have been developed if there were no boundary condition (Ks) and the beam was free to expand (i.e. Ks=0). The second part of the equation is the thermal strain. This strain can be calculated, in all cases, as the change in the temperature multiplied by the coefficient of thermal expansion of the beam material.

Case D: Assume that the beam is free to expand at the right end and there is a positive change in temperature at the bottom sensor, and a lower positive change in temperature at the top sensor (gradient temperature effect). The beam is free to expand and deform, but no stress is developed. Because there is a temperature gradient the beam attains some curvature.

$\Delta T_B > \Delta T_T > 0$ $\varepsilon_T = \alpha * \Delta T_T \neq \varepsilon_B = \alpha * \Delta T_B$

Case E: Assume a point load is applied at the mid-span of the beam and the change in temperature is zero.

$\Delta T_T = \Delta T_B = 0$ $LL > 0$

$\varepsilon_B = M*c/EI$

$\varepsilon_T = -M*c'/EI$

Where,

- M= Moment at mid-span developed due to a point live load (M=LL*L/4)
- c= Distance from bottom surface to the neutral axis
- c'= Distance from top surface to the neutral axis
- I= Moment of inertia
- A= Cross sectional area

Assume superposition of cases C, D and E. Then the monitored strain can be calculated according to the following equations:

$$\varepsilon_T = -\frac{Mc'}{EI} + \frac{P}{EA} + \alpha\Delta T_T \quad Equation\ 8.4$$

$$\varepsilon_B = +\frac{Mc}{EI} + \frac{P}{EA} + \alpha\Delta T_B \quad Equation\ 8.5$$

Where,

- ε_T = Measured strain at the top sensor
- ε_B= Measured strain at the bottom sensor
- M= Moment results due to a point load (LL*L/4)
- E= modulus of elasticity
- I= Moment of inertia
- P= Axial force, due to the spring constant multiplied by the unrestricted displacement (Ks*δU)
- A= Cross-sectional area
- α= Coefficient of thermal expansion
- ΔT_T= Change in temperature at the top sensor
- ΔT_B= Change in temperature at the bottom sensor
- c= Distance from bottom sensor to the neutral axis
- c'= Distance from top sensor to the neutral axis

The computed strain in the previous equations represents the total strain, which is composed of mechanical strain and thermal strain due to the temperature change and the applied load effect. In general, the strain induced by temperature can be classified into two categories, strain in a force free status and strain caused by stresses induced

by temperature and a restrained boundary condition. Thus, the total strain that an FBG sensor measures has two parts; the first part is the free status (α*ΔT) and the other component is the mechanical strain due to the stresses induced by temperature and applied loads.

The SHM system at the IRIB records the total strain computed by the previous equation. Even though the type of loads in the case for IRIB are more complicated than the simple beam cases due to the existence of prestressing forces losses, complicated live loads, environmental loads, and other effects, but all of the loads fall in the categories of structural forces (moment and axial force) that were presented in the simple beam cases. By studying the simple beam case one can gain a better understanding of the total strain that is measured, as well as the strain that should be considered in the rating process. Figure 8.2 shows the total strain distribution along the assumed cross section.

The top and bottom sensors measure strain and relative change in temperature. By solving the two equations (8.4 and 8.5), if the section properties are known it is possible to determine the structural forces (moment and axial force). Note that the top and bottom sensors measure the ΔT_B, ΔT_T, ε_B, and ε_T, continuously. By subtracting equation 8.4 from equation 8.5, the moment obtained from SHM data becomes:

$$M_{SHM} = \frac{EI}{h}[(\varepsilon_B - \varepsilon_T) - \alpha(\Delta T_B - \Delta T_T)] \quad Equation\ 8.6$$

Where,

- M_{SHM}= Moment obtained by SHM data

To determine the axial force (P), by rearranging equation 8.6 it becomes:

$$\frac{P}{A} = E\varepsilon_B - E\alpha\Delta T_B - \frac{M * c}{I} \quad Equation\ 8.7$$

Substituting the moment from equation 8.6 yields:

$$\frac{P}{EA} = \varepsilon_B - \alpha\Delta T_B - \frac{c}{h}[(\varepsilon_B - \varepsilon_T) - \alpha(\Delta T_B - \Delta T_T)] \quad Equation\ 8.8$$

By expanding and rearranging the terms one gets:

$$\frac{P}{EA} = \varepsilon_B - \alpha\Delta T_B - \frac{c}{h}\varepsilon_B + \frac{c}{h}\varepsilon_T + \alpha\frac{c}{h}\Delta T_B - \alpha\frac{c}{h}\Delta T_T \quad Equation\ 8.9$$

$$\frac{P}{EA} = \varepsilon_B\left(1 - \frac{c}{h}\right) - \alpha\Delta T_B\left(1 - \frac{c}{h}\right) + \frac{c}{h}(\varepsilon_T - \alpha\Delta T_T) \quad Equation\ 8.10$$

$$\frac{P}{EA} = \frac{c'}{h}(\varepsilon_B - \alpha\varepsilon_B) + \frac{c}{h}(\varepsilon_T - \alpha\varepsilon_T) \quad Equation\ 8.11$$

$$P_{SHM} = \frac{EA}{h}[c'(\varepsilon_B - \alpha\Delta T_B) + c(\varepsilon_T - \alpha\Delta T_T)] \quad Equation\ 8.12$$

Where,

- P_{SHM}= Axial force obtained by SHM data

Since the structural health monitoring forces (M_{SHM} and P_{SHM}) can be obtained, the structural health monitoring stresses based on SHM data can also be calculated. The strain collected by an FBG sensor has two components, strain free status ($\alpha*\Delta T$) and the strain caused by the stresses induced by temperature and other loads and by restrained boundary conditions. However, for the purpose of calculating a rating factor for the service limit states, only the stresses induced by temperature and restrained boundary conditions should be only considered. The strains due to the free status case should be removed.

Equations 8.4 and 8.5 can be rearranged to get the SHM stresses directly by subtracting the $\alpha*\Delta T$ term and multiplying by the modulus of elasticity. This yields the new equations which are presented in equations 8.13 and 8.14. The left term in

equations 8.13 and 8.14 represents the SHM stresses in the top and the bottom sensors, respectively.

$$E\varepsilon_T - E\alpha\Delta T_T = -\frac{M * c'}{I} + \frac{P}{A} \quad Equation\ 8.13$$

$$\mathrm{E}\varepsilon_B - E\alpha\Delta T_B = +\frac{M * c}{I} + \frac{P}{A} \quad Equation\ 8.14$$

Equations 8.6, 8.12, 8.13 and 8.14 show the structural forces and the stresses based on the collected SHM data. Due to the continuity of the SHM data, these structural forces and stresses are of vital importance for the bridge evaluation process.

8.5 Data Collection for Rating Purposes

The conventional rating equation (Equation 6.1) only takes into consideration section capacity, dead loads, and live loads. As a result, a rating factor can be computed for a bridge once it is designed, and that rating factor will not change over time until changes to the capacity (or less likely to the dead load or live load) occur. Changes to the section capacity could be due to section loss, damage, prestressed losses, etc.

Another rating process that has been developed in recent years is called In-Service Rating Factor (ISRF). In this rating process, the conventional rating equation is used with the design capacity, design dead loads, and field measured "in-service" live loads (instead of the design live loads). The ISRF proposed in this chapter is different from the conventional ISRF, because it also includes the long term effects in the numerator portion of the equation. The in-service load effects can be obtained using the Equations 8.6, 8.12, 8.13, and 8.14.

SHM data contains vital information about the bridge's behavior, including environmental effects (thermal, wind, etc.), prestressing losses, concrete shrinkage,

etc. The major contribution of this chapter is to compute SHM forces and SHM stresses from continuous SHM data to produce a continuous rating factor over time at each strain sensor location.

In order to explain the rating methodology and associated rating equations, two protocols for collecting SHM data are proposed in this chapter. The protocols were established to enable the application of two new rating methods. The two protocols are applied to the SHM system of the IRIB and been in service for 12 months up to date. The following section explains the two protocols of data collection and the need behind each of them.

8.5.1 Protocols for Data Collection

The strain measured by a strain sensor represents the total amount of strain at that time. The total strain is composed of mechanical strain and thermal strain. The thermal strain is always calculated by multiplying the coefficient of thermal expansion by the change in temperature. The mechanical strain is due to long term stresses developed as a result of boundary conditions, such as temperature change, prestressed losses, concrete shrinkage, etc. and/or short term stresses such as live loads, earthquakes, gust wind, etc.

The type of load effects captured in the measured data depends upon the frequency at which the data is collected. Long term effects can best be captured by recording data at low frequencies while short term effects can best be captured by recording data at high frequencies. As a result, two protocols for data collection are being used. They will be referred to as the low frequency and high frequency protocols.

8.5.1.1 Low Frequency Data Collection Protocol

In order to determine long term load effects, a low frequency data collection protocol is utilized. The low frequency protocol is based on data sampled at 125 Hz and then averaged and saved at 10 minute intervals (the data over the 10 minute interval is averaged to create one data point per sensor). The SHM system on the IRIB saves the low frequency data from all sensors for a one day period in a single text file. The dominant load effect captured in the low frequency strain data is due to thermal effects. The collected data also is affected by prestressed forces losses, concrete shrinkage, and other long term effects. A sample of the measured yearly and weekly low frequency data for sensor SW_22 is shown in Figure 8.3-A and -B, respectively.

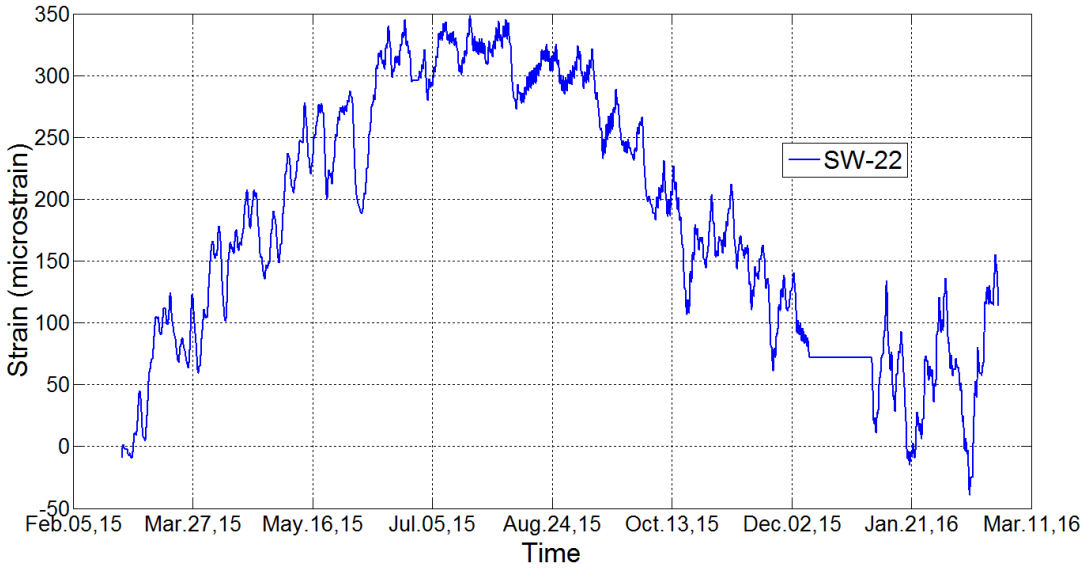

Figure 8.3-A. A Year Sample of the Low Frequency Data for Sensor SW_22

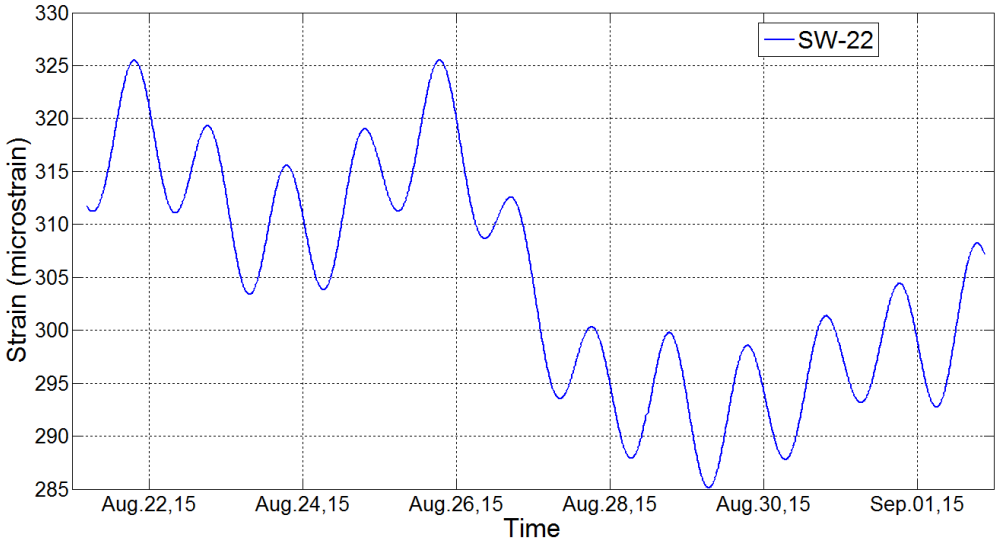

Figure 8.3-B. A Week Sample of the Low Frequency Data for Sensor SW_22

It is obvious from the low frequency data shown in Figure 8.3-A and -B that the thermal effects dominate the observed strains over this long and short period of time. The trend of increasing strain was due to the increasing temperature from February through August. While the strain due to the thermal effects is much higher than other long term load effects, the low frequency data does have other long term effects embedded within the readings. These effects can be hard to see because they are overwhelmed by the thermal effects.

The low frequency protocol does not capture short term load effects such as the live loads or wind induced effects due to the effective sample rate (once every ten minutes) is too low to capture these effects. In both rating equations (conventional and extended), the live load is used in the denominator of the equation. Therefore, the thermal effects captured in the low frequency data should be included in the numerator portion of the rating equation.

The low frequency data that is collected can be used directly in the rating method as will be explained later in this chapter. By doing so, the obtained rating factors can be compared to the design rating factors, which are based on design capacity, design dead load, and design live load. For long term monitoring periods, the rating factors computed based on measured data can show very vital information about the bridge and its ability of carrying the design live loads.

8.5.1.2 High Frequency Data Collection Protocol

In order to capture short term load effects, a high frequency data collection protocol is utilized. When trucks cross a bridge, the time to cross the bridge, or to pass a location of interest, can be very short. For the IRIB, the SHM system can collect data up to 125 Hz on Interrogator A and up to 250 Hz on Interrogator B. To minimize the size of the resulting data files, but to ensure that the frequency was suitable to capture fast moving vehicles, a recording frequency for the high frequency protocol of 25 Hz was selected. This frequency was confirmed and justified to be sufficient for trucks passing the bridge with high speed. This was confirmed by studying the data of a dynamic passes from the conducted load tests. All strain and temperature sensors in the edge girders are collected at this rate and the data is saved in hourly text files.

The rating equations use the live load effect in the denominator portion of the equation. The In-Service Rating Factor (ISRF) can be obtained directly by using the high frequency data in the denominator portion of the rating equation. When doing so, thermal effects can also be included in the numerator portion of the equation to get rating factors that reflect both actual live loads and thermal effects. These high frequency rating factors are explained later in this chapter.

Samples of the high frequency data are shown by the blue continuous line in Figures 8.4 and 8.5. Note that the high frequency data also includes the thermal effects and the other long term load effects. In order to separate the short term loads from the long term loads, signal processing is required.

8.5.1.2.1 Signal Processing

As mentioned, the high frequency data includes short and long term load effects. It also includes noise from the SHM system. In order to clean up the signal and the eliminate embedded noise, a moving average process is conducted. Also, decomposition of the signal into short term load effects and long term load effects is necessary. A smoothing average function is a good technique to eliminate the noise from the signal. Several parametric studies were performed on data samples to make sure that the processed signals were not losing the actual measured data. As a result of those parametric studies, a smoothing function over a 4-second (100 point intervals) moving average was selected and used in the rating process. In our case, the moving average function in Matlab is used over the 100 point intervals.

Figures 8.4 and 8.5 show samples of the high frequency collected data for sensors SW_7 and SW_8 (top and bottom strain sensors at midspan) during the first week of March 2015. The raw data is represented by the blue continuous lines in both figures and labeled as "Total." The blue line shows the slow changes caused by temperature changes superimposed on top of that are the live load effects (seen as spikes in the raw data). These spikes are most evident in Figure 8.5. The spikes in Figure 8.5 are mostly in the positive direction, and that is because the sensor is on the bottom of the girder and experiences tension when a vehicles crosses.

After applying the smoothing function on the raw data, the resulting data (shown in red) represents the strain due to the long term effects and is labeled the "Trend." In order to get the short term load effects one can subtract the "Trend" data from the "Total" data. The resulting data (shown in green) represents the short term strain which is mainly caused by traffic on the bridge.

The short term data is continuous over time. The short term data is of particular interest when peaks occur as these peaks likely represent live load effects (most likely heavy vehicles crossing the bridge). In dealing with the data, a threshold value was established above which the peaks were of interest (meaning the live loads were significant). The threshold values were determined for each sensor based on live load strains measured during the controlled load tests.

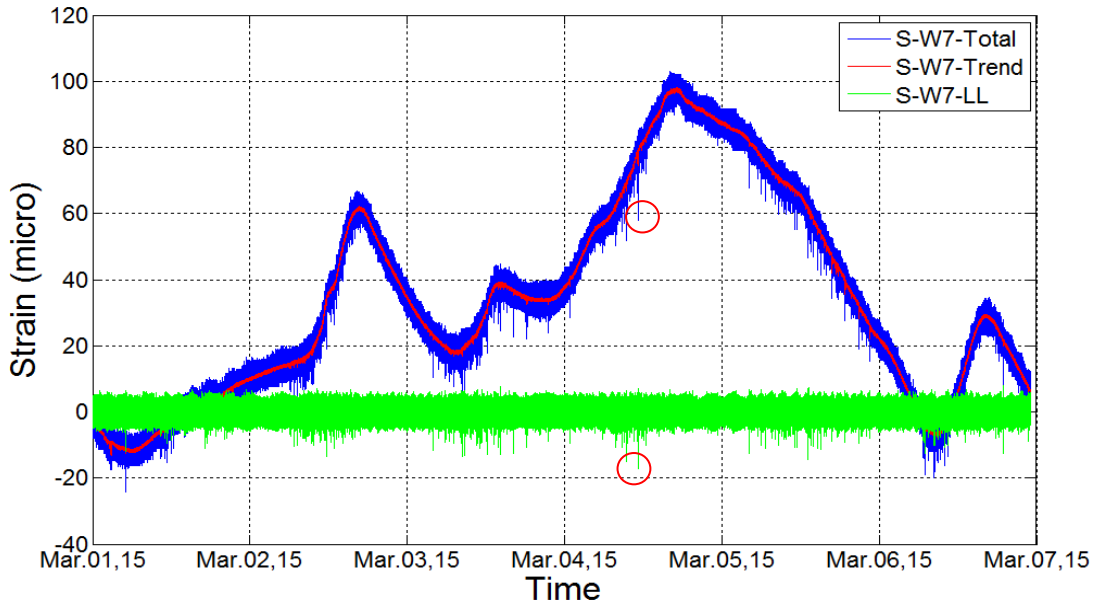

Figure 8.4. Sample of High Frequency Signal for Sensor SW_7 and Signal Processing Shows Long and Short Terms Signals

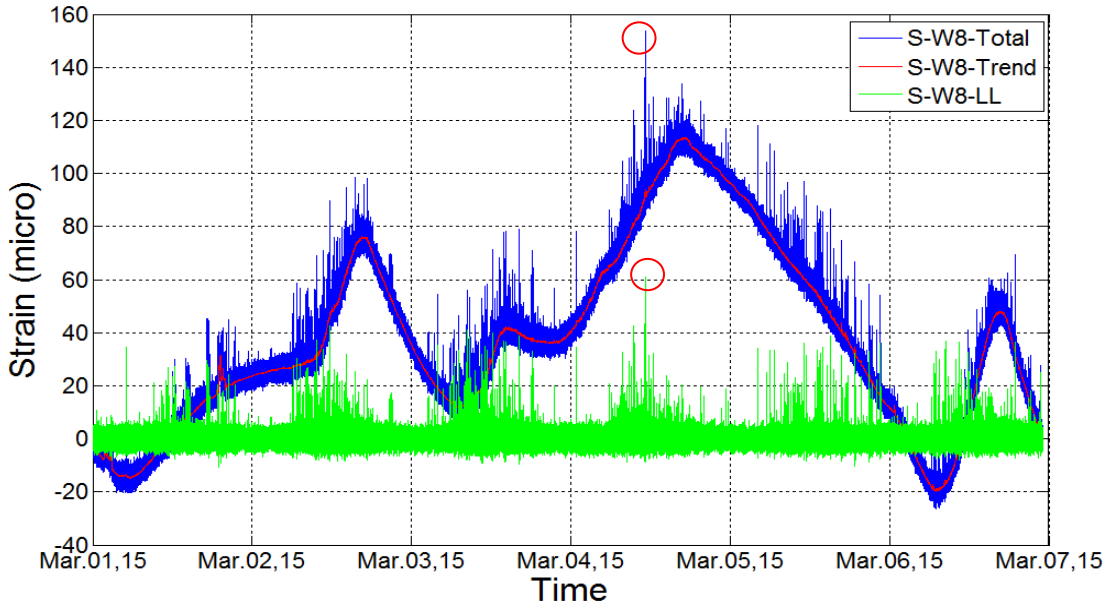

Figure 8.5. Sample of High Frequency Signal for Sensor SW_8 and Signal Processing Shows Long and Short Terms Signals

8.6 Updated Rating Equations with SHM Forces and Stresses

The new updated rating equations include forces and stresses from the collected SHM data. According to the previous section, some of that data is based on a low frequency (long term loads) and/or high frequency (short term loads). The long term loads are used in the numerator portion of the new rating equations and the short term is used in the denominator portion of the rating equation.

As a result, two new methods for ratings are proposed in this section. The two rating methods are different from each other and they can be used individually or in combination to evaluate the health or load carrying capacity of the bridge.

8.6.1 Low Frequency Rating Method

The first method is based on the monitored low frequency data, which is effected only by long term loads. In this approach, the capacities, dead loads, and live

loads, are taken from the design information. However, the extracted forces and stresses based on the SHM data are incorporated into the dead load term in the numerator. By adding the low frequency data into the numerator portion of the rating equation, a continuous rating factor that varies with time can be obtained. The new rating factor thereby includes the long term change in dead load forces and/or stresses due to thermal effects, creep, shrinkage, prestressed losses, etc.

8.6.2 High Frequency Rating Method

The second rating method uses design capacities and dead loads, while incorporating the extracted change to dead load forces or stresses captured by the SHM data caused by long term load effects, and also incorporating live load forces or stresses captured by the high frequency SHM data. In this case, the results represent the actual rating factors based on the current traffic taking in consideration the long term load effects. In addition, the new rating factor can be compared to the conventional In-Service Rating Factor (ISRF).

As mentioned earlier, according to the Manual for Bridge Evaluation (MBE), prestressed concrete bridges are rated for three different limit states. Since the Indian River Inlet Bridge (IRIB) is a prestressed concrete bridge, the following sections will present the conventional rating equations used for rating prestressed concrete bridges and compare those ratings to the new method of rating utilizing SHM data.

8.6.3 Service I and Service III Limit States

The conventional rating equation for Service I and Service III limit states is:

$$R.F = \frac{C - f_{DL}}{f_{LL}} \quad Equation\ 8.15$$

Where,

- C= Capacity, -0.6 fc' for Service I (flexural compression), and 3√fc' for Service III (flexural tension) limit state
- f_{DL}= Dead load stresses with the appropriate factor of safety from design level
- f_{LL}= Live load stresses with the appropriate factor of safety from design level

Using design stress values leads to a constant rating factor that does not change with time. The only way the rating will change over time is by incorporating a change to the section capacity due to section loss, losses in prestressed forces, etc.

The equation for the low frequency rating method, which uses the long term SHM data, is expressed as:

$$R.F = \frac{C - f_{DL} - f_{SHM-LF}}{f_{LL}} \quad Equation\ 8.16$$

Where,

- $f_{SHM\text{-}LF}$ = Stresses obtained from low frequency SHM data and can be calculated using equations 8.13 or 8.14 based on the sensor location

The $f_{SHM\text{-}LF}$ term represents the measured stresses from long term effects which can be obtained from the collected low frequency data. The primary component of these stresses are thermal effects, however, the data can include other long term phenomena such as prestressed losses and creep and shrinkage effects.

The equation for the high frequency rating method, which uses short term SHM data, is expressed as:

$$R.F = \frac{C - f_{DL} - f_{SHM-Trend-HF}}{f_{LL-SHM-HF}} \quad Equation\ 8.17$$

Where,

- C and f_{DL}= As defined previously
- $f_{SHM\text{-}Trend\text{-}HF}$ = Stresses obtained from high frequency trend SHM data and can be calculated based on equations 8.13 or 8.14 based on the sensor location
- $f_{LL\text{-}SHM\text{-}HF}$ = Stresses obtained from high frequency SHM data and can be calculated based on equations 8.13 or 8.14 based on the sensor location

The new equations 8.16 and 8.17 can be used to obtain the rating factors from Service I and Service III limit states based on the collected SHM data.

8.6.4 Strength I Limit State

The Strength I limit state rates both flexure and axial forces.

8.6.4.1 Flexural

The conventional rating equation for the Strength I limit state is:

$$R.F = \frac{CM - M_{DL}}{M_{LL}} \quad Equation\ 8.18$$

Where,

- CM = Moment capacity with the appropriate factor of safety from design level
- M_{DL} = Design dead load moment with the appropriate factor of safety
- M_{LL} = Design live load moment with the appropriate factor of safety

The equation for the low frequency rating method is obtained by adding the moment obtained by the low frequency SHM data to the dead load design moment. By doing so, the low frequency rating equation becomes:

$$R.F = \frac{CM - M_{DL} - M_{SHM-LF}}{M_{LL}} \quad Equation\ 8.19$$

Where,

- $M_{SHM\text{-}LF}$ = Moment obtained from the low frequency SHM data and can be calculated based on Equation 8.6

In order to obtain the high frequency rating equation for flexure, one must substitute the live load moment obtained by the high frequency SHM data in the denominator of Equation 8.19. By doing so, the new equation becomes:

$$R.F = \frac{CM - M_{DL} - M_{SHM-Trend-HF}}{M_{SHM-HF}} \quad Equation\ 8.20$$

Where,

- CM and M_{DL}= As defined before
- $M_{SHM\text{-}Trend\text{-}HF}$ = Moment obtained from the high frequency trend SHM data and can be calculated based on Equation 8.6
- $M_{SHM\text{-}HF}$ = Moment obtained from the high frequency SHM data and can be calculated based on Equation 8.6

8.6.4.2 Axial

The conventional rating equation for Strength I and Strength II limit states is:

$$R.F = \frac{CP - P_{DL}}{P_{LL}} \quad Equation\ 8.21$$

Where,

- CP = Axial load capacity with the appropriate factor of safety from design level
- P_{DL} = Design axial dead load with the appropriate factor of safety
- P_{LL} = Design axial live load with the appropriate factor of safety

The equation for the low frequency rating method is obtained by adding the obtained axial force effect captured by the low frequency SHM data to the design dead load. By doing so, the low frequency rating equation becomes:

$$R.F = \frac{CP - P_{DL} - P_{SHM-LF}}{P_{LL}} \quad Equation\ 8.22$$

Where,

- $P_{SHM\text{-}LF}$ = Axial force obtained from the low frequency SHM data and can be calculated based on Equation 8.12

The equation for the high frequency rating method for axial load is obtained by substituting the axial effects captured by the high frequency SHM data in the denominator portion of Equation 8.22. By doing so, the new equation becomes:

$$R.F = \frac{CP - P_{DL} - P_{SHM-\mathrm{Trend-HF}}}{P_{SHM-HF}} \quad Equation\ 8.23$$

Where,

- CP and P_{DL}= As defined before
- $P_{SHM\text{-}Trend\text{-}HF}$ = Axial force obtained from the trend high frequency SHM data and can be calculated based on Equation 8.12
- $P_{SHM\text{-}HF}$ = Axial force obtained from the high frequency SHM data and can be calculated based on Equation 8.12

8.7 Example Applying the Low Frequency Rating Method

This example shows calculation of the low frequency rating factors and compares it to the conventional rating factor (LRFR). In this example the low frequency data from sensors S-W7 and S-W8 (located at mid-span of west edge girder) is used to obtain the long term effects by the low frequency SHM data. These

sensors were selected because they represent a critical location and they measure the highest strains in the low frequency data collection protocol.

Table 8.1. Sample of Calculated Low Frequency Rating Factors and LRFR Conventional Rating Factors at the Center of Mid-span Location Sensors (S-W7 & S-W8)

Rating Factors for S-W7 (top) & S-W8 (bottom)		Service I	Service III	Strength I-Flexure	Strength I-Axial
Rating Factor based on Low Frequency SHM Data	Top	4.95	11.68	1.7	1.69
	Bottom	10.98	1.07		
Design Rating Factor (LRFR)	Top	4.68	11.76	1.71	1.71
	Bottom	10.41	1.26		

The top section of the table represents the low frequency rating factors for all applicable limit states. The first two columns (Service I and Service III), Equation 8.13 and 8.14 are applied first to obtain the long term effects stresses. Then Equation 8.16 is applied with the design values to obtain the low frequency rating factors. The last two columns in the table show the low frequency rating factors for strength I limit state for both flexure and axial loads. Equations 8.6 and 8.12 are applied on the low frequency data to obtain the long term moment and axial force, respectively. Then, the results are substituted in Equations 8.19 and 8.22, respectively; to obtain the low frequency rating factor for strength I limit state for flexure and axial force.

The bottom section of the table represents the rating factors based on the conventional rating factor equation (Equation 6.1). These rating factors depend on design information only. By comparing the two sections of the table, a decrease in most of the rating factors can be noted when the long term effects are included. The

controlling rating factor (i.e. lowest rating factor) has changed from 1.26 to 1.07, which represents a reduction of 15.1% of the live load carrying capacity at that location.

8.8 Example Applying the High Frequency Rating Method

The following example illustrates the application of the high frequency rating method using data collected from the IRIB. The data used is shown in Figures 8.4 and 8.5 and was collected from sensors S-W7 and S-W8 (located at mid-span of west edge girder) during the first week of March 2015. Ratings are computed for each of the three limits states using the equations presented in the prior section. The example allows a better understanding of the usefulness of the continuous rating methodology.

The two figures show data collected by the top and the bottom sensors of the west edge girder. The high frequency data is being collected at 25 Hz. This leads to a large amount of data since there are 15.12 $x10^6$ recordings in one week. In the example presented the author shows the calculated rating factors for only one event and compares it to the conventional ISRF.

The one event was recorded on March 4, 2015 at 11:11:07 a.m. The event is marked with red circles in Figures 8.4 and 8.5. A summary of the recorded and analyzed data is shown in Table 8.2. The strain readings are in microstrain and the temperature readings are in Celsius.

Table 8.2. Example One Recorded and Analyzed Data.

S-W7-Total	57.82
S-W7-Trend	78.4
S-W7-LL	-20.55
S-W7-Temp	4.3
S-W8-Total	153.66
S-W8-Trend	92.8
S-W8-LL	60.86
S-W8-Temp	5.5

Note that the total data represents a combination of the trend and the live load effects. The temperature data was collected at high frequency from the temperature sensor. However, the temperature change follows a long term rate change. Therefore, the total temperature signal is decomposed into noise (short term temperature) and trend, which is used and shown in the Table 8.1. In order to understand the difference between the current common rating factor equations and these new rating equations, the author shows the In-Service Rating Factor (ISRF) for the same event, and compares them to the new rating factors from the new approach.

Table 8.3 shows the results of the high frequency rating equations for the top and bottom sensors. Also, the table shows the conventional In-Service Rating Factors for the same event for all applicable limit states at the mentioned sensor locations.

Table 8.3. Sample of Calculated High Frequency Rating Factors and ISRF at the Center of Mid-span Location Sensors (S-W7 & S-W8)

Rating Factors for S-W7 (top) & S-W8 (bottom)		Service I	Service III	Strength I-Flexure	Strength I-Axial
Rating Factor based on High Frequency SHM Data	Top	29.39	12.17	17.1	22.21
	Bottom	55.13	3.81		
Current Common In-Service Rating Factor	Top	27.68	13.88	18.57	25.46
	Bottom	53.28	4.44		

The top section of the table represents the high frequency rating factors for all applicable limit states. In the first two columns (Service I and Service III), Equations 8.13 and 8.14 are applied first on the data shown in Table 8.1 to calculate the long term and short term stresses. Then, the stresses are substituted with the design values in Equation 8.17 to calculate the high frequency rating factors for the top and the bottom sensors. The last two columns in the table represent the high frequency rating factors for strength I limit state for both flexure and axial loads. Equations 8.6 and 8.12 are applied respectively on the Table 8.1 data to calculate the moment and the axial load obtained by the SHM data. Then, the results are substituted in Equations 8.20 and 8.23, respectively, to obtain the high frequency rating factor for strength I flexure and axial limit state.

The bottom section of the table represent the rating factors based on the current common practice, which is the In-Service rating Factors. The long term effects were removed from these rating equations. The high frequency short term data was used to obtain the live load effects. By comparing the two sections of the table, a decrease in most of the rating factors can be noted when the long term effects are included. The

controlling rating factor (i.e. lowest rating factor) has changed from 4.44 to 3.81, which represents a reduction of 14.2% of the live load carrying capacity at that location.

8.9 Automated Matlab Code and Data Analysis

The SHM system on the IRIB has been in service since May 2012. Different kinds of data formatting have been collected from the bridge. Since the new methodology was improved at the end of the February 2015, the required formatting file of the collected data was created at that time too. The two protocols for data collection have been running since the end of February 2015. The data is being collected from all strain and temperature sensors in the edge girders.

The high frequency protocol is running at a frequency of 25Hz and the low frequency data is collected once every ten minutes (average of ten minutes data collected at 125 Hz). The data is recorded continuously. For example, in every second there are 25 recordings are being saved for the high frequency data and a single data point is saved every ten minutes from the low frequency protocol. Rating factors can be calculated based on all applicable limit states for each recorded event as shown in the first example presented in this chapter. Because of the tremendous amount of data that is collected, an automated process was needed for calculating the rating factors. To this end, Matlab codes were developed to perform all the calculations and produce final results that can be easily read and understood by the end user.

Three separate Matlab codes were developed to continuously analyze the data and produce the final results that can be used by DelDOT. The three Matlab codes are described with examples of the final results in the following subsections.

8.9.1 Low Frequency Protocol

The low frequency protocol collects one data point every ten minutes. The ultimate goal behind this low frequency is to collect the long term effects and interpret them into forces and stresses. The long term effects are composed mainly from thermal effects, however, they can include prestressing losses. The low frequency data files contain timestamps for each recorded event, temperature measurements from all sensors, and strain data from all sensors in the edge girders. The data for a one day period is saved in a single text file. All the files are transferred continuously from the SHM system and saved in a single folder.

The low frequency Matlab code reads the data from each file in the folder and creates continuous vectors of the data for each sensor using all the files in the folder. Then, the equations of the low frequency rating protocol are applied to the data and the rating factor values for all limit states are saved in a Matlab file. Due to the continuity of the data, continuous rating factors can be obtained by analyzing the time history signals of the collected data. After that, the calculated rating factors are plotted for the top and the bottom sensor at each location with time.

The low frequency Matlab code saves and places all the figures in one pdf report called “Low Frequency Rating Factors”. This report contains all the low frequency rating factors from all applicable limit states for all sensors located in the edge girders. Figure 8.6 shows an example of the final plot in the Low Frequency Rating Factors report for sensors S-W7 and S-W8 for one year. The rest of the figures from the report can be seen in Appendix D.1.

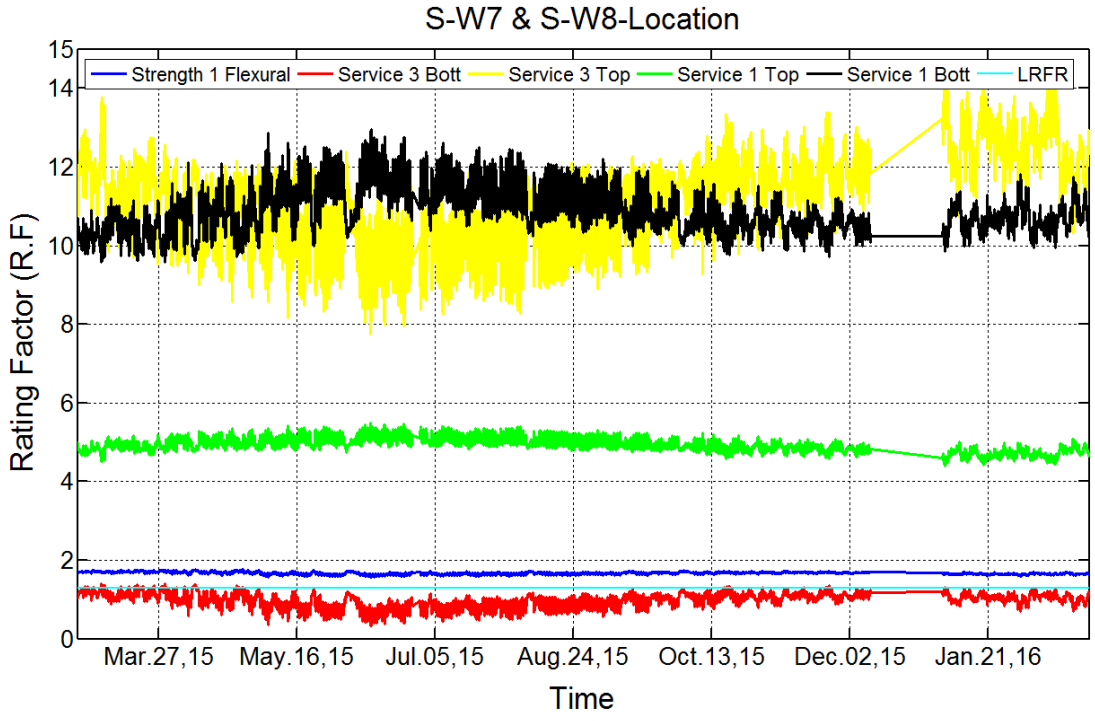

Figure 8.6. Sample of Low Frequency Rating Factors for S-W7 and S-W8

The constant cyanic line represents the rating factor at the design stage (Service III controls in this case), which represents what is currently used by transportation agencies. The dark blue line represents ratings from Strength I- Flexure limit state, these values are based on the measured strain and temperature at the top and bottom sensors. Note, with reference to the other figures of this type in Appendix D, if the lines in the figure are discontinuous, or their titles appear in the legend but lines do not shown in the figure, this means that these values exceed the Y-axis limit of the figure and are less important than the other controlling values in the figure.

8.9.2 High Frequency Protocol

The high frequency rating method is based on the collected high frequency data. The high frequency data is saved at 25 Hz for each temperature and strain sensor. A long term data set has been saved hourly since the end of February 2015. The main goal of the high frequency data collection is to capture the significant live load events (including heavy truck passes and extreme events such as earthquakes, car accidents, etc.).

Once the hour long data sets are collected, data related to significant live load events must be extracted (since much of the recorded data is capturing only low level activity). To do this, a Matlab code was written to extract only information due to events that cause the recorded strain to exceed a predetermined threshold value (a value that indicates a significant load event has occurred). The threshold value was determined based on comparisons of truck weights (>12 kips) and load test data. The Matlab code reads the hourly data files and creates continuous vectors of the data. Then, signal processing is applied for all high frequency data as explained in this chapter. After that, the code calculates the rating factors for all applicable limit states based on the equations for the high frequency rating method.

Since the high frequency rating method is not continuous, but rather is based on discrete events, the results cannot be represented by continuous lines. Therefore, the Matlab code creates figures made up of many individual points each representing a single event. In determining the single point to plot, the Matlab code compares the results from all limit states and reports only the lowest rating factor for the top and the bottom sensor locations. After the Matlab code creates individual figures for each location (pair of top and bottom sensor), it combines all of them in one pdf report called “High Frequency Rating Factors.” This report contains the high frequency

rating factors for all sensors in the edge girders for the controlling limit state. Figure 8.7 shows an example of a plot of High Frequency Rating Factors report for sensors S-W7 and S-W8 for a one year. The rest of the figures from the report can be seen in Appendix D.2.

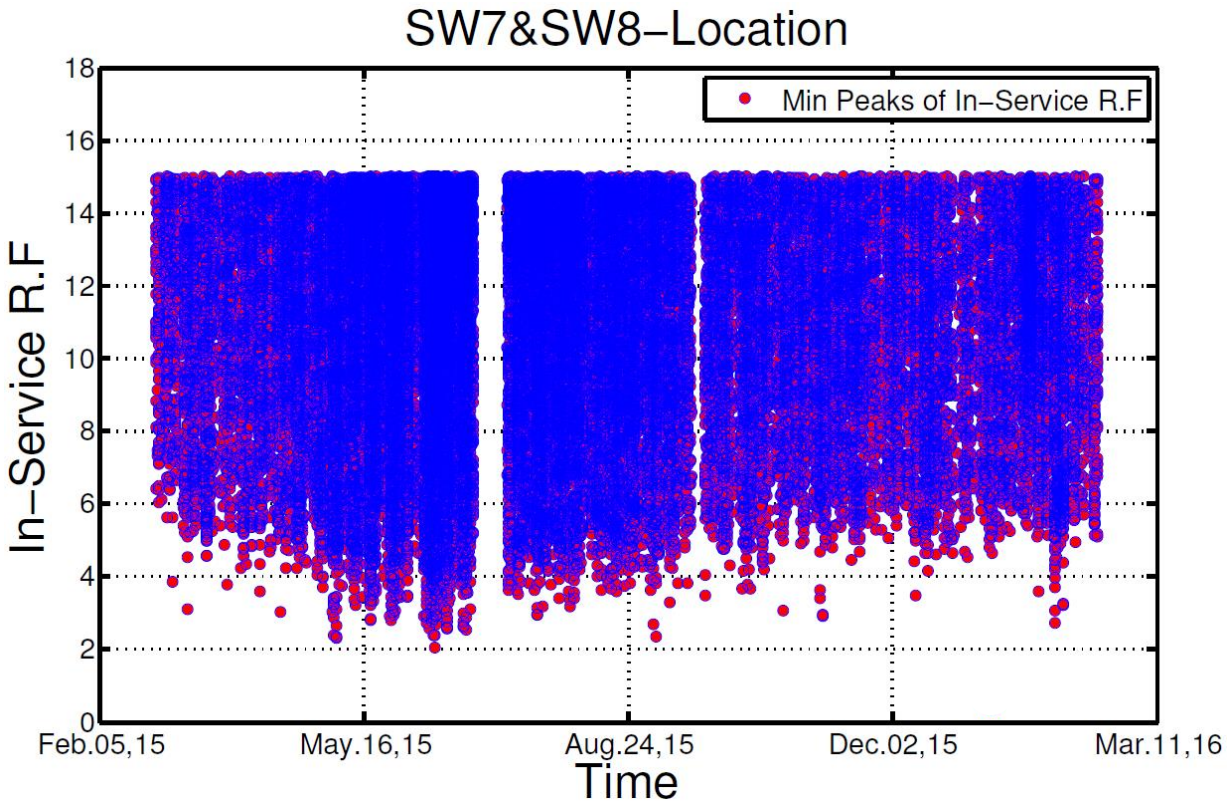

Figure 8.7. Sample of High Frequency Rating Factors Report for S-W7 and S-W8

Each of the solid circles in Figure 8.7 represents a lowest rating factor for an event based on the high frequency rating protocol that was discussed in earlier in this chapter. Also, these circles represent the lowest rating factor from all applicable limit states in the proposed period (except the gap (06/26 to 07/09) when the collected data

was subjected to some errors). Since some of the live loads on the bridge are insignificant, the author has used a threshold value for the rating factors in the plots. For example, for sensor SW-7 and SW-8, a cut off value of 15 was used as the upper limit for the plot (i.e. the upper limit on the y-axis in the figure is a value of 15).

8.9.3 Combined Low Frequency and High Frequency Results

The "Low and High Frequency Rating Factor Report" contains the controlling rating factors for all applicable limit states for the two rating methods. Since all of the rating factors are for the same sensors and there is a relation between the low and high frequency rating methods, another Matlab code was developed to combine all results into a single pdf file.

This third Matlab code condenses the results from the previous two codes. It combines the low and the high frequency ratings in one figure for each location making it easier to digest all of the rating information at a particular location. This report is named the "Low Frequency and High Frequency Rating Factors Report." Figure 8.8 shows an example of the combined frequencies report for one year at the location having sensors S-W7 and S-W8. The rest of the figures from the report can be seen in Appendix D.3.

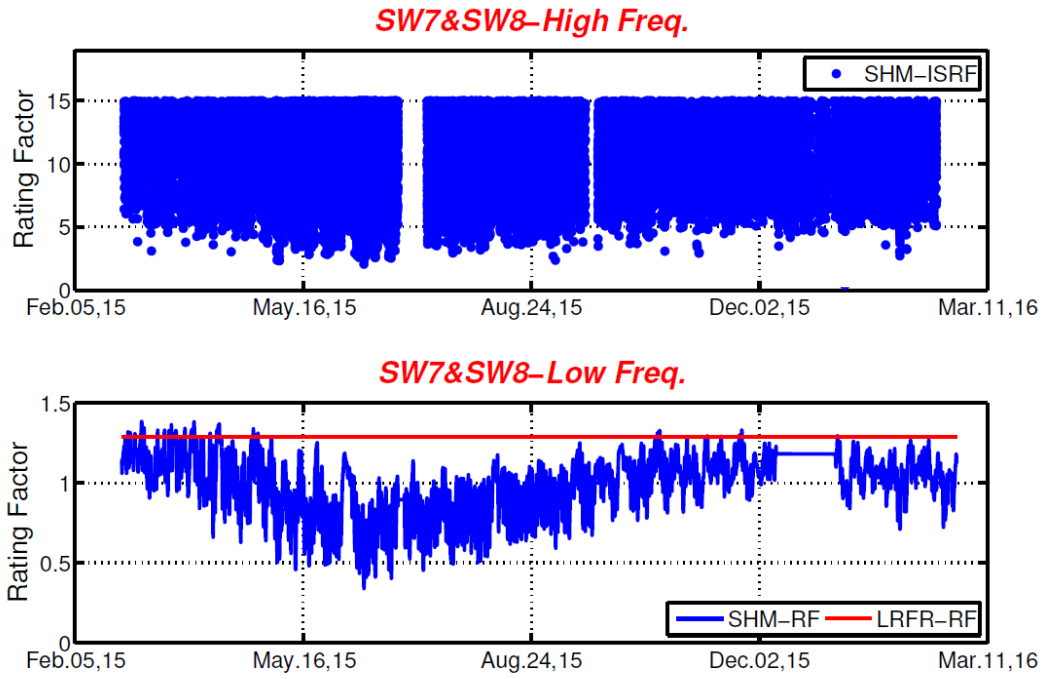

Figure 8.8. Sample of the Final Plot in the High and Low Frequency Rating Factors Report for S-W7 and S-W8

The lower figure represents the low frequency rating method. The blue line, referred to as the Structural Health Monitoring Rating Factor (SHM-RF) represents the controlling rating factor based on low frequency data. This line represents the minimum value for all of the considered limit states. For example, if the Service III limit state controlled over the first month, but the Strength I-flexure limit state controlled after that period of time, the plot would reflect that. The constant red line, referred to as the Load and Resistance Factor Rating Factor (LRFR-RF), represents the LRFR design rating factor. This value is constant since its uses only initial design information (which does not change over time) as explained in Chapter 6.

The top part of the figure represents the high frequency rating method. Each of points plotted, referred to as Structural Health Monitoring In-Service Rating Factors, represent the minimum rating factor for all of the considered limit states for the data for that particular event. Each point represents a distinct live load event that exceeded the threshold strain value. Finally, the associated Matlab code creates statistical distributions that can be used in the future.

Even though the calculated rating factors from the Matlab codes are more accurate than the conventional rating factors, because they include the long term load effects, but rating factors could still be different from the calculated ratings. The true rating factors could have been calculated, if the bridge was monitored during the construction stage, and actual dead loads were incorporated in rating equations. Initial stresses due to thermal effects and construction could have been developed when the last piece of the structure was installed during the construction. As a result, all the rating factors are based on relative change in strain and temperature measurements since the initial strain and temperature measurements are unknown. However, the range (i.e. difference between minimum and maximum calculated ratings) shows the long term load effects on rating factors. The actual rating factors can be higher or lower than the calculated ratings, but for simplification purposes, rating factors from design (LRFR-RF) were used as initial ratings.

8.10 Example Showing Strain Comparison with Rating Factor

In order to show additional benefits of this new rating methodology, example three highlights how one can investigate the effects of long term loads on ratings. The Matlab code dealing with high frequency data produces figures of maximum peaks at

all sensors and saves them in a different report called “Maximum Peaks of Strains Report”.

In this example, high frequency strain readings from sensor S-E6 are used to calculate rating factors. The high frequency data was analyzed during the period of April 10 to April 15, 2015. The highest strain during that period was measured by sensor S-E6. Usually, S-E6 does not measure the highest strain, but it could have happened due to the existence of another vehicle at that location.

On April 10, 2015, two heavy vehicles crossed the bridge at 11:11:40 am and at 4:36:55 pm. The first vehicle caused a live load strain of 45 microstrain and the second caused a strain of 35 microstrain. Based on the load tests, this level of strain would correspond to a single truck loading of approximately 90 and 70 kips, respectively, if the strain is only caused by the truck live load. Figure 8.9 shows collected and analyzed peak strains reported during that period of time with the two events marked with green and blue circles, respectively.

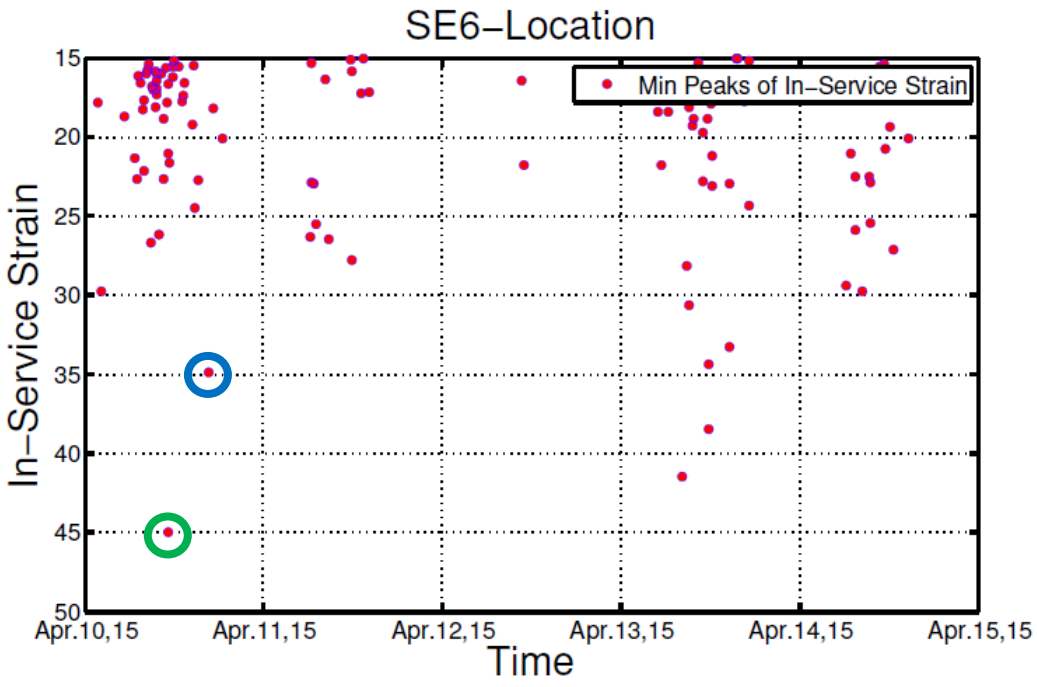

Figure 8.9. Maximum Peak Strains Recorded by Sensor S-E6

Since the recorded strains for the two vehicles are 45 and 35 microstrain respectively, a lower rating factor would be expected with the first vehicle, since it has a higher live load. However, contrary to what would have been expected, the second vehicle results in a 4.65 rating factor, which is lower than the 4.85 rating factor for the first vehicle.

The reason for the unexpected rating factor values is due to the long term effects (specifically the thermal effects). The thermal effects at the time of the second vehicle (4:36:55 pm) were higher than they were at the time of the first vehicle (11:11:40 pm). As a result, the rating factor associated with the second event (35 microstrain) is lower than a rating factor associated with the first event (45 microstrain). Figure 8.10 shows the high frequency rating factors for the two events.

The first event, circled in green, has a 4.85 rating factor while the second event, circled in blue, has a result of 4.65 rating factor.

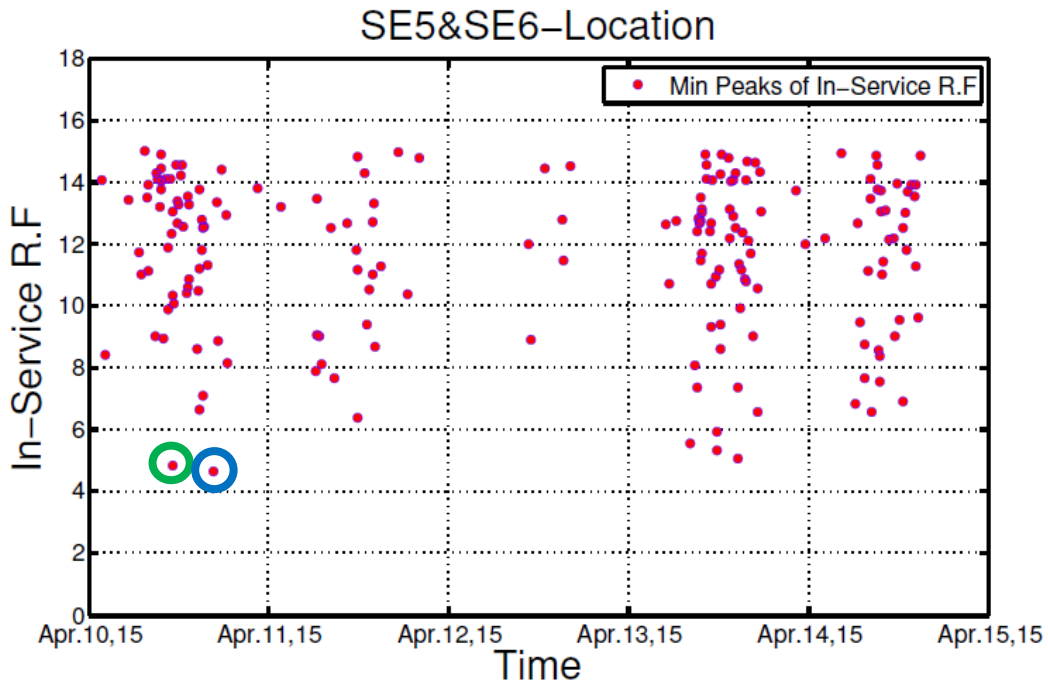

Figure 8.10. High Frequency Rating Factors

8.11 Summary

The Federal Highway Administration (FHWA) requires an LRFR rating factor greater than 1.0 for all applicable limit states for all bridges that are in-service. The conventional rating factor is assigned to a bridge based on design information and the value doesn't change with time unless damage to the bridge or section loss to a component occurs. The conventional rating equation takes into consideration the capacity, design dead load including future wearing surface, and design live load in order to obtain the Load Resistance Rating Factor (LRFR). According to the Manual

for Bridge Evaluation (MBE) other load effects could be included in the rating process, such as uniform thermal effects, gradient temperature effects, concrete creep and shrinkage. In practice, the difficulty of estimating forces for these additional phenomena, and their typically small effects compared to the other major design loads, have led designers to ignore these forces in the rating process.

The two new rating methods presented in this chapter use SHM data to produce more accurate rating factors. The Indian River Inlet Bridge (IRIB) is used as a case study for the developed rating methodology. Since the IRIB is a concrete cable-stayed bridge, the rating equations for prestressed concrete bridges are developed and derived in this chapter. Two different protocols for data collection are utilized: low frequency and high frequency. The low frequency protocol aims to capture long term effects such as thermal changes and prestressing losses due to creep and shrinkage. And also slow deterioration that might be caused by environmental factors or sustained load. The high frequency protocol aims to capture short term effects such as truck live loads, extreme events, etc.

In both cases (low and high frequency data collection) the recorded strain and temperature data is converted into structural forces and stresses (see Equations 8.6, 8.12, 8.13, and 8.14). Two rating methods are developed using the structural forces and stresses. A low frequency rating method is obtained by incorporating the long term effects into the numerator portion of the rating equation. This method uses the capacity, dead load, and live load from the design stage. The high frequency method uses the capacity and the dead load from the design stage while it uses live loads obtained from the high frequency SHM data. In addition, it also incorporates the long

term effects into the numerator portion of the equation (see Equations 8.16, 8.19, and 8.22).

A series of Matlab codes were developed to analyze the data continuously and produce low frequency and high frequency rating factors. The Matlab codes generate figures for each sensor location based on the high frequency and the low frequency rating equations considering all applicable limit states. The results are then compared to the conventional rating factors. Files with a pdf format are produced at the end of the analyses. The last pdf file contains plots of both the controlling low and high frequency rating factors as shown in Appendix D.

8.12 Conclusions

Based on the continuous strain and temperature data that has been gathered from the edge girders of the IRIB, structural forces and stresses have been computed using Equations 8.6, 8.12, 8.13, and 8.14. These structural forces and stresses have been applied to the developed rating equations to produce continuous rating factors based on two ratings methods (low frequency and high frequency).

The high frequency method uses the design capacity, design dead load, and uses the live loads as well as long term effects (thermal, prestressing losses) from the SHM data. This rating method produces the actual rating factors of the bridge. These rating factors are more accurate than the conventional In-Service Rating Factors, because it takes to consideration the long term load effects in addition to the monitored live loads. Since the high frequency method is continuous as well as the low frequency method, all heavy trucks including permit vehicles are included in these calculations. Therefore, this method provides DelDOT with comprehensive actual rating factors on the bridge since the beginning of its service life. Table 8.4

summarizes the one year analyzed data results for the High Frequency Rating Factor (SHM-RF) and compares them to the design rating factor (LRFR) from all sensors that provided full amount of data for the one year of interest.

Table 8.4. Comparison between High Frequency Ratings and Design Ratings

Comparing Controlling High Frequency Rating Factors with Design Rating Factors				
Sensor	**Limit State Controlling**	**Controlling LRFR (Design)**	**Controlling SHM-RF**	**Difference (D)** $D = \frac{(SHM-RF)-LRFR}{LRFR} x100\%$
S-E5 & S-E6	Service III-Bottom	1.71	2.37	38.5%
S-W7 & S-W8	Service III-Bottom	1.29	2.06	59.9%
S-E7 & S-E8	Service III-Bottom	1.67	2.50	50.1%
S-W9 & S-W10	Service III-Bottom	1.91	6.24	225.9%
S-W11 & S-W12	Service III-Bottom	1.82	4.80	163.3%
S-W13 & S-W14	Service III-Bottom	2.17	5.87	171.0%
S-W17 & S-W18	Service III-Bottom	3.04	6.32	107.9%
S-E17 & S-E18	Service III-Bottom	3.93	7.52	91.3%
S-W21 & S-W22	Service III-Bottom	1.16	5.31	356.3%

The lowest rating factor from the high frequency data is 2.06 reported at mid-span location and was based on Service III limit state. This value represents the controlling rating factor for the one year of interest. A difference of 59.9 % can be calculated by comparing the controlling high frequency rating factor (2.06) to the design LRFR rating factor (1.29) at the same location. These difference factors show that the design live load (HL-93) is conservative; it has a 59.9 % higher effect than the live load produced the actual controlling high frequency rating factor. The controlling rating factor in most of the cases was based on Service III limit state. Strength I limit state controlled over some time (i.e. S-W21 and S-W22), but most of the time Service III controlled over other limit states. Strength I limit state controls when a higher

gradient temperature is affecting. Since the edge girder in the IRIB is a concrete solid section, the gradient temperature effects were not significant. However, if the rated component has a hollow cross section (i.e. box girder) and/or made uses different construction material like steel, gradient temperature effects could have a bigger influence.

The low frequency approach uses the design capacity, design dead load, design live load, and it incorporates a new term in the numerator portion of the rating equation that accounts for long term effects (thermal, prestressing losses). In order to show the effects of long term load effects (i.e. thermal loads, prestressing losses) on rating factors, Table 8.5 summarizes the one year analyzed data results for the Low Frequency Rating Factor (SHM-RF) and compares them to the design rating factor (LRFR) from all sensors that provided full amount of data for the one year of interest. The table highlights the difference in the live load carrying capacity as a result of including the long term load effects. Note that the low frequency rating factors have low values comparing to the high frequency rating factors; that is because design live load is used to calculate the low frequency rating factors.

Table 8.5. Comparison between Low Frequency Ratings and Design Ratings

Comparing Controlling Low Frequency Rating Factors with Design Rating Factors				
Sensor	**Limit State Controlling**	**Controlling SHM-RF**	**Controlling LRFR (Design)**	**Difference (D)** $D = \frac{LRFR-(SHM-RF)}{LRFR} x100\%$
S-E5 & S-E6	Service III-Bottom	0.61	1.71	64.3%
S-W7 & S-W8	Service III-Bottom	0.34	1.29	73.7%
S-E7 & S-E8	Service III-Bottom	0.74	1.67	55.8%
S-W9 & S-W10	Service III-Bottom	1.48	1.91	22.5%
S-W11 & S-W12	Service III-Bottom	1.64	1.82	9.9%
S-W13 & S-W14	Service III-Bottom	1.36	2.17	37.1%
S-W17 & S-W18	Service III-Bottom	2.03	3.04	33.3%
S-E17 & S-E18	Service III-Bottom	2.52	3.93	35.9%
S-W21 & S-W22	Service III-Bottom	1.00	1.16	14.5%

The maximum difference in the live load carrying capacity reached 73.7 % of the design live load carrying capacity at mid-span location based on Service III limit state. The controlling rating factor in most of the cases was based on Service III limit state. Strength I limit state controlled over some time (i.e. S-W21 and S-W22), but most of the time Service III controlled over other limit states. Strength I limit state controls when a higher gradient temperature is affecting.

The major effect of thermal loads was also proven from this approach. In most of the figures of the low frequency rating method, the rating factor values followed the daily and seasonal change in temperature and almost end up at the same level where they started at the beginning of the year. The IRIB is a new bridge, it is not expected to show deterioration (i.e. excessive prestressing losses) in this very early stage of its service life, therefore most of the changes that occurred in the low frequency rating factor values were associated with thermal effects.

The lowest rating factor on a bridge from all of the applicable limit states determines the controlling rating factor for the bridge. According to the design firm, the location of sensors SW-21/22 represents the controlling location on the bridge (i.e. lowest rating factor). However, after computing continuous rating factors using the new methodology, the lowest controlling rating factor occurs at mid-span of the bridge (sensors SW-7/8).

The calculated rating factors from the low frequency approach can be used to evaluate and monitor the long term behavior of the bridge. Since the rating process is continuous over time, anomalies can be noticed directly from the figures. For example, if one of the prestressing tendons breaks, that will lead to a change in strain reading at the sensor(s), which will affect the rating factor values in the figure. The long term effects included in the numerator portion of the equation includes thermal effects and prestressing losses due to creep and shrinkage. In order to distinguish between these phenomenon's and to determine if the change in the rating factor was according to thermal effects or prestressing losses, a correlation analysis based on the one year analyzed data is suggested. Correlation analyses between rating factors from low frequency method with the monitored temperature can be conducted at each sensor location. By having that slope, changes can be verified whether they are a result of a change in temperature or are associated with some other phenomena (i.e. prestressing losses, creep, and shrinkage). Also, the slope can be used to predict rating factors based on expected temperature provided by the weather forecast. Furthermore, the change in the slope over time (i.e. three months period) can be used to monitor the long term behavior of the bridge.

The numerator portion of the proposed rating methods (low frequency and high frequency) includes the same terms (capacity, dead load, and long term effects), but they have different terms in the denominator portion of the equation. By comparing the values from the two rating methods, any live load produces higher effect than the design load (HL-93) can directly be verified when the rating factor from the high frequency method falls below the rating factor from the low frequency method. This should raise an immediate attention of DelDOT at these locations because it may indicate developed cracks in the edge girder if the controlling limit state is service or a probability of failure if strength limit state controls. This also can help with detecting heavy trucks (> 80kips) passing the bridge without a valid permit from DelDOT.

Both rating methods convert measured strain and temperature data into rating factors. To engineers working at transportation agencies and in industry, the rating factors are more useful and more understandable than the pure strain and temperature data. This approach reduces the gap between the huge amount of monitored data and direct application of SHM data.

Also, the concept of using continuous rating factors and their variation with time to understand the effect of thermal loads and other long term load effects was presented in this chapter. A conventional rating factor value is associated with the bridge's initial design information and does not change over time unless quantifiable changes to the bridge or to bridge components due to section loss, damage, prestressed losses, etc. occur. The results from the proposed rating methods show that the conventional rating factor may not completely reflect the actual rating factor for a bridge because the actual rating factor does vary with time (specifically due to long term effects such as thermal loads and prestress losses). In fact, it has been shown that

thermal effects can have a significant effect on rating factors. Rating factors can be underestimated (i.e. be unconservative) when thermal effects are not considered in the rating process, especially for long span bridges. As shown for the IRIB case, the thermal stresses and structural forces are significant when compared to the conventional major design loads such as dead and live loads and therefore should not be ignored.

To make the computation of rating factors efficient, and to produce easy to read plots of the most important results, a series of Matlab codes have been developed for each of the two rating methods. The Matlab codes produce continuous rating factors at sensor locations based on the two methods and considering all applicable limit states. This is done for all sensors in the west and east edge girders, and the results are saved in the form of pdf files.

Chapter 9

RELIABILITY ANALYSIS BASED ON STRUCTURAL HEALTH MONITORING DATA

9.1 Background

The safety and serviceability of bridges is a paramount concern for bridge engineers. According to the American Society of Civil Engineers (ASCE), one out of every nine bridges in the United States is classified as structurally deficient and is in urgent need of repair (ASCE 2013) . Bridge maintenance is very costly, especially when the structure is on a major road and the repairs require shutting down the bridge completely or partially. The Federal Highway Administration (FHWA) estimates that it will cost nine billion dollars per year more than what we are currently spending on maintenance to repair our deficient bridges (ASCE 2013).

In order to achieve an optimum level of bridge maintenance and improve the decision making process, it is important to be able to quantify the reliability of bridges. The new code was calibrated based on a target reliability index that results in a consistent and uniform level of safety. Therefore, bridges designed according to the Load Resistance Factor Design (LRFD) method should achieve reliability indices equal to or higher than the target reliability.

On the other hand, it is difficult to determine the reliability indices for existing bridges that were designed based upon earlier design philosophies such as Allowable Stress Design (ASD) and Load Factor Design (LFD). Structural Health Monitoring (SHM) can help with evaluating and maintaining existing bridges. As a result of the

revolution in new information technologies and advanced sensing systems, the number of bridges using Structural Health Monitoring (SHM) systems has increased. Large amounts of data are measured and recorded by the SHM systems. Despite the fact that the collected data has vital information about the health of these bridges, transportation agencies are still lacking a direct implementation of the monitored data into the maintenance and decision making processes. Many of today's transportation agencies lack the knowledge needed to directly use the monitored data for bridge evaluation. In fact, a good amount of the currently collected and stored SHM data goes unused.

Reliability analysis based on SHM data is a very powerful technique that can be used to determine the reliability indices for structural components. By using SHM data, the load effects and structural responses can be determined in a better way than using conventional finite element models. Furthermore, the continuity of the data reduces the uncertainties for the estimated random variables which in turn leads to more accurate reliability indices.

9.2 Literature Review

Reliability analysis has been a very active research topic during the last two decades. After the AASHTO LRFD Bridge Design Specifications was calibrated based on a target reliability index, the idea of evaluating the reliability indices for existing bridges has become more common. By comparing the reliability index of an existing bridge to the code standards, bridge safety can be evaluated. The reliability index can also be used to prioritize and optimize bridge inspection and maintenance procedures for existing bridges.

Imai and Frangopol in 2001 conducted early research in which Finite Element (FE) models were used for estimating load effects (including dead loads, live loads, temperature loads, etc.) and incorporated them with the coefficients of variation used in the literature at that time to quantify the reliability indices for the Innoshima Bridge. Following the rapid growth and availability of structural health monitoring techniques, the ability to measure the structural responses of bridges has become more feasible than it used to be. Reliability analysis using simulated structural health monitoring data from FE analyses was first presented by Ni et al. in 2006. The authors used continuous long term monitored strains to obtain the probability distribution functions for the load effects, while the resistance distribution functions were obtained based on the material strength or material tests.

In 2008, Frangopol et al. presented a real life example of reliability evaluation using SHM data from the Lehigh River Bridge SR-33. The analysis was based on short term and long term monitored data that was collected over a 38 month period. The authors used the long term monitoring data to investigate the overall influence of temperature on the truss bridge, and to determine the long term effects of concrete creep and shrinkage on the instrumented truss members.

The concept of reliability assessment and performance prediction based on extreme monitored data was first presented by Frangopol et al. in 2008b. The authors presented a general approach for the development of performance functions based on monitored extreme data and the estimation of possible monitoring interruption periods for a bridge in Wisconsin. Also, in 2008 a method of conducted reliability assessment and performance prediction based on Bayesian updating was proposed by Strauss et al.

In 2008, novel research into reliability analysis was conducted by Catbas, F & Frangopol that extended the reliability analysis methodology based on SHM data. The authors conducted reliability analysis based on distributions estimated for dead, live, and wind loads. Also, the researchers used long term SHM data to estimate the probability distribution function for temperature effects. The investigators found that temperature loads have a significant effect on overall system reliability.

A direct use for SHM data in reliability analysis was presented in 2009 by Liu et al. In this research the authors introduced the concept of the condition function and the prediction function illustrated by monitored live loads obtained by SHM system. The research was applied to a bridge in Pennsylvania, which was monitored for four years from 2001 to 2005. The research showed the use of SHM data in structural safety evaluation, and as a platform for reliability assessment of infrastructures.

All of the previously cited research was based on reliability indices that were derived from the estimated probability of failure. In 2011 Jiao and Sun proposed a new approach for reliability analysis based on direct failure probabilities. Assuming that the structural resistance is independent from the structural responses, a formulation of failure probability was determined and probability density functions of the strain at sensor locations were developed and verified. The authors applied their new approach to four years of recorded data from the Donghai Bridge in China.

In 2012, Li et al. studied reliability analysis of cable-stayed bridges based on SHM data. A summary of the framework of reliability analysis based on SHM data was explained in this research. The monitored vehicle loads and environmental effects were used to produce probability distribution functions for the load effects. An updated FE model was used to calculate the load effects at the unmonitored locations.

Reliability indices for the main bridge components were estimated by using flexural capacity as a limit state in the reliability analysis.

Following the introduction over the past several years of long term bridge monitoring systems, the methodology for conducting reliability analysis based on structural health monitoring data has evolved. However, most of the research has focused on estimating the reliability index of older bridges. Recently, there have been a few real-life examples of using reliability indices for decision making in the areas of optimizing and prioritizing bridge inspection and maintenance.

9.3 Contribution

Serviceability and safety of bridges are essential for transportation agencies. The maintenance process has a crucial effect on the health of bridges. Also the maintenance of bridges is very costly, especially when it involves a major road and the repair requires shutting down the bridge completely or partially. In order to help the Delaware Department of Transportation (DelDOT) in optimizing their decision making process for the inspection and maintenance of the Indian River Inlet Bridge (IRIB), reliability analysis using SHM data is conducted and evaluated in this chapter.

The research described herein advances the state-of-the-art in several areas. First, the IRIB is a new bridge that was designed according to the AASHTO LRFD Bridge Design Specifications. This makes it different from much of the prior research studies that focused on older bridges designed based on older design philosophies. Second, from the very opening of the bridge in the spring of 2012, there has been a very large amount of data collected from the SHM system on the IRIB from a wide array of sensors. Reliability analyses have proven to be an efficient approach to representing the large amount of data, and for being able to create a trackable baseline

of safety. Third, reliability analysis can be applied to different limit states. Since the author was able to extract the design loads and stresses used in the design process, performing reliability analysis using different limit states can be conducted and compared. Most of the prior research is based solely on Strength limit state since the AASHTO code was calibrated for only that limit state. This research is unique in that it performs reliability analyses for several limit states based on SHM data. Fourth, this research is the first example in the United States conducted on a new bridge (designed according to the AASHTO LRFD code) from the first day of its service life. By tracking indices over the life of the bridge, long term performance can be established and health problems can be detected.

9.4 Reliability Method

The reliability of any bridge can be defined as the ability to meet the required functions within the bridge's remaining service life. In other words, reliability analysis is a statistical approach that takes into consideration all loads that affect a structure and subtracts them from its resistance. In general, reliability analysis results are presented in terms of reliability indices. A reliability index can be defined as an accurate overall measure of the structural safety; it represents the probability of failure if the ultimate limit state is used, or it represents the probability of exceedance in case of serviceability limit states.

There are two methods for determining structural reliability, the First Order Reliability Method (FORM) and the Second Order Reliability Method (SORM). FORM provides an excellent approximation for linear and some nonlinear cases. However, SORM should be used for all nonlinear cases and for improving the results obtained by FORM. In the case of the IRIB, since linear limit state functions are used,

the FORM is considered to be an accurate approximation (Li et al. 2012) and was used in this study.

Adequate structural safety for any bridge requires that the resistance (R) of any component on the bridge is greater than the load effects (Q) on the same component (i.e., R> Q). However, in order to make a comparison between the resistance and the load effects, they need to have the same units, and that can be achieved by selecting a certain limit state (i.e. Z (*X*)), then

$$Z(X) = g[R(X), Q(X)] = R(X) - Q(X) \quad Equation\ 9.1$$

Where,

- Z(*X*): Limit state function
- $X = \{X_1, X_2, \ldots, X_n\}^T$: Vector of random variables
- R(*X*) : Resistance
- Q(*X*) : Load effects

Then, Z(*X*) = 0 represents the limit state, and Z(*X*) < 0 is the failure state.

A graphical presentation of the load effect, resistance, and the limit state function is shown in Figure 7.1. In general, the reliability index can be calculated as the inverse of the standard normal distribution function for the probability of failure (shaded area), as shown in Equation 9.2.

$$\beta = \varphi^{-1}(P_f) \quad Equation\ 9.2$$

Where,

- φ^{-1}: Inverse of the standard normal distribution function
- P_f : Probability of failure (shaded area in Figure 7.1)

Calculating the reliability index based on a closed form solution can be achieved only in two special cases: (1) when both Q and R are normal random variables, then the solution becomes as indicated in Equation 7.1; or (2) when both Q and R are lognormal random variables and the reliability index can be calculated as shown in Equation 7.3. However, in all other cases, available procedures such as Monte Carlo Simulation produce approximate results (Kulicki et al. 2007). If Monte Carlo Simulation is used and no failures were detected (probability of failure is equal to zero) after applying a sufficient number of iterations (i.e. 10^6), then another method can be used to obtain the reliability indices such as the Hasofer-Lind method (Nowak & Collins 2013).

Hasofer-Lind method evaluates the limit state function at a point known as the "design point" instead of the mean values. The design point is a point on the failure surface (g=0). Since this design point is not generally known in advance, an iterative technique must be used to solve for the reliability index (Nowak & Collins 2013). Hasofer-Lind method requires information about the means and standard deviations of the random variables. However, if more detailed information on the type of distribution for each random variable is known, then the procedure can be improved as shown by the Rackwitz-Fiessler method (Nowak & Collins 2013).

Hasofer-Lind method and Rackwitz-Fiessler method follow the same procedure (iteration process at the "design point") except that knowledge of distributions for each random variable is required in Rackwitz-Fiessler method to calculate the equivalent normal parameters as shown in Equations 9.7 and 9.8. The Rackwitz-Fiessler method can be used to obtain reliability indices using SHM data.

In this study, Rackwitz-Fiessler method is used and linear limit states are assumed in all cases. The general equations of the reliability method using the Rackwitz-Fiessler procedure based on the non-normal procedure are described in Equations 9.3 through 9.8 (Li et al., 2012):

$$Z = g(X_1^*, X_2^*, \dots, X_n^*) = 0 \qquad Equation\ 9.3$$

$$\beta = \frac{\alpha_0 + \sum_{i=1}^{n} \alpha_i \mu_{X_i}^e}{\sqrt{\sum_{i=1}^{n} \left(\alpha_i \sigma_{X_i}^e\right)^2}} \qquad Equation\ 9.4$$

$$x_i^* = \mu_{X_i}^e + \alpha_i \beta \sigma_{X_i}^e \qquad Equation\ 9.5$$

$$\alpha_i = -\frac{\sum_{i=1}^{n} \frac{\partial g}{\partial X_i}\ \sigma_{X_i}^e}{\sqrt{\sum_{i=1}^{n} \left(\frac{\partial g}{\partial X_i}\ \sigma_{X_i}^e\right)^2}} \qquad Equation\ 9.6$$

$$\mu_{X_i}^e = x_i^* - \sigma_{X_i}^e \left[\Phi^{-1}\left(F_X(x_i^*)\right)\right] \qquad Equation\ 9.7$$

$$\sigma_{X_i}^e = \frac{1}{f_{X(x_i^*)}} \phi\left[\Phi^{-1}\left(F_X(x_i^*)\right)\right] \qquad Equation\ 9.8$$

Where,

- X_i (i=1,2,…,n) : The $_i$th variable related with resistance and load effects. In this case study the limit state is assumed to be linear. Dead loads, live loads, and thermal loads were subtracted from resistance as will be explained later in this chapter.

- $X_i$and X_i^e : Non-normal random variable and equivalent normal random variables, respectively. For normal random variable $X_i^e = X_i$; the mean value and standard deviation of X_i and X_i^e are (μ_{X_i}, σ_{X_i}) and ($\mu_{X_i}^e$, $\sigma_{X_i}^e$), respectively

- $F_X(x_i^*)$, $f_{x(x_i^*)}$: Cumulative distribution function and probability density function of variable X_i at checking point x_i^*

- $\Phi^{-1}(.),\phi(.)$: Inverse cumulative standard normal distribution function and standard normal probability density function

- $\frac{\partial g}{\partial X_i}$: Partial deferential of *g(X)* with respect to parameter X_i

The procedure for Rackwitz-Fiessler method is described in Reliability of Structures (Nowak & Collins 2013) as follows:

1. Formulate the limit state function. Determine the probability distributions and appropriate parameters for all random variables X_i (i=1,2,…,n) involved.

2. Obtain an initial design point $\{x_i^*\}$ by assuming values for n-1 of random variables X_i. (Mean values are often a reasonable choice). Solve the limit state equation g=0 for the remaining random variable. This ensures that the design point is on the failure boundary.

3. For each of the design point values x_i^* corresponding to a non-normal distribution, determine the equivalent normal mean $\mu_{X_i}^e$ and standard deviation $\sigma_{X_i}^e$ using equations 9.7 and 9.8.

4. Determine the reduced variates $\{z_i^*\}$ corresponding to the design point $\{x_i^*\}$ using Equation 9.9.

$$z_i^* = \frac{x_i^* - \mu_{X_i}^e}{\sigma_{X_i}^e} \qquad Equation\ 9.9$$

5. Determine the partial derivatives of the limit state function with respect to the reduced variates using Equation 9.10.

$$\frac{\partial g}{\partial Z_i} = \frac{\partial g}{\partial X_i}\sigma_{X_i}^e \qquad Equation\ 9.10$$

6. Calculate an estimate of β using Equation 9.4.

7. Calculate the sensitivity factors (α) using equation 9.6.

8. Determine a new design point in reduced variates for n-1 of variables of the variables using Equation 9.11.

$$z_i^* = \alpha_i\beta \qquad Equation\ 9.11$$

9. Determine the corresponding design point values in original coordinates for the n-1 values in step 7 using equation 9.5. Note that $z_i^* = \alpha_i \beta$.

10. Determine the value of the remaining random variable (i.e., the one not found in steps 8 and 9) by solving the limit state function g=0.

11. Repeat steps 3 through 10 until β and the design point $\{x_i^*\}$ converge.

9.5 General Framework

A summary of the general framework for the reliability analysis based on SHM data that was followed for the IRIB is shown in Figure 9.1. The SHM system has been in service since May 2012. Various types of data have been collected from the bridge using the SHM system. In addition to the continuously monitored data collected from the SHM system, a series of diagnostic load tests have been conducted on the bridge as indicated in Chapter 5.

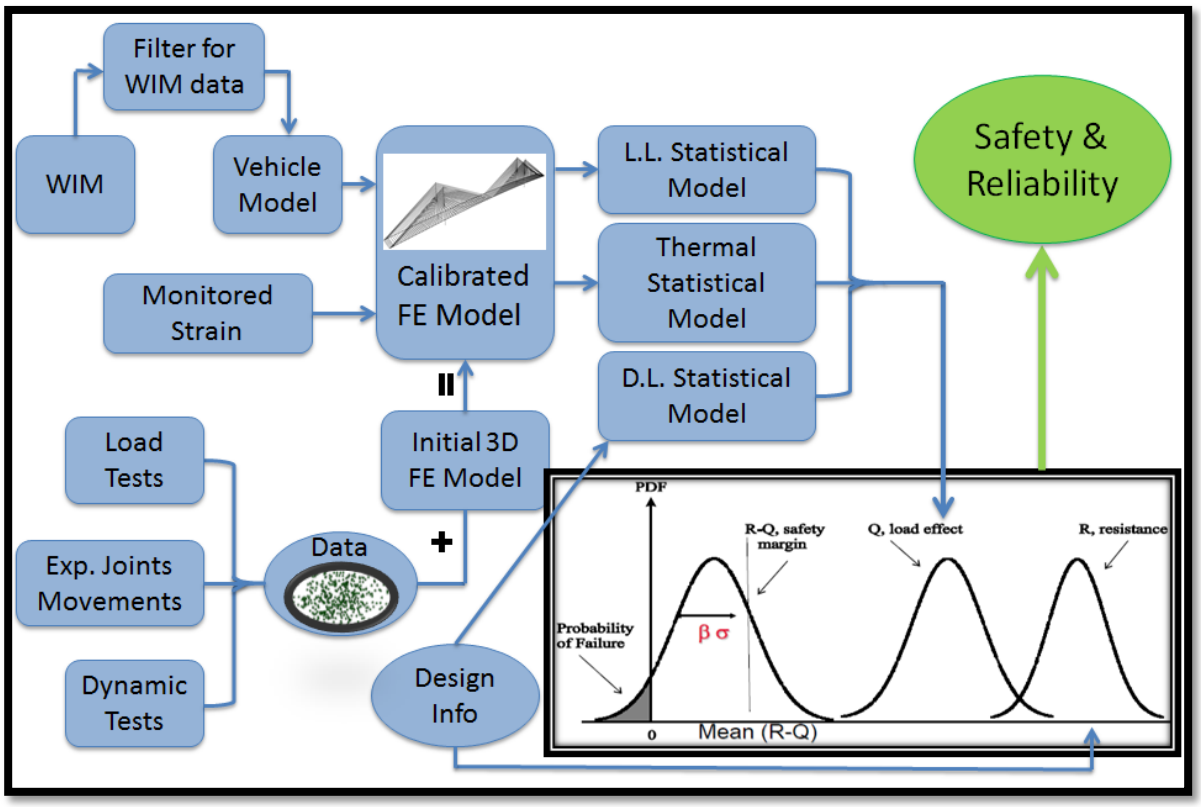

Figure 9.1. Framework for Reliability Analysis Based on SHM

The first step in the flow chart involves the initial 3D finite element model that was described in Chapter 4. Next, the initial model was calibrated based on load test data. As described earlier, the model was calibrated at the sensors locations by changing the concrete strength based on a range of cylinder test data collected during construction.

The collection of continuous high frequency data, recorded at a frequency of 25 Hz, was initiated at the end of February 2015. Before that, only low frequency data was collected. Since the amount of high frequency data collected at the time of writing is not enough to create a live load model, three years of WIM data was analyzed and

applied to bridge influence lines created using the calibrated model to produce the live load model effects.

The collected low frequency monitored strain and temperature data includes the environmental effects such as thermal effects, wind, etc. A correlation study was conducted using the monitored strain data and the collected temperature data to produce the environmental statistical model. Also, an approximation method is applied to the monitored locations to predict the environmental effects at the unmonitored locations.

Since the bridge was not monitored during the construction stage, a dead load model was developed based on extracted design information as explained in Chapter 5. The same statistical model properties used in the *Updating the Calibration Report* for the AASHTO Code (Kulicki et al. 2007) was used in this analysis.

The reliability analysis performed herein considered several limit states. The resistance model was established based on the type of limit state being considered. For example, for the Strength I (Flexure) limit state, the extracted moment capacities from interaction diagrams (as explained in Chapter 5) were used in combination with the statistical parameters from the *Updating the Calibration Report* for the AASHTO Code to create the statistical resistance model. Other limit states, such as Service Limit State, use the material strength as a resistance model.

Due to the inherent variability within the SHM data, it was found that loads and resistance do not follow normal distributions, therefore, Rackwitz-Fiessler procedure based on non-normal distribution were used to determine reliability indices. Indices were computed along the west edge girder of the bridge using different limit states.

9.6 Load Effects Statistical Models

In order to measure reliability in terms of probability of failure, load effects and resistance have to be expressed in Probability Distribution Functions (PDF), where loads and resistance are treated as random variables. The type of the PDF and the associated parameter(s) determine the shape of the PDF. The total load effect (Q) is defined as the summation of the load effects acting on the bridge (such as dead load, live load, thermal effects, etc.). Therefore, the statistical parameters of the total load effect are determined by the statistical parameters of each individual load component.

There are several types of loads that act on a bridge. According to the AASHTO LRFD Bridge Design Specifications, there are several loads and load combinations that should be considered when designing a bridge. In fact, some of these loads have a more significant effect than others. Also, the significance of a particular load type will vary from one bridge to another based on the geographical location (for example, thermal, wind, or earthquake loads). The safety factors applied to these loads come from studies of reliability analysis and/or experience or empirical studies. Therefore, there are some uncertainties in the estimation of the design loads. Structural health monitoring techniques can clearly help determine the actual load effects on bridges and reduce that uncertainty involved in using design loads.

SHM systems can be used to determine the actual types of loads affecting bridges. By utilizing the real time data, the actual live load effects and environmental effects such as thermal, wind, etc. can be accounted for more accurately than by simply using non-site specific design loads (which by nature need to be conservative and will typically produce maximum effects to ensure bridge safety). Also, the availability of continuous SHM data makes it possible for engineers to consider the actual effects of long term loads such as those related to the loss of prestressing forces.

In order to establish representative statistical models for load effects, a large amount of SHM data is needed. The more data that is used, the better the statistical models are. In addition to the low frequency data that has been saved every 10 minutes since May 2012, four load tests were conducted on the bridge. Also, high frequency data collection has been ongoing since the end of February 2015. The use and benefits of each type of SHM data used in the reliability analysis will be explained later in this chapter.

The total load effects in a reliability analysis can be obtained by adding all loads of the individual load effects acting on the bridge. It is obvious that the primary two load effects to be included in that load combination are the dead and live loads. Also, the monitored data showed that the environmental loads, primarily the thermal effects, have a significant influence on the computed reliability indices. The procedure for obtaining each statistical load model is described in the following subsections.

9.6.1 Dead Load Statistical Model

One of the objectives of installing the SHM system on the IRIB was to provide DelDOT with information that would help guide their engineers in the future maintenance and operation of the bridge. The bridge itself was built under a design/build contract; thus, the design and construction of the SHM system was also a design/build project. While this presented unique challenges to the team, the installation of the SHM system did not in any way affect the construction schedule of the bridge. Due to the complexity of the SHM system, and the timeline for construction, the bridge was not monitored during construction. As a result, extracted design dead loads, which include structural forces (moment and axial loads) and stresses, were used to establish the dead load statistical model.

In so doing, the author has used statistical parameters from NCHRP Report 20-7/186 (Kulicki et al. 2007) to create the dead load PDF's. A bias factor of 1.05 and a coefficient of variation of 0.1 were used with the design dead loads to generate normal PDF's. The factors used for cast-in-place concrete were obtained from Table 7.1. Additional details regarding the dead load statistical model are presented in Chapter 7.

In summary, the dead load statistical model was assumed to be normally distributed and was generated using bias factors and coefficients of variations obtained from NCHRP Report 20-7/186. Since the reliability analysis is performed using different limit states, more than one dead load statistical model was developed since the dead load model has to have the same units as the resistance model. Examples of dead load statistical models are presented later in this chapter.

9.6.2 Live Load Statistical Model

The current design live load in the AASHTO LRFD Bridge Design Specifications is the HL-93 load, which consists of HS-20 44 truck, a lane load of 0.64 kip/feet, a tandem load, and two trucks back to back for the negative moment regions. However, the HL-93 does not represent the actual traffic on a bridge. Rather it was developed to achieve a certain level of safety for bridges. Thus, the SHM data reflects the actual in-situ live load effects at the monitored locations on the bridge.

The SHM system at the IRIB has been in service since May 2012. However, high frequency data has only been collected since February 2015. Since the amount of collected data was not enough at the time of writing to create a representative live load model for the bridge, another source for the live load data was needed. To address this issue, weigh-in-motion (WIM) data for the last three years (taken from weigh stations near the IRIB) was used to create the live load statistical model. Moving forward,

actual live load response data can be used to develop the live load models needed to perform future reliability analyses. The results presented here can be used as a baseline for this future analysis.

9.6.2.1 Weigh-In-Motion Data

In general, Departments of Transportation (DOTs) use Automatic Traffic Recorder (ATR) stations to collect traffic inventory data throughout the United States. Each state has its own ATR stations spread throughout the state. Some of these ATR stations are called Weigh-In-Motion stations. The Weigh-In-Motion stations utilize devices that capture and record axle weights, axles spacing, direction of travel, speed, and gross vehicle weights as vehicles drive over the measurement site.

Each state in the US has several WIM stations spread throughout the state. The state of Delaware had 27 WIM stations at the time of writing. The stations are typically located at the boundaries of the states on major roads. Two of Delaware's WIM stations are very close to the IRIB, one located north and one located south of the bridge (stations 8076 and 8099 respectively). Figure 9.2 shows a map of all of the ATR stations in the state of Delaware as of 2014. The two stations of interest near the IRIB location are marked on the map.

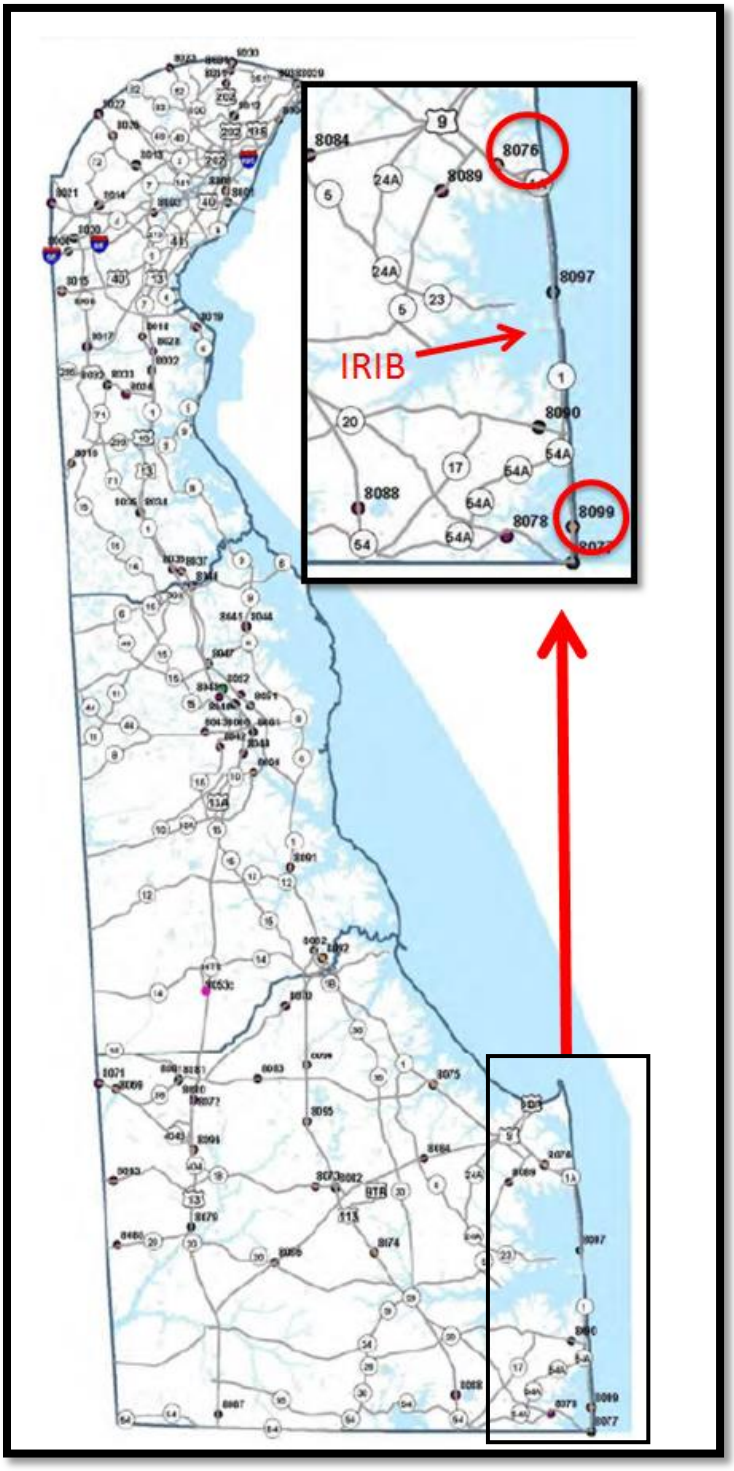

Figure 9.2. Automatic Traffic Recorder (ATR) Locations in Delaware Including Two WIM Stations of Interest

While WIM data from all WIM stations was requested from DelDOT, only the data from the two WIM stations (8076 and 8099) was used in order to determine an accurate live load statistical model for the IRIB. The provided WIM data was collected between the period of January 2011 and June 2014.

9.6.2.1.1 Weigh-In-Motion Data Processing

The WIM stations record data continuously creating an event every time a live load passes over a station. As a result, a large amount of data is generated by WIM stations on daily basis. WIM station data is saved in daily "White Files" with an extension designating the year the file was collected. For example, files saved in the year of 2011 have the extension of ".11." Each of the "White Files" contains continuous numbers in each row, and each row represents an event during that day. Figure 9.3 shows an example of "White File" data.

```
W10008076521101010009   03290504903906701307508806701307 1
W10008076521101010005   004502017041028
W10008076121101010005   012402062040061
W10008076131101010008   01590404202904024204002303 7
W10008076131101010008   01760404402704216904403104 6
W10008076131101010008   01290403402703420203002302 9
W10008076121101010005   015302070042083
W10008076131101010005   014402066041078
W10008076121101010005   014002066053075
W10008076131101010008   01770404703004326804502504 3
W10008076511101010005   001802011041008
W10008076131101010008   01630404302804033504002603 9
```

Figure 9.3. Example of WIM "White File" Data

Each row in this file represents a recorded vehicle. The rows then can be broken down into columns of different widths that describe the vehicle. Table 9.1 is taken from the

Federal Highway Administration's (FHWA) *Traffic Monitoring Guide* (2013) and shows the description of the columns/widths and their respective meaning.

Table 9.1. WIM Data Record Format (fhwa.dot.gov 2013)

Field	Columns	Width	Description
1	1	1	Record Type
2	2-3	2	FIPS State Code
3	4-9	6	Station ID
4	10	1	Direction of Travel Code
5	11	1	Lane of Travel
6	12-15	4	Year of Data
7	16-17	2	Month of Data
8	18-19	2	Day of Data
9	20-21	2	Hour of Data
10	22-23	2	Vehicle Class
11	24-26	3	Open
12	27-32	6	Total Weight of Vehicle
13	33-34	2	Number of Axles
14	35-39	5	Axle Weight 1
15	40-43	4	Axles 1-2 Spacing
16	44-48	5	Axle Weight 2
17	49-52	4	Axles 2-3 Spacing
18	53-57	5	Axle Weight 3
19	58-61	4	Axles 3-4 Spacing
20	62-66	5	Axle Weight 4
21	67-70	4	Axles 4-5 Spacing
22	71-75	5	Axle Weight 5
23	76-79	4	Axles 5-6 Spacing
24	80-84	5	Axle Weight 6
25	85-88	4	Axles 6-7 Spacing
26	89-93	5	Axle Weight 7
27	94-97	4	Axles 7-8 Spacing
28	98-102	5	Axle Weight 8
29	103-106	4	Axles 8-9 Spacing
30	107-111	5	Axle Weight 9
31	112-115	4	Axles 9-10 Spacing
32	116-120	5	Axle Weight 10
33	121-124	4	Axles 10-11 Spacing
34	125-129	5	Axle Weight 11
35	130-133	4	Axles 11-12 Spacing
36	134-138	5	Axle Weight 12
37	139-142	4	Axles 12-13 Spacing
38	143-147	5	Axle Weight 13

The data provided by DelDOT for the WIM stations were in one folder. In order to pick the files of interest, a Matlab code was used to separate the WIM files based on the WIM station number. As a result, two main folders, one for station 8076 and one for station 8099 were created. Those two files contain the WIM data of interest. Next, a Matlab code was developed and used to analyze the raw data and transfer all of the recorded events into Microsoft EXCEL sheets which were used to filter the data.

The number of collected events for station 8076 is 2,594,671, and for station 8099 is 415,012. This yields a total of 3,009,683 events or records. According to the NCHRP Project 12-76 report, high speed WIM data is subjected to various errors, which need to be recognized and considered in the data review process so that unreliable data and unlikely trucks and cars can be eliminated. Therefore, before creating a live load statistical model, the WIM data was scrubbed and filtered to ensure that only data meeting the quality checks would be included in the live load statistical model.

9.6.2.1.2 Weigh-In-Motion Data Scrubbing

The National Cooperative Highway Research Program (NCHRP) Protocols for Collecting and Using Traffic Data in Bridge Design Project 12-76 (2008) developed protocols for collecting and using traffic data for bridge design. Since high speed WIM data is subjected to various errors, the data needs to be evaluated in the data review phase to ensure the quality of the data used in the bridge design live load model.

By using protocols similar to the ones used in NCHRP Report 12-76, the data for the two WIM stations 8076 and 8099 were filtered before the live load statistical

model was generated. For example, it is important to check speed data, because stop-and-go traffic can cause difficulty in separating vehicles. Also, traffic with a very large axle spacing or very small axle spacings could mean two trucks get combined together.

The following protocols were stated in NCHRP Report 12-76 and applied to the DE WIM data to produce the live load statistical model for the IRIB. Any record that satisfied one or more of the following constraints was removed from the dataset.

1. Speed < 10 mph
2. Speed > 100 mph
3. Truck length > 120 ft
4. Total number of axles < 3
5. Record where the sum of axle spacing is greater than the length of truck.
6. Gross Vehicle Weight (GVW) < 12 Kips
7. Record where an individual axle > 70 Kips
8. Record where the steer axle > 25 Kips
9. Record where the steer axle < 6 Kips
10. Record where the first axle spacing < 5 feet
11. Record where any axle spacing < 3.4 feet
12. Record where any axle < 2 Kips
13. Record which has GVW +/- sum of the axle weights by more than10%. This may indicate that the axle records provided may not be complete or accurate.

The filtering process was conducted using a Microsoft EXCEL filter. The data was filtered separately for each of the two WIM stations. The number of recorded

vehicles at station 8076 after filtering was 311,360 compared to 2,594,671 vehicles before filtering (or 12% of the station 8076 events). The number of recorded vehicles at station 8099 after filtering is 69,912 vehicles compared to 415,012 vehicles before filtering (or 16.8% of the station 8099 events). Note that cars were removed from the dataset according to protocol number 4, and that explains the big difference between the recorded events and the useful records that will be used to create the live load statistical model. The filtered vehicles from the two WIM stations were added together resulting in a total of 381,272 vehicles. These vehicles were recorded at the two WIM stations during the period from January 2011 to June 2014. These 381,272 records from the two WIM stations were used to create the live load statistical model.

9.6.2.1.3 Results of Weigh-In-Motion Data Scrubbing

The scrubbed data from the two WIM stations were combined together to create a total of 381,272 vehicles, which represents 12.7% of the original data. Since the WIM data has a couple of entries, such as total weight, total length, axles weights, axles spacings, speed, etc., it is difficult to present the actual data (examples of the WIM data are presented in this chapter for some of these entries, the rest of data is shown in Appendix E). Figures 9.4, 9.5, and 9.6 show histograms of the Gross Vehicle Weight (GVW), total length of vehicles, and number of axles for all filtered WIM data. Note that according to filtering protocol number 6, the GVW is greater than 12 kips for all filtered vehicles. Also according to Figure 9.4, most of the vehicles average about 35 kips. The maximum length of vehicle recorded is 120 feet, and the maximum number of axles recorded for any individual vehicle is 9.

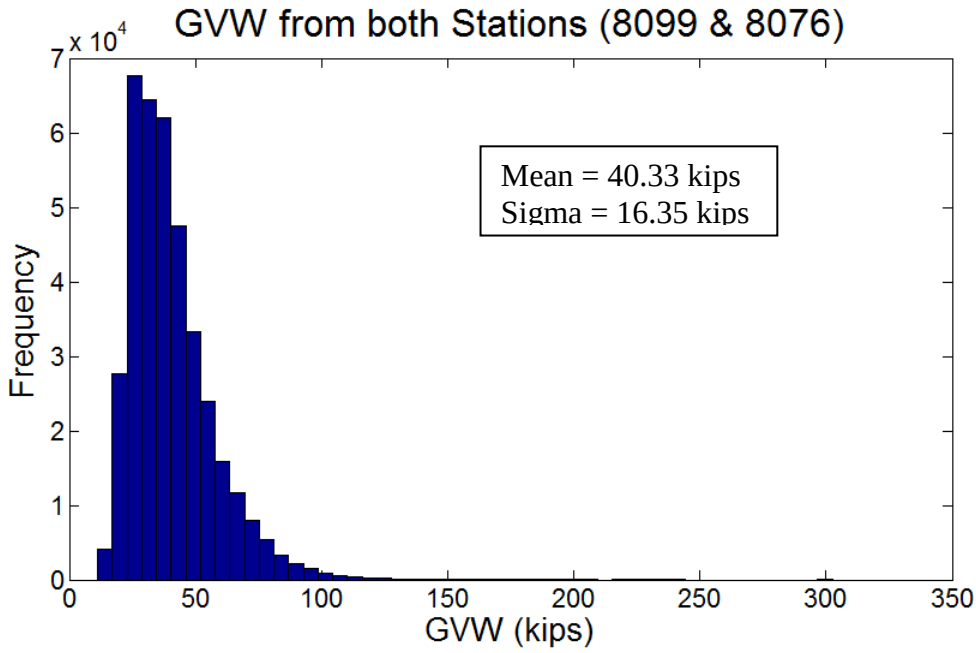

Figure 9.4. Gross Vehicle Weight for Filtered Weigh-In-Motion Data

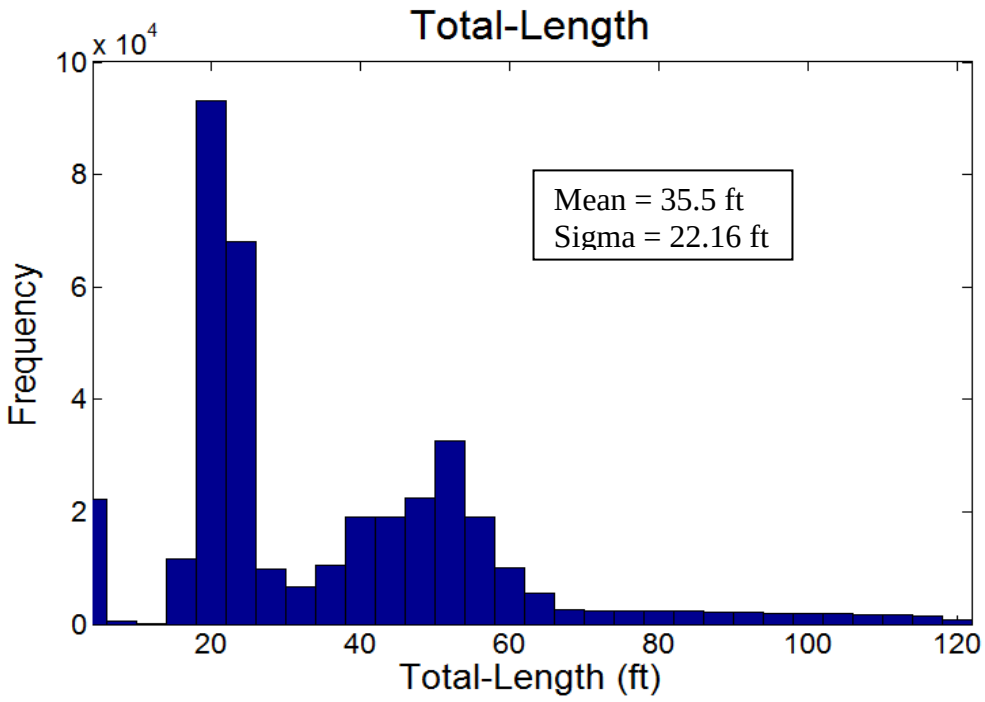

Figure 9.5. Total Length of Vehicles for Filtered Weigh-In-Motion Data

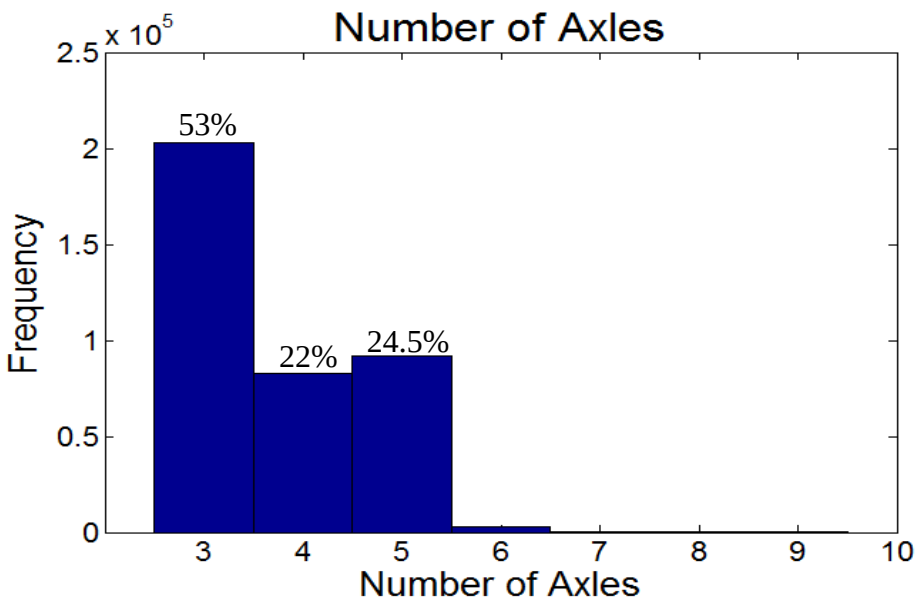

Figure 9.6. Total Number of Axles for Filtered Weigh-In-Motion Data

9.6.2.2 Trucks Simulation in 3D CSiBridge Model

In order to get the live load statistical load effect model, the structural response of the IRIB bridge caused by these filtered WIM vehicles must be determined. Since the edge girder of IRIB is monitored at 11 locations only along the bridge, the 3D finite element model is an excellent tool for evaluating the structural response at the unmonitored locations.

In general, live load analysis is performed as a moving load analysis to find the maximum responses from a moving load. The moving load analysis can be performed by creating influence lines for structural forces at each node in the FE model. After that, the live load is applied to the influence lines of each node to obtain the maximum live load structural responses produced by the applied live load. That requires creating truck models for each WIM event and analyzing the CSiBridge model for each event. To accomplish this, the author has used the influence lines created at each node from a

moving load analysis and used a Matlab code to create the live loads from the WIM data and applied them to the influence lines to obtain the structural responses from each filtered WIM record along the edge girder.

First, the influence lines for moment and axial forces are obtained from the 3D CSiBridge model for a moving load of 1 kip. There are 160 beam elements that make up the edge girder in the model. Since the west edge girder sees larger strains than does the east edge girder (due to the existence of a pedestrian walkway on the east side of the bridge), to represent the influence lines response the author used 0.1 feet meshing along the west edge girder. This leads to 17,500 nodes. The moving load analysis is then used to create influence lines along the west edge girder, and the influence lines for moment and axial forces for the 160 locations at the center of these beam elements are obtained from the analysis.

The resulting influence lines for moments and axial forces for those 160 locations are saved in text files with a name of the beam element number. For example, for beam element number 1, influence lines are saved in text file called W1. The W states for the west edge girder and the number states for the beam element order in the model. Also, each text file has two columns, the first one is the moment influence lines and the second one is the influence lines for the axial force.

9.6.2.3 Final Live Load Model

The Matlab code imports the filtered WIM data from Microsoft EXCEL sheets and creates equivalent vectors for the vehicle loads based on the axle weights and axle spacings provided in the recorded WIM data. Then it applies the 381,272 vectors (vehicles) on the influence lines of each beam element (W1, W2, through W160) using the convolution command in Matlab to obtain the maximum structural responses

(moments and axial forces). The "CONV" command in Matlab is used to return the convolution of vectors if they are vectors of polynomial coefficients and that is equivalent to multiplying the two polynomials. The benefit of using this command is that it cuts the analysis time to around 1/10 of what is needed if standard commands are used to multiply the polynomial vectors to find the maximum responses.

In addition obtaining the maximum moment and maximum axial forces using the Matlab, the code also is used to calculate the stresses at the top and the bottom of the edge girder using the design section properties and Equation 5.3. These stresses are then converted into strains using the design material properties and Equation 4.1. All of the results are then saved in Microsoft EXCEL sheets for each member along the west edge girder. In addition, the Matlab code creates histograms of the structural responses for each member along the edge girder, and fits the data into Probability Distribution Functions and determines their statistical parameters.

Using this methodology, the live loads from the two WIM stations recorded for three and a half years have been applied to each member in the model and the maximum structural responses and stresses have been computed and saved for each vehicle of the filtered WIM data. By doing this the author found that the distribution for these responses fits a log-normal distribution and the statistical parameters were saved to a Microsoft EXCEL sheet. Figures 9.7, 9.8, and 9.9 represent samples of the final live load statistical model and show their associated parameters for those members.

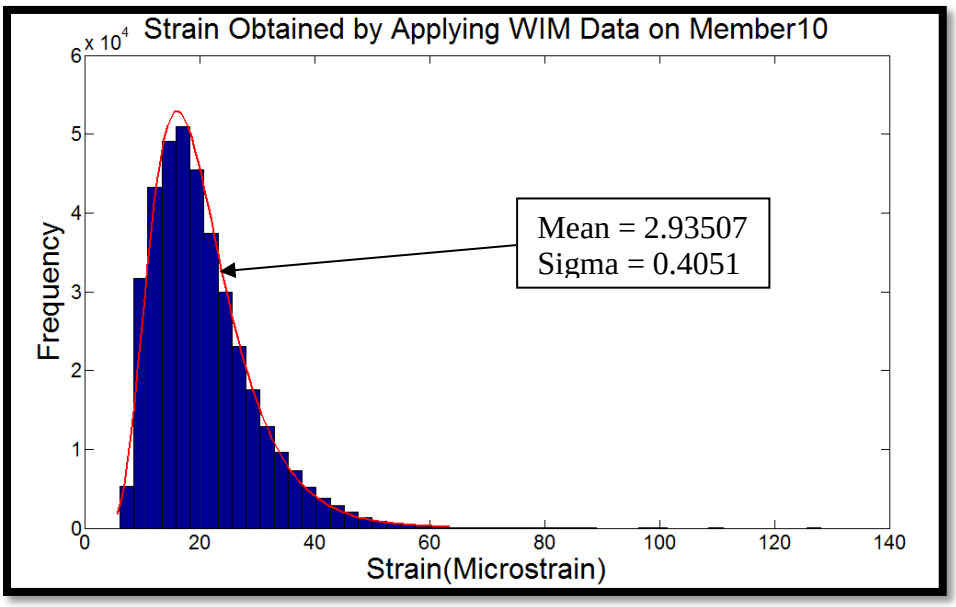

Figure 9.7. Final Strain Distribution Obtained By WIM Data and Log-normal Distribution Parameters for Member 10

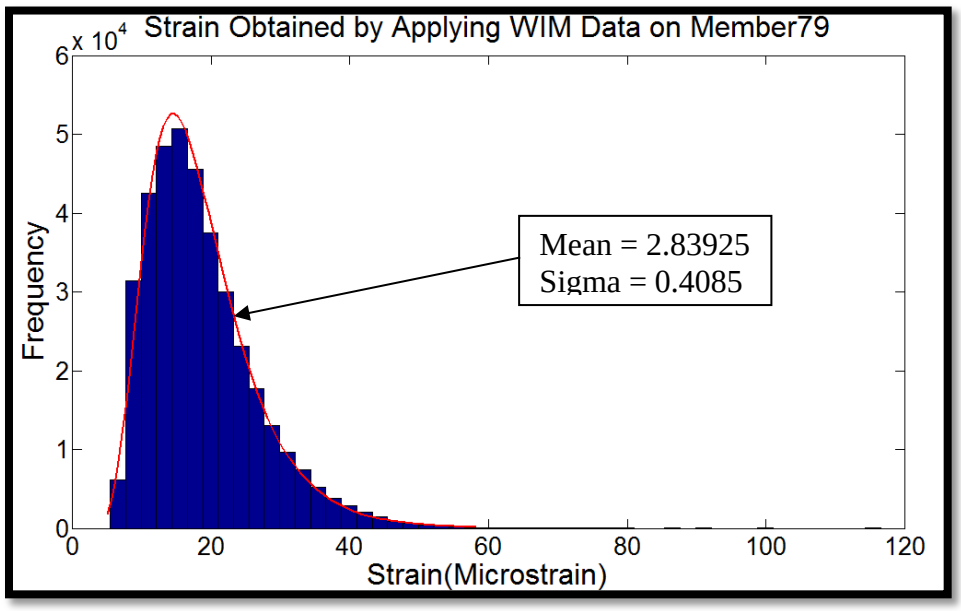

Figure 9.8. Final Strain Distribution Obtained By WIM Data and Log-normal Distribution Parameters for Member 89 at Mid-span location

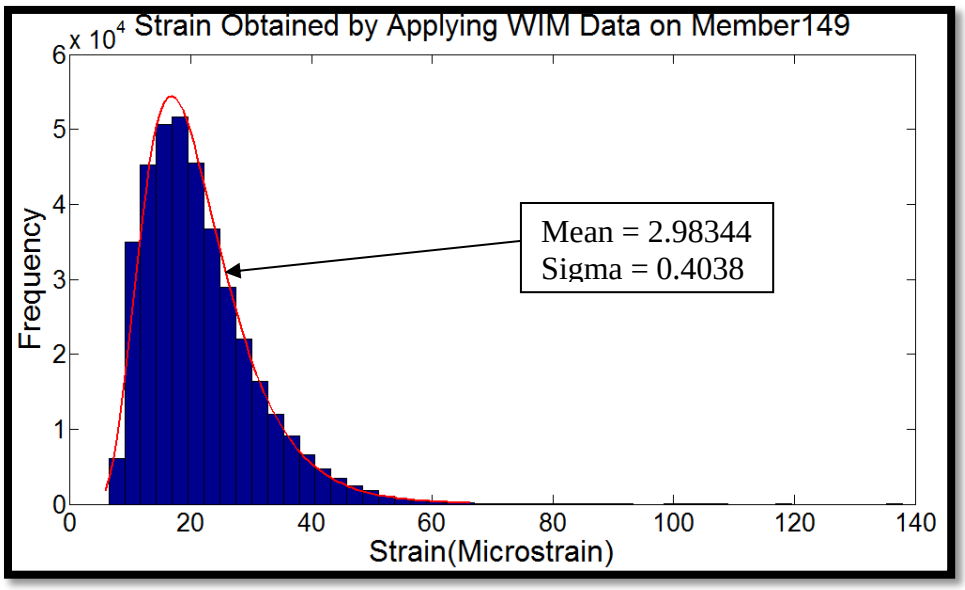

Figure 9.9. Final Strain Distribution Obtained By WIM Data and Log-normal Distribution Parameters for Member 149 at Controlling Location

9.6.3 Environmental Statistical Model

Thermal loads and wind loads are the most common component of an environmental load model. Although the design process for bridges includes thermal loads and wind loads, it is still very difficult to estimate the actual loads and their effects on structures. Continuous SHM data can be used to better quantify the effects of these environmental loads on bridges.

The main component of environmental loads of interest for the IRIB bridge is thermal loads. Thermal loads occur as a result of the cyclic change in temperature throughout the day or a cyclic change over the year due to seasonal changes. These changes in temperature cause bridge expansion or contraction. If boundary conditions restrain the bridge movements, as explained in Chapter 8, internal stresses and forces

are developed. The change in temperature could be uniform through a cross-section, or can vary though the cross-section (i.e. have a gradient).

9.6.3.1 Sample of Collected Data

The low frequency data collected by the SHM system on the IRIB has been collected since May 2012. The low frequency data includes strain and temperature measurements from sensors in the west and east edge girders. Since thermal loads follow a slow trend, the low frequency data collection protocol is suitable for capturing the thermal load effects.

Even though the SHM system has been in service since May 2012, and the low frequency data has been collected since that time, the strain equation used to calculate the strain and the temperature based on the change of the wave length was not very accurate in the early years. An updated equation, shown in Chapter 3 as Equation 3.1, was applied in the end of February 2015 and has been used since then. Since the amount of data collected since February 2015 was not suitable to generate a reliable thermal statistical model, a different procedure was followed to obtain the thermal statistical model. It should be noted that this procedure can be changed in the future once a sufficient amount of data becomes available directly from the SHM system. A sample of the collected low frequency strain data can be seen in Figure 9.10 for sensor SW-22. It is obvious from the figure that the strain data follows both a daily and seasonal temperature change.

Figure 9.10. Sample of Low Frequency Strain Data for Sensor SW-22

In order to create a representative model for the thermal effects, at least one year of data is needed to capture the seasonal effects. Since the data that has been collected from the SHM system (at that time) represents less than a full year, another source of temperature data is required. The Delaware Environmental Observing System (DOES) was used to provide the required temperature data.

9.6.3.2 Delaware Environmental Observing System (DEOS) Data

The DEOS system has been measuring real-time environmental conditions for Delaware and surrounding regions for the past 10 years. There are several stations spread throughout the state of Delaware. One of these stations is the Indian River Inlet

Station (DE-LSS Station). This station is located two miles north of the IRIB. A map that shows the location of DE-LSS station is given in Figure 9.11.

Figure 9.11. DE-LSS DEOS Station Location Compared to the IRIB Location

A host of environmental condition are recorded at DEOS stations including temperatures, wind speed, humidity, etc. Since the station is very close to the IRIB, researchers decided to use data from DEOS station DE-LSS to create the environmental model. Daily average, daily minimum, and daily maximum temperature and wind speed data for the years of 2010 through 2014 were requested from the DEOS office at the University of Delaware. Figure 9.12 shows a sample of the tables provided by the DEOS office for the DE-LSS station for January 1, 2013. Figure 9.13 shows the daily average temperature and wind speed at the DE-LSS station for the June 2012 to June 2014.

Indian River Inlet, DE-LSS Station

ID	DIRL	Network	DEOS
City/State	Indian River Inlet/DE	Elevation	15 ft.
Latitude	38° 38' N	Longitude	75° 4' W

24-Hour Summary for January 1, 2013

Hour	Temp (°F)	Temp (°C)	Dew Point (°F)	Dew Point (°C)	Rel Hum. (%)	Wind Spd. (MPH)	Wind Spd. (m/s)	Wind Dir (°)	Wind Gust (MPH)	Wind Gust (m/s)	Heat Inde (°F)
0	42.7	5.9	30.2	-1.0	61	7.3	3.3	232.2 (SW)	10.0@00:10	4.5	N/A
1	41.7	5.4	31.6	-0.2	67	6.6	3.0	231.2 (SW)	10.0@02:00	4.4	N/A
2	42.1	5.6	29.0	-1.7	60	8.2	3.7	245.2 (WSW)	11.9@02:35	5.3	N/A
3	41.5	5.3	29.2	-1.5	61	5.8	2.6	236.3 (WSW)	8.9@03:10	4.0	N/A
4	41.3	5.2	29.1	-1.6	62	5.3	2.4	255.9 (WSW)	8.9@04:25	4.0	N/A
5	41.0	5.0	29.4	-1.5	63	4.5	2.0	268.7 (W)	6.2@05:15	2.8	N/A
6	40.7	4.8	30.2	-1.0	66	3.7	1.7	267.3 (W)	5.4@06:20	2.4	N/A
7	41.4	5.2	28.9	-1.7	61	4.2	1.9	254.3 (WSW)	6.9@08:00	3.1	N/A
8	42.3	5.7	29.0	-1.7	59	4.3	1.9	244.5 (WSW)	6.6@09:00	2.9	N/A
9	42.8	6.0	30.2	-1.0	61	4.4	2.0	214.6 (SW)	6.7@10:00	3.0	N/A
10	43.9	6.6	31.6	-0.2	62	5.0	2.2	242.4 (WSW)	8.5@10:55	3.8	N/A
11	45.0	7.2	30.1	-1.0	56	6.5	2.9	265.3 (W)	11.4@12:00	5.1	N/A
12	45.4	7.4	30.7	-0.7	56	6.5	2.9	264.8 (W)	9.7@12:40	4.4	N/A
13	45.3	7.4	30.9	-0.6	57	6.3	2.8	261.8 (W)	10.2@13:25	4.6	N/A
14	44.8	7.1	30.8	-0.6	58	5.5	2.5	260.3 (W)	9.5@15:00	4.3	N/A
15	43.8	6.6	31.7	-0.1	62	6.4	2.8	273.7 (W)	9.3@15:40	4.2	N/A
16	42.8	6.0	31.7	-0.1	65	4.8	2.2	272.0 (W)	8.3@16:05	3.7	N/A
17	41.6	5.4	32.4	0.2	69	3.7	1.6	276.6 (W)	5.1@17:35	2.3	N/A
18	40.7	4.9	32.0	-0.0	71	3.5	1.6	296.3 (WNW)	5.4@18:55	2.4	N/A
19	40.2	4.6	31.7	-0.2	71	3.3	1.5	285.4 (WNW)	4.7@19:05	2.1	N/A
20	39.9	4.4	31.4	-0.4	71	2.6	1.2	310.1 (NW)	5.3@20:10	2.4	N/A
21	39.5	4.2	31.8	-0.1	74	2.4	1.1	306.5 (NW)	4.9@22:00	2.2	N/A
22	39.8	4.4	30.6	-0.8	69	6.1	2.7	329.4 (NNW)	11.4@22:35	5.1	N/A
23	39.4	4.1	30.6	-0.8	70	5.7	2.5	324.9 (NW)	10.7@23:05	4.8	N/A

Summary

High Temp. (°F)	Low Temp. (°F)	Avg. Temp. (°F)	Avg. Dew Point (°F)	Avg. Rel Hum (%)	Avg. Wind Spd (MPH)	Avg. Wind Dir (°)	Peak Gust (MPH)	Max. Heat Inde (°F)
46.0	39.0	42.1	30.6	64	5.1	266.9 (W)	11.9	N/A

Note: All observations were obtained from the Delaware Environmental Observing System network

Figure 9.12. Sample of DEOS Table Shows Minimum, Maximum, and Average Temperature with Wind Speed for January 1, 2013

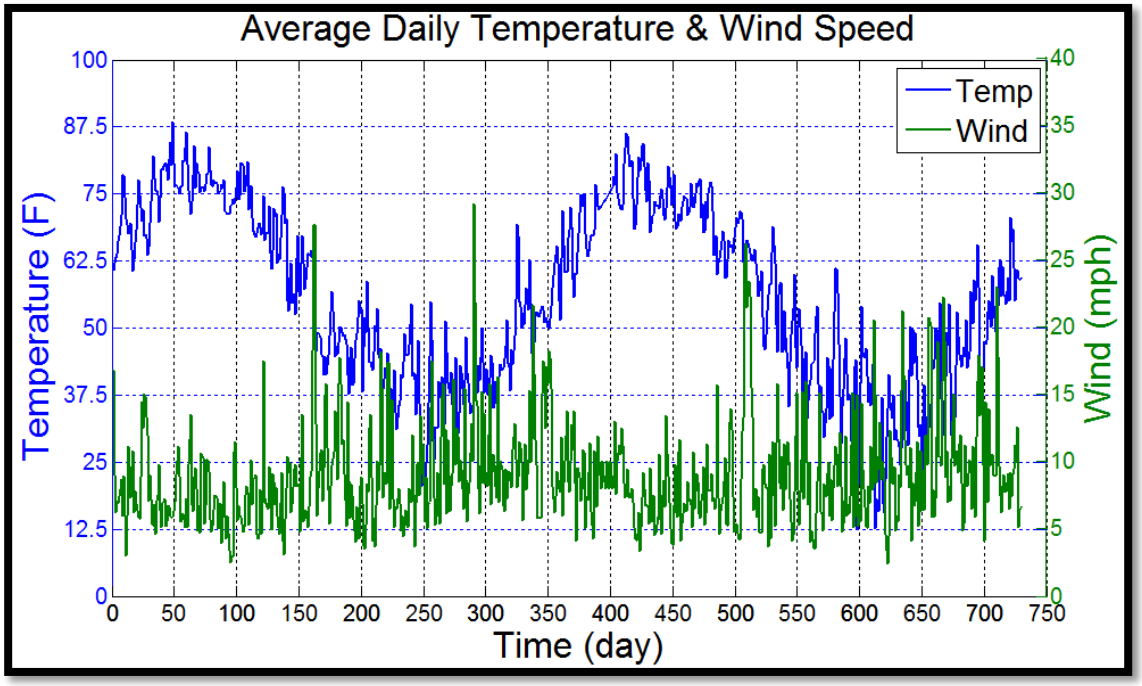

Figure 9.13. Average Daily Temperature and Wind Speed for June 2012 to June 2014 at DE-LSS station

Actual temperature readings can be used to find daily and seasonal temperature fluctuations that cause bridge movements and cause internal forces and stresses. In order to find the actual temperature fluctuations during a given day, first the difference between the maximum and minimum temperatures from the same daily temperature records are calculated. This was done by subtracting the minimum temperature from maximum temperature at that day; this allowed for capturing the positive daily fluctuations. In order to capture the negative daily fluctuations; maximum temperature for a given day was subtracted from the next day minimum temperature; this process allowed for capturing the negative daily fluctuations. However, to find the temperature fluctuations during the year (seasonal fluctuations), the difference between daily

averages and the baseline average found over the five years was 13.2 Celsius. The daily fluctuations and the seasonal fluctuations were added together to form the overall temperature fluctuations for the IRIB for 2010 through 2014. Figure 9.13 shows a combined histogram of daily and seasonal temperature fluctuations for the five years; Figure 9.14 shows a histogram of the maximum daily wind speed for the five years.

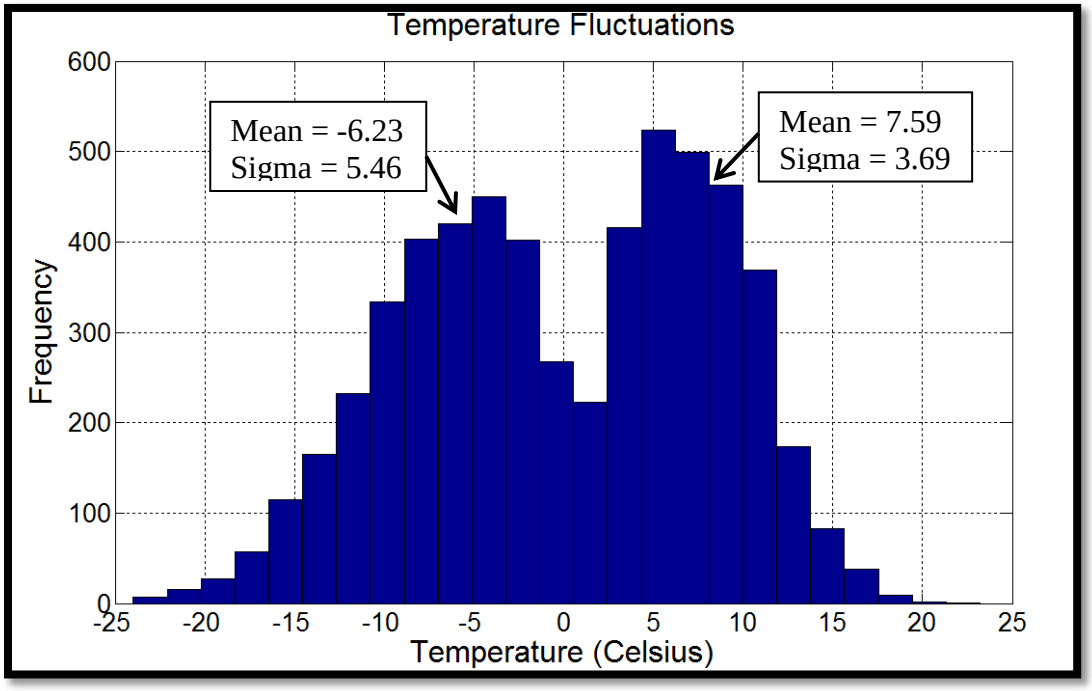

Figure 9.14. Daily and Seasonal Temperature Fluctuations (2010 to 2014)

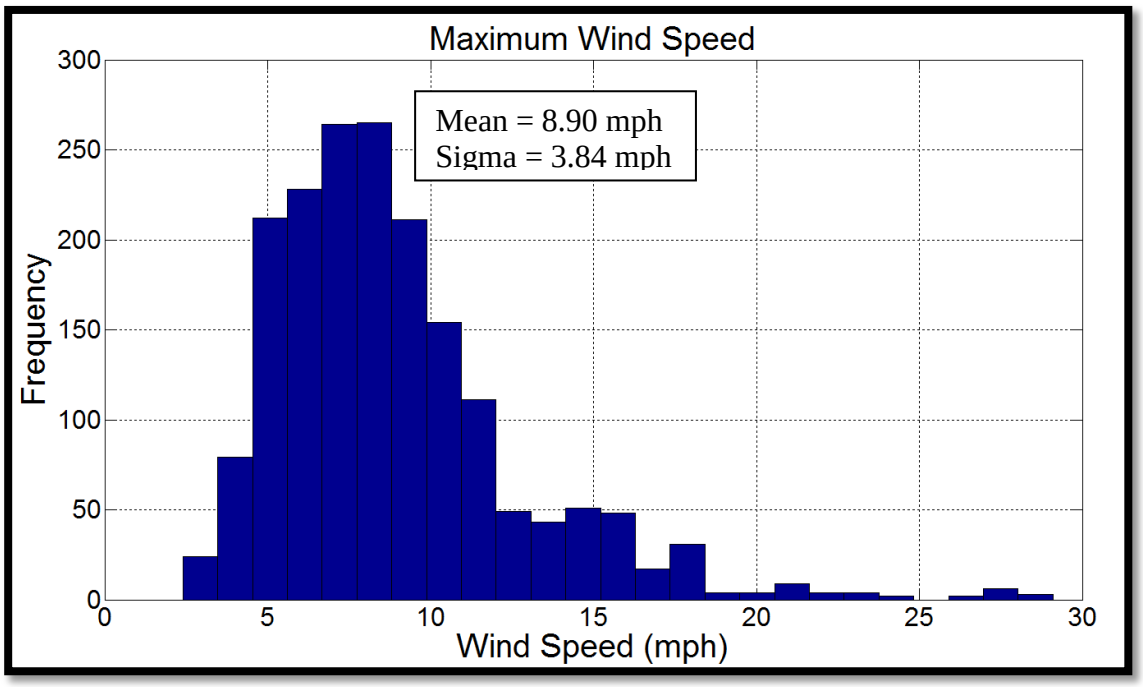

Figure 9.15. Maximum Daily Wind Speed (2010 to 2014)

9.6.3.3 Correlation and Regression Analysis

Since the strain data coming directly from the SHM system of IRIB is not enough data to create a robust thermal model because it represents less than a full year, regression analysis was used to predict strains based on the DEOS temperature data. A regression analysis was performed to find the effects of an increase or decrease of one degree Celsius at each strain sensor location in the edge girders using the available data at that time. A record of temperature and strain data was recorded between March 7, 2014 and May 7, 2014 was used to conduct regression analysis at each sensor location with the associated recorded (measured) temperature at that same sensor. Figure 9.16 shows an example of the regression analysis results for the

monitored strain and measured temperature from sensor SE-22 for the two months period.

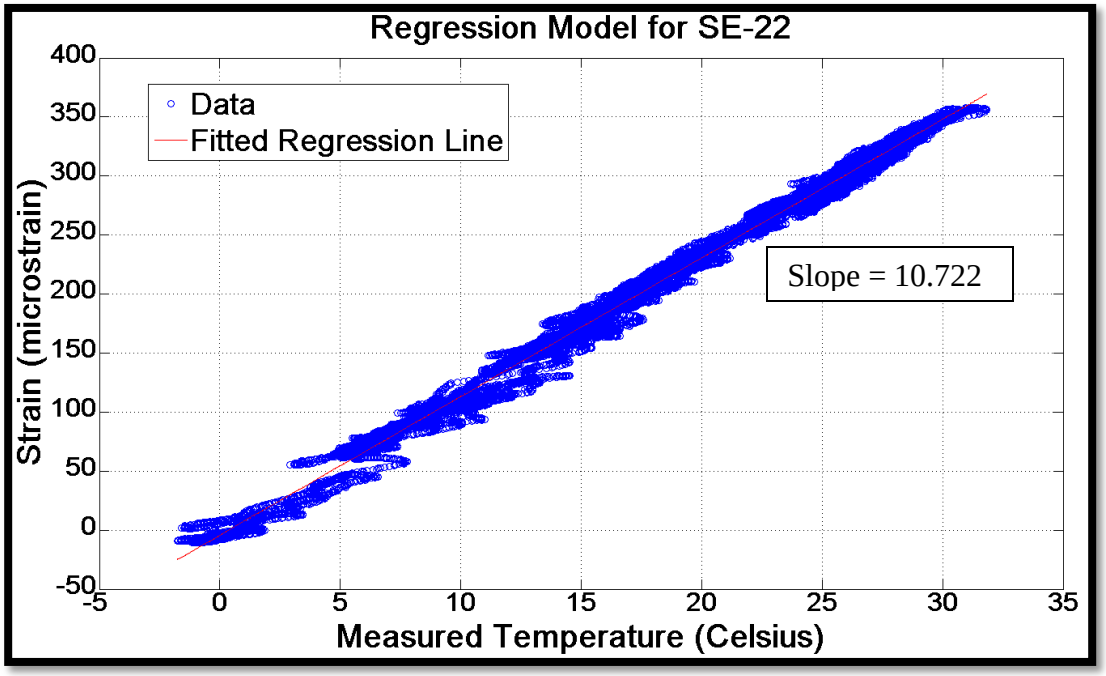

Figure 9.16. Regression Model for Sensor SE-22 with all Measured Data Between March 7, 2014 to May 7, 2014

Figure 9.16 shows a good linear correlation between the measured strain and the measured temperature. The slope in the figure represents the strain increment caused by a unit temperature variation. For example, for sensor SE-22, if temperature increases 1 degree Celsius, the strain increases by 10.722 microstrain. By having these slopes, predicting strains at all sensor locations based on temperature changes is possible. Also, a change in the slope over time can indicate a change in the behavior of

the bridge and possible change in bearing functionality. Table 9.2 shows these slopes for all sensors located in the edge girders.

It was assumed that the temperature fluctuations calculated from the DEOS data have the same magnitudes at the sensor locations. Figure 9.17 shows a comparison between the measured temperature at sensor SE-22 and the recorded temperature data from DEOS system at DE-LSS station for the two months period. It can be seen from the figure that the temperature swings at the sensor location are not as great as they are for the DEOS data, and there is a small lag in the sensor data (as one would expect); however, the general trend of the changes track the DEOS data well, with the overall fluctuations varying from 0.4 to 23 Celsius. The overall fluctuations are assumed to be the same in this analysis for simplifying purposes. However, once conducting this analysis in the future, actual measured strain in can be used and there will be no need to consider this assumption.

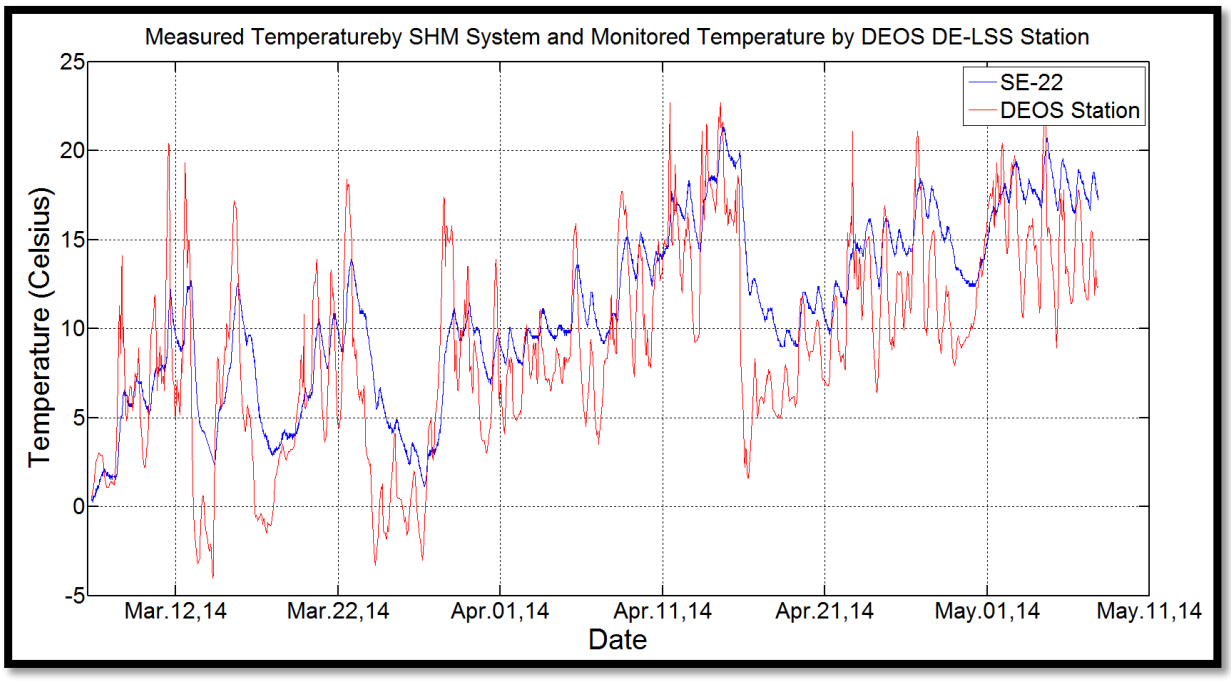

Figure 9.17. Comparison Between Measured Temperature at sensor SE-22 and Recorded Temperature by DEOS System at DE-LSS Station

The expectation is that the temperature fluctuations are the main cause of the structural response captured by the low frequency data. In order to prove this, correlation analysis between the strain from the low frequency data and the recorded temperature readings were made. The correlation coefficients between the measured strain and the recorded temperature change were found at all sensors locations. The correlation coefficients were high at all sensor locations, which indicate that the temperature changes are indeed the predominant load affecting the collected low frequency strain data. Table 9.2 shows the correlation coefficients between measured strain and the recorded temperature change for all strain sensors in the edge girders. As a result, the wind data is ignored in this study and temperature is considered to be the only load included in the environmental model.

Table 9.2. Correlation Coefficients and Regression Model Slopes between measured Strain and Temperature

Sensor	Correlation Coefficient	Regression Model Slope	Sensor	Correlation Coefficient	Regression Model Slope
S-W1	0.977	9.670	**S-E1**	NaN	NaN
S-W2	0.909	8.760	**S-E2**	NaN	NaN
S-W3	0.965	9.090	**S-E3**	0.973	10.110
S-W4	0.957	12.630	**S-E4**	0.974	10.840
S-W5	0.977	8.870	**S-E5**	0.968	10.730
S-W6	0.931	14.790	**S-E6**	0.940	14.060
S-W7	0.967	10.340	**S-E7**	0.980	10.780
S-W8	0.916	12.339	**S-E8**	0.921	12.530
S-W9	0.953	10.410	**S-E9**	NaN	NaN
S-W10	0.967	11.750	**S-E10**	NaN	NaN
S-W11	0.978	10.670	**S-E11**	0.969	11.708
S-W12	0.965	12.640	**S-E12**	0.970	13.350
S-W13	0.981	9.920	**S-E13**	0.981	10.440
S-W14	0.975	11.430	**S-E14**	0.974	12.120
S-W15	0.976	9.460	**S-E15**	0.966	10.470
S-W16	NaN	NaN	**S-E16**	0.974	11.107
S-W17	NaN	NaN	**S-E17**	NaN	NaN
S-W18	NaN	NaN	**S-E18**	NaN	NaN
S-W19	0.963	10.930	**S-E19**	0.964	9.410
S-W20	0.955	12.460	**S-E20**	0.982	17.674
S-W21	0.967	10.910	**S-E21**	NaN	NaN
S-W22	0.987	10.220	**S-E22**	0.995	10.722

9.6.3.4 Final Environmental Model

The analyses that have been performed involving the thermal loads show that the environmental model is composed primarily of thermal loads (since the linear correlation is high between the measured strain and temperature). As a result, wind loads have been ignored in this study. Since the measured data from the SHM system

did not represent a full year of data, DEOS data was used to calculate temperature fluctuations in 2010 through 2014. Regression analysis was then performed using the monitored strain and measured temperature data at each sensor location to determine the slope that can be used for predicting strains based on temperature fluctuations.

In order to determine the final thermal model, the distribution function for the temperature fluctuations must be found. A histogram of the temperature fluctuations is shown in Figure 9.14. A Matlab code was developed to fit the histogram in a reasonable distribution function. The statistical distribution results indicate that the distribution function of the temperature fluctuations can be fitted by two weighted normal distributions. In addition to the estimation of the PDF parameters, the Matlab code develops the Cumulative Distribution Functions (CDF) both empirically and theoretically for the empirical and theoretical PDF's. Equation 9.10 shows the general case of cumulative density function for two weighted normal distribution functions.

$$\mathrm{F(X)} = P_1\varphi\left(\frac{X-\mu_{X1}}{\sigma_1}\right) + P_2\varphi\left(\frac{X-\mu_{X2}}{\sigma_2}\right) \quad Equation\ 9.10$$

Where,

- F(X): Theoretical cumulative density function
- P_1, P_2: Weighted probability for the first and second normal distributions, respectively
- $\varphi(.)$: Cumulative probability function of standard normal distribution
- X : Random variable (temperature fluctuation)
- μ_1, μ_2 : Mean value of the first and second normal distributions, respectively
- σ_1, σ_2: Standard deviation for the first and second normal distributions, respectively

The parameters for the two weighted normal distribution and their cumulative distribution functions are given in Table 9.3 The empirical and theoretical PDF's and CDF's for the temperature fluctuations from the DEOS data are presented in Figure 9.18.

Table 9.3. Parameters Estimation for Cumulative Distribution Function

Distribution number	P_i	μ_i	σ_i
1	0.549	-6.234	5.458
2	0.451	7.59	3.689

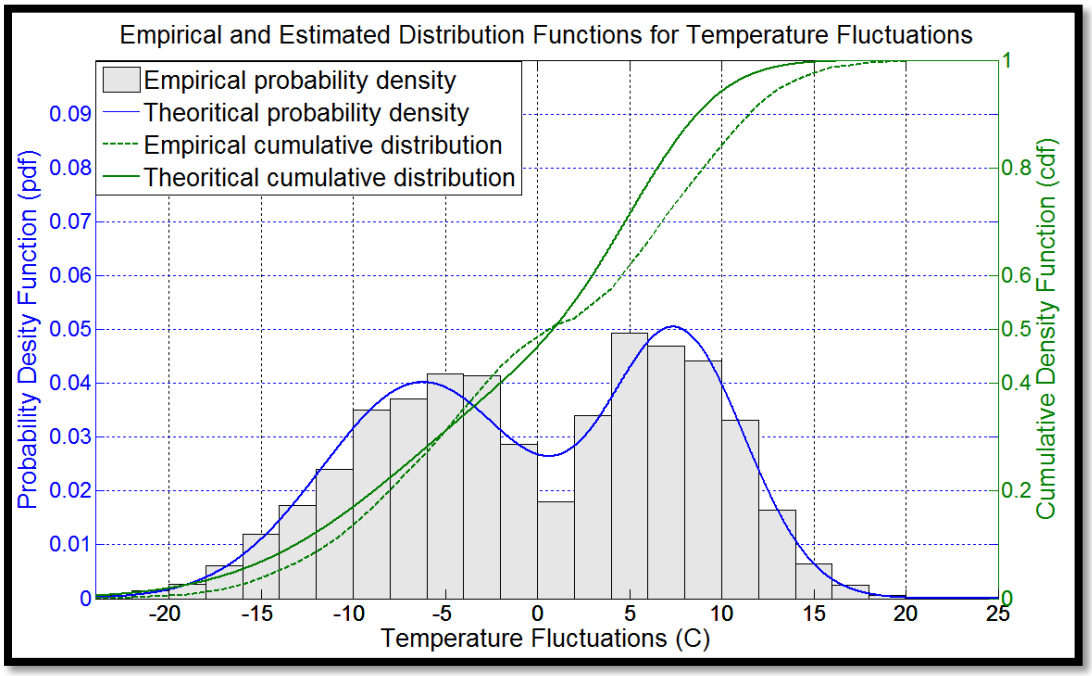

Figure 9.18. Empirical and Theoretical Probability Distribution Function and Cumulative Distribution Function For Temperature Fluctuations

For the monitored locations, the final distribution model can be obtained by multiplying the slopes given by the regression analysis shown in Table 9.2 by the probability density function obtained by the Matlab Code. The results will have the shape of the PDF shown in Figure 9.18, but the values for each sensor will vary based on the slope obtained from the regression model. For example, for sensor SE-22, the slope from the regression model is 10.722 microstrain per unit temperature. That value would be multiplied by the estimated values of the mean and standard deviation of the weighted normal distributions. Therefore, the shape of the new weighted normal distribution follows the same distribution shown in Figure 9.18, but the mean value and the standard deviation of the new distribution are generated by multiplying the slope with the values of the mean and the standard deviation in Table 9.3. The results for sensor SE-22 are presented in Table 9.4.

Table 9.4. Calculated Parameters for The CDF At Sensor SE-22

Distribution number	P_i	μ_i	σ_i
1	0.549	-66.8409	58.5207
2	0.451	81.38	39.5535

As mentioned previously, the west edge girder is monitored at 11 locations along the bridge. In order to find the effect of temperature changes at unmonitored locations, slopes of regression analysis are needed. A linear approximation was used between each two monitored locations to estimate the slopes at the unmonitored locations. As a result, slopes for the 160 members of the west edge girder were estimated.

The linear approximation is established by performing linear correlation between the data coming from sensors adjacent to each other. Linear correlation factors are obtained between measured strains at sensors adjacent to each other. The strain correlation coefficients were very high, implying that, there is a strong linear correlation between the strains measured along the edge girder. Similarly, the linear correlation coefficients were obtained for the measured temperature (sensor temperature) along the edge girder. The correlation coefficients were again very high, implying that there is a strong linear correlation between the measured temperatures along the edge girder.

Since the strain between two sensors that are next to each other correlates very well, as does the measured temperature at those sensors, a linear approximation can be performed to estimate the regression slopes for the unmonitored locations between sensors that are adjacent to each other. By doing this, regression slopes for the 149 unmonitored locations were determined. The final thermal statistical models were obtained at each member location by multiplying the slope of the regression analysis by the values of the mean and standard deviation in Table 9.3. The resulted PDF's follow the same distribution of the PDF in Figure 9.18, but have different mean and standard deviation values based on the regression slopes as explained earlier in this section.

9.7 Resistance Statistical Model

The statistical parameters used in the National Cooperative Highway Research Project (NCHRP) *Updating the Calibration Report* (20-7/186) were also used for the resistance statistical model in this analysis. In NCHRP Report (20-7/186), three uncertainties were considered for the resistance model, material factor (M), fabrication

factor (F), and professional factor (P). The resistance model (R) is obtained by multiplying the three factors by the nominal resistance (R_n), $R = M \cdot F \cdot P \cdot R_n$. The mean value can be expressed as $\mu_R = \mu_M \cdot \mu_F \cdot \mu_P \cdot R$, and the coefficient of variation can be expressed as the square root of the summation of the variances, $V_R = \sqrt{V_M^2 + V_F^2 + V_P^2}$. The result of the product of random variables will produce lognormal random variables.

The final resistance model used for the code calibration had a lognormal distribution. Table 7.3 presents the statistical parameters for the resistance components. In this reliability analysis, and for all of the limit states used, a bias factor of 1.05 and a coefficient of variation of 0.075 were used (with the assumption of lognormal distribution for the design resistance capacities of the bridge).

The dead load statistical model is assumed to be normally distributed; however, the live load statistical model, the environmental statistical model, and the resistance model are not assumed to be normally distributed. Therefore, the closed form solutions that were presented in Equations 7.1 or 7.3 are not valid for this case. Therefore, Monte Carlo Simulation, or another technique such Rackwitz-Fiessler, is needed to find the reliability indices.

9.8 Reliability Analysis in Matlab Code

The Matlab code used to perform the reliability analysis based on design information presented in Chapter 7 was expanded and refined to perform a reliability analysis based on SHM data. The Matlab code used the Monte Carlo Simulation tool as explained in Chapter 7. The new code takes into consideration the statistical live load model and the statistical environmental model for all limit states. A sufficient number of iterations are assured by inspecting the number of failures at each location.

Monte Carlo was used first to conduct the analysis along the west edge girder. However, no failures were detected (probability of failure is equal to zero) even after applying sufficient number of iterations (i.e. 10^6). For that reason, another method should be used to obtain the reliability indices such as the Hasofer-Lind method. Hasofer-Lind method evaluates the limit state function at the design point instead of mean values. Furthermore, because the distributions of random variables were available, the procedure was improved as explained earlier in this chapter by using Rackwitz-Fiessler method.

The Rackwitz-Fiessler method is used to obtain the reliability indices from the SHM data. To do so requires the knowledge of probability distribution functions. If the random variables do not follow a normal distribution, then the equivalent normal parameters should be used. The Rackwitz-Fiessler analysis was conducted using a Matlab code for all the applicable limit states using the equations presented earlier in this chapter. The analysis was conducted at 160 locations along the west edge girder. Those locations represent the centers of the beams that form the west edge girder in the finite element model.

9.9 Analysis Results

This chapter discusses the reliability analysis based on SHM data. Different limit states were used to determine the reliability indices along the west edge girder. The dead load effects, live load effects, and thermal effects represent the load effects model. The resistance model follows the limit state type.

A normal distribution was assumed for dead loads and was created by using the mean value from the extracted design loads with a bias factor and a coefficient of variation. The analysis for the WIM data showed that the live load effects can be

presented in lognormal distribution. The thermal effects can be fitted in two weighted normal distributions as discussed previously. On the other hand, the resistance model is assumed to have a lognormal distribution that can be obtained by verifying the mean value as a design value and a bias factor and coefficient of variation as discussed earlier in this chapter.

The reliability indices based on design information were obtained and discussed in Chapter 7. Since the LRFD code was calibrated for only the Strength I limit state, the focus in Chapter 7 was to compare the calculated β factors for the Strength I limit state to the target reliability index (β_T). The β factors from the other limit states cannot be compared to β_T, but their results are used as a baseline for reliability analysis based on the SHM data. However, the thermal effects are not included in calculating the reliability indices based on design information. Therefore, a number of comparisons of results obtained when thermal effects were included and excluded were made to show their effects on the reliability analysis.

Strength I, and Service I and III limit states were applied to obtain the reliability indices based on SHM data. The procedure for all limit states was nearly identical. The moment effects were used in the case of Strength I flexural limit state, while stresses that came from moments and axial forces effects were used in the Service limit states. Normal distributions with bias factors of 1.05 and a coefficient of variation of 0.1 were used with the extracted dead load moment or stress design values to generate the dead load statistical model at each member along the west edge girder. The WIM data analysis showed that the live load moments and stresses can be expressed in lognormal distributions. After obtaining the strains and the fluctuations as explained earlier in this chapter, the thermal moments and stresses were calculated

using Equation 9.10. The resistance model for the Strength I flexural limit state was created using the extracted flexural capacities from interaction diagrams as explained in Chapter 5. An equation was applied to the compressive strength of concrete to obtain stresses in the case of the Service limit states. For Service III, $3\sqrt{f'c}$ was used as a mean value for the lognormal distribution, and $-0.6f'c$ was used for the Service I limit state. A bias factor of 1.05 and a coefficient of variation of 0.075 with a lognormal distribution were used to create the resistance model at the center of each member along the west edge girder.

The analysis was conducted for each limit state taking into consideration all load effects at the same time, or excluding the thermal loads to see their effects on the reliability analysis. In other words, the reliability analysis based on SHM data was conducted using all load effects (dead, live, and thermal loads) and using only the dead and live load effects without including the thermal effects. This comparison shows the thermal load effects on the reliability indices. Also, the results from the reliability analysis based on design information are shown on the same figure. This is done to provide a comparison between the reliability indices based on design and SHM data. The reliability indices for Strength I flexural, Service III, and Service I limit states are presented in Figures 9.19, 9.20, and 9.21, respectively. A discussion of these figures is found in the following section.

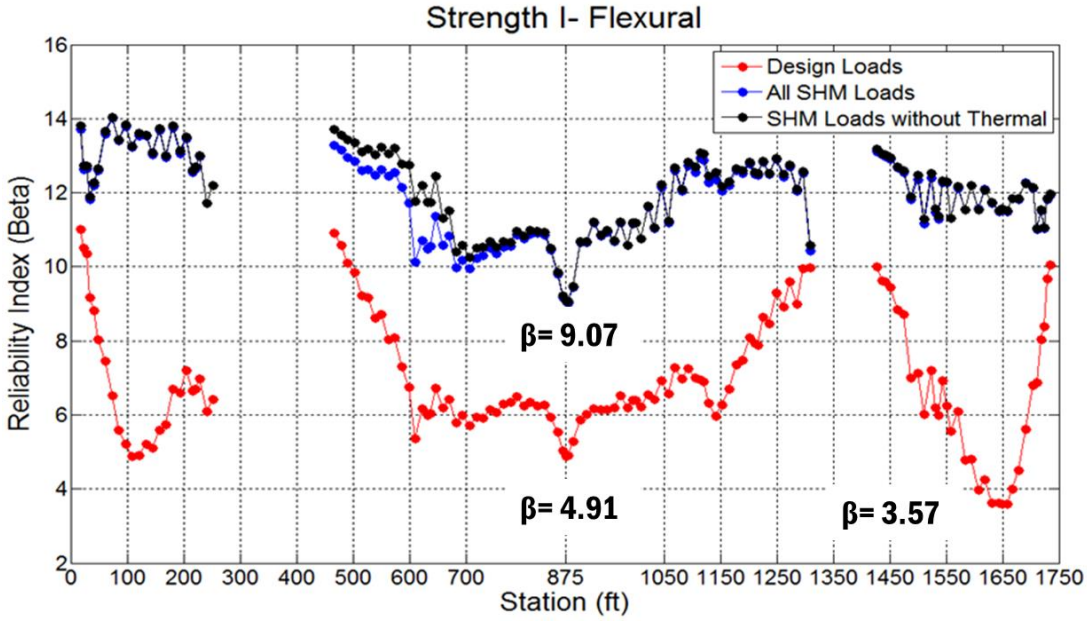

Figure 9.19. Reliability Indices Based on Design and SHM Data Along West Edge Girder for Strength I-Flexural

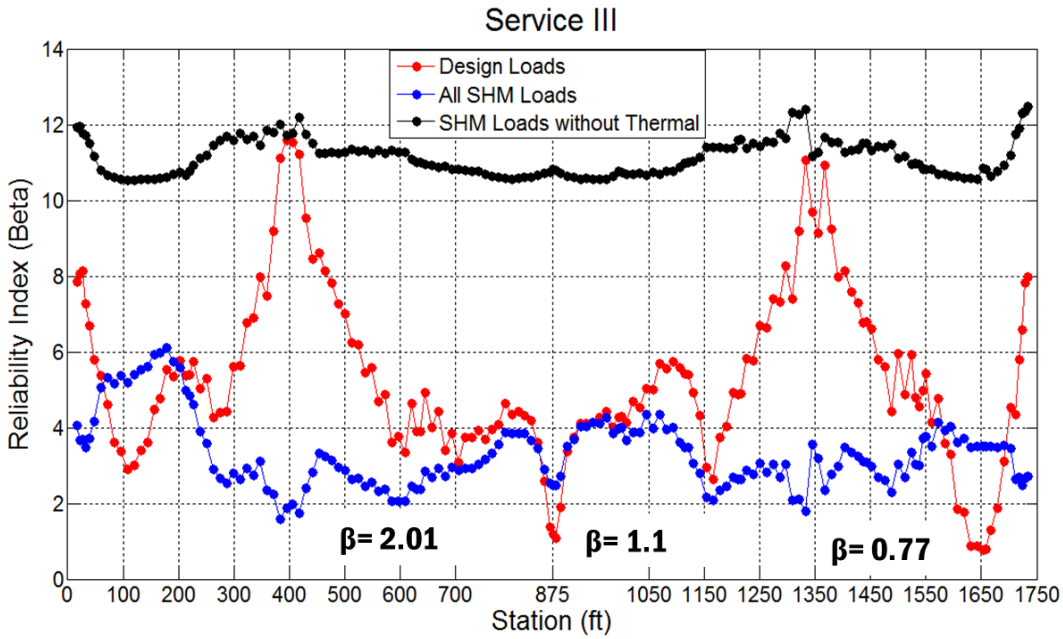

Figure 9.20. Reliability Indices Based on Design and SHM Data Along West Edge Girder for Service III

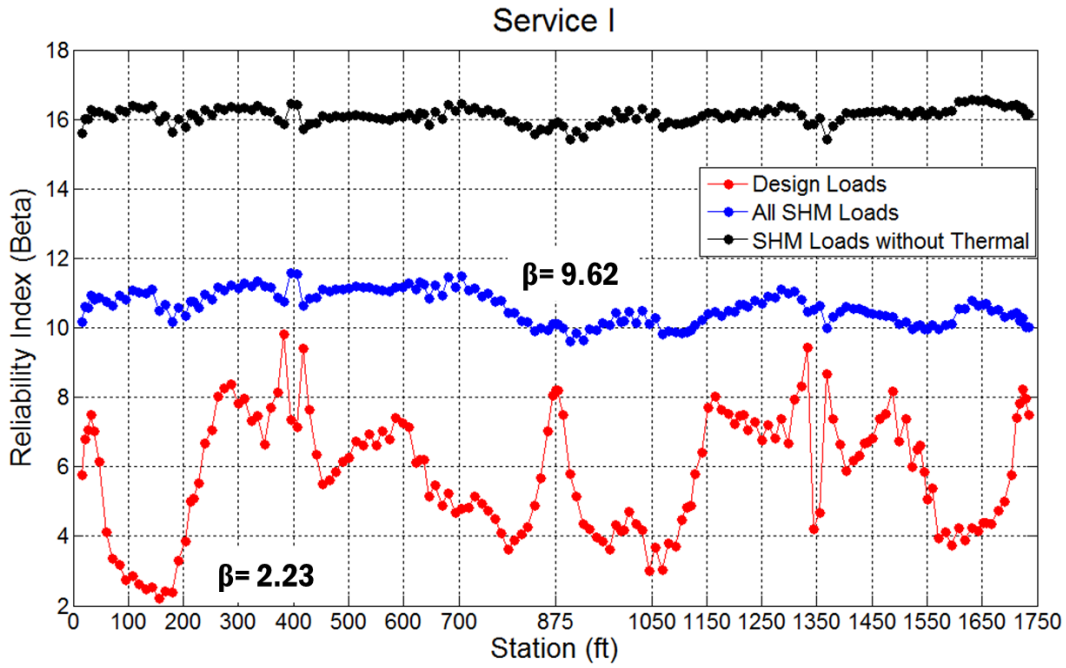

Figure 9.21. Reliability Indices Based on Design and SHM Data Along West Edge Girder for Service I

9.10 Discussion and Conclusions

Bridges that are designed according to the AASHTO LRFD Bridge Specifications should achieve a uniform level of safety. That level of safety is represented by the probability of failure, which can be represented by a target reliability index. Since the code was only calibrated for the Strength I flexural limit state, performing a reliability analysis using the design loads and resistance should result in a reliability near the target reliability (β_T =3.5). It can be seen from Figure 9.19 that the lowest reliability index along the west edge girder is 3.57 (at 1,649 ft from pier 4), which is very close to the target reliability as indicated before in Chapter 7. This location (1,649 ft) is also associated with the bridge controlling load rating factor according to design (i.e. lowest rating factor). Therefore, the lowest reliability

index was expected to be at this location since design loads only are used in this analysis.

Reliability analysis based on design information was also performed for Service I and III limit states. The current AASHTO code was not calibrated for Service limit state, but a new NCHRP Report that was published at the end of 2015 (*Bridges for Service Life Beyond 100 Years: Service Limit State Design*), contains a new proposed calibration for the AASHTO code. Large sample of bridges were used in this study. The study showed that the calculated reliability indices for different bridges from the sample were in the range of 0.5 to 1.0 (Kulicki et al. 2015). Even though the IRIB was not designed according to the new proposed changes for the code, but that provide a good reference to compare the computed reliability indices from service limit states with that range (0.5-1.0).

It can be seen from Figure 9.21 that the lowest reliability index from Service I limit state is 2.23 located at 155 ft from pier 4. The lowest reliability index from Service III limit state is 0.77 located at 1,649 ft from pier 4. Both of these locations were expected, because they are associated with the bridge controlling load rating factor of these limit states. The reliability index based on design for Service I limit state is above the range (0.5-1.0), and for Service III falls in the range. Therefore, one conclusion that can be drawn from the reliability analysis results based on design, that the IRIB satisfies the requirements of the current code and shows good agreement with the sample of analyzed bridges for the Service limit state calibration.

Reliability analysis was performed using SHM data for the same limit states. This analysis was performed twice, once considering dead, live, and thermal loads in the statistical models in the analysis, and another time considering just dead and live

loads in the statistical models (and excluding the thermal loads). This analysis was meant to show the effects of thermal loads on reliability analysis. See Figures 9.19-9.21.

Several results and conclusions can be drawn from Figure 9.19. The lowest reliability index based on design information was 3.57 at 1,649 ft from pier 4. The second region that shows the second lowest reliability index from the same figure is the mid span location (880 ft location from pier 4). It shows a reliability index of 4.91. The lowest reliability index from the reliability analysis performed using all load effects was 9.07 at the mid span location. This leads to a conclusion that the mid span location experienced more loads than the controlling rating factor location from design. Also, by comparing the reliability indices based on the two types of analyses (design and include all load effects) for the mid span location, the reliability index increased from 4.91 to 9.07. In general, special attention should be given to these locations with low reliability indices in future inspections.

The lowest reliability index based on design information from Service III is 0.77 at 1,649 ft from pier 4. The second region that shows the second lowest reliability index from the same figure is the mid span location (880 ft location from pier 4). It shows a reliability index of 1.10. The lowest reliability index from the reliability analysis performed using all load effects is 2.05 at 585 ft from pier 4 location. This leads to a conclusion that this location (585 ft) experienced more loads than the controlling rating factor location from design. Also, by comparing the reliability indices based on the two types of analyses (design and include all load effects) for the 585 ft location, the reliability index decreased from 3.62 to 2.05. In general, special

attention should be given to these locations with low reliability indices in future inspections.

The lowest reliability index based on design information from Service I is 2.23 at 155 ft from pier 4. The second region that shows the second lowest reliability index from the same figure is the 1045 ft from pier 4. It shows a reliability index of 3.02. The lowest reliability index from the reliability analysis performed using all load effects is 9.62 located at 901ft from pier 4. This leads to a conclusion that this location experienced more loads than the controlling rating factor location from design. Also, by comparing the reliability indices based on the two types of analyses (design and include all load effects) for the 155 ft location, the reliability index increased from 2.23 to 10.51. In general, special attention should be given to these locations with low reliability indices in future inspections.

The thermal effects on reliability indices can be seen and concluded also from the previous figures. The effects of thermal loads on the reliability analysis can be observed from the difference between the blue and black lines in the previous figures. For strength limit state thermal loads did not have a big influence on reliability indices, and that is because thermal load effects depend on the gradient temperature values (i.e. difference between top and bottom sensor temperature readings). A correlation analysis was conducted between the measured temperature at top sensor locations and the measured temperature at the bottom sensor locations showed very high correlation coefficients, which indicated a small gradient temperature effect on the edge girders. Since the edge girder of the IRIB is a solid concrete section, a very small gradient temperature effect was expected. Therefore including or excluding temperature effects did not influence the reliability indices obtained by Strength I limit

state. However, the thermal effects on reliability indices based on Service I and Service III limit states is obvious. For Service III limit state the lowest reliability index (based on all loads) is 2.05 and that increased to 11.33 when thermal loads were excluded. For Service I limit state the lowest reliability index was 10.51(based on all loads) and that increased to 15.95 when thermal loads were excluded.

The load combination that includes the dead, live, and thermal loads effects is the closest to the actual reliability indices for the bridge. These reliability indices can be compared directly to the reliability indices based on design information. If the reliability index is a lot lower than the design reliability index, that means that the probability of failure or probability of exceedance for the load effects are higher than the design loads, therefore special attention needs to be paid to those locations during inspection. In general, the locations associated with low reliability indices should be considered areas of interest in the future inspections.

This analysis can be performed yearly based on SHM data, and deterioration may be detected by comparing the reliability analysis from different years.

Chapter 10

CONCLUSIONS

10.1 Research Overview

This research study was conducted with the goal of developing methods for assisting transportation agencies in their efforts to ensure the structural safety and serviceability of their bridges through the use of Structural Health Monitoring (SHM) systems. The research results demonstrate the significant potential of incorporating SHM data in the inspection and evaluation process, and how the data can be used to enhance ensuing maintenance, repair, and rehabilitation decisions.

The Indian River Inlet Bridge (IRIB) was used as a study case in this research. The IRIB is a prestressed concrete bridge located in southern Delaware. It is managed and maintained by the Delaware Department of Transportation (DelDOT). The bridge has a permanent SHM system that was installed during the construction of the bridge. This is the first bridge in the United States to have a comprehensive, permanent SHM system installed during the initial construction stage with the expectation that it will track the bridges performance over its life.

10.2 Principal Contributions, Findings, and Conclusions

There are several important contributions, findings, and conclusions that resulted from the research that has been conducted and reported in this dissertation. First, let us review the more ancillary contributions of this work. These contributions are specific to the IRIB bridge and are of significant practical use to DelDOT.

Furthermore, these efforts have enabled the primary objectives of the study, the use of SHM data in bridge evaluation, to be achieved. The ancillary achievements can be summarized as follows; (1) developing a Finite Element (FE) model for the IRIB, (2) extracting the design loads and stresses from the design documents that the designer, AECOM, submitted to DelDOT, (3) producing rating factors for the edge girder and providing DelDOT with sample calculations. The developed 3-D FE model showed a good comparison to the design loads. Also, the FE model was compared to the measured data during the load tests; the model yielded good results using the values of the tested concrete compressive strength from the 56-day cylinder breaks. The FE model can be used by DelDOT for future evaluation purposes such as overall bridge load rating and for permit truck evaluation. The extracted design loads and stresses were used for re-rating the edge girder of the bridge. AECOM provided DelDOT with rating factor values, but the loads and stresses used in these calculations were not provided. Rating factors along the west edge girder were calculated and the design loads used in these calculations were documented.

Beyond these ancillary efforts, the majority of the research conducted was aimed at developing two new bridge evaluation methods; (1) a bridge rating factor method using SHM data, and (2) a reliability analysis method based on SHM data.

In the first method, continuous SHM data collected from the IRIB was converted into structural forces and incorporated into the conventional rating equation to yield continuous rating factors over time. The new approach takes into consideration the available SHM data which includes, among other influences, live loads, thermal loads, and prestressing losses to obtain improved rating factors for various bridge components. The continuous rating factor approach was performed

using all applicable limit states for the IRIB bridge. In this approach we were able to; (1) make a direct use of SHM data in bridge load rating, (2) develop a new simple, concise, and easily interpreted method of reporting SHM data to transportation agencies, and (3) show the impact of thermal load effects on the bridge load rating of a particular long-span bridge.

The key findings from applying the continuous rating factor approach on the IRIB are; (1) the lowest rating factor from the high frequency method is 2.06 (actual rating factor) reported at the west mid-span location and was based on Service III limit state,(2) the maximum difference in the live load carrying capacity from the low frequency method reached 73.7 % of the design live load carrying capacity at mid-span location based on Service III limit state, (3) the two methods (high frequency and low frequency) showed that the lowest rating factors obtained by the two methods are 2.06 (actual rating factor obtained by using actual loads on the bridge) and 0.34 (rating factor obtained by using design loads and long term effects) are at the mid-span location, not at the SW-21/22 (1,649 ft from pier 4) location as indicated from design. The design rating factor (LRFR) at the mid-span location is 1.29, while the lowest rating factors resulting from the new methods (high and low frequency) at the same location are 2.06 and 0.34, respectively. The 2.06 rating factor represents an actual rating factor on the bridge, by comparing this factor to design LRFR rating factor (1.29) one can see that design loads are conservative. However, the low frequency rating factor is low as 0.34, due to the fact of using design live loads in the denominator. A big difference between design LRFR rating factor (1.29) and the low frequency rating factor (0.34) shows the significant effect of long term loads (mainly thermal loads) on rating factors. Also, according to the design firm the location of

sensors SW-21/22 (1,649 ft from pier 4) represents the controlling location on the bridge (i.e. lowest rating factor), but after computing continuous rating factors using the new methodology, the lowest controlling rating factor occurs at mid-span of the bridge (sensors SW-7/8).

In the second method, reliability analysis based on design loads and SHM data was performed. In this approach, loads and resistances were expressed as Probability Distribution Functions (PDF), where loads and resistances were treated as random variables. The concept of estimating the probability of failure or probability of exceedance was presented and expressed by reliability indices for bridge components. The reliability analysis was conducted in two stages, first using design loads and second using long-term SHM data. The analysis was performed considering the various limit states and using Monte Carlo simulation in combination with the Rackwitz-Fiessler method. The resistance model, dead model, and live load model were considered in the reliability analysis based on design information. In this analysis, the same statistical parameters used for the load effects model and the resistance model in the AASHTO LRFD calibration were also used to perform this analysis. In the second analysis, the load effects consisted of dead loads, live loads, and thermal loads. The live load statistical model was created using data from Weigh-In-Motion stations close to the IRIB in combination with the 3-D finite element model. The thermal load statistical model was created using data from Delaware Environmental Observing System (DEOS) and correlation analysis between measured strain and temperature data on the IRIB. Reliability indices for the west edge girder were estimated along the bridge for various limit states. Using this approach we were able to; (1) establish a new reliability-based method by which transportation agencies

can utilize SHM data to ensure the structural safety of their bridges using the various applicable limit states, (2) ensure the structural safety of bridges at the design level and at the service level by comparing the estimated reliability indices to the target reliability indices that used in the calibration of the LRFD code, and (3) help DelDOT to guide their maintenance and inspection procedures for the IRIB; the use of this method can be confirmed by tying results of actual bridge inspection data to the reliability analysis results.

The key finding from applying reliability analysis based on design loads on the IRIB is; (1) the design loads of the IRIB achieve the design requirements for Strength I limit state. The lowest reliability index along the west edge girder is 3.57 (at 1,649 ft from pier 4), which is very close to the target reliability index of 3.5 used for the LRFD code calibration. This location (1,649 ft) is also associated with the bridge controlling load rating factor according to design (i.e. lowest rating factor). Therefore, the lowest reliability index was expected to be at this location since design loads only are used in this analysis. The lowest reliability index from Service I limit state is 2.23 located at 155 ft from pier 4 and the lowest reliability index from Service III limit state is 0.77 located at 1,649 ft from pier 4. Both of these locations were expected, because they are associated with the bridge controlling load rating factor of these limit states. The reliability index based on design for Service I limit state is above the new code calibration range (0.5-1.0), and for Service III falls in the range. Therefore, one conclusion that can be drawn from the reliability analysis results based on design is that the IRIB satisfies the requirements of the current code and shows a good agreement with the sample of analyzed bridges for the Service limit state calibration.

The main key findings from applying reliability analysis based on SHM data on the IRIB are; (1) the lowest reliability index from the reliability analysis performed on Strength I limit state using all load effects was 9.07 at the mid-span location. This leads to a conclusion that the mid span location experienced more loads than the controlling rating factor location from design. (2)The lowest reliability index from the reliability analysis performed on Service III limit state using all load effects was 2.05 at 585 ft from pier 4 location. This leads to a conclusion that this location (585 ft) experienced more loads than the controlling rating factor location from design. Also, by comparing the reliability indices based on the two types of analyses (design and include all load effects) for the 585 ft location, the reliability index decreased from 3.62 to 2.01. In general, special attention should be given to these locations with low reliability indices in future inspections. (3) The lowest reliability index from the reliability analysis performed using the Service I limit state and considering all load effects is 9.62 located at 901 ft from pier 4. This leads to a conclusion that this location experienced more loads than the controlling rating factor location from design. Also, by comparing the reliability indices based on the two types of analyses (design and include all load effects) for the 155 ft location, the reliability index increased from 2.23 to 10.51. In general, special attention should be given to these locations with low reliability indices in future inspections. (4) The thermal effects on reliability indices based on Service I and Service III limit states is obvious. For Service III limit state the lowest reliability index (based on all loads) is 2.01 and that increased to 11.33 when thermal loads were excluded. For Service I limit state the lowest reliability index was 10.51(based on all loads) and that increased to 15.95 when thermal loads were excluded.

10.3 Future Work

The primary goal of the research presented in this study was to develop new techniques for utilizing structural health monitoring data for bridge evaluation. The aim was to help transportation agencies bridge the gap between collecting and analyzing the massive amounts of data generated by SHM systems and the actual application of the SHM data to the maintenance, inspection, evaluation, and decision making procedures that are currently used for bridges.

The proposed continuous rating factor method demonstrated a direct use of SHM data for bridge load rating. The method highlighted the importance of thermal effects on the load ratings of this long-span bridge. The method also represents a new and concise way of reporting the meaning of the collected SHM data in a way that transportation agencies are familiar with. The method provides rating factors only at the monitored locations. To overcome this limitation, and to further improve the procedure, the following future research areas are suggested; (1) Developing a calibrated finite element model for the bridge that reflects the changing condition of the bridge so that rating factors can continue to be determined at the unmonitored locations, (2) Collecting SHM data during the construction stage of future instrumented bridges so that the dead loads can be based on actual SHM data during construction and not have to rely on design information, and (3) Using statistical quantification of rating factors over time to indicate changes in bridge performance. The SHM system on the IRIB is a continuous long-term system. The SHM data and resulting changes in ratings over time should provide important insights into deterioration and capacity changes that can be estimated through rigorous statistical evaluation.

The proposed reliability analysis method based on using SHM data was performed for various limit states. The method of determining reliability indices using SHM data and comparing them to reliability indices based on design loads was presented. Since reliability analysis utilizes a large amount of monitored data, this approach can provide vital information about the health of the monitored bridge. In terms of future work, the following future research areas can improve and maximize the results of the presented method; (1) conducting statistical studies on the reliability indices over time to quantify changes in the structural performance over time, (2) developing predictive models that are based on statistical data and allow the DOT to manage and optimize the maintenance operations on the bridge, (3) comparing the results of the reliability analysis method to real inspection data, and (4) studying the correlation between the rating factor method based on SHM data and the reliability analysis method based on using SHM data. This comparison may lead to new ways in which transportation agencies can estimate long-term structural performance based on shorter-term evaluations.

REFERENCES

AASHTO, 2011. *"Manual for Bridge Evaluation (2nd Edition),"* Washington, D.C.: American Association of State Highway and Transportation Officials (AASHTO).

Abell, M., 2012. Computers & Structures Inc. -Articles Tutorials-Shell Element. , p.2000.

AECOM, 2012a. *Load Rating Calculations - Edge Girder-Indian River Inlet Bridge*,

AECOM, 2012b. *Load Rating Manual Indian River Inlet (Charles W. Cullen) Bridge SR-1 over the Indian River Inlet (Br. 3-156)*,

Allen, T.M., Nowak, A.S. & Bathurust, R.J., 2005. *Calibration to determine load and resistance factors for geotechnical and structural design*, Available at: http://trid.trb.org/view.aspx?id=760804.

ASCE, 2013 Report Card for America's Infrastructure, 2013. *2013 Report Card for America's Infrastructure Findings*,

Catbas, F, N. & Frangopol, D.., 2008. Systems-based monitoring approaches for improved infrastructure management under uncer- tainty: Novel approach. In H.-M. Koh & D. M. Frangopol, eds. *4th Int. Conf., on Bridge maintenance, Safety, and Management, IABMAS-08*. CRC/Balkema, Taylor & Fracis Group, London, pp. 3072–3078.

Farrar, C.R. & Worden, K., 2007. An introduction to structural health monitoring. *Philosophical transactions of the Royal Society*, 365(1851), pp.303–15.

Frangopol, D.M., Strauss, A. & Kim, S., 2008a. Bridge reliability assessment based on monitoring. *Journal of Bridge Engineering*, 13(3), pp.258–270. Available at: http://ascelibrary.org/doi/abs/10.1061/(ASCE)1084-0702(2008)13:3(258).

Frangopol, D.M., Strauss, A. & Kim, S., 2008b. Use of monitoring extreme data for the performance prediction of structures: General approach. *Engineering Structures*, 30(12), pp.3644–3653. Available at: http://dx.doi.org/10.1016/j.engstruct.2008.06.010.

Hu, J. et al., 2006. *BASELINE MODELING OF THE OWENSBORO CABLE-STAYED*

BRIDGE OVER THE OHIO RIVER,

Imai, K. & Frangopol, D.M., 2001. Reliability-Based Assesment of Suspension Bridges: Application To The Innoshima Bridge. *Journal of Bridge Engineering*, 6(December), pp.288–289.

Jiao, M.J. & Sun, L.M., 2011. Bridge reliability assessment based on the PDF of long-term monitored extreme strains. *Nondestructive Characterization for Composite Materials, Aerospace Engineering, Civil Infrastructure, and Homeland Security 2011*, 7983, pp.1–10. Available at: <Go to ISI>://WOS:000294472700015.

Kulicki, J.M. et al., 2015. *Bridges for Service Life Beyond 100 Years : Service Limit State Design*, Washington, D.C.

Kulicki, J.M. et al., 2007. *UPDATING THE CALIBRATION REPORT FOR AASHTO LRFD CODE*,

Lai, L.-Y. ("Leon"), 2013. Thermal Effects on Load Rating of Reinforced Concrete Arch Bridges. In *Structures Congress 2013*. Structures Congress 2013, pp. 479–490. Available at: http://ascelibrary.org/doi/abs/10.1061/9780784412848.043.

Li, H., Li, S. & Ou, J., 2012. Reliability assessment of cable-stayed bridges based on structural health monitoring techniques. *Structure and Infrastructure Engineering*, 8(9), pp.829–845. Available at: http://www.scopus.com/inward/record.url?eid=2-s2.0-84861401721&partnerID=40&md5=0615119074714ed75b469f658e95831a.

Liu, M., Frangopol, D.M. & Kim, S., 2009. Bridge Safety Evaluation Based on Monitored Live Load Effects. *Journal of Bridge Engineering*, 14(August), pp.257–269.

Marquez, P., 2013. *LOAD RATING OF THE INDIAN RIVER INLET BRIDGE USING A STRUCTURAL HEALTH MONITORING SYSTEM*. University of Delaware.

Morcous, G., Hanna, K. & Tadros, M.K., 2010. *Load Rating of Complex Bridges*,

Nelson, E.T., 2012. Indian River Inlet Bridge – Surviving the Storms. , pp.12–16.

Ni, Y.Q., Hua, X.G. & Ko, J.M., 2006. Reliability based assessment of bridges using long term monitoring data. *Key Engineering Materials*, 321-323, pp.217–222.

Nowak, A. & Collins, K., 2013. *Reliability of Structures* 2nd ed.,

Nowak, A.S., 1999. *Calibrartion of LRFD Bridge Design Code*,

Shenton, H.W. et al., 2016. *Load Tests of the Charles W . Cullen Bridge at Indian River Inlet*,

State of California Department of Transportation/Division of Engineering Services, 2015. Bridge Design Practice. In *Bridge Design Practice*. CALTRANS. Available at: http://www.dot.ca.gov/hq/esc/techpubs/manual/bridgemanuals/bridge-design-practice/bdp.html.

Strauss, A., Frangopol, D.M. & Kim, S., 2008. Use of monitoring extreme data for the performance prediction of structures: Bayesian updating. *Engineering Structures*, 30(12), pp.3654–3666. Available at: http://dx.doi.org/10.1016/j.engstruct.2008.06.009.

Xu, Y.-L. & Xia, Y., 2012. *Structural Health Monitoring of Long-Span Suspension Bridges* First edit., London and New York: Spon Press.

Zhou, G.D. & Yi, T.H., 2013. Thermal Load in Large-Scale Bridges: A state-of-the-Art Review. *International Journal of Distributed Sensor Networks*, 2013, p.17.

Appendix A

DESIGN, LEGAL, AND PERMIT TRUCKS CONFIGURATIONS

A.1 Load Rating Manual Truck Configurations

The Design, Legal, and Permit Loads can be seen in figuresA.1 through A.4.

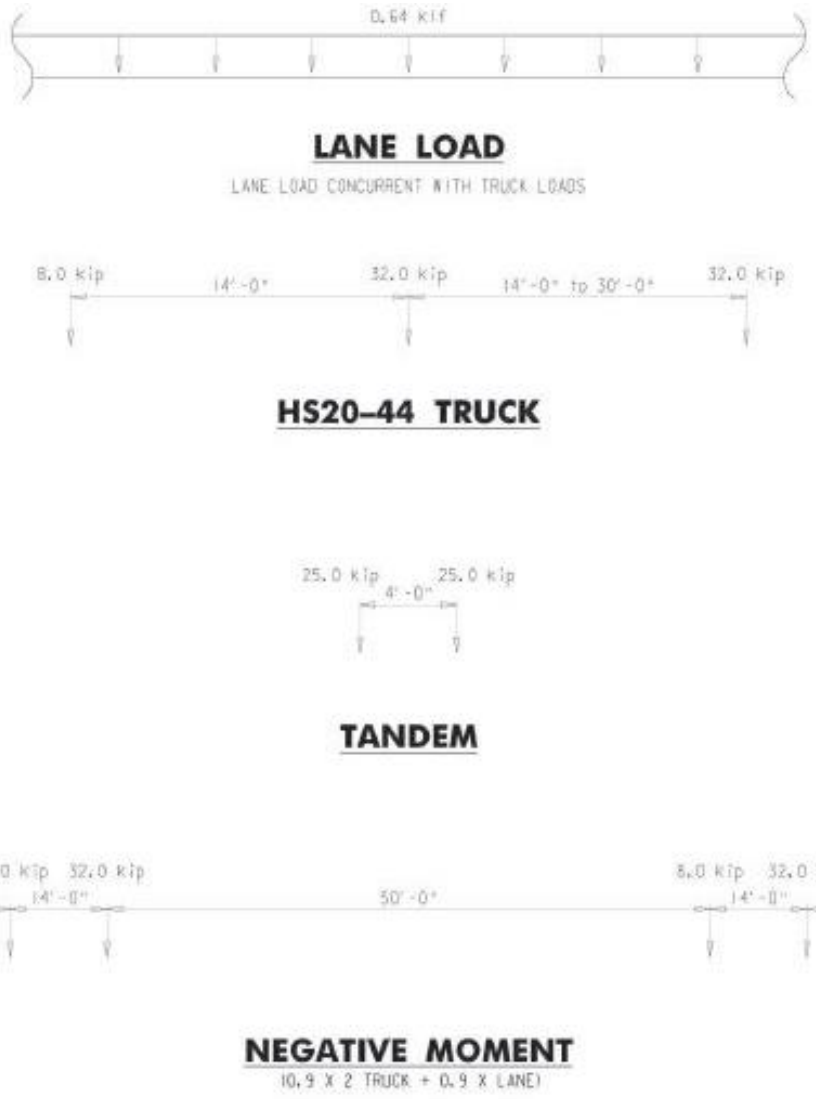

Figure A.1. Rating Truck Axle Configurations and Wheel Weights for Design

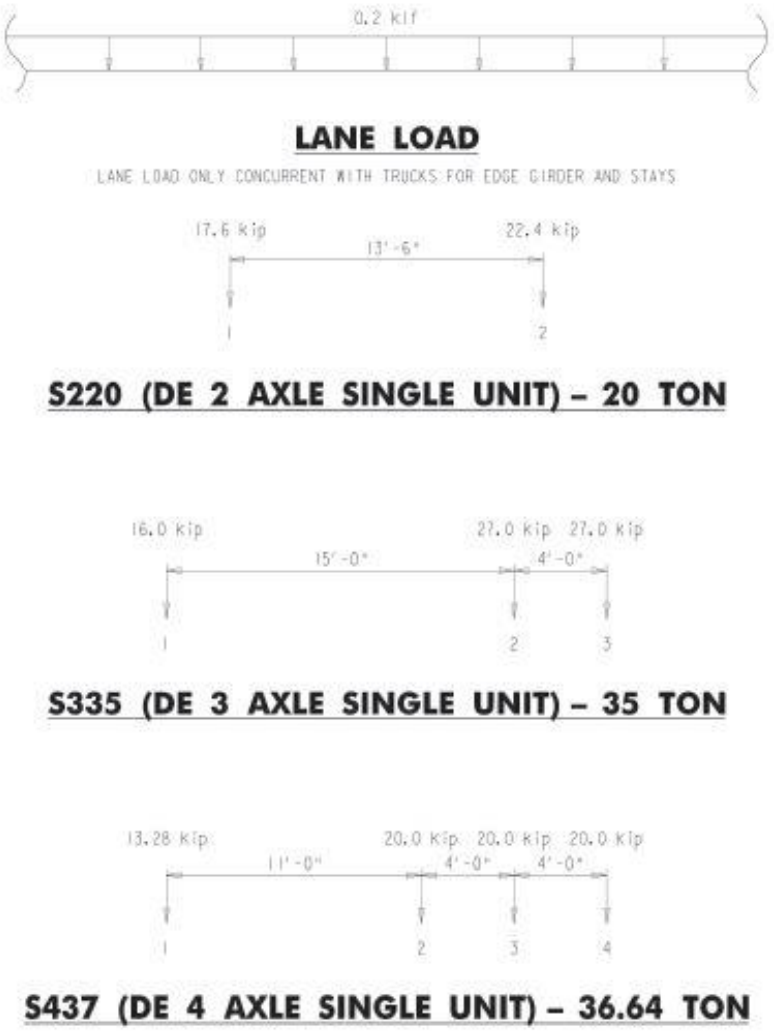

Figure A.2. Rating Truck Axle Configurations and Wheel Weights for Legal Loads

T330 (DE 3 AXLE SEMI) – 30 TON

T435 (DE 4 AXLE SEMI) – 35 TON

T540 (DE 5 AXLE SEMI) – 40 TON

LEGAL 2 of 2

Figure A.3. Rating Truck Axle Configurations and Wheel Weights for Legal Loads

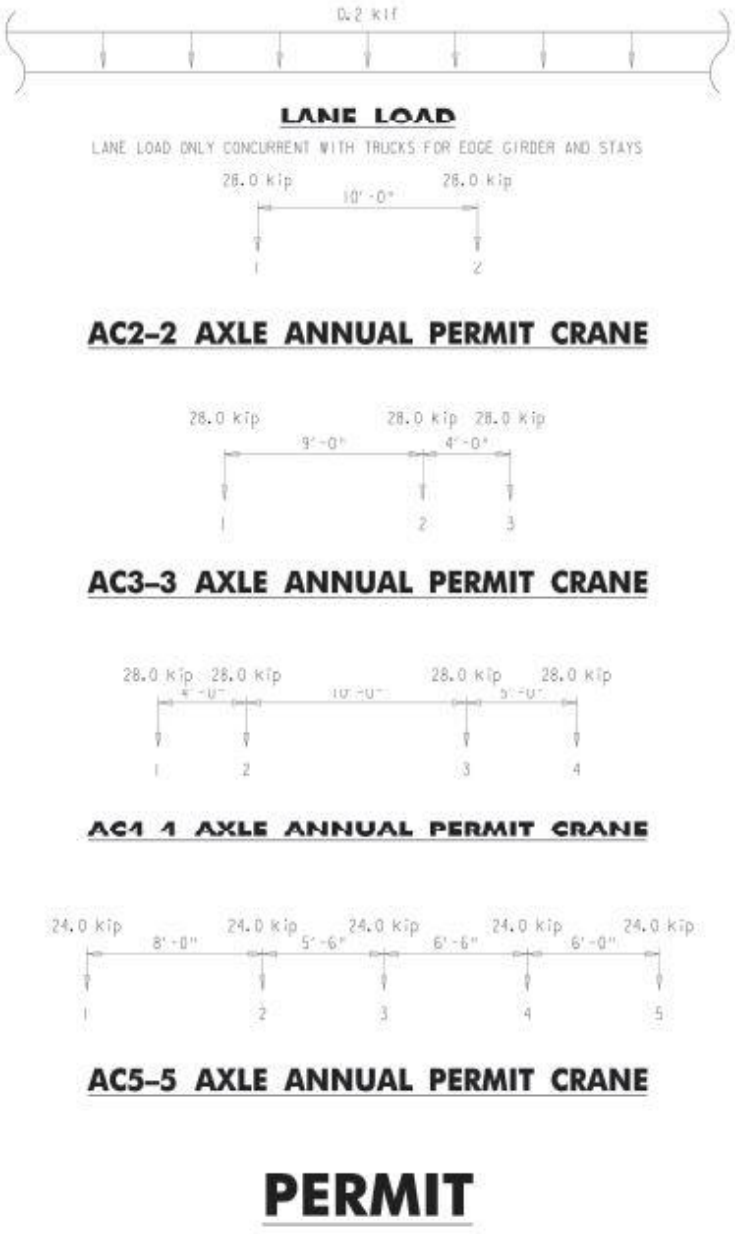

Figure A.4. Rating Truck Axle Configurations and Wheel Weights for Permit Loads

Appendix B

LOAD RATING

B.1 Extracted live and Dead Load Stresses with Calculated Rating Factors for Service I and Service III Limit States

Table B.1. Rating Factors for Service I and Service III

Member number	Station (feet)	Service III Capaity (ksf)	Service I Capaity (ksf)	Dead load stresses (Day 10,000)		HL-93 - 4 Lanes Stresses							
						Maximum Force Envelope				Minimum Force Envelope			
				Top (ksf)	Bottom (ksf)	Top (ksf)	Bottom (ksf)	Servive III Bottom Rating Factor	Servive I Top Rating Factor	Top (ksf)	Bottom (ksf)	Servive III Top Rating Factor	Servive I Bottom Rating Factor
WG003	1291+38.08	34.83	-561.6	-132	-156	-51.0	89.0	2.68	8.42	72.5	-131.0	2.88	3.09
WG004	1291+38.08	34.83	-561.6	-132	-156	-37.5	70.0	3.41	11.45	62.5	-121.5	3.34	3.34
WG004	1291+43.67	34.83	-561.6	-126	-167	-31.5	59.5	4.24	13.84	53.5	-107.0	3.75	3.69
WG005	1291+43.67	34.83	-561.6	-163	-145	-31.0	59.0	3.82	12.87	52.0	-104.0	4.74	4.00
WG005	1291+49.25	34.83	-561.6	-165	-141	-29.5	56.5	3.89	13.44	41.0	-86.0	6.10	4.89
WG006	1291+49.25	34.83	-561.6	-165	-141	-26.5	53.5	4.11	14.95	38.5	-87.0	6.50	4.83
WG006	1291+54.83	34.83	-561.6	-159	-151	-31.0	61.0	3.81	12.98	33.0	-78.5	7.35	5.23
WG007	1291+54.83	34.83	-561.6	-198	-130	-32.0	62.0	3.32	11.38	33.5	-79.0	8.67	5.46
WG007	1291+60.42	34.83	-561.6	-190	-144	-37.5	72.0	3.10	9.92	30.5	-74.0	9.20	5.65
WG008	1291+60.42	34.83	-561.6	-189	-143	-37.5	72.0	3.09	9.93	32.0	-81.0	8.75	5.16
WG008	1291+66.00	34.83	-561.6	-181	-157	-45.5	86.0	2.79	8.36	31.5	-79.5	8.56	5.09
WG009	1291+66.00	34.83	-561.6	-200	-158	-45.5	86.5	2.79	7.94	31.5	-79.5	9.33	5.07
WG010	1291+78.00	34.83	-561.6	-177	-195	-67.5	121.5	2.37	5.70	40.0	-94.0	6.62	3.90
WG011	1291+78.00	34.83	-561.6	-186	-221	-66.0	120.5	2.65	5.69	43.5	-103.0	6.35	3.31
WG012	1291+90.00	34.83	-561.6	-170	-248	-87.0	155.0	2.28	4.51	51.5	-116.0	4.96	2.70
WG013	1291+90.00	34.83	-561.6	-169	-249	-85.5	153.0	2.31	4.59	50.5	-114.5	5.06	2.73
WG014	1292+02.00	34.83	-561.6	-163	-259	-103.0	181.5	2.02	3.87	59.0	-129.0	4.19	2.34
WG015	1292+02.00	34.83	-561.6	-201	-234	-99.5	176.5	1.91	3.62	61.0	-134.5	4.84	2.43
WG016	1292+14.00	34.83	-561.6	-189	-255	-114.5	201.0	1.80	3.26	65.5	-141.5	4.26	2.17
WG017	1292+14.00	34.83	-561.6	-187	-257	-113.0	198.0	1.84	3.32	64.0	-140.0	4.32	2.17
WG018	1292+26.00	34.83	-561.6	-182	-264	-122.5	213.5	1.75	3.10	67.5	-145.5	4.02	2.04
WG019	1292+26.00	34.83	-561.6	-219	-237	-118.0	205.5	1.65	2.90	68.5	-147.5	4.63	2.20
WG020	1292+38.00	34.83	-561.6	-205	-260	-126.0	218.5	1.68	2.83	68.5	-148.0	4.38	2.04
WG021	1292+38.00	34.83	-561.6	-205	-259	-124.5	215.5	1.70	2.86	68.0	-147.0	4.41	2.06
WG022	1292+50.00	34.83	-561.6	-203	-264	-127.0	220.5	1.69	2.83	66.5	-145.5	4.46	2.05
WG023	1292+50.00	34.83	-561.6	-211	-255	-121.5	209.5	1.73	2.89	66.5	-146.0	4.62	2.10
WG024	1292+62.00	34.83	-561.6	-191	-288	-124.0	214.5	1.88	2.99	64.0	-141.0	4.41	1.94
WG025	1292+62.00	34.83	-561.6	-212	-281	-122.5	211.5	1.86	2.86	62.5	-139.5	4.93	2.01
WG026	1292+74.00	34.83	-561.6	-217	-272	-119.5	207.0	1.85	2.88	58.5	-133.0	5.39	2.18
WG027	1292+74.00	34.83	-561.6	-166	-281	-114.0	195.5	2.02	3.47	57.5	-132.5	4.37	2.12
WG028	1292+86.00	34.83	-561.6	-144	-319	-113.0	194.5	2.27	3.70	53.0	-124.0	4.21	1.96
WG029	1292+86.00	34.83	-561.6	-168	-306	-111.5	192.0	2.22	3.53	52.0	-122.5	4.87	2.08
WG030	1292+98.00	34.83	-561.6	-173	-298	-106.0	183.0	2.28	3.67	46.0	-113.0	5.63	2.33
WG031	1292+98.00	34.83	-561.6	-133	-305	-99.5	171.0	2.48	4.31	45.0	-112.0	4.66	2.29
WG032	1293+10.00	34.83	-561.6	-122	-322	-98.0	167.5	2.67	4.49	39.0	-102.0	5.02	2.35
WG033	1293+10.00	34.83	-561.6	-148	-306	-96.0	165.5	2.57	4.31	38.5	-101.0	5.92	2.53
WG034	1293+22.00	34.83	-561.6	-174	-261	-90.0	155.0	2.39	4.30	32.0	-91.0	8.17	3.30
WG035	1293+22.00	34.83	-561.6	-147	-261	-84.0	144.0	2.57	4.94	31.0	-89.5	7.33	3.36
WG036	1293+34.00	34.83	-561.6	-136	-278	-83.0	141.5	2.76	5.13	26.5	-81.5	8.06	3.48
WG037	1293+34.00	34.83	-561.6	-165	-254	-81.5	139.5	2.59	4.87	25.5	-81.0	9.78	3.79
WG038	1293+46.00	34.83	-561.6	-193	-209	-76.5	131.5	2.32	4.82	21.0	-73.5	13.54	4.80
WG039	1293+46.00	34.83	-561.6	-161	-210	-72.0	122.0	2.51	5.56	20.5	-73.0	11.94	4.82
WG040	1293+58.00	34.83	-561.6	-151	-226	-71.5	121.5	2.69	5.74	17.0	-67.0	13.66	5.00
WG041	1293+58.00	34.83	-561.6	-179	-200	-70.5	120.0	2.45	5.43	17.0	-67.0	15.71	5.39
WG042	1293+70.00	34.83	-561.6	-204	-158	-67.0	114.0	2.11	5.33	14.5	-63.0	20.62	6.41
WG043	1293+70.00	34.83	-561.6	-181	-156	-62.5	106.0	2.25	6.09	15.0	-64.0	17.99	6.34
WG044	1293+82.00	34.83	-561.6	-169	-177	-63.5	107.5	2.46	6.19	15.0	-64.0	16.94	6.02
WG045	1293+82.00	34.83	-561.6	-195	-149	-62.5	106.0	2.17	5.86	14.0	-63.5	20.56	6.50
WG046	1293+94.00	34.83	-561.6	-218	-112	-59.5	101.5	1.80	5.77	15.0	-64.5	21.09	6.98
WG047	1293+94.00	34.83	-561.6	-204	-105	-56.5	95.0	1.84	6.33	15.5	-66.0	19.26	6.91
WG048	1294+06.00	34.83	-561.6	-186	-134	-57.5	96.5	2.19	6.53	15.5	-66.0	17.84	6.48
WG049	1294+06.00	34.83	-561.6	-209	-115	-57.0	96.0	1.95	6.18	15.5	-65.0	19.68	6.88
WG050	1294+18.00	34.83	-561.6	-208	-116	-54.5	91.5	2.06	6.48	16.0	-66.5	18.99	6.70
WG051	1294+18.00	34.83	-561.6	-204	-123	-51.5	87.0	2.27	6.94	16.5	-67.5	18.09	6.50
WG052	1294+30.00	34.83	-561.6	-190	-145	-52.0	87.5	2.57	7.14	16.5	-68.0	17.06	6.12
WG053	1294+30.00	34.83	-561.6	-211	-126	-51.5	86.5	2.33	6.81	16.5	-67.0	18.60	6.50
WG054	1294+42.00	34.83	-561.6	-208	-130	-48.5	81.5	2.53	7.28	17.5	-70.0	17.37	6.16
WG055	1294+42.00	34.83	-561.6	-203	-140	-46.0	77.5	2.81	7.81	17.5	-70.0	16.95	6.03
WG056	1294+54.00	34.83	-561.6	-190	-159	-46.0	77.0	3.15	8.07	18.5	-71.5	15.20	5.63
WG057	1294+54.00	34.83	-561.6	-214	-136	-45.0	76.0	2.80	7.73	17.5	-70.5	17.76	6.04
WG058	1294+66.00	34.83	-561.6	-207	-148	-41.0	69.5	3.28	8.66	19.5	-74.0	15.47	5.60
WG059	1294+66.00	34.83	-561.6	-197	-163	-39.5	67.0	3.69	9.23	19.5	-74.0	14.86	5.39
WG060	1294+78.00	34.83	-561.6	-188	-178	-37.0	63.0	4.22	10.10	21.0	-76.0	13.26	5.05

WG061	1294+78.00	34.83	-561.6	-188	-121	-47.0	65.5	2.97	7.95	34.5	-79.5	8.07	5.54
WG062	1294+90.00	34.83	-561.6	-186	-125	-38.5	54.5	3.65	9.77	39.0	-85.5	7.07	5.11
WG063	1294+90.00	34.83	-561.6	-180	-131	-39.0	54.5	3.79	9.77	36.5	-82.0	7.37	5.26
WG064	1295+02.00	34.83	-561.6	-136	-110	-23.0	28.0	6.47	18.50	29.0	-56.5	7.36	7.99
WG065	1295+02.00	34.83	-561.6	-165	-81	-22.0	27.5	5.26	18.04	28.5	-56.5	8.76	8.51
WG066	1295+14.00	34.83	-561.6	-127	-76	-11.5	13.5	10.26	37.77	28.0	-47.5	7.23	10.22
WG068	1295+14.00	34.83	-561.6	-245	-70	-12.0	18.0	7.25	26.37	48.5	-100.5	7.21	4.90
WG069	1295+25.00	34.83	-561.6	-198	-134	-6.0	10.0	21.12	60.65	66.0	-123.5	4.40	3.46
WG070	1295+25.00	34.83	-561.6	-198	-134	-5.5	9.5	22.17	66.04	64.0	-122.0	4.56	3.51
WG071	1295+36.00	34.83	-561.6	-234	-86	-12.0	19.0	7.92	27.28	50.0	-102.5	6.73	4.64
WG073	1295+36.00	34.83	-561.6	-120	-83	-10.5	12.5	11.80	42.02	27.5	-48.0	7.06	9.97
WG074	1295+48.00	34.83	-561.6	-146	-102	-22.0	27.5	6.23	18.88	29.0	-57.0	7.81	8.06
WG075	1295+48.00	34.83	-561.6	-146	-102	-21.5	26.5	6.45	19.33	28.5	-56.0	7.94	8.21
WG076	1295+60.00	34.83	-561.6	-150	-178	-39.5	55.5	4.79	10.43	37.0	-82.5	6.23	4.65
WG077	1295+60.00	34.83	-561.6	-148	-177	-35.5	51.0	5.18	11.66	37.5	-84.0	6.08	4.58
WG078	1295+72.00	34.83	-561.6	-151	-172	-46.5	65.5	3.94	8.84	34.0	-79.5	6.82	4.91
WG079	1295+72.00	34.83	-561.6	-179	-200	-34.5	59.5	4.93	11.09	20.0	-75.0	13.37	4.82
WG080	1295+84.00	34.83	-561.6	-162	-228	-38.0	65.5	5.01	10.51	19.0	-74.0	12.98	4.51
WG081	1295+84.00	34.83	-561.6	-161	-219	-38.5	66.0	4.80	10.40	18.5	-73.5	13.24	4.67
WG082	1295+96.00	34.83	-561.6	-171	-203	-44.0	75.5	3.93	8.88	18.0	-71.5	14.29	5.02
WG083	1295+96.00	34.83	-561.6	-177	-193	-43.5	74.0	3.85	8.84	17.5	-71.5	15.12	5.16
WG084	1296+08.00	34.83	-561.6	-164	-214	-45.0	76.5	4.07	8.84	18.0	-72.0	13.79	4.82
WG085	1296+08.00	34.83	-561.6	-165	-199	-46.0	78.0	3.75	8.63	17.5	-71.0	14.25	5.11
WG086	1296+20.00	34.83	-561.6	-173	-186	-50.5	86.5	3.19	7.69	17.5	-70.5	14.86	5.33
WG087	1296+20.00	34.83	-561.6	-176	-181	-49.5	85.0	3.17	7.78	17.0	-70.5	15.53	5.40
WG088	1296+32.00	34.83	-561.6	-168	-195	-51.0	87.0	3.30	7.73	18.5	-72.0	13.68	5.09
WG089	1296+32.00	34.83	-561.6	-172	-175	-52.5	89.5	2.92	7.43	17.5	-71.0	14.74	5.45
WG090	1296+44.00	34.83	-561.6	-177	-166	-56.5	96.0	2.62	6.81	18.5	-72.0	14.29	5.49
WG091	1296+44.00	34.83	-561.6	-177	-166	-55.5	94.5	2.66	6.94	18.0	-72.0	14.68	5.49
WG092	1296+56.00	34.83	-561.6	-167	-181	-56.0	95.5	2.83	7.04	20.0	-74.0	12.64	5.14
WG093	1296+56.00	34.83	-561.6	-169	-162	-58.0	98.5	2.49	6.77	19.0	-73.0	13.42	5.48
WG094	1296+68.00	34.83	-561.6	-171	-159	-61.5	105.0	2.30	6.34	20.5	-75.0	12.57	5.37
WG095	1296+68.00	34.83	-561.6	-169	-164	-60.0	103.0	2.41	6.55	20.5	-74.5	12.40	5.34
WG096	1296+80.00	34.83	-561.6	-161	-175	-60.5	103.5	2.54	6.62	22.5	-78.0	10.89	4.95
WG097	1296+80.00	34.83	-561.6	-162	-154	-62.5	107.5	2.20	6.40	21.5	-76.5	11.42	5.32
WG098	1296+92.00	34.83	-561.6	-163	-151	-66.5	113.0	2.06	5.99	23.5	-79.0	10.52	5.20
WG099	1296+92.00	34.83	-561.6	-162	-154	-64.5	111.0	2.12	6.20	23.0	-79.0	10.70	5.16
WG100	1297+04.00	34.83	-561.6	-157	-163	-64.0	110.0	2.24	6.33	25.0	-82.0	9.57	4.87
WG101	1297+04.00	34.83	-561.6	-167	-135	-66.5	114.5	1.85	5.93	25.0	-80.5	10.10	5.30
WG102	1297+16.00	34.83	-561.6	-169	-133	-69.0	119.0	1.76	5.70	27.0	-84.0	9.42	5.11
WG103	1297+16.00	34.83	-561.6	-168	-134	-67.5	116.0	1.81	5.84	26.5	-83.5	9.55	5.13
WG104	1297+28.00	34.83	-561.6	-165	-138	-67.0	115.5	1.87	5.92	29.0	-87.5	8.61	4.84
WG105	1297+28.00	34.83	-561.6	-185	-130	-70.0	121.5	1.69	5.38	28.5	-86.0	9.64	5.02
WG106	1297+40.00	34.83	-561.6	-176	-145	-72.0	125.5	1.79	5.36	30.5	-89.5	8.63	4.65
WG107	1297+40.00	34.83	-561.6	-165	-171	-70.5	122.5	2.10	5.63	30.5	-89.0	8.18	4.39
WG108	1297+52.00	34.83	-561.6	-162	-175	-70.0	122.0	2.15	5.70	33.5	-94.0	7.36	4.12
WG109	1297+52.00	34.83	-561.6	-186	-156	-74.5	129.5	1.84	5.04	33.0	-92.0	8.37	4.41
WG110	1297+64.00	34.83	-561.6	-173	-178	-77.5	135.0	1.97	5.02	35.5	-96.5	7.31	3.98
WG111	1297+64.00	34.83	-561.6	-134	-222	-75.5	131.5	2.44	5.67	35.0	-96.0	6.01	3.54
WG112	1297+76.00	34.83	-561.6	-155	-186	-76.0	132.5	2.08	5.35	38.5	-100.5	6.17	3.74
WG113	1297+76.00	34.83	-561.6	-191	-179	-80.5	140.0	1.91	4.60	38.0	-99.0	7.43	3.86
WG114	1297+88.00	34.83	-561.6	-181	-197	-84.0	146.5	1.98	4.53	40.5	-103.5	6.65	3.52
WG115	1297+88.00	34.83	-561.6	-149	-226	-82.0	143.5	2.27	5.03	40.5	-103.0	5.69	3.26
WG116	1298+00.00	34.83	-561.6	-173	-188	-83.0	145.0	1.92	4.68	43.5	-107.5	5.97	3.48
WG117	1298+00.00	34.83	-561.6	-220	-180	-88.0	153.5	1.75	3.88	43.5	-106.0	7.32	3.60
WG118	1298+12.00	34.83	-561.6	-209	-198	-92.0	160.5	1.81	3.83	46.0	-110.5	6.63	3.29
WG119	1298+12.00	34.83	-561.6	-181	-225	-90.0	157.5	2.06	4.23	46.0	-110.0	5.87	3.06
WG120	1298+24.00	34.83	-561.6	-202	-191	-92.0	160.0	1.76	3.91	48.5	-114.5	6.09	3.24
WG121	1298+24.00	34.83	-561.6	-235	-194	-96.5	168.5	1.69	3.39	49.0	-113.0	6.87	3.26
WG122	1298+36.00	34.83	-561.6	-227	-206	-101.5	176.0	1.71	3.30	51.0	-117.0	6.41	3.04
WG123	1298+36.00	34.83	-561.6	-201	-226	-99.0	173.5	1.88	3.65	51.0	-116.5	5.77	2.88
WG124	1298+48.00	34.83	-561.6	-197.7	-192.9	-79.5	152.5	1.87	4.58	40.0	-105.0	7.27	3.51
WG125	1298+48.00	34.83	-561.6	-211.3	-201.5	-83.5	160.0	1.85	4.20	40.5	-103.0	7.60	3.50
WG126	1298+60.00	34.83	-561.6	-204.2	-214.5	-87.0	166.5	1.87	4.11	41.5	-105.5	7.20	3.29
WG127	1298+60.00	34.83	-561.6	-184	-224	-85.0	163.0	1.98	4.44	41.5	-104.5	6.59	3.23
WG128	1298+72.00	34.83	-561.6	-192	-209	-86.0	164.5	1.85	4.30	42.5	-107.0	6.68	3.30
WG129	1298+72.00	34.83	-561.6	-205	-219	-90.0	172.5	1.84	3.96	42.5	-104.5	7.06	3.28
WG130	1298+84.00	34.83	-561.6	-198	-232	-93.0	177.5	1.88	3.91	43.0	-105.0	6.76	3.14
WG131	1298+84.00	34.83	-561.6	-179	-241	-91.0	174.5	1.97	4.20	42.5	-104.5	6.30	3.07
WG132	1298+96.00	34.83	-561.6	-185	-231	-91.0	175.0	1.90	4.14	42.5	-105.0	6.46	3.15
WG133	1298+96.00	34.83	-561.6	-194	-248	-95.0	182.0	1.94	3.87	43.0	-102.0	6.65	3.08
WG134	1299+08.00	36.14	-604.8	-184	-265	-97.0	185.5	2.02	4.34	42.0	-100.0	6.51	3.39
WG135	1299+08.00	36.14	-604.8	-159	-283	-95.0	182.0	2.18	4.70	41.5	-99.5	5.82	3.23
WG136	1299+20.00	36.14	-604.8	-162	-278	-93.5	180.0	2.17	4.74	40.5	-97.5	6.07	3.35
WG137	1299+20.00	36.14	-604.8	-165	-274	-97.5	187.0	2.06	4.51	40.0	-93.5	6.24	3.54
WG138	1299+32.00	36.14	-604.8	-162	-278	-98.0	188.0	2.08	4.52	37.5	-89.5	6.57	3.65
WG139	1299+32.00	36.14	-604.8	-144	-275	-96.0	184.5	2.10	4.80	37.5	-89.0	5.95	3.71
WG140	1299+44.00	36.14	-604.8	-147	-270	-93.5	180.5	2.11	4.90	35.5	-85.0	6.39	3.94
WG141	1299+44.00	36.14	-604.8	-147	-270	-97.5	187.0	2.03	4.69	34.5	-80.5	6.59	4.16
WG142	1299+56.00	36.14	-604.8	-144	-275	-96.0	184.5	2.10	4.80	31.5	-74.5	7.11	4.43
WG143	1299+56.00	36.14	-604.8	-123	-260	-94.5	181.0	2.04	5.10	31.0	-74.5	6.35	4.63
WG144	1299+68.00	36.14	-604.8	-130	-246	-91.5	175.5	2.00	5.19	28.5	-69.0	7.24	5.20
WG145	1299+68.00	36.14	-604.8	-138	-233	-95.5	182.5	1.83	4.88	27.0	-63.0	8.02	5.91
WG146	1299+80.00	36.14	-604.8	-139	-232	-94.5	180.5	1.85	4.93	23.0	-56.5	9.42	6.59
WG147	1299+80.00	36.14	-604.8	-126	-205	-92.0	177.0	1.69	5.20	23.0	-56.0	8.76	7.14
WG148	1299+92.00	36.14	-604.8	-147	-167	-90.0	173.0	1.46	5.08	20.5	-51.0	11.11	8.59
WG149	1299+92.00	36.14	-604.8	-155	-158	-94.5	180.5	1.33	4.77	19.0	-45.5	12.46	9.82
WG149	1300+00.00	36.14	-604.8	-156	-155	-95.0	181.5	1.31	4.73	18.0	-44.5	13.24	10.10
WG150	1300+00.00	36.14	-604.8	-161	-147	-94.5	180.5	1.26	4.70	18.5	-44.0	13.22	10.41
WG150	1300+08.00	36.14	-604.8	-158	-152	-95.5	182.0	1.28	4.68	20.5	-48.0	11.76	9.44

WG151	1300+08.00	36.14	-604.8	-152	-163	-90.0	171.5	1.44	5.04	22.0	-51.5	10.59	8.59
WG152	1300+20.00	36.14	-604.8	-146	-172	-96.5	183.0	1.41	4.75	25.5	-58.0	8.88	7.47
WG153	1300+20.00	36.14	-604.8	-125	-211	-94.5	180.0	1.71	5.08	24.5	-56.5	8.14	6.97
WG154	1300+32.00	36.14	-604.8	-107	-243	-99.5	188.0	1.84	5.01	29.0	-65.0	6.09	5.57
WG155	1300+32.00	36.14	-604.8	-137	-239	-94.0	178.0	1.92	4.98	30.0	-69.5	7.16	5.26
WG156	1300+44.00	36.14	-604.8	-135	-242	-100.5	189.0	1.83	4.68	33.5	-76.0	6.33	4.77
WG157	1300+44.00	36.14	-604.8	-125	-260	-98.5	186.0	1.98	4.88	32.5	-74.0	6.13	4.66
WG158	1300+56.00	36.14	-604.8	-115	-277	-102.5	194.0	2.01	4.78	37.0	-82.0	5.07	3.99
WG159	1300+56.00	36.14	-604.8	-149	-266	-97.5	183.5	2.05	4.67	37.0	-85.0	6.21	3.98
WG160	1300+68.00	36.14	-604.8	-150	-265	-102.5	193.0	1.94	4.44	39.5	-89.5	5.85	3.80
WG161	1300+68.00	36.14	-604.8	-148	-268	-100.5	189.5	2.00	4.54	38.5	-88.0	5.95	3.83
WG162	1300+80.00	36.14	-604.8	-142	-279	-103.5	194.5	2.02	4.47	41.5	-93.0	5.32	3.50
WG163	1300+80.00	36.14	-604.8	-166	-271	-97.5	184.0	2.08	4.50	41.0	-96.0	6.13	3.48
WG164	1300+92.00	36.14	-604.8	-166	-272	-101.0	190.0	2.02	4.35	43.0	-99.0	5.83	3.36
WG165	1300+92.00	36.14	-604.8	-161	-278	-99.5	187.0	2.09	4.46	42.0	-96.5	5.83	3.38
WG166	1301+04.00	34.83	-561.6	-158	-284	-100.0	188.0	2.12	4.04	44.0	-100.0	5.47	2.77
WG167	1301+04.00	34.83	-561.6	-190	-252	-94.0	177.5	2.02	3.95	43.0	-101.5	6.54	3.05
WG168	1301+16.00	34.83	-561.6	-198	-239	-95.5	180.5	1.89	3.81	43.5	-103.0	6.68	3.14
WG169	1301+16.00	34.83	-561.6	-174	-249	-94.0	177.5	2.00	4.13	42.0	-100.5	6.21	3.12
WG170	1301+28.00	34.83	-561.6	-168	-259	-93.0	175.5	2.09	4.23	43.0	-102.5	5.89	2.95
WG171	1301+28.00	34.83	-561.6	-195	-234	-86.5	164.5	2.04	4.24	42.0	-103.5	6.84	3.17
WG172	1301+40.00	34.83	-561.6	-201	-222	-87.5	166.0	1.93	4.12	41.0	-103.0	7.20	3.30
WG173	1301+40.00	34.83	-561.6	-172	-242	-86.0	163.5	2.11	4.53	40.0	-100.5	6.46	3.18
WG174	1301+52.00	34.83	-561.6	-167	-251	-84.5	160.0	2.23	4.68	40.0	-101.0	6.29	3.08
WG175	1301+52.00	34.83	-561.6	-189	-236	-78.5	149.5	2.26	4.75	39.0	-101.5	7.17	3.21
WG176	1301+64.00	34.83	-561.6	-207	-242	-100.0	173.5	2.00	3.55	50.0	-114.5	6.04	2.79
WG177	1301+64.00	34.83	-561.6	-167	-274	-98.0	170.5	2.27	4.02	48.5	-112.0	5.21	2.57
WG178	1301+76.00	34.83	-561.6	-160	-287	-95.5	166.5	2.41	4.21	48.0	-111.0	5.07	2.48
WG179	1301+76.00	34.83	-561.6	-180	-256	-88.0	154.0	2.36	4.33	47.0	-112.0	5.72	2.73
WG180	1301+88.00	34.83	-561.6	-186	-247	-89.5	156.0	2.26	4.20	45.0	-109.5	6.12	2.87
WG181	1301+88.00	34.83	-561.6	-144	-282	-87.5	153.5	2.58	4.78	43.5	-107.0	5.13	2.61
WG182	1302+00.00	34.83	-561.6	-140	-288	-86.0	150.5	2.68	4.91	43.0	-105.5	5.07	2.59
WG183	1302+00.00	34.83	-561.6	-148	-258	-79.0	139.0	2.64	5.24	42.0	-106.5	5.43	2.85
WG184	1302+12.00	34.83	-561.6	-155	-247	-81.5	143.0	2.46	4.99	40.0	-104.0	5.92	3.03
WG185	1302+12.00	34.83	-561.6	-136	-280	-79.5	140.5	2.80	5.35	38.5	-101.5	5.56	2.77
WG186	1302+24.00	34.83	-561.6	-159	-242	-79.0	139.0	2.49	5.09	37.5	-100.0	6.46	3.19
WG187	1302+24.00	34.83	-561.6	-142	-239	-72.5	128.5	2.66	5.79	36.5	-100.5	6.04	3.21
WG188	1302+36.00	34.83	-561.6	-152	-222	-75.0	132.5	2.43	5.47	34.5	-97.5	6.75	3.48
WG189	1302+36.00	34.83	-561.6	-140	-242	-73.5	130.0	2.66	5.73	33.5	-95.5	6.53	3.34
WG190	1302+48.00	34.83	-561.6	-166	-200	-73.0	129.0	2.28	5.42	32.0	-94.0	7.84	3.85
WG191	1302+48.00	34.83	-561.6	-155	-193	-67.0	119.5	2.39	6.07	31.5	-94.5	7.52	3.90
WG192	1302+60.00	34.83	-561.6	-167	-174	-69.5	124.0	2.11	5.68	29.5	-92.0	8.53	4.21
WG193	1302+60.00	34.83	-561.6	-158	-188	-68.0	122.0	2.28	5.94	28.5	-90.0	8.45	4.15
WG194	1302+72.00	34.83	-561.6	-187	-140	-68.0	121.5	1.80	5.51	27.5	-88.0	10.08	4.79
WG195	1302+72.00	34.83	-561.6	-175	-129	-63.0	113.0	1.81	6.13	27.0	-89.0	9.72	4.87
WG196	1302+84.00	34.83	-561.6	-189	-105	-65.5	117.0	1.50	5.69	25.5	-86.0	10.98	5.31
WG197	1302+84.00	34.83	-561.6	-179	-115	-64.5	115.0	1.63	5.93	24.5	-84.5	10.93	5.28
WG198	1302+96.00	34.83	-561.6	-187	-104	-64.0	114.5	1.51	5.86	23.5	-83.0	11.78	5.52
WG199	1302+96.00	34.83	-561.6	-169	-121	-59.0	107.0	1.82	6.66	23.0	-84.0	11.07	5.24
WG200	1303+08.00	34.83	-561.6	-165	-128	-61.0	110.5	1.84	6.50	22.0	-81.5	11.35	5.32
WG201	1303+08.00	34.83	-561.6	-174	-136	-60.5	109.5	1.95	6.41	21.0	-81.0	12.40	5.25
WG202	1303+20.00	34.83	-561.6	-180	-126	-59.0	107.0	1.88	6.47	20.0	-79.5	13.40	5.48
WG203	1303+20.00	34.83	-561.6	-176	-133	-55.0	100.5	2.08	7.02	20.0	-80.0	13.15	5.36
WG204	1303+32.00	34.83	-561.6	-162	-154	-56.5	102.0	2.32	7.07	19.0	-78.5	12.94	5.19
WG205	1303+32.00	34.83	-561.6	-182	-141	-55.5	101.0	2.18	6.84	18.5	-77.5	14.64	5.42
WG206	1303+44.00	34.83	-561.6	-187	-133	-53.5	97.5	2.15	7.01	18.0	-77.0	15.39	5.56
WG207	1303+44.00	34.83	-561.6	-181	-142	-50.0	91.5	2.42	7.61	17.5	-77.5	15.43	5.41
WG208	1303+56.00	34.83	-561.6	-168	-164	-51.0	93.0	2.67	7.72	17.0	-76.5	14.91	5.20
WG209	1303+56.00	34.83	-561.6	-188	-148	-50.5	92.5	2.47	7.39	16.5	-75.5	16.90	5.48
WG210	1303+68.00	34.83	-561.6	-192	-143	-47.5	88.0	2.52	7.79	17.0	-76.0	16.65	5.51
WG211	1303+68.00	34.83	-561.6	-185	-153	-44.5	83.0	2.83	8.46	16.5	-76.5	16.66	5.34
WG212	1303+80.00	34.83	-561.6	-172	-175	-44.5	83.0	3.16	8.77	16.5	-76.0	15.63	5.08
WG213	1303+80.00	34.83	-561.6	-196	-150	-44.0	81.5	2.84	8.32	16.0	-75.5	18.01	5.45
WG214	1303+92.00	34.83	-561.6	-199	-145	-40.0	75.5	2.97	9.06	17.0	-77.0	17.22	5.41
WG215	1303+92.00	34.83	-561.6	-193	-155	-37.5	72.0	3.30	9.82	17.0	-77.5	16.77	5.24
WG216	1304+04.00	34.83	-561.6	-187	-165	-36.5	70.5	3.55	10.25	18.0	-79.5	15.43	4.99
WG217	1304+10.00	34.83	-561.6	-213	-137	-36.5	69.5	3.09	9.56	17.5	-78.0	17.69	5.44
WG218	1304+16.00	34.83	-561.6	-214	-136	-31.5	62.5	3.41	11.03	20.0	-82.5	15.56	5.16
WG219	1304+16.00	34.83	-561.6	-205	-152	-30.0	60.0	3.88	11.90	19.5	-82.0	15.35	5.00
WG220	1304+28.00	34.83	-561.6	-197	-164	-28.0	56.0	4.44	13.03	23.0	-88.0	12.58	4.52
WG221	1304+28.00	34.83	-561.6	-203	-100	-37.0	57.5	2.92	9.68	39.5	-92.0	7.54	5.02
WG222	1304+40.00	34.83	-561.6	-208	-93	-30.0	48.5	3.30	11.78	47.5	-103.0	6.40	4.55
WG223	1304+40.00	34.83	-561.6	-201	-105	-30.5	50.0	3.49	11.84	44.0	-98.5	6.69	4.64
WG224	1304+52.00	34.83	-561.6	-152	-92	-18.0	26.5	5.98	22.77	35.0	-68.0	6.67	6.91
WG225	1304+52.00	34.83	-561.6	-163	-82	-17.5	26.0	5.62	22.80	34.0	-67.0	7.26	7.16
WG226	1304+64.00	34.83	-561.6	-126	-77	-11.0	16.5	8.49	39.65	34.5	-59.0	5.81	8.21
WG228	1304+64.00	34.83	-561.6	-134	-211	1.0	40.0	7.69	NaN	21.5	-129.5	9.81	2.70
WG229	1304+75.00	34.83	-561.6	-158	-179	1.5	39.5	6.76	NaN	39.0	-153.0	6.18	2.50
WG230	1304+75.00	34.83	-561.6	-165	-169	1.0	39.5	6.44	NaN	39.0	-152.5	6.39	2.58
WG231	1304+86.00	34.83	-561.6	-161	-174	-10.0	55.0	4.75	40.09	27.5	-137.5	8.89	2.82
WG233	1304+86.00	34.83	-561.6	-101	-105	-11.5	14.0	12.49	40.07	30.5	-49.5	5.56	9.22
WG234	1304+98.00	34.83	-561.6	-124	-129	-23.5	29.0	7.05	18.63	32.0	-59.0	6.19	7.34
WG235	1304+98.00	34.83	-561.6	-124	-129	-23.0	28.5	7.18	19.03	31.5	-58.5	6.30	7.40
WG236	1305+10.00	34.83	-561.6	-162	-162	-42.5	60.0	4.10	9.40	41.0	-86.0	6.01	4.65
WG237	1305+10.00	34.83	-561.6	-157	-164	-39.0	55.5	4.48	10.38	41.5	-86.5	5.77	4.59
WG238	1305+22.00	34.83	-561.6	-163	-155	-50.0	69.5	3.41	7.98	38.5	-83.0	6.41	4.90

WG239	1305+22.00	34.83	-561.6	-187	-186	-37.5	64.5	4.28	9.98	23.5	-78.5	11.82	4.78
WG240	1305+34.00	34.83	-561.6	-175	-206	-41.5	71.0	4.23	9.31	23.0	-77.5	11.43	4.59
WG241	1305+34.00	34.83	-561.6	-174	-197	-42.0	71.0	4.08	9.22	22.5	-76.5	11.62	4.77
WG242	1305+46.00	34.83	-561.6	-186	-178	-47.0	79.5	3.35	8.00	21.5	-74.5	12.82	5.14
WG243	1305+46.00	34.83	-561.6	-191	-172	-46.5	78.5	3.29	7.98	21.5	-74.0	13.10	5.26
WG244	1305+58.00	34.83	-561.6	-177	-194	-47.0	80.0	3.58	8.17	21.0	-74.0	12.63	4.97
WG245	1305+58.00	34.83	-561.6	-179	-178	-48.0	81.5	3.27	7.97	20.5	-72.5	13.03	5.29
WG246	1305+70.00	34.83	-561.6	-186	-167	-52.0	88.5	2.85	7.22	19.5	-71.0	14.17	5.56
WG247	1305+70.00	34.83	-561.6	-188	-164	-51.0	86.0	2.88	7.33	19.0	-70.5	14.65	5.65
WG248	1305+82.00	34.83	-561.6	-183	-173	-51.5	87.0	2.98	7.36	19.0	-70.5	14.30	5.52
WG249	1305+82.00	34.83	-561.6	-183	-157	-52.5	89.0	2.69	7.21	18.5	-68.5	14.71	5.91
WG250	1305+94.00	34.83	-561.6	-190	-145	-56.0	94.5	2.37	6.63	17.5	-67.0	16.07	6.22
WG251	1305+94.00	34.83	-561.6	-192	-142	-55.0	93.0	2.37	6.71	17.5	-66.5	16.23	6.32
WG252	1306+06.00	34.83	-561.6	-188	-150	-54.5	92.5	2.49	6.86	17.0	-66.5	16.36	6.19
WG253	1306+06.00	34.83	-561.6	-190	-129	-57.0	96.5	2.13	6.52	16.5	-64.5	17.04	6.70
WG254	1306+18.00	34.83	-561.6	-195	-122	-60.5	102.0	1.92	6.07	15.5	-62.5	18.49	7.04
WG255	1306+18.00	34.83	-561.6	-183	-169	-59.5	101.0	2.52	6.37	15.0	-62.5	18.11	6.29
WG256	1306+30.00	34.83	-561.6	-170	-190	-60.0	101.5	2.76	6.53	15.5	-62.5	16.49	5.95
WG257	1306+30.00	34.83	-561.6	-183	-160	-63.0	105.5	2.31	6.01	14.5	-60.5	18.79	6.64
WG258	1306+42.00	34.83	-561.6	-187	-155	-67.5	114.0	2.08	5.55	14.0	-60.0	19.81	6.78
WG259	1306+42.00	34.83	-561.6	-176	-199	-66.5	112.0	2.61	5.80	14.0	-60.0	18.82	6.04
WG260	1306+54.00	34.83	-561.6	-166	-216	-68.0	115.0	2.73	5.82	16.5	-63.5	15.19	5.44
WG261	1306+54.00	34.83	-561.6	-187	-182	-71.5	121.5	2.23	5.23	16.0	-62.5	17.36	6.07
WG262	1306+66.00	34.83	-561.6	-190	-177	-79.0	133.0	1.99	4.71	21.5	-71.0	13.07	5.41
WG263	1306+66.00	34.83	-561.6	-179	-224	-77.5	131.0	2.47	4.94	21.0	-70.5	12.70	4.79
WG264	1306+78.00	34.83	-561.6	-171	-236	-81.5	137.5	2.46	4.79	27.0	-80.5	9.53	4.04
WG265	1306+78.00	34.83	-561.6	-186	-209	-85.0	144.5	2.11	4.42	27.5	-80.0	10.04	4.41
WG266	1306+90.00	34.83	-561.6	-189	-205	-94.0	159.5	1.88	3.97	35.0	-92.5	7.98	3.85
WG267	1306+90.00	34.83	-561.6	-177	-250	-92.5	157.0	2.27	4.16	34.5	-92.0	7.67	3.39
WG268	1307+02.00	34.83	-561.6	-174	-255	-98.0	166.0	2.18	3.96	42.0	-104.5	6.20	2.93
WG269	1307+02.00	34.83	-561.6	-188	-234	-102.0	174.0	1.93	3.66	42.0	-103.5	6.63	3.17
WG270	1307+14.00	34.83	-561.6	-189	-233	-111.5	189.5	1.76	3.34	50.5	-117.5	5.53	2.80
WG271	1307+14.00	34.83	-561.6	-178	-256	-110.0	187.0	1.95	3.49	49.5	-116.5	5.37	2.62
WG272	1307+26.00	34.83	-561.6	-202	-216	-115.0	195.0	1.61	3.13	57.5	-129.0	5.15	2.68
WG273	1307+26.00	34.83	-561.6	-235	-203	-118.5	202.5	1.46	2.75	57.0	-127.5	5.92	2.82
WG274	1307+38.00	34.83	-561.6	-235	-204	-125.5	214.5	1.39	2.60	64.0	-138.5	5.27	2.59
WG275	1307+38.00	34.83	-561.6	-225	-224	-124.5	211.5	1.53	2.71	63.0	-138.0	5.15	2.45
WG276	1307+50.00	34.83	-561.6	-246	-191	-126.0	215.5	1.31	2.51	69.0	-147.5	5.08	2.51
WG277	1307+50.00	34.83	-561.6	-264	-184	-129.0	221.0	1.24	2.31	68.0	-144.5	5.49	2.61
WG278	1307+62.00	34.83	-561.6	-260	-190	-131.5	225.0	1.25	2.29	72.0	-151.5	5.12	2.45
WG279	1307+62.00	34.83	-561.6	-238	-198	-129.5	222.5	1.31	2.50	71.0	-150.5	4.79	2.41
WG280	1307+74.00	34.83	-561.6	-253	-172	-127.0	218.0	1.19	2.43	74.5	-155.5	4.83	2.50
WG281	1307+74.00	34.83	-561.6	-253	-173	-128.5	221.5	1.17	2.40	72.0	-150.5	5.00	2.58
WG282	1307+86.00	34.83	-561.6	-246	-184	-124.5	214.5	1.27	2.53	72.0	-150.5	4.88	2.51
WG283	1307+86.00	34.83	-561.6	-224	-191	-122.5	212.5	1.33	2.76	72.0	-149.5	4.49	2.48
WG284	1307+98.00	34.83	-561.6	-236	-171	-112.5	196.0	1.31	2.89	70.5	-147.5	4.80	2.65
WG285	1307+98.00	34.83	-561.6	-236	-171	-113.0	197.0	1.31	2.88	67.5	-141.0	5.01	2.77
WG286	1308+10.00	34.83	-561.6	-227	-185	-100.0	175.0	1.57	3.35	62.0	-132.5	5.28	2.84
WG287	1308+10.00	34.83	-561.6	-204	-188	-99.0	173.0	1.61	3.61	61.5	-131.5	4.85	2.84
WG288	1308+22.00	34.83	-561.6	-215	-171	-80.5	143.0	1.80	4.31	55.5	-121.5	5.63	3.22
WG289	1308+22.00	34.83	-561.6	-216	-171	-79.5	141.5	1.82	4.35	52.0	-111.5	6.02	3.51
WG290	1308+34.00	34.83	-561.6	-214	-173	-59.5	107.5	2.41	5.85	43.5	-98.5	7.14	3.95
WG291	1308+34.00	34.83	-561.6	-221	-121	-57.0	104.0	1.88	5.97	42.5	-96.5	7.53	4.56
WG291	1308+39.58	34.83	-561.6	-223	-119	-49.0	91.0	2.12	6.92	39.5	-92.0	8.14	4.81
WG292	1308+39.58	34.83	-561.6	-194	-129	-46.5	86.0	2.39	7.91	34.5	-79.5	8.29	5.44
WG292	1308+45.17	34.83	-561.6	-202	-116	-39.5	74.0	2.54	9.10	33.5	-78.0	8.84	5.72
WG293	1308+45.17	34.83	-561.6	-202	-115	-37.5	70.0	2.68	9.58	32.0	-75.5	9.26	5.92
WG293	1308+50.75	34.83	-561.6	-211	-101	-31.5	60.5	2.80	11.12	34.5	-79.5	8.91	5.80
WG294	1308+50.75	34.83	-561.6	-177	-121	-30.0	56.0	3.47	12.84	33.0	-73.0	8.00	6.04
WG294	1308+56.33	34.83	-561.6	-182	-114	-27.5	53.0	3.50	13.82	40.0	-84.0	6.76	5.33
WG295	1308+56.33	34.83	-561.6	-182	-113	-26.0	50.5	3.67	14.61	40.5	-85.0	6.68	5.27
WG295	1308+61.92	34.83	-561.6	-175	-124	-29.5	56.0	3.55	13.11	51.0	-101.0	5.14	4.33
WG296	1308+61.92	34.83	-561.6	-133	-149	-57.0	99.5	2.31	7.51	81.0	-145.5	2.59	2.84

B.2 Extracted live and Dead Load Forces with the Calculated Rating Factors for Strength I Inventory Limit State

Table B.2. Rating Factors for Strength I-Flexural Inventory

Member Number	Station (feet)	Axial Capacity	Moment Capacity	Factored Axial Dead load	Factored Axial Live Load	Factored Dead Load Moment	Factored Live Load Moment	Rating Factor inv Axial	Rating Factor inv moment
WG003	1291+38.08	-128	26223	-1314	339	-741	8548	3.50	3.15
WG004	1291+38.08	830	25100	-1308	515	-738	6561	4.15	3.94
WG004	1291+43.67	1083	24805	-1272	515	-1323	5983	4.58	4.37
WG005	1291+43.67	342	25671	-2240	514	800	5377	5.02	4.63
WG005	1291+49.25	310	25708	-2204	514	1096	5468	4.89	4.50
WG006	1291+49.25	876	25046	-2213	632	1079	5237	4.89	4.58
WG006	1291+54.83	492	25495	-2178	632	567	6363	4.22	3.92
WG007	1291+54.83	-587	26762	-3227	631	2744	6477	4.18	3.71
WG007	1291+60.42	-870	27094	-3191	631	1975	7827	3.68	3.21
WG008	1291+60.42	-657	26845	-3183	716	1982	7965	3.53	3.12
WG008	1291+66.00	-932	27168	-3148	716	1210	9642	3.09	2.69
WG009	1291+66.00	-1651	28012	-3940	716	1872	9728	3.20	2.69
WG010	1291+78.00	-2051	28483	-3864	716	-263	14159	2.53	2.03
WG011	1291+78.00	-2784	29344	-4855	761	-834	14168	2.72	2.13
WG012	1291+90.00	-3015	29615	-4783	761	-2387	18404	2.32	1.74
WG013	1291+90.00	-2992	29588	-4780	764	-2398	18194	2.34	1.76
WG014	1292+02.00	-3136	29757	-4747	764	-3043	21457	2.11	1.53
WG015	1292+02.00	-3987	30650	-5670	747	-721	20253	2.25	1.55
WG016	1292+14.00	-4069	30732	-5647	747	-1965	23197	2.11	1.41
WG017	1292+14.00	-4041	30704	-5639	751	-2105	22949	2.13	1.43
WG018	1292+26.00	-4098	30761	-5636	751	-2572	24708	2.05	1.35
WG019	1292+26.00	-4889	31555	-6425	690	-235	23214	2.23	1.37
WG020	1292+38.00	-4918	31584	-6430	690	-1649	24968	2.19	1.33
WG021	1292+38.00	-4904	31571	-6433	694	-1619	24646	2.20	1.35
WG022	1292+50.00	-4916	31582	-6437	694	-1943	25128	2.19	1.33
WG023	1292+50.00	-5127	31794	-6551	599	-1322	23869	2.38	1.39
WG024	1292+62.00	-5677	32346	-7176	599	-2073	24474	2.50	1.41
WG025	1292+62.00	-6261	32933	-7843	603	-1029	23876	2.62	1.42
WG026	1292+74.00	-6964	31806	-8593	603	220	22968	2.70	1.38
WG027	1292+74.00	-5439	30020	-6752	496	-1978	22364	2.65	1.43
WG028	1292+86.00	-6274	30997	-7713	496	-2101	22177	2.90	1.49
WG029	1292+86.00	-6862	31686	-8383	500	-774	21535	3.04	1.51
WG030	1292+98.00	-7524	31842	-9147	500	483	20101	3.25	1.56
WG031	1292+98.00	-6341	30514	-7684	398	-1241	19346	3.38	1.64
WG032	1293+10.00	-6923	31162	-8384	398	-2977	19359	3.67	1.76
WG033	1293+10.00	-7463	31772	-8998	401	-1467	18708	3.83	1.78
WG034	1293+22.00	-8111	29320	-9680	401	784	16849	3.91	1.69
WG035	1293+22.00	-7203	28244	-8702	311	-231	15967	4.82	1.78
WG036	1293+34.00	-7663	28790	-9093	311	-2323	16201	4.59	1.92
WG037	1293+34.00	-8169	29389	-9662	314	-442	15476	4.76	1.93
WG038	1293+46.00	-8857	25446	-10341	314	1869	14010	4.73	1.68
WG039	1293+46.00	-7804	24205	-9436	237	698	13186	6.90	1.78
WG040	1293+58.00	-8463	24981	-9868	237	-922	13532	5.94	1.91
WG041	1293+58.00	-8893	25488	-10347	238	1040	12815	6.10	1.91
WG042	1293+70.00	-9581	22239	-11024	238	3144	12104	6.05	1.58
WG043	1293+70.00	-8714	21221	-10379	176	2352	11252	9.44	1.68
WG044	1293+82.00	-9206	21798	-10508	176	-94	11720	7.38	1.87
WG045	1293+82.00	-9580	22237	-10913	178	1891	11290	7.49	1.80
WG079	1295+72.00	-10339	29421	-12228	151	-661	6476	12.52	4.65
WG080	1295+84.00	-10410	29508	-12228	151	-2311	7615	12.06	4.18

WG081	1295+84.00	-10161	29199	-11963	155	-2017	7570	11.59	4.12
WG082	1295+96.00	-10233	29289	-11963	155	-1083	8303	11.13	3.66
WG083	1295+96.00	-10226	29280	-11972	157	-495	7991	11.13	3.73
WG084	1296+08.00	-10246	29305	-11972	157	-1775	8636	11.01	3.60
WG085	1296+08.00	-9904	28830	-11632	174	-1180	8639	9.94	3.47
WG086	1296+20.00	-9960	28929	-11632	174	-421	9315	9.61	3.15
WG087	1296+20.00	-9940	28895	-11626	176	-102	9088	9.56	3.19
WG088	1296+32.00	-9950	28912	-11626	176	-948	9521	9.50	3.14
WG089	1296+32.00	-9595	28286	-11284	205	-59	9545	8.25	2.97
WG090	1296+44.00	-9647	28377	-11284	205	375	10301	8.00	2.72
WG091	1296+44.00	-9625	28338	-11279	208	378	10119	7.97	2.76
WG092	1296+56.00	-9621	28331	-11279	208	-518	10367	7.99	2.78
WG093	1296+56.00	-9204	27595	-10868	245	249	10552	6.78	2.59
WG094	1296+68.00	-9243	27664	-10868	245	396	11205	6.62	2.43
WG095	1296+68.00	-9219	27621	-10864	248	90	11078	6.62	2.49
WG096	1296+80.00	-9216	27616	-10864	249	-615	11313	6.63	2.50
WG097	1296+80.00	-8703	26711	-10344	296	114	11596	5.54	2.29
WG098	1296+92.00	-8740	26776	-10344	296	227	12240	5.42	2.17
WG099	1296+92.00	-8718	26737	-10340	299	79	12070	5.42	2.21
WG100	1297+04.00	-8710	26723	-10340	299	-511	12190	5.45	2.23
WG101	1297+04.00	-8432	26232	-10079	353	859	12331	4.67	2.06
WG102	1297+16.00	-8462	26286	-10079	353	894	12879	4.59	1.97
WG103	1297+16.00	-8438	26244	-10074	354	831	12591	4.63	2.02
WG104	1297+28.00	-7546	21541	-9389	354	392	12735	5.21	1.66
WG105	1297+28.00	-8047	22105	-9621	409	752	13256	3.85	1.61
WG106	1297+40.00	-7961	22009	-9450	409	2779	13314	3.64	1.44
WG107	1297+40.00	-8089	22152	-9642	410	1548	13306	3.79	1.55
WG108	1297+52.00	-6762	26455	-8628	410	997	13565	4.55	1.88
WG109	1297+52.00	-7179	26949	-8808	470	1526	14190	3.47	1.79
WG110	1297+64.00	-7095	26849	-8632	470	3121	14524	3.27	1.63
WG111	1297+64.00	-6584	26245	-8121	471	142	15031	3.27	1.74
WG112	1297+76.00	-5378	30768	-7047	471	2094	14765	3.54	1.94
WG113	1297+76.00	-6482	32082	-8214	530	2909	15381	3.26	1.90
WG114	1297+88.00	-6509	32114	-8149	531	4670	15805	3.09	1.74
WG115	1297+88.00	-5973	31475	-7594	531	2503	16072	3.05	1.80
WG116	1298+00.00	-4606	35556	-6163	531	4567	15906	2.93	1.95
WG117	1298+00.00	-6075	37193	-7902	590	5728	16481	3.10	1.91
WG118	1298+12.00	-6065	37181	-7766	590	7513	17283	2.88	1.72
WG119	1298+12.00	-5583	36633	-7289	591	5603	17186	2.89	1.81
WG120	1298+24.00	-3971	40228	-5570	591	7189	17258	2.71	1.91
WG121	1298+24.00	-5140	41714	-6994	646	7000	18226	2.87	1.90
WG122	1298+36.00	-5058	41610	-6778	646	8672	19044	2.66	1.73
WG123	1298+36.00	-4473	40865	-6168	647	7060	18946	2.62	1.78
WG124	1298+48.00	-3132	45133	-4789	647	7794	19270	2.56	1.94
WG125	1298+48.00	-3809	45957	-5643	697	7150	20377	2.63	1.90
WG126	1298+60.00	-3761	45898	-5495	697	8542	20976	2.49	1.78
WG127	1298+60.00	-3128	45129	-4813	698	7267	20926	2.41	1.81
WG128	1298+72.00	-2167	50721	-3904	698	8208	21119	2.49	2.01
WG129	1298+72.00	-2863	51520	-4752	741	8332	22023	2.55	1.96
WG130	1298+84.00	-2909	51573	-4725	741	9540	22535	2.45	1.87
WG131	1298+84.00	-2331	50909	-4110	742	8364	22437	2.40	1.90
WG132	1298+96.00	-1351	55676	-3165	742	9059	22506	2.44	2.07
WG133	1298+96.00	-2062	56496	-4015	773	8769	23464	2.53	2.03
WG134	1299+08.00	-2034	56465	-3929	773	9833	23672	2.45	1.97
WG135	1299+08.00	-1367	55697	-3224	774	7943	23771	2.40	2.01
WG136	1299+20.00	-1297	55608	-3142	774	8317	23590	2.38	2.00
WG137	1299+20.00	-1360	55688	-3203	790	8667	24343	2.33	1.93
WG138	1299+32.00	-1307	55622	-3134	790	8452	24561	2.31	1.92
WG139	1299+32.00	-476	54580	-2217	792	7766	24313	2.20	1.93
WG140	1299+44.00	-432	54525	-2190	792	8020	23841	2.22	1.95
WG141	1299+44.00	-500	54611	-2221	787	8116	24563	2.19	1.89
WG142	1299+56.00	-479	54584	-2219	787	7670	24475	2.21	1.92
WG143	1299+56.00	707	53100	-886	789	7356	24127	2.02	1.90
WG144	1299+68.00	736	53063	-884	789	8241	23211	2.05	1.93
WG145	1299+68.00	603	53230	-914	760	9220	23756	2.00	1.85
WG146	1299+80.00	617	53212	-914	760	9205	23519	2.02	1.87
WG147	1299+80.00	1725	51825	346	761	9824	22901	1.81	1.83
WG148	1299+92.00	1715	51837	346	761	12406	21652	1.80	1.82
WG149	1299+92.00	1488	52122	249	714	13119	22443	1.73	1.74
WG149	1300+00.00	1479	52132	249	714	13277	22514	1.72	1.73
WG150	1300+00.00	1468	52146	240	720	13861	22405	1.71	1.71

WG150	1300+08.00	1466	52149	239	720	13532	22624	1.70	1.71
WG151	1300+08.00	1401	52231	265	624	12745	21476	1.82	1.84
WG152	1300+20.00	1334	52315	262	624	12149	23148	1.72	1.74
WG153	1300+20.00	1394	52239	270	624	9501	23490	1.80	1.82
WG154	1300+32.00	1370	52269	267	624	7377	25145	1.77	1.79
WG155	1300+32.00	213	53718	-995	578	8839	23482	2.09	1.91
WG156	1300+44.00	148	53799	-1001	578	8680	24965	1.99	1.81
WG157	1300+44.00	207	53725	-968	578	7471	24885	2.03	1.86
WG158	1300+56.00	176	53765	-974	578	6380	26137	1.99	1.81
WG159	1300+56.00	-950	55175	-2235	557	8313	24380	2.31	1.92
WG160	1300+68.00	-1002	55240	-2240	557	8528	25418	2.22	1.84
WG161	1300+68.00	-981	55214	-2239	557	8298	25054	2.26	1.87
WG162	1300+80.00	-1000	55237	-2245	557	7676	25731	2.23	1.85
WG163	1300+80.00	-1752	56158	-3109	548	9045	24096	2.47	1.96
WG164	1300+92.00	-1793	56204	-3125	548	9135	24695	2.43	1.91
WG165	1300+92.00	-1739	56144	-3089	548	8627	24433	2.46	1.94
WG166	1301+04.00	-1836	56250	-3228	548	5956	25185	2.54	2.00
WG167	1301+04.00	-2370	56832	-3851	547	8733	23087	2.71	2.08
WG168	1301+16.00	-3296	52012	-4729	547	9735	23003	2.62	1.84
WG169	1301+16.00	-2537	51146	-3904	547	8216	23037	2.50	1.86
WG170	1301+28.00	-2664	51292	-4105	547	5086	23508	2.64	1.97
WG171	1301+28.00	-3124	51820	-4666	550	7324	21497	2.81	2.07
WG172	1301+40.00	-4094	46303	-5578	550	8081	21236	2.70	1.80
WG173	1301+40.00	-3322	45365	-4745	550	5942	21470	2.59	1.84
WG174	1301+52.00	-3338	45384	-4833	550	3056	21660	2.72	1.95
WG175	1301+52.00	-3826	45976	-5438	556	5545	19590	2.90	2.06
WG176	1301+64.00	-5284	41897	-6918	556	6549	19224	2.94	1.84
WG177	1301+64.00	-4524	40930	-6105	556	3937	19612	2.84	1.89
WG178	1301+76.00	-4473	40865	-6128	556	1062	19725	2.98	2.02
WG179	1301+76.00	-4489	40885	-6200	565	4363	17419	3.03	2.10
WG180	1301+88.00	-6178	37314	-7929	565	5421	17119	3.10	1.86
WG181	1301+88.00	-5366	36393	-7063	565	2558	17631	3.00	1.92
WG182	1302+00.00	-5446	36481	-7240	565	-663	18021	3.17	2.06
WG183	1302+00.00	-5019	36011	-6826	574	1700	16079	3.15	2.13
WG184	1302+12.00	-6343	31917	-8103	574	2763	15922	3.07	1.83
WG185	1302+12.00	-6354	31929	-8174	574	802	16204	3.17	1.92
WG186	1302+24.00	-6512	32118	-8399	574	35	16050	3.28	2.00
WG187	1302+24.00	-5712	31165	-7749	582	79	14909	3.50	2.09
WG188	1302+36.00	-7028	26770	-8818	582	1136	14814	3.08	1.73
WG189	1302+36.00	-7016	26757	-8852	582	-82	14906	3.15	1.80
WG190	1302+48.00	-7095	26850	-8977	582	-531	14724	3.23	1.86
WG191	1302+48.00	-6451	26088	-8689	588	195	13477	3.81	1.92
WG192	1302+60.00	-8005	22058	-9835	588	1455	13429	3.11	1.53
WG193	1302+60.00	-7943	21988	-9807	589	556	13443	3.17	1.59
WG194	1302+72.00	-7990	22041	-9879	589	477	13264	3.21	1.63
WG195	1302+72.00	-7254	21213	-9468	593	1102	12160	3.74	1.65
WG196	1302+84.00	-8189	25804	-10239	593	2602	12299	3.46	1.89
WG197	1302+84.00	-8016	25499	-10097	594	1897	12050	3.50	1.96
WG198	1302+96.00	-8047	25554	-10097	594	2691	11998	3.45	1.91
WG199	1302+96.00	-7655	24862	-9810	597	1415	11175	3.61	2.10
WG200	1303+08.00	-7677	24901	-9810	597	1095	11551	3.57	2.06
WG201	1303+08.00	-8119	25681	-10364	598	1131	11402	3.75	2.15
WG202	1303+20.00	-8127	25696	-10364	598	1785	11176	3.74	2.14
WG203	1303+20.00	-8017	25501	-10378	601	1428	10420	3.93	2.31
WG204	1303+32.00	-7990	25453	-10378	601	181	10730	3.97	2.36
WG205	1303+32.00	-8418	26208	-10858	602	1383	10532	4.05	2.36
WG206	1303+44.00	-8401	26178	-10858	602	1910	10171	4.08	2.39
WG207	1303+44.00	-8277	25960	-10873	606	1382	9532	4.29	2.58
WG208	1303+56.00	-8232	25880	-10873	606	154	9697	4.36	2.65
WG209	1303+56.00	-8630	26582	-11298	607	1493	9567	4.40	2.62
WG210	1303+68.00	-8574	26483	-11298	607	1842	9076	4.49	2.72
WG211	1303+68.00	-8430	26230	-11303	612	1216	8562	4.70	2.92
WG212	1303+80.00	-8345	26080	-11303	612	-61	8540	4.84	3.06
WG213	1303+80.00	-8735	26768	-11683	613	1725	8417	4.81	2.98
WG214	1303+92.00	-8626	26576	-11683	613	2089	7765	4.99	3.15
WG215	1303+92.00	-8470	26299	-11694	620	1479	7346	5.20	3.38
WG216	1304+04.00	-8395	26167	-11694	620	912	7217	5.32	3.50
WG217	1304+10.00	-8785	26857	-12052	621	2892	7086	5.26	3.38
WG218	1304+16.00	-8575	26486	-12052	621	3003	6312	5.60	3.72
WG219	1304+16.00	-8379	26140	-12059	629	2071	6026	5.85	3.99
WG220	1304+28.00	-8156	25745	-12059	629	1389	5599	6.21	4.35

WG239	1305+22.00	-10377	29468	-12193	152	4	6869	11.94	4.29
WG240	1305+34.00	-10438	29544	-12193	152	-1128	7888	11.54	3.89
WG241	1305+34.00	-10238	29295	-11945	150	-843	7844	11.42	3.84
WG242	1305+46.00	-10300	29372	-11945	150	223	8497	11.01	3.43
WG243	1305+46.00	-10336	29417	-11984	148	652	8350	11.10	3.45
WG244	1305+58.00	-10341	29423	-11984	148	-676	8821	11.07	3.41
WG245	1305+58.00	-10063	29079	-11645	148	-42	8793	10.70	3.31
WG246	1305+70.00	-10106	29131	-11645	148	646	9421	10.41	3.02
WG247	1305+70.00	-10111	29138	-11653	147	784	9253	10.52	3.06
WG248	1305+82.00	-10109	29135	-11653	147	249	9367	10.54	3.08
WG249	1305+82.00	-9781	28613	-11258	150	821	9540	9.87	2.91
WG250	1305+94.00	-9815	28673	-11258	150	1505	10117	9.64	2.69
WG251	1305+94.00	-9823	28688	-11269	148	1701	9937	9.74	2.72
WG252	1306+06.00	-9814	28671	-11269	148	1179	9892	9.80	2.78
WG253	1306+06.00	-9459	28046	-10857	161	2052	10247	8.66	2.54
WG254	1306+18.00	-8995	21551	-10197	161	2833	10872	7.44	1.72
WG255	1306+18.00	-9545	22196	-10856	161	702	10770	8.15	2.00
WG256	1306+30.00	-9033	21595	-10726	161	678	10932	10.54	1.91
WG257	1306+30.00	-8916	21457	-10203	188	2267	11267	6.84	1.70
WG258	1306+42.00	-8288	24774	-9525	188	2991	12126	6.57	1.80
WG259	1306+42.00	-8842	25428	-10191	188	966	12011	7.18	2.04
WG260	1306+54.00	-8174	24640	-9758	188	576	12532	8.43	1.92
WG261	1306+54.00	-8189	24658	-9451	243	2651	12920	5.19	1.70
WG262	1306+66.00	-7558	28665	-8772	243	3306	14231	4.99	1.78
WG263	1306+66.00	-8122	29333	-9456	243	1188	14107	5.49	1.99
WG264	1306+78.00	-7656	28780	-9065	243	1558	14795	5.79	1.84
WG265	1306+78.00	-7545	28649	-8849	314	3112	15502	4.15	1.65
WG266	1306+90.00	-6947	31189	-8167	314	3704	17255	3.88	1.59
WG267	1306+90.00	-7465	31774	-8802	314	1620	17026	4.26	1.77
WG268	1307+02.00	-6886	31120	-8102	314	2048	18103	3.88	1.61
WG269	1307+02.00	-6847	31077	-8158	400	3367	18901	3.27	1.47
WG270	1307+14.00	-6200	30911	-7394	400	2681	20720	2.98	1.36
WG271	1307+14.00	-6298	31025	-7535	399	1391	20537	3.10	1.44
WG272	1307+26.00	-5480	30069	-6574	399	1689	21468	2.74	1.32
WG273	1307+26.00	-6299	31027	-7600	498	3422	22190	2.61	1.24
WG274	1307+38.00	-5620	32289	-6850	498	2634	23656	2.47	1.25
WG275	1307+38.00	-5700	32370	-6972	496	1508	23375	2.57	1.32
WG276	1307+50.00	-5180	31847	-6347	496	2251	23917	2.36	1.24
WG277	1307+50.00	-5617	32286	-6954	594	3181	24459	2.25	1.19
WG278	1307+62.00	-5625	32295	-6949	594	2899	25099	2.23	1.17
WG279	1307+62.00	-4940	31607	-6207	592	1761	24799	2.14	1.20
WG280	1307+74.00	-4964	31631	-6202	592	3356	24429	2.09	1.16
WG281	1307+74.00	-5160	32500	-6223	668	3340	24760	**1.59**	**1.18**
WG282	1307+86.00	-4862	31528	-6226	667	2756	24153	2.04	1.19
WG283	1307+86.00	-4163	30827	-5470	666	1656	23861	1.96	1.22
WG284	1307+98.00	-4161	30824	-5494	666	2866	22198	2.00	1.26
WG285	1307+98.00	-4130	30793	-5517	699	2840	22266	1.98	1.26
WG286	1308+10.00	-4039	30702	-5550	699	2009	20055	2.16	1.43
WG287	1308+10.00	-3253	29895	-4698	699	1049	19779	2.07	1.46
WG288	1308+22.00	-3170	29798	-4770	698	2040	16599	2.29	1.67
WG289	1308+22.00	-3198	29830	-4788	675	2066	16348	2.36	1.70
WG290	1308+34.00	-2939	29526	-4864	675	1852	12668	2.85	2.18
WG291	1308+34.00	-2169	28621	-3886	676	3995	12201	2.54	2.02
WG291	1308+39.58	-1999	28422	-3922	676	4110	10495	2.84	2.32
WG292	1308+39.58	-1221	27507	-3006	606	2673	9960	2.95	2.49
WG292	1308+45.17	-1024	27275	-3041	606	3444	8296	3.33	2.87
WG293	1308+45.17	-940	27177	-3051	607	3494	7849	3.48	3.02
WG293	1308+50.75	-647	26832	-3086	607	4304	6341	4.02	3.55
WG294	1308+50.75	10	26060	-2190	497	2285	5910	4.43	4.02
WG294	1308+56.33	253	25775	-2225	497	2683	5045	4.99	4.58
WG295	1308+56.33	438	25558	-2228	499	2705	4631	5.34	4.93
WG295	1308+61.92	427	25570	-2264	499	1997	4736	5.39	4.98
WG296	1308+61.92	-86	26173	-1181	362	-440	9728	3.03	2.74

B.3 Extracted live and Dead Load Forces with the Calculated Rating Factors for Strength I Operating Limit State

Table B.3. Rating Factors for Strength I-Flexural Operating

Member Number	Station (feet)	Axial Capacity	Moment Capacity	Factored Axial Dead load	Factored Axial Live Load	Factored Dead Load Moment	Factored Live Load Moment	Rating Factor inv Axial	Rating Factor inv moment
WG003	1291+38.08	-128	26223	-1314	178	-741	5930	6.67	4.55
WG004	1291+38.08	830	25100	-1308	265	-738	4663	8.06	5.54
WG004	1291+43.67	1083	24805	-1272	265	-1323	4159	8.88	6.28
WG005	1291+43.67	342	25671	-2240	266	800	3538	9.71	7.03
WG005	1291+49.25	310	25708	-2204	266	1096	3389	9.47	7.26
WG006	1291+49.25	876	25046	-2213	334	1079	3161	9.26	7.58
WG006	1291+54.83	492	25495	-2178	334	567	3689	8.00	6.76
WG007	1291+54.83	-587	26762	-3227	334	2744	3684	7.90	6.52
WG007	1291+60.42	-870	27094	-3191	334	1975	4320	6.95	5.81
WG008	1291+60.42	-657	26845	-3183	384	1982	4312	6.58	5.77
WG008	1291+66.00	-932	27168	-3148	384	1210	5177	5.77	5.01
WG009	1291+66.00	-1651	28012	-3940	384	1872	5206	5.96	5.02
WG010	1291+78.00	-2051	28483	-3864	384	-263	7805	4.72	3.68
WG011	1291+78.00	-2784	29344	-4855	417	-834	7846	4.97	3.85
WG012	1291+90.00	-3015	29615	-4783	417	-2387	10490	4.24	3.05
WG013	1291+90.00	-2992	29588	-4780	424	-2398	10351	4.21	3.09
WG014	1292+02.00	-3136	29757	-4747	424	-3043	12380	3.80	2.65
WG015	1292+02.00	-3987	30650	-5670	421	-721	11398	4.00	2.75
WG016	1292+14.00	-4069	30732	-5647	421	-1965	13314	3.74	2.46
WG017	1292+14.00	-4041	30704	-5639	427	-2105	13171	3.74	2.49
WG018	1292+26.00	-4098	30761	-5636	427	-2572	14319	3.60	2.33
WG019	1292+26.00	-4889	31555	-6425	398	-235	13176	3.86	2.41
WG020	1292+38.00	-4918	31584	-6430	398	-1649	14428	3.80	2.30
WG021	1292+38.00	-4904	31571	-6433	403	-1619	14229	3.79	2.33
WG022	1292+50.00	-4916	31582	-6437	403	-1943	14622	3.77	2.29
WG023	1292+50.00	-5127	31794	-6551	353	-1322	13828	4.04	2.39
WG024	1292+62.00	-5677	32346	-7176	353	-2073	14334	4.25	2.40
WG025	1292+62.00	-6261	32933	-7843	357	-1029	13861	4.42	2.45
WG026	1292+74.00	-6964	31806	-8593	358	220	13262	4.56	2.38
WG027	1292+74.00	-5439	30020	-6752	297	-1978	13188	4.42	2.43
WG028	1292+86.00	-6274	30997	-7713	297	-2101	13149	4.84	2.52
WG029	1292+86.00	-6862	31686	-8383	301	-774	12624	5.05	2.57
WG030	1292+98.00	-7524	31842	-9147	301	483	11701	5.39	2.68
WG031	1292+98.00	-6341	30514	-7684	241	-1241	11493	5.57	2.76
WG032	1293+10.00	-6923	31162	-8384	241	-2977	11735	6.06	2.91
WG033	1293+10.00	-7463	31772	-8998	244	-1467	11188	6.28	2.97
WG034	1293+22.00	-8111	29320	-9680	245	784	9879	6.42	2.89
WG035	1293+22.00	-7203	28244	-8702	190	-231	9510	7.88	2.99
WG036	1293+34.00	-7663	28790	-9093	190	-2323	9900	7.51	3.14
WG037	1293+34.00	-8169	29389	-9662	193	-442	9267	7.74	3.22
WG038	1293+46.00	-8857	25446	-10341	193	1869	8209	7.69	2.87
WG039	1293+46.00	-7804	24205	-9436	145	698	7824	11.22	3.00
WG040	1293+58.00	-8463	24981	-9868	145	-922	8199	9.66	3.16
WG041	1293+58.00	-8893	25488	-10347	148	1040	7561	9.82	3.23
WG042	1293+70.00	-9581	22239	-11024	148	3144	7124	9.74	2.68
WG043	1293+70.00	-8714	21221	-10379	108	2352	6637	15.42	2.84
WG044	1293+82.00	-9206	21798	-10508	108	-94	7019	12.05	3.12
WG045	1293+82.00	-9580	22237	-10913	110	1891	6656	12.12	3.06
WG079	1295+72.00	-10339	29421	-12228	94	-661	3782	20.11	7.95
WG080	1295+84.00	-10410	29508	-12228	94	-2311	4656	19.36	6.83

WG081	1295+84.00	-10161	29199	-11963	97	-2017	4589	18.65	6.80
WG082	1295+96.00	-10233	29289	-11963	97	-1083	4928	17.90	6.16
WG083	1295+96.00	-10226	29280	-11972	98	-495	4669	17.87	6.38
WG084	1296+08.00	-10246	29305	-11972	98	-1775	5208	17.66	5.97
WG085	1296+08.00	-9904	28830	-11632	106	-1180	5138	16.26	5.84
WG086	1296+20.00	-9960	28929	-11632	106	-421	5466	15.74	5.37
WG087	1296+20.00	-9940	28895	-11626	108	-102	5301	15.63	5.47
WG088	1296+32.00	-9950	28912	-11626	108	-948	5656	15.54	5.28
WG089	1296+32.00	-9595	28286	-11284	121	-59	5574	14.00	5.09
WG090	1296+44.00	-9647	28377	-11284	121	375	6025	13.58	4.65
WG091	1296+44.00	-9625	28338	-11279	122	378	5913	13.51	4.73
WG092	1296+56.00	-9621	28331	-11279	122	-518	6133	13.54	4.70
WG093	1296+56.00	-9204	27595	-10868	139	249	6168	12.01	4.43
WG094	1296+68.00	-9243	27664	-10868	139	396	6556	11.73	4.16
WG095	1296+68.00	-9219	27621	-10864	141	90	6503	11.70	4.23
WG096	1296+80.00	-9216	27616	-10864	141	-615	6749	11.72	4.18
WG097	1296+80.00	-8703	26711	-10344	162	114	6841	10.11	3.89
WG098	1296+92.00	-8740	26776	-10344	162	227	7248	9.89	3.66
WG099	1296+92.00	-8718	26737	-10340	164	79	7150	9.88	3.73
WG100	1297+04.00	-8710	26723	-10340	164	-511	7329	9.93	3.72
WG101	1297+04.00	-8432	26232	-10079	191	859	7258	8.61	3.50
WG102	1297+16.00	-8462	26286	-10079	191	894	7630	8.45	3.33
WG103	1297+16.00	-8438	26244	-10074	192	831	7464	8.53	3.40
WG104	1297+28.00	-7546	21541	-9389	192	392	7653	9.61	2.76
WG105	1297+28.00	-8047	22105	-9621	221	752	7921	7.13	2.70
WG106	1297+40.00	-7961	22009	-9450	221	2779	7797	6.75	2.47
WG107	1297+40.00	-8089	22152	-9642	221	1548	7921	7.02	2.60
WG108	1297+52.00	-6762	26455	-8628	221	997	8195	8.44	3.11
WG109	1297+52.00	-7179	26949	-8808	252	1526	8502	6.46	2.99
WG110	1297+64.00	-7095	26849	-8632	252	3121	8567	6.09	2.77
WG111	1297+64.00	-6584	26245	-8121	253	142	9214	6.09	2.83
WG112	1297+76.00	-5378	30768	-7047	253	2094	8883	6.61	3.23
WG113	1297+76.00	-6482	32082	-8214	283	2909	9145	6.11	3.19
WG114	1297+88.00	-6509	32114	-8149	284	4670	9235	5.79	2.97
WG115	1297+88.00	-5973	31475	-7594	284	2503	9653	5.71	3.00
WG116	1298+00.00	-4606	35556	-6163	284	4567	9366	5.48	3.31
WG117	1298+00.00	-6075	37193	-7902	314	5728	9560	5.82	3.29
WG118	1298+12.00	-6065	37181	-7766	314	7513	9975	5.41	2.97
WG119	1298+12.00	-5583	36633	-7289	314	5603	10040	5.43	3.09
WG120	1298+24.00	-3971	40228	-5570	314	7189	9943	5.09	3.32
WG121	1298+24.00	-5140	41714	-6994	343	7000	10521	5.41	3.30
WG122	1298+36.00	-5058	41610	-6778	343	8672	10928	5.02	3.01
WG123	1298+36.00	-4473	40865	-6168	343	7060	10994	4.95	3.07
WG124	1298+48.00	-3132	45133	-4789	343	7794	11146	4.84	3.35
WG125	1298+48.00	-3809	45957	-5643	369	7150	11848	4.97	3.28
WG126	1298+60.00	-3761	45898	-5495	369	8542	12070	4.70	3.09
WG127	1298+60.00	-3128	45129	-4813	369	7267	12207	4.57	3.10
WG128	1298+72.00	-2167	50721	-3904	369	8208	12256	4.71	3.47
WG129	1298+72.00	-2863	51520	-4752	391	8332	12759	4.83	3.38
WG130	1298+84.00	-2909	51573	-4725	391	9540	12953	4.65	3.25
WG131	1298+84.00	-2331	50909	-4110	391	8364	13055	4.55	3.26
WG132	1298+96.00	-1351	55676	-3165	391	9059	13063	4.64	3.57
WG133	1298+96.00	-2062	56496	-4015	407	8769	13646	4.80	3.50
WG134	1299+08.00	-2034	56465	-3929	407	9833	13682	4.66	3.41
WG135	1299+08.00	-1367	55697	-3224	407	7943	13989	4.57	3.41
WG136	1299+20.00	-1297	55608	-3142	407	8317	13888	4.54	3.41
WG137	1299+20.00	-1360	55688	-3203	415	8667	14282	4.44	3.29
WG138	1299+32.00	-1307	55622	-3134	415	8452	14481	4.40	3.26
WG139	1299+32.00	-476	54580	-2217	415	7766	14446	4.20	3.24
WG140	1299+44.00	-432	54525	-2190	415	8020	14190	4.24	3.28
WG141	1299+44.00	-500	54611	-2221	413	8116	14598	4.17	3.19
WG142	1299+56.00	-479	54584	-2219	413	7670	14646	4.21	3.20
WG143	1299+56.00	707	53100	-886	412	7356	14506	3.86	3.15
WG144	1299+68.00	736	53063	-884	412	8241	13915	3.93	3.22
WG145	1299+68.00	603	53230	-914	398	9220	14112	3.81	3.12
WG146	1299+80.00	617	53212	-914	398	9205	14010	3.85	3.14
WG147	1299+80.00	1725	51825	346	397	9824	13603	3.47	3.09
WG148	1299+92.00	1715	51837	346	397	12406	12592	3.45	3.13
WG149	1299+92.00	1488	52122	249	378	13119	12939	3.27	3.01
WG149	1300+00.00	1479	52132	249	378	13277	12994	3.25	2.99
WG150	1300+00.00	1468	52146	240	381	13861	12933	3.22	2.96

WG150	1300+08.00	1466	52149	239	381	13532	13055	3.22	2.96
WG151	1300+08.00	1401	52231	265	342	12745	12454	3.32	3.17
WG152	1300+20.00	1334	52315	262	342	12149	13441	3.13	2.99
WG153	1300+20.00	1394	52239	270	343	9501	13949	3.28	3.06
WG154	1300+32.00	1370	52269	267	343	7377	15111	3.22	2.97
WG155	1300+32.00	213	53718	-995	323	8839	13981	3.74	3.21
WG156	1300+44.00	148	53799	-1001	323	8680	14796	3.56	3.05
WG157	1300+44.00	207	53725	-968	324	7471	14889	3.63	3.11
WG158	1300+56.00	176	53765	-974	323	6380	15684	3.55	3.02
WG159	1300+56.00	-950	55175	-2235	314	8313	14444	4.09	3.24
WG160	1300+68.00	-1002	55240	-2240	314	8528	14953	3.94	3.12
WG161	1300+68.00	-981	55214	-2239	315	8298	14770	4.00	3.18
WG162	1300+80.00	-1000	55237	-2245	315	7676	15178	3.96	3.13
WG163	1300+80.00	-1752	56158	-3109	310	9045	14077	4.37	3.35
WG164	1300+92.00	-1793	56204	-3125	310	9135	14347	4.29	3.28
WG165	1300+92.00	-1739	56144	-3089	311	8627	14267	4.34	3.33
WG166	1301+04.00	-1836	56250	-3228	311	5956	14966	4.48	3.36
WG167	1301+04.00	-2370	56832	-3851	310	8733	13435	4.78	3.58
WG168	1301+16.00	-3296	52012	-4729	310	9735	13206	4.62	3.20
WG169	1301+16.00	-2537	51146	-3904	310	8216	13416	4.40	3.20
WG170	1301+28.00	-2664	51292	-4105	310	5086	14010	4.64	3.30
WG171	1301+28.00	-3124	51820	-4666	312	7324	12590	4.95	3.53
WG172	1301+40.00	-4094	46303	-5578	312	8081	12292	4.76	3.11
WG173	1301+40.00	-3322	45365	-4745	312	5942	12693	4.56	3.11
WG174	1301+52.00	-3338	45384	-4833	312	3056	13098	4.80	3.23
WG175	1301+52.00	-3826	45976	-5438	315	5545	11615	5.13	3.48
WG176	1301+64.00	-5284	41897	-6918	315	6549	11231	5.20	3.15
WG177	1301+64.00	-4524	40930	-6105	315	3937	11773	5.02	3.14
WG178	1301+76.00	-4473	40865	-6128	315	1062	12122	5.26	3.28
WG179	1301+76.00	-4489	40885	-6200	318	4363	10404	5.37	3.51
WG180	1301+88.00	-6178	37314	-7929	318	5421	10047	5.50	3.17
WG181	1301+88.00	-5366	36393	-7063	318	2558	10697	5.33	3.16
WG182	1302+00.00	-5446	36481	-7240	319	-663	11245	5.63	3.30
WG183	1302+00.00	-5019	36011	-6826	322	1700	9842	5.61	3.49
WG184	1302+12.00	-6343	31917	-8103	322	2763	9565	5.46	3.05
WG185	1302+12.00	-6354	31929	-8174	322	802	9975	5.64	3.12
WG186	1302+24.00	-6512	32118	-8399	322	35	9913	5.85	3.24
WG187	1302+24.00	-5712	31165	-7749	325	79	9241	6.26	3.36
WG188	1302+36.00	-7028	26770	-8818	326	1136	8999	5.50	2.85
WG189	1302+36.00	-7016	26757	-8852	326	-82	9213	5.63	2.91
WG190	1302+48.00	-7095	26850	-8977	326	-531	9088	5.77	3.01
WG191	1302+48.00	-6451	26088	-8689	328	195	8267	6.82	3.13
WG192	1302+60.00	-8005	22058	-9835	328	1455	8028	5.58	2.57
WG193	1302+60.00	-7943	21988	-9807	329	556	8159	5.67	2.63
WG194	1302+72.00	-7990	22041	-9879	329	477	7991	5.75	2.70
WG195	1302+72.00	-7254	21213	-9468	330	1102	7262	6.71	2.77
WG196	1302+84.00	-8189	25804	-10239	330	2602	7204	6.21	3.22
WG197	1302+84.00	-8016	25499	-10097	331	1897	7079	6.29	3.33
WG198	1302+96.00	-8047	25554	-10097	331	2691	7027	6.20	3.25
WG199	1302+96.00	-7655	24862	-9810	332	1415	6553	6.49	3.58
WG200	1303+08.00	-7677	24901	-9810	332	1095	6768	6.42	3.52
WG201	1303+08.00	-8119	25681	-10364	333	1131	6693	6.75	3.67
WG202	1303+20.00	-8127	25696	-10364	333	1785	6555	6.72	3.65
WG203	1303+20.00	-8017	25501	-10378	334	1428	6117	7.07	3.94
WG204	1303+32.00	-7990	25453	-10378	334	181	6313	7.15	4.00
WG205	1303+32.00	-8418	26208	-10858	335	1383	6180	7.29	4.02
WG206	1303+44.00	-8401	26178	-10858	335	1910	5963	7.34	4.07
WG207	1303+44.00	-8277	25960	-10873	337	1382	5595	7.71	4.39
WG208	1303+56.00	-8232	25880	-10873	337	154	5687	7.84	4.52
WG209	1303+56.00	-8630	26582	-11298	338	1493	5619	7.90	4.46
WG210	1303+68.00	-8574	26483	-11298	338	1842	5325	8.07	4.63
WG211	1303+68.00	-8430	26230	-11303	340	1216	5029	8.45	4.97
WG212	1303+80.00	-8345	26080	-11303	340	-61	5012	8.70	5.22
WG213	1303+80.00	-8735	26768	-11683	341	1725	4947	8.65	5.06
WG214	1303+92.00	-8626	26576	-11683	341	2089	4557	8.97	5.37
WG215	1303+92.00	-8470	26299	-11694	344	1479	4317	9.37	5.75
WG216	1304+04.00	-8395	26167	-11694	344	912	4239	9.59	5.96
WG217	1304+10.00	-8785	26857	-12052	345	2892	4169	9.47	5.75
WG218	1304+16.00	-8575	26486	-12052	345	3003	3710	10.08	6.33
WG219	1304+16.00	-8379	26140	-12059	349	2071	3552	10.56	6.78
WG220	1304+28.00	-8156	25745	-12059	349	1389	3291	11.20	7.40

WG239	1305+22.00	-10377	29468	-12193	91	4	4066	19.87	7.25
WG240	1305+34.00	-10438	29544	-12193	91	-1128	4783	19.21	6.41
WG241	1305+34.00	-10238	29295	-11945	90	-843	4726	19.02	6.38
WG242	1305+46.00	-10300	29372	-11945	90	223	4986	18.34	5.85
WG243	1305+46.00	-10336	29417	-11984	89	652	4901	18.56	5.87
WG244	1305+58.00	-10341	29423	-11984	89	-676	5275	18.51	5.71
WG245	1305+58.00	-10063	29079	-11645	88	-42	5190	17.94	5.61
WG246	1305+70.00	-10106	29131	-11645	88	646	5524	17.45	5.16
WG247	1305+70.00	-10111	29138	-11653	87	784	5428	17.72	5.22
WG248	1305+82.00	-10109	29135	-11653	87	249	5516	17.75	5.24
WG249	1305+82.00	-9781	28613	-11258	88	821	5600	16.79	4.96
WG250	1305+94.00	-9815	28673	-11258	88	1505	5945	16.41	4.57
WG251	1305+94.00	-9823	28688	-11269	87	1701	5840	16.64	4.62
WG252	1306+06.00	-9814	28671	-11269	87	1179	5819	16.75	4.72
WG253	1306+06.00	-9459	28046	-10857	94	2052	6031	14.93	4.31
WG254	1306+18.00	-8995	21551	-10197	94	2833	6409	12.83	2.92
WG255	1306+18.00	-9545	22196	-10856	93	702	6380	14.10	3.37
WG256	1306+30.00	-9033	21595	-10726	93	678	6513	18.22	3.21
WG257	1306+30.00	-8916	21457	-10203	106	2267	6649	12.14	2.89
WG258	1306+42.00	-8288	24774	-9525	106	2991	7154	11.67	3.05
WG259	1306+42.00	-8842	25428	-10191	105	966	7120	12.80	3.44
WG260	1306+54.00	-8174	24640	-9758	105	576	7481	15.03	3.22
WG261	1306+54.00	-8189	24658	-9451	136	2651	7602	9.31	2.89
WG262	1306+66.00	-7558	28665	-8772	136	3306	8341	8.95	3.04
WG263	1306+66.00	-8122	29333	-9456	135	1188	8307	9.85	3.39
WG264	1306+78.00	-7656	28780	-9065	136	1558	8643	10.40	3.15
WG265	1306+78.00	-7545	28649	-8849	176	3112	9036	7.39	2.83
WG266	1306+90.00	-6947	31189	-8167	176	3704	9996	6.92	2.75
WG267	1306+90.00	-7465	31774	-8802	176	1620	9869	7.61	3.06
WG268	1307+02.00	-6886	31120	-8102	176	2048	10430	6.92	2.79
WG269	1307+02.00	-6847	31077	-8158	226	3367	10886	5.81	2.55
WG270	1307+14.00	-6200	30911	-7394	226	2681	11863	5.29	2.38
WG271	1307+14.00	-6298	31025	-7535	224	1391	11796	5.51	2.51
WG272	1307+26.00	-5480	30069	-6574	224	1689	12227	4.87	2.32
WG273	1307+26.00	-6299	31027	-7600	280	3422	12642	4.64	2.18
WG274	1307+38.00	-5620	32289	-6850	280	2634	13397	4.39	2.21
WG275	1307+38.00	-5700	32370	-6972	278	1508	13249	4.57	2.33
WG276	1307+50.00	-5180	31847	-6347	278	2251	13473	4.20	2.20
WG277	1307+50.00	-5617	32286	-6954	331	3181	13792	4.04	2.11
WG278	1307+62.00	-5625	32295	-6949	331	2899	14060	4.00	2.09
WG279	1307+62.00	-4940	31607	-6207	328	1761	13909	3.86	2.15
WG280	1307+74.00	-4964	31631	-6202	328	3356	13603	3.77	2.08
WG281	1307+74.00	-5160	32500	-6223	367	3340	13807	**2.89**	**2.11**
WG282	1307+86.00	-4862	31528	-6226	367	2756	13357	3.72	2.15
WG283	1307+86.00	-4163	30827	-5470	364	1656	13217	3.59	2.21
WG284	1307+98.00	-4161	30824	-5494	364	2866	12170	3.67	2.30
WG285	1307+98.00	-4130	30793	-5517	377	2840	12231	3.68	2.29
WG286	1308+10.00	-4039	30702	-5550	377	2009	10860	4.01	2.64
WG287	1308+10.00	-3253	29895	-4698	373	1049	10741	3.87	2.69
WG288	1308+22.00	-3170	29798	-4770	373	2040	8823	4.29	3.15
WG289	1308+22.00	-3198	29830	-4788	353	2066	8718	4.50	3.18
WG290	1308+34.00	-2939	29526	-4864	353	1852	6588	5.45	4.20
WG291	1308+34.00	-2169	28621	-3886	354	3995	6371	4.85	3.86
WG291	1308+39.58	-1999	28422	-3922	354	4110	5505	5.43	4.42
WG292	1308+39.58	-1221	27507	-3006	313	2673	5244	5.70	4.74
WG292	1308+45.17	-1024	27275	-3041	313	3444	4478	6.44	5.32
WG293	1308+45.17	-940	27177	-3051	314	3494	4225	6.72	5.61
WG293	1308+50.75	-647	26832	-3086	314	4304	3602	7.77	6.25
WG294	1308+50.75	10	26060	-2190	256	2285	3391	8.59	7.01
WG294	1308+56.33	253	25775	-2225	256	2683	3181	9.68	7.26
WG295	1308+56.33	438	25558	-2228	257	2705	3018	10.37	7.57
WG295	1308+61.92	427	25570	-2264	257	1997	3394	10.46	6.94
WG296	1308+61.92	-86	26173	-1181	194	-440	6508	5.66	4.09

B.4 Extracted live and Dead Load Shear Forces with the Calculated Rating Factors for Strength I Inventory and Operating

Table B.4. Rating Factors for Strength I-Shear Inventory and Operating

Member Number	Station (feet)	Facored Dead Load Shear (VDL) (kips)	Factored Live Load Shear (VLL) (kips)	Shear Capacity (φVn)	Strength I Shear Inventory Rating Factor	Facored Dead Load Shear (VDL) (kips)	Factored Live Load Shear (VLL) (kips)	Shear Capacity (φVn)	Strength I Shear Operating Rating Factor
WG003	1291+38.08	19.7	1887.0	2241.5	NaN	-19.7	1887.0	2265.9	
WG004	1291+38.08	45.6	317.8	2567.9	7.9	68.3	163.0	2270.1	13.5
WG004	1291+43.67	149.9	163.0	2261.1	13.0	149.9	163.0	2270.1	13.0
WG005	1291+43.67	92.0	401.4	2476.5	5.9	92.0	401.4	2356.3	5.6
WG005	1291+49.25	14.2	401.4	2476.5	6.1	14.2	401.4	2356.3	5.8
WG006	1291+49.25	325.4	155.7	2263.9	12.5	325.4	155.7	2269.9	12.5
WG006	1291+54.83	350.3	155.7	2263.8	12.3	350.3	155.7	2269.9	12.3
WG007	1291+54.83	76.7	373.9	2475.6	6.4	108.8	172.1	2299.0	12.7
WG007	1291+60.42	188.5	172.1	2264.2	12.1	188.5	172.1	2299.0	12.3
WG008	1291+60.42	517.7	90.1	2313.0	19.9	517.7	90.1	2442.4	21.4
WG008	1291+66.00	540.2	90.1	2313.0	19.7	540.2	90.1	2442.4	21.1
WG009	1291+66.00	337.5	107.0	2366.5	19.0	337.5	107.0	2567.9	20.8
WG010	1291+78.00	422.6	107.0	1779.2	12.68	422.6	107.0	1945.8	14.24
WG011	1291+78.00	36.3	-316.6	1672.4	5.17	36.3	-316.6	1770.8	5.48
WG012	1291+90.00	214.1	103.8	1284.4	10.31	214.1	103.8	1945.8	16.68
WG013	1291+90.00	318.8	141.1	1246.2	6.57	318.8	141.1	1863.5	10.95
WG014	1292+02.00	345.6	141.2	1270.1	6.55	345.6	141.2	1875.1	10.83
WG015	1292+02.00	13.5	-286.3	1679.0	5.82	13.5	-286.3	1789.6	6.20
WG016	1292+14.00	182.0	155.5	1265.1	6.97	182.0	155.5	1866.3	10.83
WG017	1292+14.00	420.7	193.1	1237.8	4.23	420.7	193.1	1847.9	7.39
WG018	1292+26.00	434.1	193.6	1260.3	4.27	434.1	193.6	1858.8	7.36
WG019	1292+26.00	19.3	-268.1	1697.7	6.26	29.6	198.5	1847.4	9.16
WG020	1292+38.00	190.0	198.9	1262.4	5.39	190.0	198.9	1858.4	8.39
WG021	1292+38.00	249.9	238.0	1239.4	4.16	249.9	238.0	1844.9	6.70
WG022	1292+50.00	263.3	239.0	1262.1	4.18	263.3	239.0	1856.0	6.66
WG023	1292+50.00	85.8	222.3	1244.4	5.21	85.8	222.3	1847.9	7.93
WG024	1292+62.00	245.2	223.0	1254.0	4.52	245.2	223.0	1846.3	7.18
WG025	1292+62.00	-141.2	-219.6	1741.6	7.29	-141.2	-219.6	1847.5	7.77
WG026	1292+74.00	-61.6	-217.0	1725.7	7.67	-61.6	-217.0	1833.4	8.16
WG027	1292+74.00	110.4	226.9	1248.3	5.01	110.4	226.9	1850.3	7.67
WG028	1292+86.00	270.7	227.6	1255.8	4.33	270.7	227.6	1845.8	6.92
WG029	1292+86.00	-128.6	-214.5	1761.8	7.61	-128.6	-214.5	1861.8	8.08
WG030	1292+98.00	-40.9	-211.9	1743.2	8.03	-40.9	-211.9	1844.8	8.51
WG031	1292+98.00	115.8	217.4	1743.6	7.49	115.8	217.4	1846.7	7.96
WG032	1293+10.00	67.7	218.0	1751.8	7.73	67.7	218.0	1842.0	8.14
WG033	1293+10.00	-360.0	-207.3	1767.7	6.79	-360.0	-207.3	1864.5	7.26
WG034	1293+22.00	-449.1	-204.6	1769.5	6.45	-449.1	-204.6	1867.2	6.93
WG035	1293+22.00	114.5	201.0	1758.6	8.18	114.5	201.0	1865.3	8.71
WG036	1293+34.00	101.8	201.5	1798.6	8.42	101.8	201.5	1945.8	9.15
WG037	1293+34.00	-337.6	-195.1	1755.0	7.26	-337.6	-195.1	1853.1	7.77
WG038	1293+46.00	-458.2	-192.3	1747.9	6.71	-458.2	-192.3	1847.1	7.22
WG039	1293+46.00	117.1	184.7	1810.4	9.17	117.1	184.7	1945.8	9.90
WG040	1293+58.00	131.3	185.1	1809.7	9.07	131.3	185.1	1945.8	9.80
WG041	1293+58.00	-276.9	-181.3	1765.8	8.21	-276.9	-181.3	1865.6	8.76
WG042	1293+70.00	-430.3	-178.3	1771.0	7.52	-430.3	-178.3	1871.3	8.08
WG043	1293+70.00	156.1	179.2	1758.1	8.94	156.1	179.2	1859.1	9.50
WG044	1293+82.00	182.6	179.3	1789.5	8.96	182.6	179.3	1945.8	9.83
WG045	1293+82.00	-207.3	-174.5	1760.5	8.90	-207.3	-174.5	1859.9	9.47
WG046	1293+94.00	-391.8	-171.9	1750.1	7.90	-391.8	-171.9	1850.5	8.49
WG047	1293+94.00	209.4	189.1	1188.4	5.18	209.4	189.1	1804.5	8.44
WG048	1294+06.00	302.1	188.9	1213.9	4.83	302.1	188.9	1816.6	8.02
WG049	1294+06.00	-7.1	232.2	1697.5	7.28	-7.1	232.2	1812.4	7.77
WG050	1294+18.00	65.8	232.8	1218.1	4.95	65.8	232.8	1820.8	7.54

WG051	1294+18.00	188.2	208.3	1702.1	7.27	188.2	208.3	1816.3	7.82
WG052	1294+30.00	267.1	208.2	1727.8	7.02	267.1	208.2	1828.3	7.50
WG053	1294+30.00	3.8	255.0	1710.6	6.69	3.8	255.0	1823.1	7.13
WG054	1294+42.00	81.7	255.9	1737.5	6.47	81.7	255.9	1835.8	6.85
WG055	1294+42.00	270.5	226.2	1730.6	6.45	270.5	226.2	1838.6	6.93
WG056	1294+54.00	323.0	226.1	1758.5	6.35	323.0	226.1	1851.3	6.76
WG057	1294+54.00	78.6	276.1	1761.7	6.10	78.6	276.1	1860.5	6.45
WG058	1294+66.00	158.6	277.3	1790.6	5.89	158.6	277.3	1873.5	6.18
WG059	1294+66.00	267.2	255.4	1815.1	6.06	267.2	255.4	1945.8	6.57
WG060	1294+78.00	309.3	255.7	1838.0	5.98	309.3	255.7	1945.8	6.40
WG061	1294+78.00	-16.5	307.7	1682.8	5.42	-16.5	307.7	1780.0	5.73
WG062	1294+90.00	67.8	309.6	1780.0	5.53	67.8	309.6	1780.0	5.53
WG063	1294+90.00	310.3	265.1	1658.6	5.09	310.3	265.1	1780.0	5.54
WG064	1295+02.00	325.6	273.9	2581.8	8.24	325.6	273.9	2581.8	8.24
WG065	1295+02.00	-31.9	378.2	2581.8	6.74	-31.9	378.2	2581.8	6.74
WG066	1295+14.00	135.5	386.8	3383.7		135.5	386.8	3383.7	
WG068	1295+14.00	211.5	507.8	1612.3		211.5	507.8	1708.9	
WG069	1295+25.00	365.9	512.6	1624.9		365.9	512.6	1780.0	
WG070	1295+25.00	-337.1	-469.4	1676.3		-337.1	-469.4	1780.0	
WG071	1295+36.00	-182.6	-465.7	1673.5		-182.6	-465.7	1780.0	
WG073	1295+36.00	-99.2	-381.4	3383.7		-99.2	-381.4	3383.7	
WG074	1295+48.00	38.1	-374.0	2581.8	6.80	38.1	-374.0	2581.8	6.80
WG075	1295+48.00	138.9	186.5	2331.1	11.75	138.9	186.5	2412.2	12.19
WG076	1295+60.00	289.2	206.8	1467.1	5.70	289.2	206.8	1494.3	5.83
WG077	1295+60.00	-92.6	-259.2	1780.0	6.51	-92.6	-259.2	1780.0	6.51
WG078	1295+72.00	-4.6	-255.2	1780.0	6.96	-4.6	-255.2	1780.0	6.96
WG079	1295+72.00	114.2	186.3	1638.8	8.18	114.2	186.3	1714.7	8.59
WG080	1295+84.00	244.4	186.3	1640.6	7.49	244.4	186.3	1731.1	7.98
WG081	1295+84.00	-200.8	-257.7	1805.4	6.23	-200.8	-257.7	1945.8	6.77
WG082	1295+96.00	-118.0	-254.1	1803.4	6.63	-118.0	-254.1	1945.8	7.19
WG083	1295+96.00	105.1	228.0	1670.8	6.87	105.1	228.0	1776.1	7.33
WG084	1296+08.00	210.5	228.2	1695.8	6.51	210.5	228.2	1788.5	6.91
WG085	1296+08.00	-173.1	-247.3	1749.7	6.38	-173.1	-247.3	1852.9	6.79
WG086	1296+20.00	-93.9	-243.7	1747.0	6.78	-93.9	-243.7	1851.5	7.21
WG087	1296+20.00	95.7	242.2	1700.6	6.63	95.7	242.2	1800.1	7.04
WG088	1296+32.00	174.9	242.5	1723.7	6.39	174.9	242.5	1811.4	6.75
WG089	1296+32.00	-125.6	-234.7	1729.4	6.83	-125.6	-234.7	1837.2	7.29
WG090	1296+44.00	-46.4	-231.1	1726.6	7.27	-46.4	-231.1	1835.7	7.74
WG091	1296+44.00	132.8	255.3	1713.2	6.19	132.8	255.3	1810.4	6.57
WG092	1296+56.00	199.5	255.7	1736.1	6.01	199.5	255.7	1821.6	6.34
WG093	1296+56.00	-88.4	-227.6	1721.9	7.18	-88.4	-227.6	1830.6	7.65
WG094	1296+68.00	-10.5	-224.1	1715.6	7.61	-10.5	-224.1	1825.6	8.10
WG095	1296+68.00	164.6	264.3	1722.1	5.89	164.6	264.3	1817.1	6.25
WG096	1296+80.00	218.1	264.8	1747.0	5.77	218.1	264.8	1830.1	6.09
WG097	1296+80.00	-103.6	-223.2	1719.4	7.24	-103.6	-223.2	1828.3	7.73
WG098	1296+92.00	-23.9	-221.2	1716.4	7.65	-23.9	-221.2	1825.4	8.14
WG099	1296+92.00	148.9	274.0	1213.7	3.89	148.9	274.0	1813.5	6.08
WG100	1297+04.00	189.1	274.6	1736.5	5.64	189.1	274.6	1824.0	5.95
WG101	1297+04.00	-121.9	-219.7	1723.4	7.29	-121.9	-219.7	1829.6	7.77
WG102	1297+16.00	-81.7	-216.2	1720.8	7.58	-81.7	-216.2	1828.0	8.08
WG103	1297+16.00	131.7	266.5	1213.8	4.06	131.7	266.5	1813.6	6.31
WG104	1297+28.00	170.0	267.4	1242.6	4.01	170.0	267.4	1831.7	6.21
WG105	1297+28.00	369.5	249.1	1158.0	3.17	369.5	249.1	1758.6	5.58
WG106	1297+40.00	232.7	249.1	1184.2	3.82	232.7	249.1	1776.5	6.20
WG107	1297+40.00	196.3	274.2	1228.0	3.76	196.3	274.2	1826.4	5.94
WG108	1297+52.00	214.5	275.2	1265.7	3.82	214.5	275.2	1853.5	5.96
WG109	1297+52.00	357.9	252.2	1167.9	3.21	357.9	252.2	1771.1	5.60
WG110	1297+64.00	229.0	252.2	1180.8	3.77	229.0	252.2	1773.1	6.12
WG111	1297+64.00	-417.8	-181.0	1678.8	6.97	-417.8	-181.0	1790.9	7.59
WG112	1297+76.00	-359.7	-178.4	1696.6	7.49	-359.7	-178.4	1809.3	8.13
WG113	1297+76.00	282.8	256.0	1187.0	3.53	282.8	256.0	1790.3	5.89
WG114	1297+88.00	175.5	255.9	1214.3	4.06	175.5	255.9	1806.2	6.37
WG115	1297+88.00	-443.4	-191.7	1688.7	6.50	-443.4	-191.7	1801.9	7.09
WG116	1298+00.00	-378.8	-188.8	1673.7	6.86	-378.8	-188.8	1788.6	7.47
WG117	1298+00.00	292.6	259.8	1248.2	3.68	292.6	259.8	1851.1	6.00
WG118	1298+12.00	200.9	259.7	1264.0	4.09	200.9	259.7	1855.9	6.37
WG119	1298+12.00	-405.3	-204.0	1679.1	6.24	-405.3	-204.0	1794.4	6.81
WG120	1298+24.00	-346.6	-201.0	1680.4	6.64	-346.6	-201.0	1797.0	7.22
WG121	1298+24.00	194.6	263.2	1230.3	3.94	194.6	263.2	1835.6	6.23
WG122	1298+36.00	163.8	263.2	1271.9	4.21	163.8	263.2	1865.3	6.46
WG123	1298+36.00	-358.7	-212.6	1671.8	6.18	-358.7	-212.6	1790.3	6.73
WG124	1298+48.00	-334.1	-210.7	1677.7	6.38	-334.1	-210.7	1795.9	6.94
WG125	1298+48.00	246.4	267.5	1216.2	3.63	246.4	267.5	1827.0	5.91

WG126	1298+60.00	130.1	267.5	1223.0	4.09	130.1	267.5	1823.0	6.33
WG127	1298+60.00	-334.0	-220.8	1691.2	6.15	-334.0	-220.8	1809.7	6.68
WG128	1298+72.00	-288.8	-217.7	1678.4	6.38	-288.8	-217.7	1798.7	6.94
WG129	1298+72.00	273.8	262.1	1204.0	3.55	273.8	262.1	1819.9	5.90
WG130	1298+84.00	167.6	262.1	1238.0	4.08	167.6	262.1	1842.1	6.39
WG131	1298+84.00	-244.4	-225.4	1667.6	6.31	-244.4	-225.4	1791.8	6.87
WG132	1298+96.00	-197.4	-222.3	1666.8	6.61	-197.4	-222.3	1792.2	7.17
WG133	1298+96.00	378.2	259.9	1195.0	3.14	378.2	259.9	1816.7	5.53
WG134	1299+08.00	300.9	259.9	1228.3	3.57	300.9	259.9	1857.0	5.99
WG135	1299+08.00	-162.9	-222.6	1710.3	6.95	-162.9	-222.6	1837.1	7.52
WG136	1299+20.00	-135.0	-219.6	1703.7	7.14	-135.0	-219.6	1832.0	7.73
WG137	1299+20.00	31.7	253.2	1201.8	4.62	31.7	253.2	1847.8	7.17
WG138	1299+32.00	78.6	253.3	1225.3	4.53	78.6	253.3	1860.4	7.03
WG139	1299+32.00	-166.9	-216.4	1699.5	7.08	-166.9	-216.4	1829.2	7.68
WG140	1299+44.00	-89.1	-213.5	1692.9	7.51	-89.1	-213.5	1824.1	8.13
WG141	1299+44.00	87.7	246.7	1198.8	4.50	87.7	246.7	1850.6	7.15
WG142	1299+56.00	130.0	246.9	1222.4	4.42	130.0	246.9	1863.1	7.02
WG143	1299+56.00	-290.1	-204.2	1687.3	6.84	-290.1	-204.2	1819.6	7.49
WG144	1299+68.00	-209.1	-201.4	1680.6	7.31	-209.1	-201.4	1814.5	7.97
WG145	1299+68.00	-29.9	-237.8	1658.2	6.85	-29.9	-237.8	1802.5	7.45
WG146	1299+80.00	12.7	230.3	1235.6	5.31	12.7	230.3	1870.2	8.07
WG147	1299+80.00	-414.2	-201.9	1673.0	6.23	-414.2	-201.9	1810.2	6.91
WG148	1299+92.00	-287.6	-199.1	1665.7	6.92	-287.6	-199.1	1804.8	7.62
WG149	1299+92.00	-152.6	-265.4	1663.9	5.69	-152.6	-265.4	1808.6	6.24
WG149	1300+00.00	-131.5	-265.4	1663.8	5.77	-131.5	-265.4	1806.0	6.31
WG150	1300+00.00	32.1	250.2	1163.4	4.52	32.1	250.2	1297.2	5.06
WG150	1300+08.00	96.7	250.2	1166.0	4.27	96.7	250.2	1299.7	4.81
WG151	1300+08.00	215.7	182.0	1158.7	5.18	215.7	182.0	1802.3	8.72
WG152	1300+20.00	258.3	182.1	1161.7	4.96	258.3	182.1	1813.7	8.54
WG153	1300+20.00	470.4	207.0	1159.3	3.33	470.4	207.0	1805.5	6.45
WG154	1300+32.00	541.0	207.4	1169.5	3.03	541.0	207.4	1816.4	6.15
WG155	1300+32.00	88.3	194.8	1157.9	5.49	88.3	194.8	1817.9	8.88
WG156	1300+44.00	130.8	194.7	1182.2	5.40	130.8	194.7	1828.5	8.72
WG157	1300+44.00	340.5	208.2	1162.9	3.95	340.5	208.2	1818.9	7.10
WG158	1300+56.00	397.0	208.5	1185.9	3.78	397.0	208.5	1829.3	6.87
WG159	1300+56.00	-30.0	-301.9	1710.2	5.57	-30.0	-301.9	1840.3	6.00
WG160	1300+68.00	12.3	-298.1	1704.2	5.68	12.3	-298.1	1835.3	6.12
WG161	1300+68.00	222.2	220.4	1172.4	4.31	222.2	220.4	1825.5	7.27
WG162	1300+80.00	279.7	220.7	1195.3	4.15	279.7	220.7	1836.2	7.05
WG163	1300+80.00	44.3	215.1	1180.3	5.28	44.3	215.1	1833.7	8.32
WG164	1300+92.00	86.3	215.0	1204.7	5.20	86.3	215.0	1845.7	8.18
WG165	1300+92.00	236.6	231.9	1187.4	4.10	236.6	231.9	1836.4	6.90
WG166	1301+04.00	220.3	232.4	1179.5	4.13	220.3	232.4	1799.3	6.79
WG167	1301+04.00	-273.6	-297.1	1688.1	4.76	-273.6	-297.1	1806.8	5.16
WG168	1301+16.00	-288.3	-293.5	1687.8	4.77	-288.3	-293.5	1807.2	5.18
WG169	1301+16.00	346.1	238.3	1155.3	3.40	346.1	238.3	1783.1	6.03
WG170	1301+28.00	337.7	238.9	1189.6	3.57	337.7	238.9	1805.4	6.14
WG171	1301+28.00	-187.4	-296.3	1691.6	5.08	-187.4	-296.3	1805.1	5.46
WG172	1301+40.00	-238.2	-292.8	1679.8	4.92	-238.2	-292.8	1794.4	5.31
WG173	1301+40.00	426.5	237.3	1194.4	3.24	426.5	237.3	1814.7	5.85
WG174	1301+52.00	422.5	238.0	1198.1	3.26	422.5	238.0	1809.2	5.83
WG175	1301+52.00	-120.6	-294.3	1705.7	5.39	-120.6	-294.3	1814.1	5.75
WG176	1301+64.00	-211.1	-292.6	1711.4	5.13	-211.1	-292.6	1819.9	5.50
WG177	1301+64.00	494.1	231.6	1159.4	**2.87**	494.1	231.6	1781.5	5.56
WG178	1301+76.00	463.7	232.2	1701.8	5.33	463.7	232.2	1810.6	5.80
WG179	1301+76.00	-137.1	-298.6	1710.3	5.27	-137.1	-298.6	1816.0	5.62
WG180	1301+88.00	-112.2	-295.1	1712.4	5.42	-112.2	-295.1	1818.7	5.78
WG181	1301+88.00	493.5	218.2	1680.6	5.44	493.5	218.2	1798.9	5.98
WG182	1302+00.00	474.5	218.7	1698.7	5.60	474.5	218.7	1805.7	6.09
WG183	1302+00.00	-248.3	-298.3	1727.2	4.96	-248.3	-298.3	1831.0	5.31
WG184	1302+12.00	-233.2	-294.8	1712.2	5.02	-233.2	-294.8	1817.2	5.37
WG185	1302+12.00	-64.6	-249.7	1737.0	6.70	-64.6	-249.7	1832.0	7.08
WG186	1302+24.00	-296.1	-246.7	1729.7	5.81	-296.1	-246.7	1825.8	6.20
WG187	1302+24.00	-337.1	-293.6	1661.9	4.51	-337.1	-293.6	1767.1	4.87
WG188	1302+36.00	-333.7	-290.1	1680.7	4.64	-333.7	-290.1	1785.9	5.01
WG189	1302+36.00	-130.6	-244.7	1739.9	6.58	-130.6	-244.7	1834.3	6.96
WG190	1302+48.00	-319.2	-241.7	1747.9	5.91	-319.2	-241.7	1842.9	6.30
WG191	1302+48.00	-370.6	-288.2	1651.9	4.45	-370.6	-288.2	1757.2	4.81
WG192	1302+60.00	-379.4	-284.8	1631.6	4.40	-379.4	-284.8	1738.2	4.77
WG193	1302+60.00	-156.5	-238.9	1741.8	6.64	-156.5	-238.9	1836.2	7.03
WG194	1302+72.00	-360.3	-236.1	1729.0	5.80	-360.3	-236.1	1824.7	6.20
WG195	1302+72.00	-436.7	-279.3	1646.6	4.33	-436.7	-279.3	1752.6	4.71

WG196	1302+84.00	-454.2	-275.9	1634.3	4.28	-454.2	-275.9	1741.5	**4.67**
WG197	1302+84.00	-106.1	-231.2	1716.2	6.96	-106.1	-231.2	1813.8	7.39
WG198	1302+96.00	23.1	206.5	1242.0	5.90	23.1	206.5	1837.1	8.78
WG199	1302+96.00	134.1	180.8	1208.5	5.94	134.1	180.8	1817.5	9.31
WG200	1303+08.00	174.3	180.8	1230.0	5.84	174.3	180.8	1828.0	9.15
WG201	1303+08.00	-110.8	-223.7	1730.9	7.24	-110.8	-223.7	1826.2	7.67
WG202	1303+20.00	-30.9	-222.8	1729.8	7.63	-30.9	-222.8	1825.4	8.05
WG203	1303+20.00	125.4	183.5	1202.4	5.87	125.4	183.5	1815.5	9.21
WG204	1303+32.00	231.7	183.6	1728.8	8.15	231.7	183.6	1827.5	8.69
WG205	1303+32.00	-100.9	-214.6	1732.3	7.60	-100.9	-214.6	1826.4	8.04
WG206	1303+44.00	-21.1	-212.1	1730.2	8.06	-21.1	-212.1	1825.0	8.50
WG207	1303+44.00	144.5	190.1	1706.7	8.22	144.5	190.1	1818.3	8.80
WG208	1303+56.00	237.6	190.4	1732.0	7.85	237.6	190.4	1830.2	8.36
WG209	1303+56.00	-79.9	-201.0	1727.1	8.20	-79.9	-201.0	1822.3	8.67
WG210	1303+68.00	3.5	236.8	1732.6	7.30	3.5	236.8	1830.2	7.71
WG211	1303+68.00	185.0	203.4	1716.5	7.53	185.0	203.4	1826.3	8.07
WG212	1303+80.00	264.2	204.0	1742.1	7.24	264.2	204.0	1838.1	7.72
WG213	1303+80.00	-86.7	-181.9	1714.7	8.95	-86.7	-181.9	1812.2	9.49
WG214	1303+92.00	-2.8	253.9	1747.6	6.87	-2.8	253.9	1841.2	7.24
WG215	1303+92.00	129.0	217.7	1746.4	7.43	129.0	217.7	1849.3	7.90
WG216	1304+04.00	181.9	218.4	1774.3	7.29	181.9	218.4	1861.9	7.69
WG217	1304+10.00	-30.0	270.2	1766.3	6.43	-45.1	159.3	1782.0	10.90
WG218	1304+16.00	35.3	272.4	1807.6	6.51	35.3	272.4	1945.8	7.01
WG219	1304+16.00	229.3	254.1	1833.4	6.31	229.3	254.1	1945.8	6.76
WG220	1304+28.00	271.8	255.7	1856.2	6.20	271.8	255.7	1945.8	6.55
WG221	1304+28.00	-60.6	309.1	1699.6	5.30	-89.1	121.2	1520.1	11.81
WG222	1304+40.00	3.4	312.3	1780.0	5.69	3.4	312.3	1780.0	5.69
WG223	1304+40.00	192.9	321.9	1702.6	4.69	192.9	321.9	1780.0	4.93
WG224	1304+52.00	197.2	325.1	2581.8	7.33	197.2	325.1	2581.8	7.33
WG225	1304+52.00	38.9	425.0	2581.8	5.98	38.9	425.0	2581.8	5.98
WG226	1304+64.00	200.7	428.8	3383.7		200.7	428.8	3383.7	
WG228	1304+64.00	252.8	486.5	1594.0		252.8	486.5	1686.1	
WG229	1304+75.00	406.9	490.2	1597.9		406.9	490.2	1688.3	
WG230	1304+75.00	-355.3	-617.9	1658.5		-355.3	-617.9	1780.0	
WG231	1304+86.00	-201.3	-613.7	1655.2		-201.3	-613.7	1780.0	
WG233	1304+86.00	-88.3	-404.3	3383.7		-88.3	-404.3	3383.7	
WG234	1304+98.00	64.0	-393.6	2581.8	6.40	86.6	158.5	2384.8	14.50
WG235	1304+98.00	179.3	169.2	2357.0	12.87	179.3	169.2	2444.0	13.38
WG236	1305+10.00	339.6	185.9	1469.2	6.08	339.6	185.9	1545.5	6.49
WG237	1305+10.00	-120.8	-291.9	1780.0	5.68	-120.8	-291.9	1780.0	5.68
WG238	1305+22.00	-33.3	-288.2	1780.0	6.06	-33.3	-288.2	1780.0	6.06
WG239	1305+22.00	63.1	179.1	1640.9	8.81	63.1	179.1	1757.7	9.46
WG240	1305+34.00	193.0	179.3	1660.4	8.18	193.0	179.3	1774.1	8.82
WG241	1305+34.00	-223.5	-279.1	1785.7	5.60	-223.5	-279.1	1875.1	5.92
WG242	1305+46.00	-141.1	-275.8	1783.8	5.96	-141.1	-275.8	1874.2	6.28
WG243	1305+46.00	109.1	212.1	1693.7	7.47	109.1	212.1	1806.0	8.00
WG244	1305+58.00	214.2	212.5	1718.7	7.08	214.2	212.5	1818.3	7.55
WG245	1305+58.00	-166.1	-256.3	1737.2	6.13	-166.1	-256.3	1842.1	6.54
WG246	1305+70.00	-87.3	-253.0	1734.6	6.51	-87.3	-253.0	1840.8	6.93
WG247	1305+70.00	38.0	218.6	1718.5	7.69	38.0	218.6	1825.4	8.18
WG248	1305+82.00	116.9	219.1	1741.6	7.42	116.9	219.1	1836.8	7.85
WG249	1305+82.00	-170.6	-235.1	1719.5	6.59	-170.6	-235.1	1829.0	7.05
WG250	1305+94.00	-91.8	-231.9	1716.8	7.01	-91.8	-231.9	1827.5	7.48
WG251	1305+94.00	53.0	219.8	1734.4	7.65	53.0	219.8	1838.8	8.12
WG252	1306+06.00	119.3	220.5	1759.1	7.44	119.3	220.5	1850.9	7.85
WG253	1306+06.00	-124.5	-225.5	1709.0	7.03	-124.5	-225.5	1819.0	7.51
WG254	1306+18.00	-40.2	-222.0	1698.0	7.47	-40.2	-222.0	1809.6	7.97
WG255	1306+18.00	296.5	216.6	1764.6	6.78	296.5	216.6	1859.8	7.22
WG256	1306+30.00	246.2	216.5	1799.0	7.17	246.2	216.5	1945.8	7.85
WG257	1306+30.00	-105.7	-232.3	1764.0	7.14	-105.7	-232.3	1870.5	7.60
WG258	1306+42.00	-37.9	-228.5	1768.7	7.57	-37.9	-228.5	1876.2	8.05
WG259	1306+42.00	317.3	224.4	1760.8	6.43	317.3	224.4	1861.3	6.88
WG260	1306+54.00	267.2	225.1	1756.1	6.61	267.2	225.1	1845.7	7.01
WG261	1306+54.00	-92.1	-253.6	1815.7	6.80	-92.1	-253.6	1945.8	7.31
WG262	1306+66.00	-24.8	-249.8	1808.5	7.14	-24.8	-249.8	1945.8	7.69
WG263	1306+66.00	324.8	235.5	1755.5	6.08	324.8	235.5	1855.1	6.50
WG264	1306+78.00	282.3	236.1	1794.1	6.40	282.3	236.1	1945.8	7.05
WG265	1306+78.00	-69.2	-275.0	1771.4	6.19	-69.2	-275.0	1873.3	6.56

WG266	1306+90.00	-2.9	-271.1	1773.0	6.53	-2.9	-271.1	1945.8	7.17
WG267	1306+90.00	270.1	247.9	1265.0	4.01	270.1	247.9	1866.1	6.44
WG268	1307+02.00	248.3	248.3	1272.8	4.13	248.3	248.3	1861.4	6.50
WG269	1307+02.00	-39.4	-291.2	1742.1	5.85	-39.4	-291.2	1840.7	6.19
WG270	1307+14.00	19.7	-287.4	1730.2	5.95	25.6	218.6	1945.8	8.78
WG271	1307+14.00	-276.8	-250.9	1729.3	5.79	-276.8	-250.9	1827.8	6.18
WG272	1307+26.00	-116.5	-247.3	1743.1	6.58	-116.5	-247.3	1842.1	6.98
WG273	1307+26.00	-18.2	-294.1	1745.7	5.87	-18.2	-294.1	1844.2	6.21
WG274	1307+38.00	61.1	225.0	1267.7	5.36	61.1	225.0	1863.4	8.01
WG275	1307+38.00	-239.2	-252.9	1730.1	5.90	-239.2	-252.9	1830.3	6.29
WG276	1307+50.00	-79.8	-249.3	1741.0	6.66	-79.8	-249.3	1841.6	7.07
WG277	1307+50.00	35.1	231.1	1205.2	5.06	35.1	231.1	1316.9	5.55
WG278	1307+62.00	114.9	231.3	1230.6	4.82	114.9	231.3	1328.9	5.25
WG279	1307+62.00	-206.1	-233.1	1740.5	6.58	-206.1	-233.1	1843.7	7.03
WG280	1307+74.00	-45.7	-229.6	1738.2	7.37	-45.7	-229.6	1842.2	7.82
WG281	1307+74.00	78.4	239.7	1176.1	4.58	78.4	239.7	1290.4	5.06
WG282	1307+86.00	158.7	240.2	1202.2	4.34	158.7	240.2	1302.9	4.76
WG283	1307+86.00	-178.1	-189.5	1748.5	8.29	-178.1	-189.5	1856.3	8.86
WG284	1307+98.00	-10.6	280.7	1198.3	4.23	-10.6	280.7	1799.1	6.37
WG285	1307+98.00	112.0	257.6	1141.7	4.00	112.0	257.6	1754.0	6.37
WG286	1308+10.00	192.3	258.8	1170.5	3.78	192.3	258.8	1767.7	6.09
WG287	1308+10.00	-162.5	-123.6	1786.0	13.14	-162.5	-123.6	1945.8	14.43
WG288	1308+22.00	1.1	307.6	1182.4	3.84	1.1	307.6	1769.2	5.75
WG289	1308+22.00	74.5	311.9	1128.8	3.38	74.5	311.9	1705.8	5.23
WG290	1308+34.00	101.4	315.0	1759.6	5.3	101.4	315.0	2334.2	7.1
WG291	1308+34.00	39.5	329.8	1875.9	5.6	39.5	329.8	2436.0	7.3
WG291	1308+39.58	1.5	329.8	2377.1	7.2	1.5	329.8	2436.0	7.4
WG292	1308+39.58	547.7	143.2	2255.8	11.9	547.7	143.2	2381.0	12.8
WG292	1308+45.17	525.2	143.2	2255.8	12.1	525.2	143.2	2381.0	13.0
WG293	1308+45.17	196.0	137.2	2240.2	14.9	196.0	137.2	2254.6	15.0
WG293	1308+50.75	81.8	367.0	2567.9	6.8	116.4	137.2	2254.7	15.6
WG294	1308+50.75	268.6	238.6	2240.0	8.3	268.6	238.6	2256.0	8.3
WG294	1308+56.33	243.7	238.6	2240.0	8.4	243.7	238.6	2256.1	8.4
WG295	1308+56.33	95.4	400.5	2389.3	5.7	95.4	400.5	2287.0	5.5
WG295	1308+61.92	173.4	400.5	2389.3	5.5	173.4	400.5	2287.0	5.3
WG296	1308+61.92	76.4	1270.7	2224.9	NaN	76.4	1270.7	2251.1	

Appendix C

RELIABILITY ANALYSIS BASED ON DESIGN INFORMATION

C.1 Matlab Code for Reliability Analysis Based on Design Information

```
%%Reliability Analyis Based on Design Information.
%%% Strength I limit state-Flexural

clc
clear all
close all
tic
%% Load files
DLM=load('mean_sigma_DL.txt');
LLM=load('mean_sigma_LL.txt');
RM=load('mean_sigma_R.txt');
%% Determe the number of trails
n=10^6;

for i=1:n;
p(i,1)=i/(n+1);
z(i,1)=norminv(p(i,1));
end

%% Monte Carlo Simulation
for j=1:length(DLM)    %%%number of elements along the edge girder

%%% Dead Load
DL=(1/1)*normrnd(DLM(j,1),abs(DLM(j,2)),n,1);

%%% Live Load
LL=(0.65/1)*normrnd(LLM(j,1),LLM(j,2),n,1);      %%% 0.65 is the
multiple presense factor

%%% Resistance
R=exp(((log(RM(j,1))/log(exp(1)))-(.5* (log(.075^2+1)/log(exp(1))))))
+ ((sqrt(log(.075^2+1)/log(exp(1)) ))*norminv(abs(rand(n,1)))));

%%% Limit state
Y=R-DL-LL;

%%% rearrange values in ascending order at all locations
```

```
Y_arranged=sort(Y);  %% this commadn sort each column in the matrix
in ascending order

Rate=length(find(Y_arranged(:)<=0))/n;   %%% count the negative
values, and devide them by the number of cycles, that represents the
probability of failure
Beta(j,1)=-norminv(Rate,0,1);

%% final distribution at each member location
figure(j)
histfit(Y_arranged,30,'kernel');
distribution=fitdist(Y_arranged,'Normal');
mdl=LinearModel.fit(Y_arranged,z);
Beta_3_start(j,1)=mdl.Coefficients(1,1);
end

Beta_extrapolation=-table2array(Beta_3_start);
clearvars -except keepVariables Beta Beta_extrapolation station

%% Plotting
load('station.txt');
figure(1)
plot(station,Beta,'Marker','o','MarkerSize',6,'MarkerEdgeColor','b','
MarkerFaceColor',[1 0 0]);
ylabel('Reliability Index (Beta)','FontSize',20);
xlabel('Station (ft)','FontSize',20);
xlim([0 1750]);
ylim([0 5])
set(gca,'XTick',[0 100 200 300 400 500 600 700 875 1050 1150 1250
1350 1450 1550 1650 1750]);
set(gca,'YTick',[0 1 2 3 4 5]);
grid on
set(gca,'FontSize',14);
legend('Reliability Index');
title('Strength I- Flexure');

figure(2)
plot(station,Beta_extrapolation,'Marker','o','MarkerSize',6,'MarkerEd
geColor','b','MarkerFaceColor',[1 0 0]);
ylabel('Reliability Index (Beta)','FontSize',20);
xlabel('Station (ft)','FontSize',20);
xlim([0 1750]);
ylim([0 12])
set(gca,'XTick',[0 100 200 300 400 500 600 700 875 1050 1150 1250
1350 1450 1550 1650 1750]);
set(gca,'YTick',[0 1 2 3 4 5 6 7 8 9 10 11 12]);
grid on
set(gca,'FontSize',14);
legend('Reliability Index');
title('Strength I- Flexure');
toc
```

Appendix D

CONTINUOUS RATING FACTORS USING STRUCTURAL HEALTH MONITORING DATA

D.1 Low Frequency Rating Factor Report

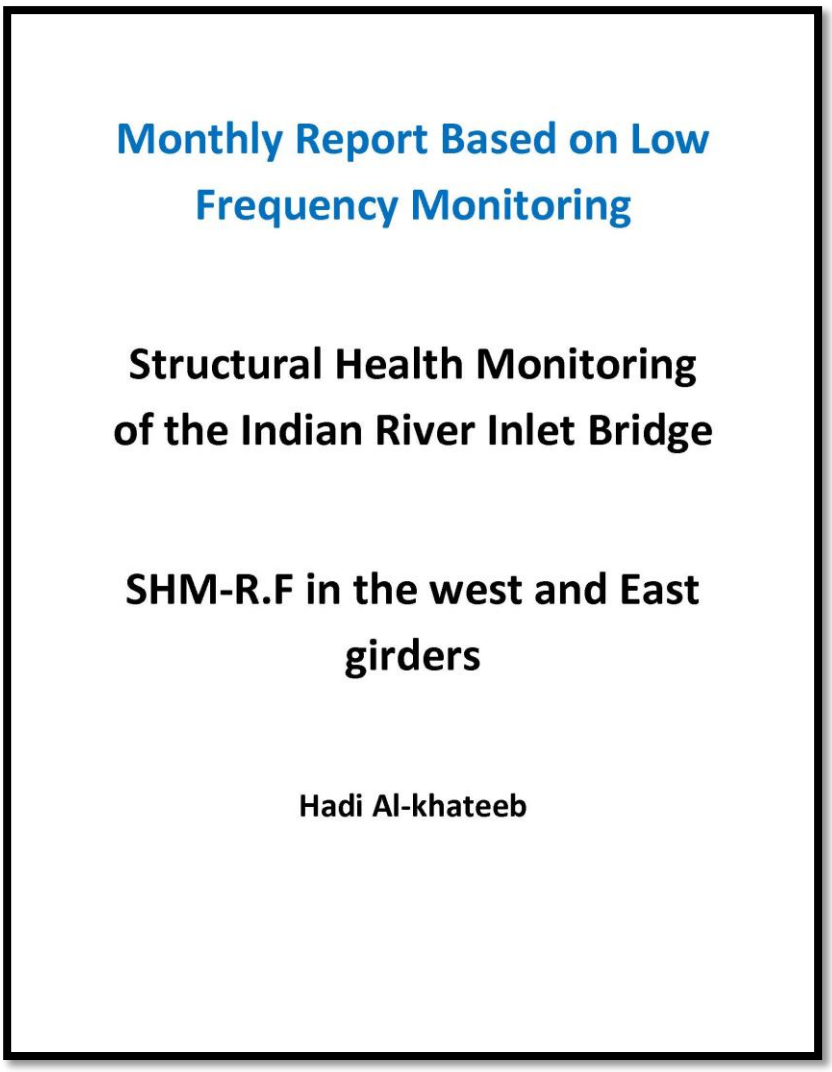

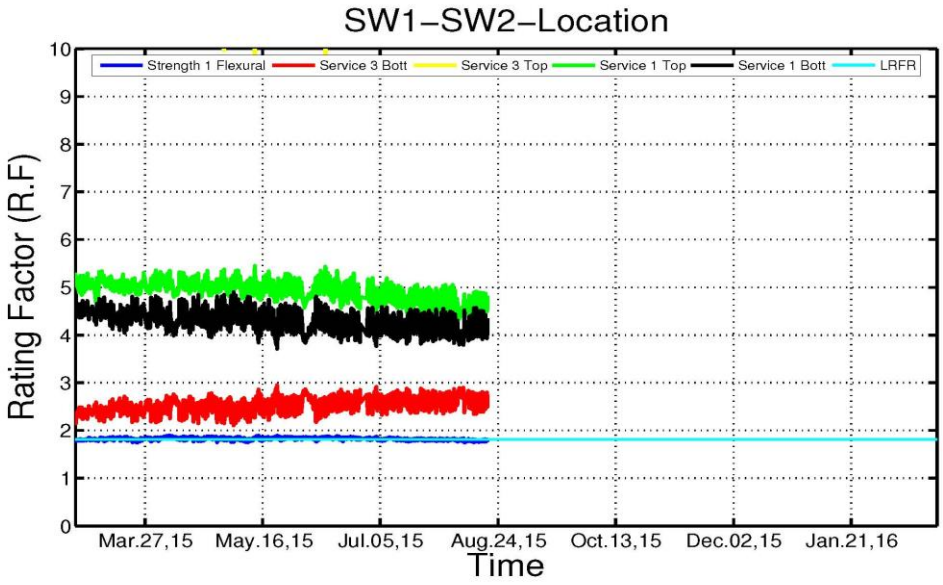
SW1–SW2–Location
Strength 1 Flexural
Service 3 Bott
Service 3 Top
Service 1 Top
Service 1 Bott
LRFR
Rating Factor (R.F)
0
1
2
3
4
5
6
7
8
9
10
Mar.27,15
May.16,15
Jul.05,15
Aug.24,15
Oct.13,15
Dec.02,15
Jan.21,16
Time

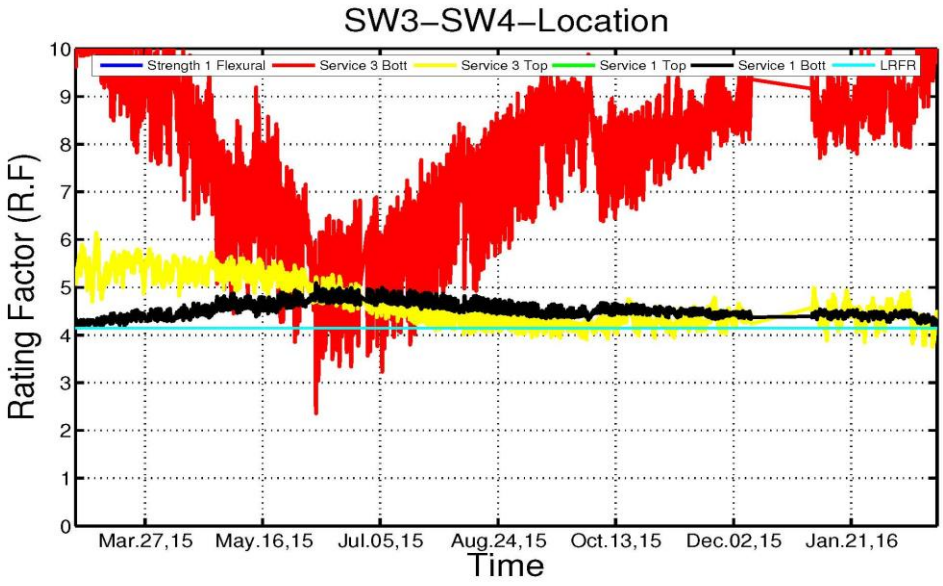
SW3–SW4–Location
Strength 1 Flexural
Service 3 Bott
Service 3 Top
Service 1 Top
Service 1 Bott
LRFR
Rating Factor (R.F)
0
1
2
3
4
5
6
7
8
9
10
Mar.27,15
May.16,15
Jul.05,15
Aug.24,15
Oct.13,15
Dec.02,15
Jan.21,16
Time

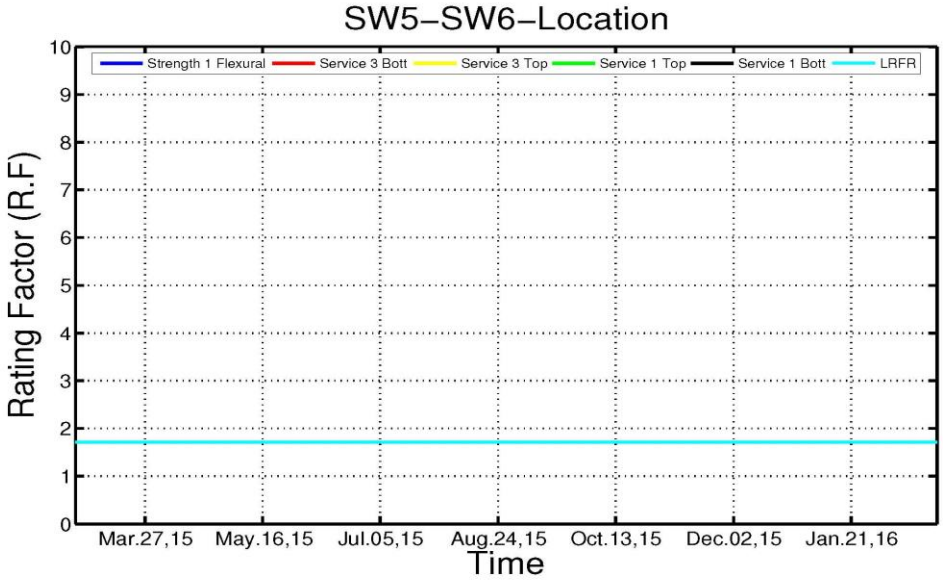
SW5–SW6–Location
Strength 1 Flexural
Service 3 Bott
Service 3 Top
Service 1 Top
Service 1 Bott
LRFR
Rating Factor (R.F)
0
1
2
3
4
5
6
7
8
9
10
Mar.27,15
May.16,15
Jul.05,15
Aug.24,15
Oct.13,15
Dec.02,15
Jan.21,16
Time

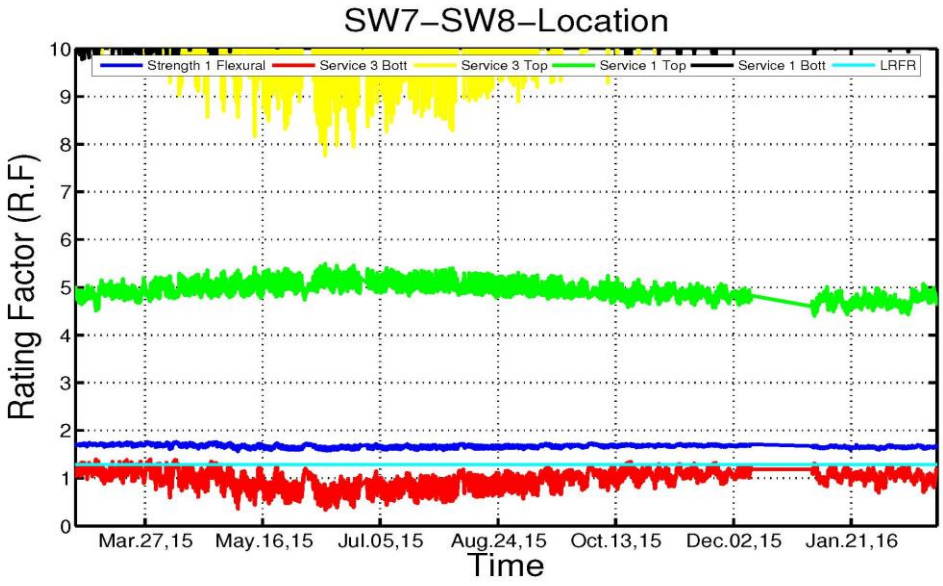
SW7–SW8–Location
Strength 1 Flexural
Service 3 Bott
Service 3 Top
Service 1 Top
Service 1 Bott
LRFR
Rating Factor (R.F)
0
1
2
3
4
5
6
7
8
9
10
Mar.27,15
May.16,15
Jul.05,15
Aug.24,15
Oct.13,15
Dec.02,15
Jan.21,16
Time

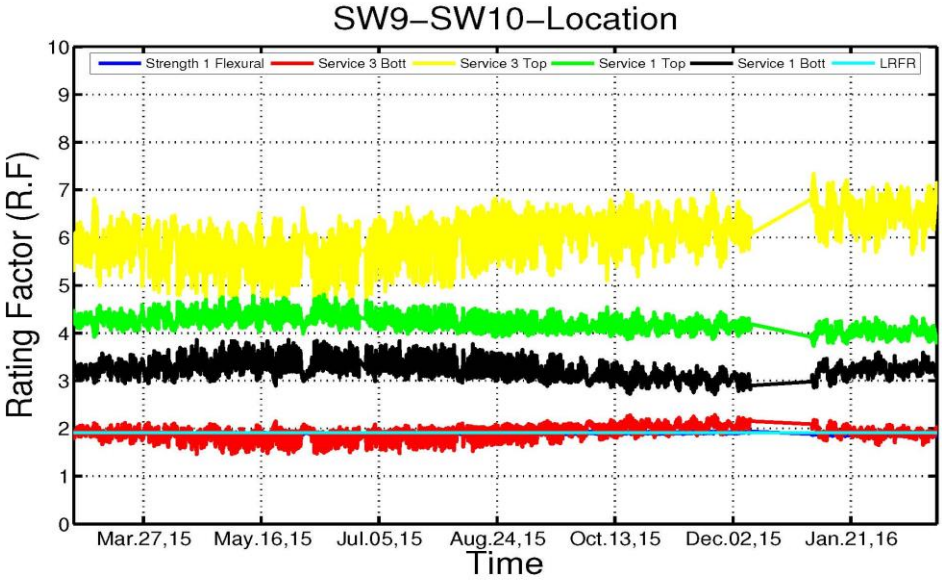
SW9–SW10–Location
Strength 1 Flexural
Service 3 Bott
Service 3 Top
Service 1 Top
Service 1 Bott
LRFR
Rating Factor (R.F)
0
1
2
3
4
5
6
7
8
9
10
Mar.27,15
May.16,15
Jul.05,15
Aug.24,15
Oct.13,15
Dec.02,15
Jan.21,16
Time

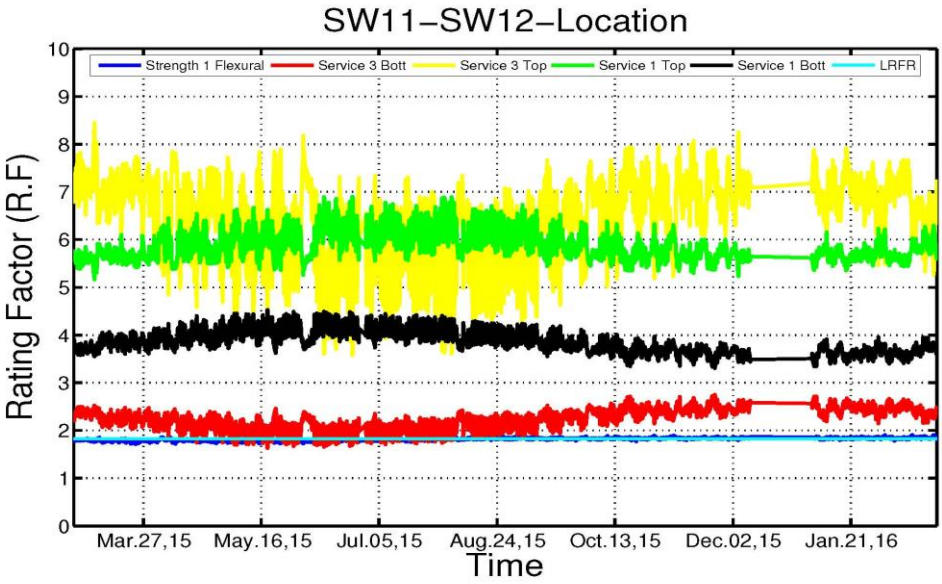
SW11–SW12–Location
Strength 1 Flexural
Service 3 Bott
Service 3 Top
Service 1 Top
Service 1 Bott
LRFR
Rating Factor (R.F)
0
1
2
3
4
5
6
7
8
9
10
Mar.27,15
May.16,15
Jul.05,15
Aug.24,15
Oct.13,15
Dec.02,15
Jan.21,16
Time

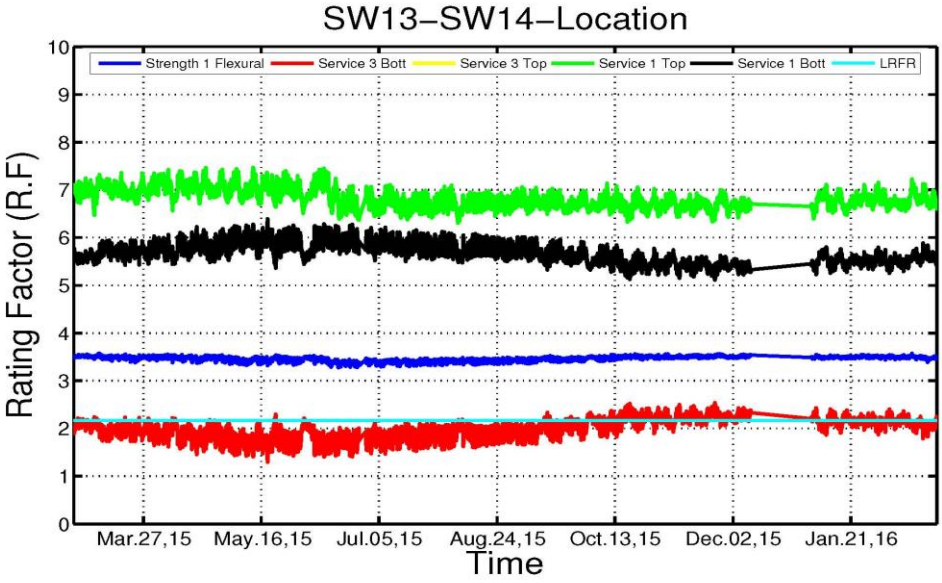
SW13–SW14–Location
Strength 1 Flexural
Service 3 Bott
Service 3 Top
Service 1 Top
Service 1 Bott
LRFR
Rating Factor (R.F)
0
1
2
3
4
5
6
7
8
9
10
Mar.27,15
May.16,15
Jul.05,15
Aug.24,15
Oct.13,15
Dec.02,15
Jan.21,16
Time

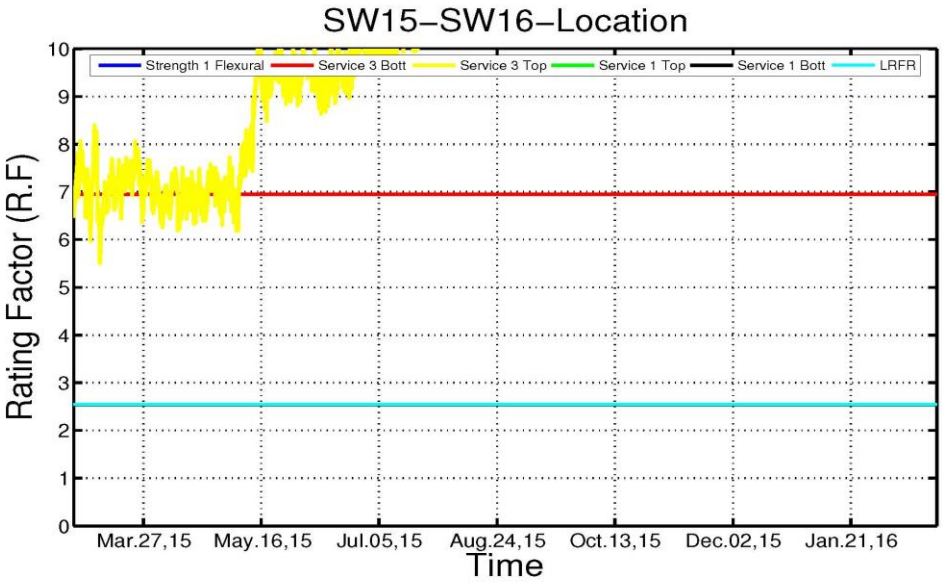
SW15–SW16–Location
Strength 1 Flexural
Service 3 Bott
Service 3 Top
Service 1 Top
Service 1 Bott
LRFR
Rating Factor (R.F)
0
1
2
3
4
5
6
7
8
9
10
Mar.27,15
May.16,15
Jul.05,15
Aug.24,15
Oct.13,15
Dec.02,15
Jan.21,16
Time

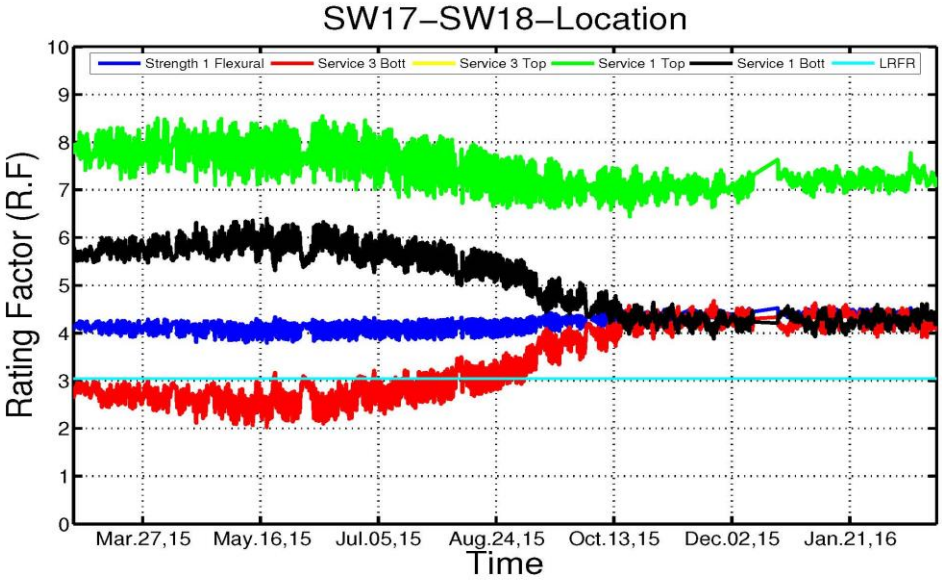
SW17–SW18–Location
Strength 1 Flexural
Service 3 Bott
Service 3 Top
Service 1 Top
Service 1 Bott
LRFR
Rating Factor (R.F)
0
1
2
3
4
5
6
7
8
9
10
Mar.27,15
May.16,15
Jul.05,15
Aug.24,15
Oct.13,15
Dec.02,15
Jan.21,16
Time

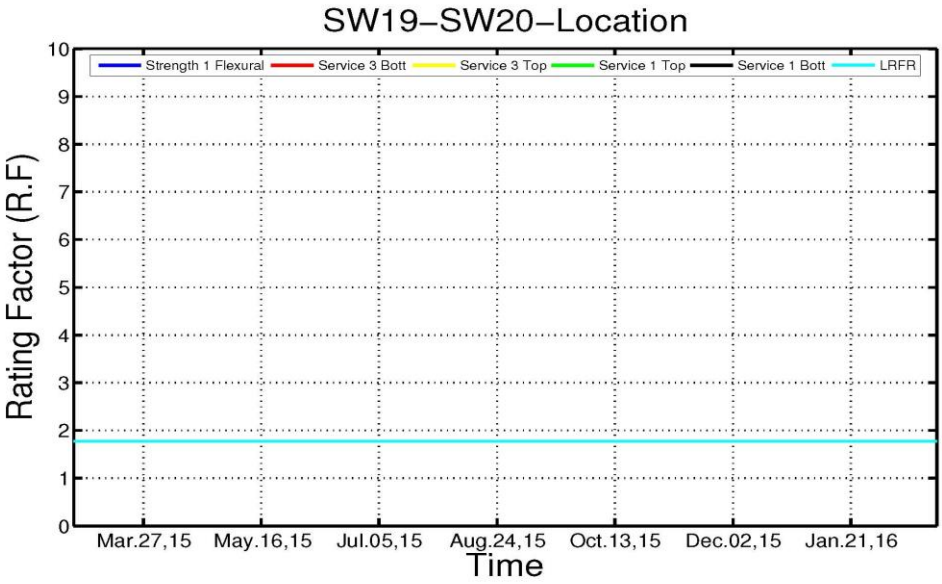
SW19–SW20–Location
Strength 1 Flexural
Service 3 Bott
Service 3 Top
Service 1 Top
Service 1 Bott
LRFR
Rating Factor (R.F)
0
1
2
3
4
5
6
7
8
9
10
Mar.27,15
May.16,15
Jul.05,15
Aug.24,15
Oct.13,15
Dec.02,15
Jan.21,16
Time

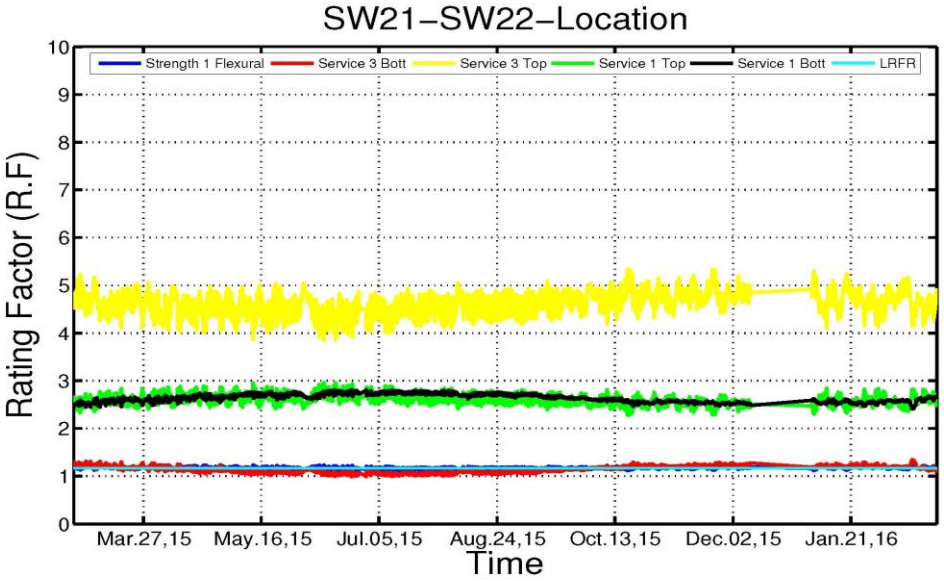
SW21–SW22–Location
Strength 1 Flexural
Service 3 Bott
Service 3 Top
Service 1 Top
Service 1 Bott
LRFR
Rating Factor (R.F)
0
1
2
3
4
5
6
7
8
9
10
Mar.27,15
May.16,15
Jul.05,15
Aug.24,15
Oct.13,15
Dec.02,15
Jan.21,16
Time

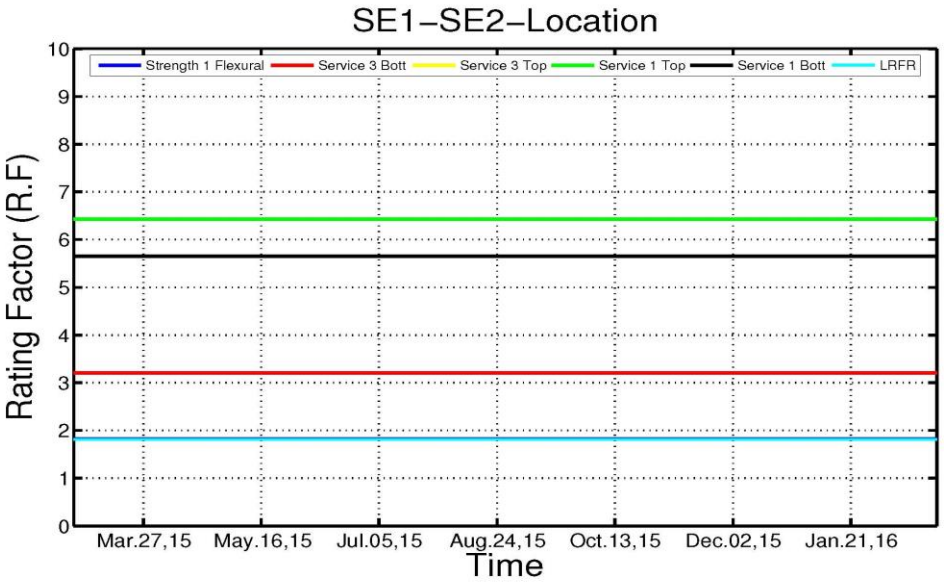
SE1–SE2–Location
Strength 1 Flexural
Service 3 Bott
Service 3 Top
Service 1 Top
Service 1 Bott
LRFR
Rating Factor (R.F)
0
1
2
3
4
5
6
7
8
9
10
Mar.27,15
May.16,15
Jul.05,15
Aug.24,15
Oct.13,15
Dec.02,15
Jan.21,16
Time

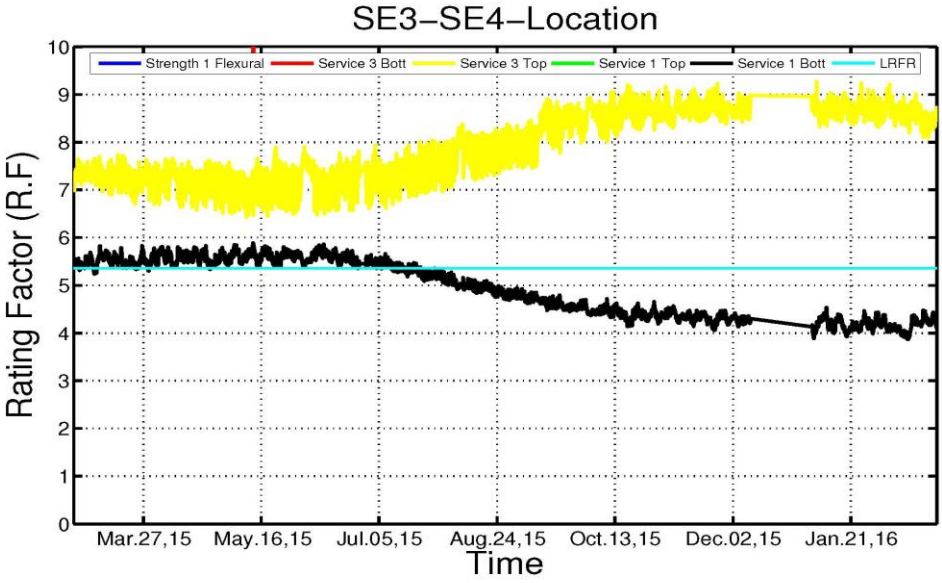
SE3–SE4–Location
Strength 1 Flexural
Service 3 Bott
Service 3 Top
Service 1 Top
Service 1 Bott
LRFR
Rating Factor (R.F)
0
1
2
3
4
5
6
7
8
9
10
Mar.27,15
May.16,15
Jul.05,15
Aug.24,15
Oct.13,15
Dec.02,15
Jan.21,16
Time

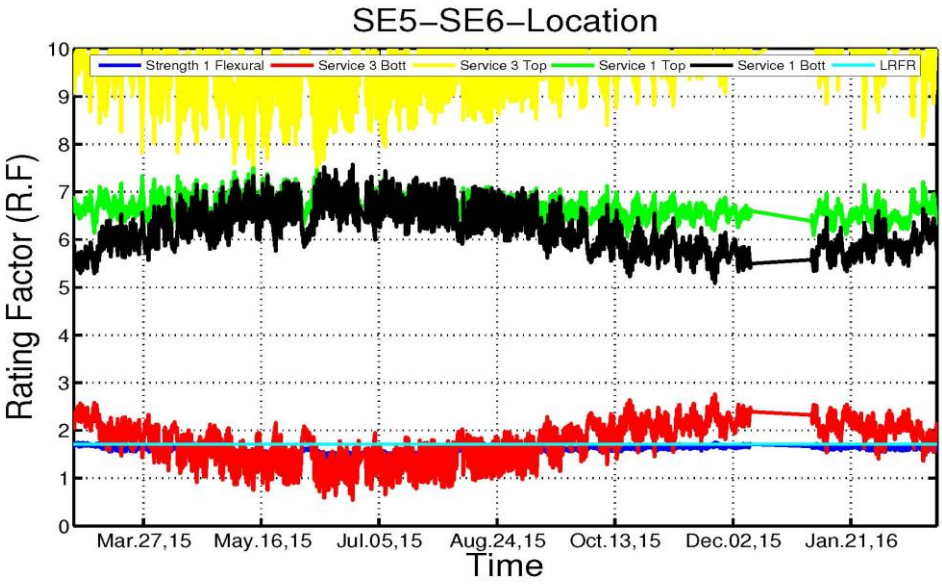
SE5–SE6–Location
Strength 1 Flexural
Service 3 Bott
Service 3 Top
Service 1 Top
Service 1 Bott
LRFR
Rating Factor (R.F)
0
1
2
3
4
5
6
7
8
9
10
Mar.27,15
May.16,15
Jul.05,15
Aug.24,15
Oct.13,15
Dec.02,15
Jan.21,16
Time

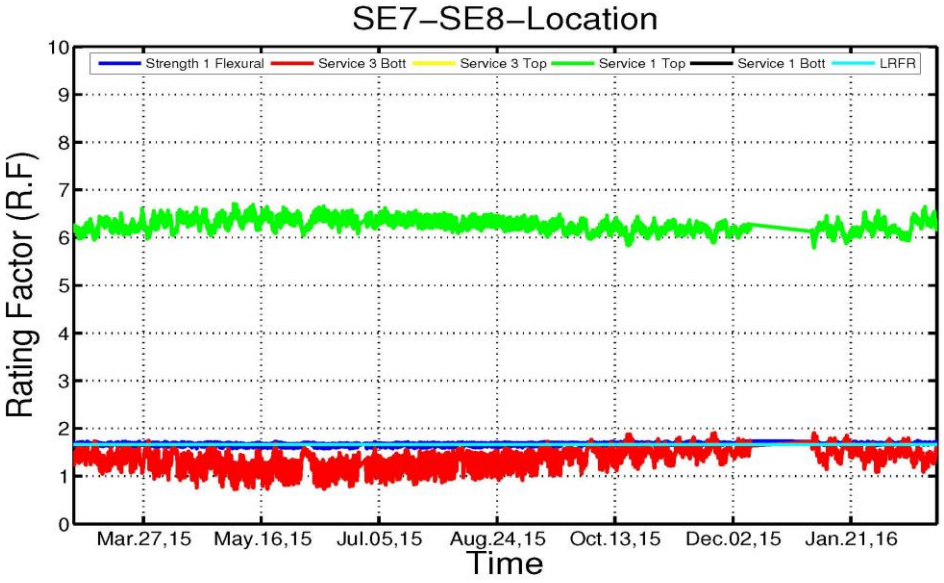
SE7–SE8–Location
Strength 1 Flexural
Service 3 Bott
Service 3 Top
Service 1 Top
Service 1 Bott
LRFR
Rating Factor (R.F)
0
1
2
3
4
5
6
7
8
9
10
Mar.27,15
May.16,15
Jul.05,15
Aug.24,15
Oct.13,15
Dec.02,15
Jan.21,16
Time

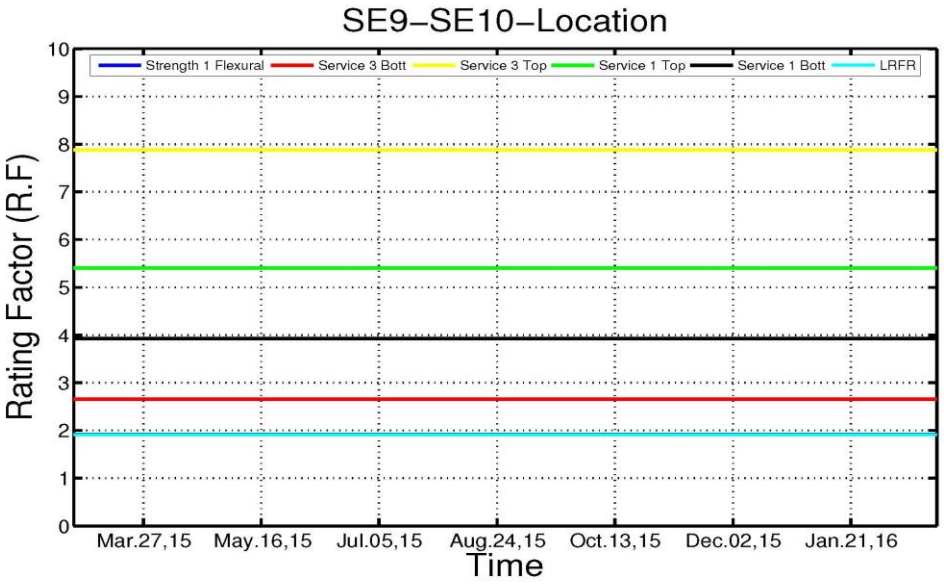
SE9–SE10–Location
Strength 1 Flexural
Service 3 Bott
Service 3 Top
Service 1 Top
Service 1 Bott
LRFR
Rating Factor (R.F)
0
1
2
3
4
5
6
7
8
9
10
Mar.27,15
May.16,15
Jul.05,15
Aug.24,15
Oct.13,15
Dec.02,15
Jan.21,16
Time

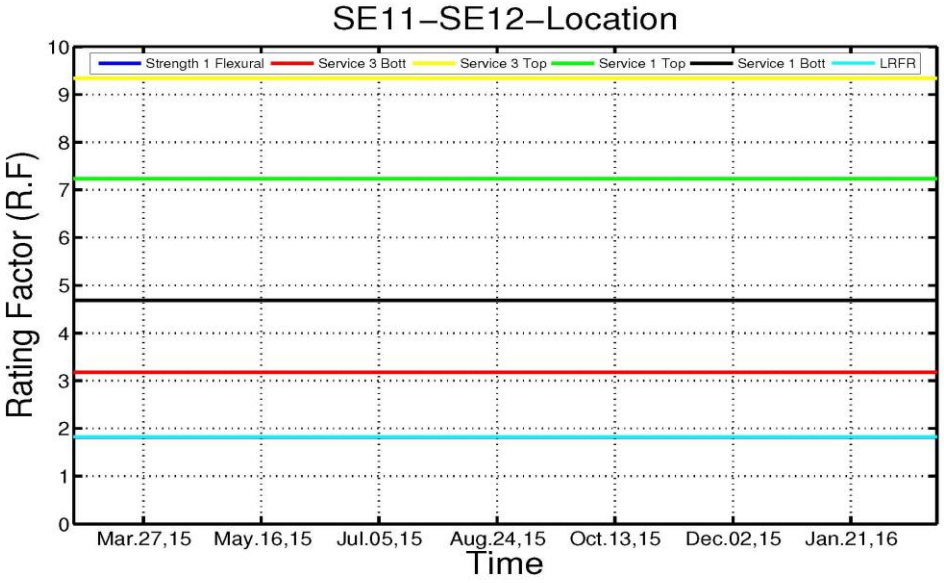
SE11–SE12–Location
Strength 1 Flexural
Service 3 Bott
Service 3 Top
Service 1 Top
Service 1 Bott
LRFR
Rating Factor (R.F)
0
1
2
3
4
5
6
7
8
9
10
Mar.27,15
May.16,15
Jul.05,15
Aug.24,15
Oct.13,15
Dec.02,15
Jan.21,16
Time

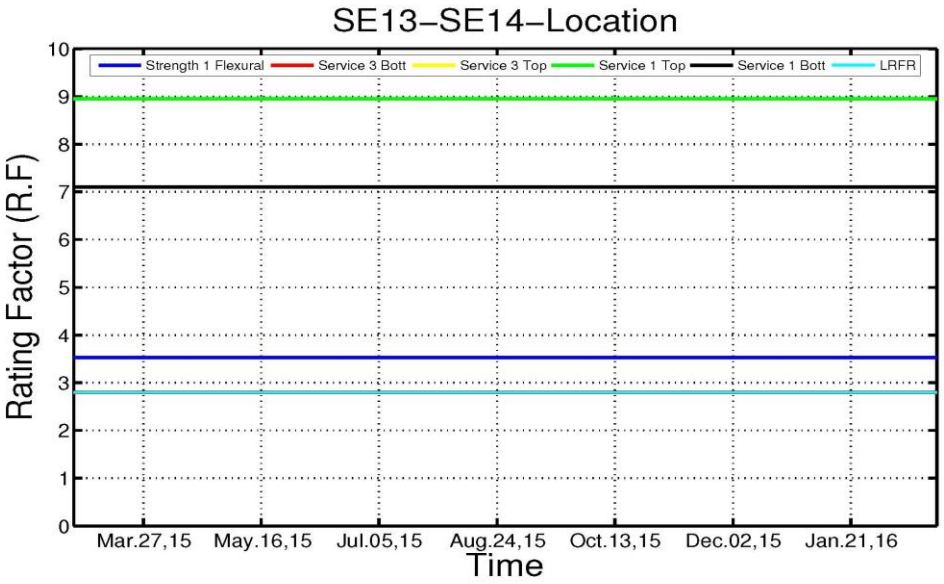
SE13–SE14–Location
Strength 1 Flexural
Service 3 Bott
Service 3 Top
Service 1 Top
Service 1 Bott
LRFR
Rating Factor (R.F)
0
1
2
3
4
5
6
7
8
9
10
Mar.27,15
May.16,15
Jul.05,15
Aug.24,15
Oct.13,15
Dec.02,15
Jan.21,16
Time

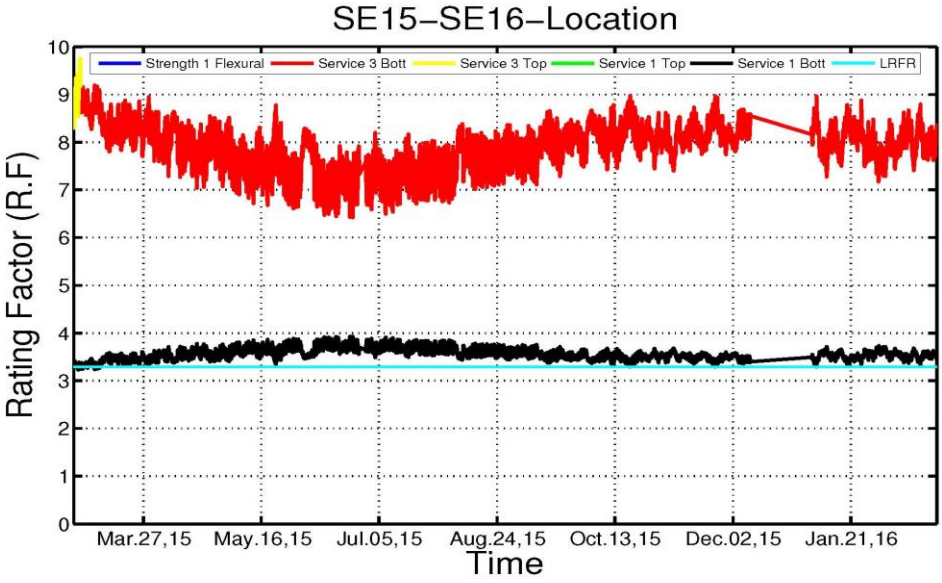
SE15–SE16–Location
Strength 1 Flexural
Service 3 Bott
Service 3 Top
Service 1 Top
Service 1 Bott
LRFR
Rating Factor (R.F)
0
1
2
3
4
5
6
7
8
9
10
Mar.27,15
May.16,15
Jul.05,15
Aug.24,15
Oct.13,15
Dec.02,15
Jan.21,16
Time

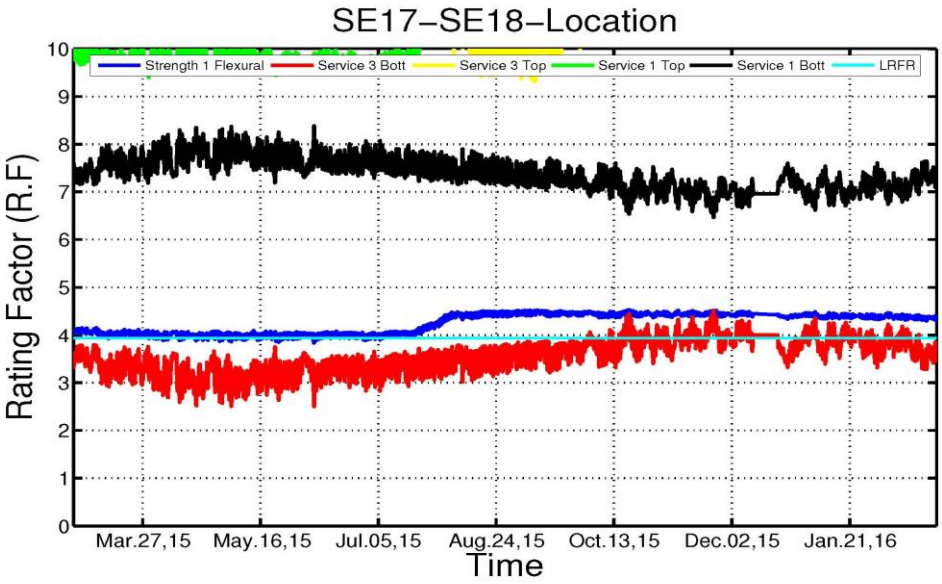
SE17–SE18–Location
Strength 1 Flexural
Service 3 Bott
Service 3 Top
Service 1 Top
Service 1 Bott
LRFR
Rating Factor (R.F)
0
1
2
3
4
5
6
7
8
9
10
Mar.27,15
May.16,15
Jul.05,15
Aug.24,15
Oct.13,15
Dec.02,15
Jan.21,16
Time

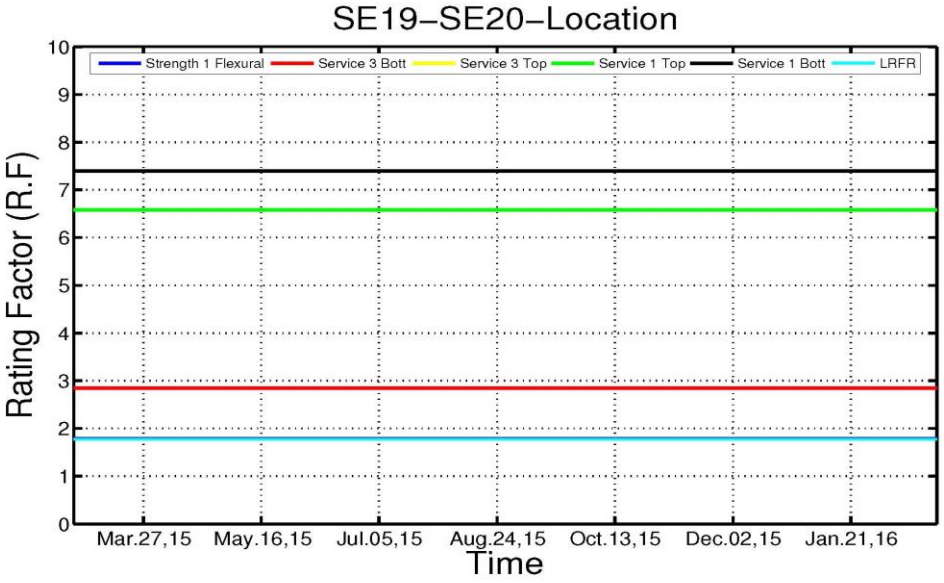
SE19–SE20–Location
Strength 1 Flexural
Service 3 Bott
Service 3 Top
Service 1 Top
Service 1 Bott
LRFR
Rating Factor (R.F)
0
1
2
3
4
5
6
7
8
9
10
Mar.27,15
May.16,15
Jul.05,15
Aug.24,15
Oct.13,15
Dec.02,15
Jan.21,16
Time

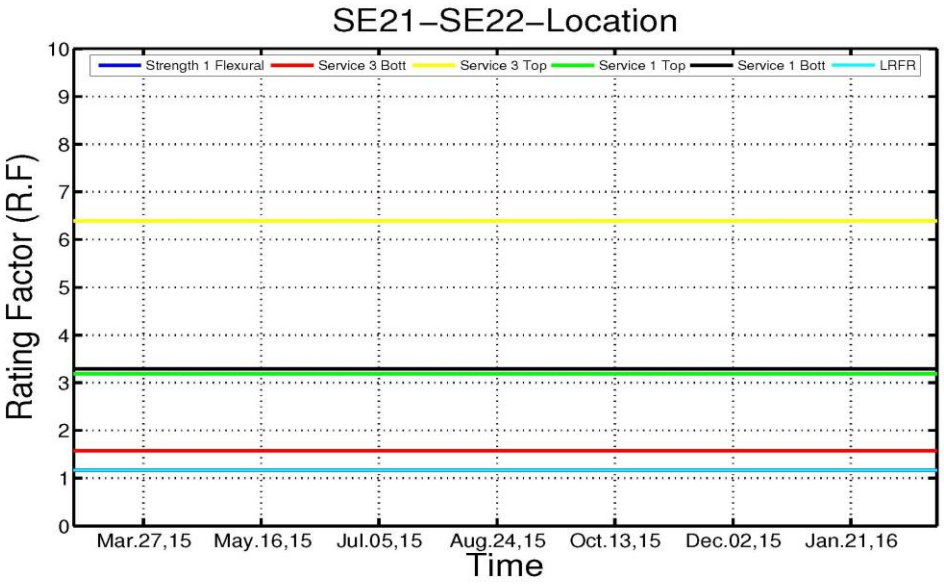
SE21–SE22–Location
Strength 1 Flexural
Service 3 Bott
Service 3 Top
Service 1 Top
Service 1 Bott
LRFR
Rating Factor (R.F)
0
1
2
3
4
5
6
7
8
9
10
Mar.27,15
May.16,15
Jul.05,15
Aug.24,15
Oct.13,15
Dec.02,15
Jan.21,16
Time

D.2 High Frequency Rating Factor Report

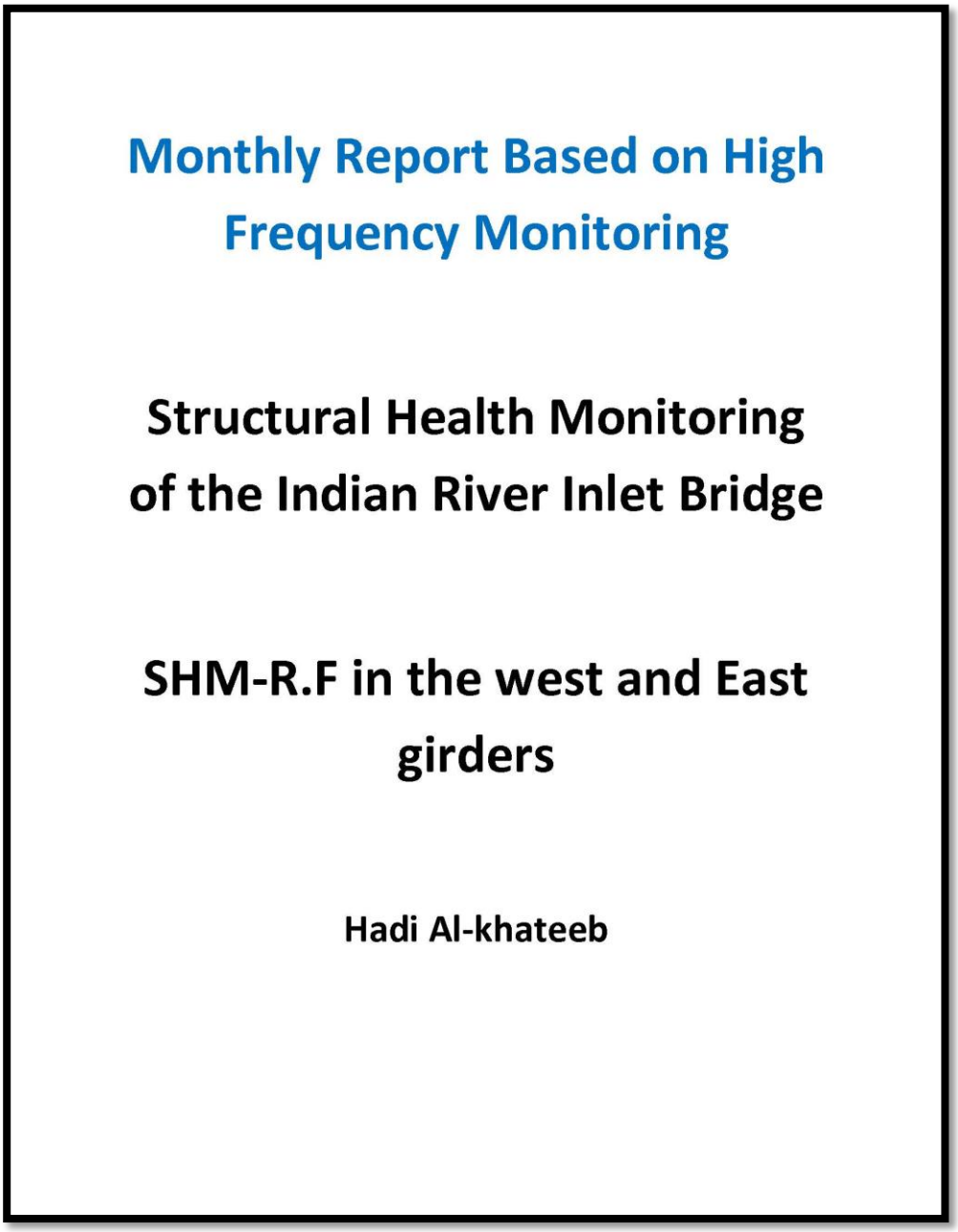

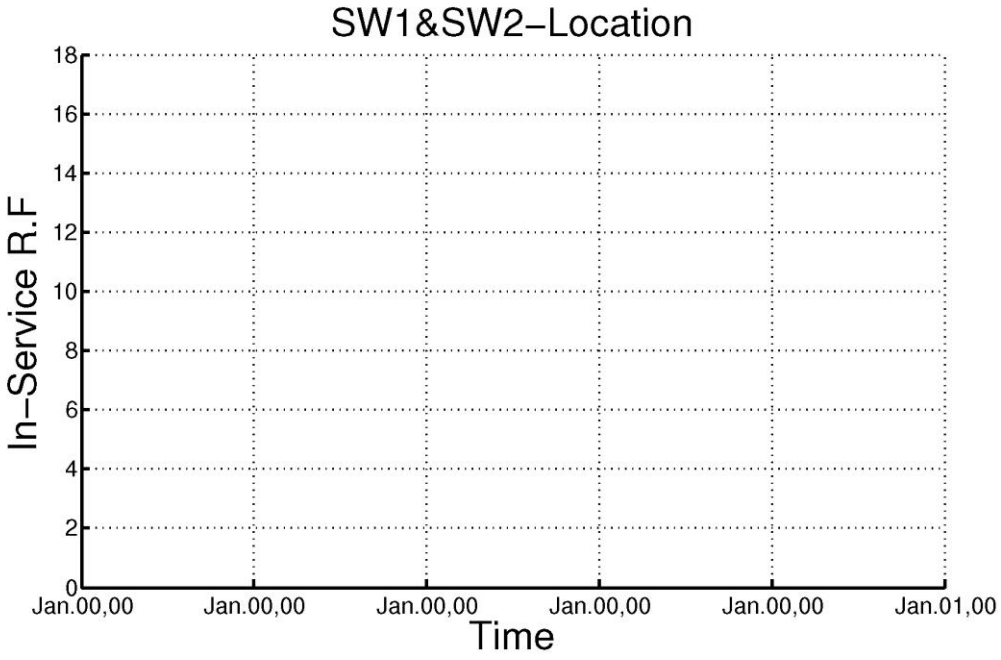
SW1&SW2–Location
In–Service R.F
0
2
4
6
8
10
12
14
16
18
Jan.00,00
Jan.00,00
Jan.00,00
Jan.00,00
Jan.00,00
Jan.01,00
Time

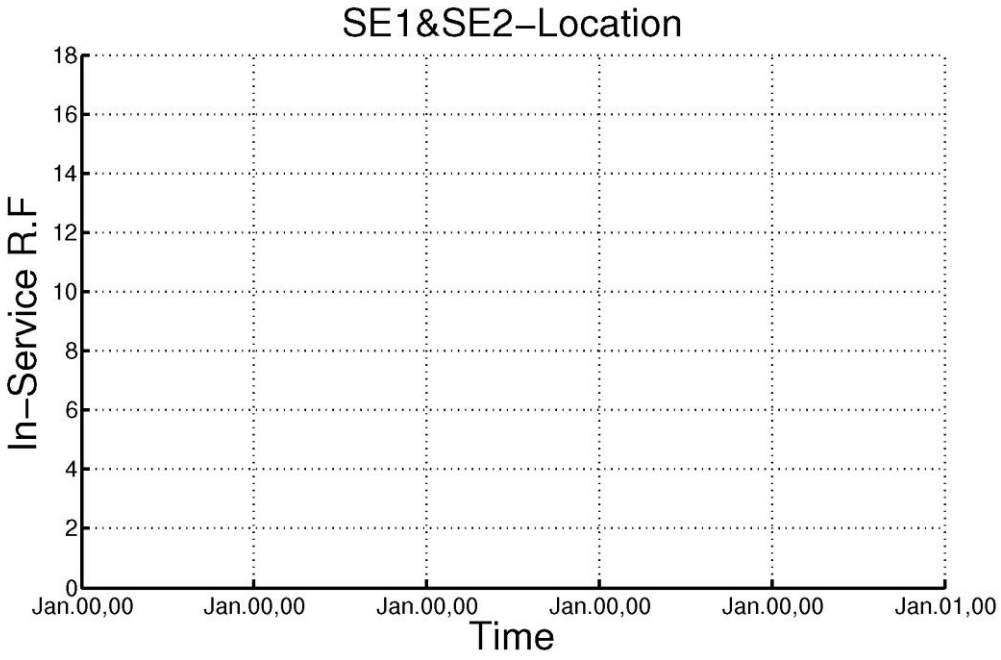
SE1&SE2–Location
In–Service R.F
0
2
4
6
8
10
12
14
16
18
Jan.00,00
Jan.00,00
Jan.00,00
Jan.00,00
Jan.00,00
Jan.01,00
Time

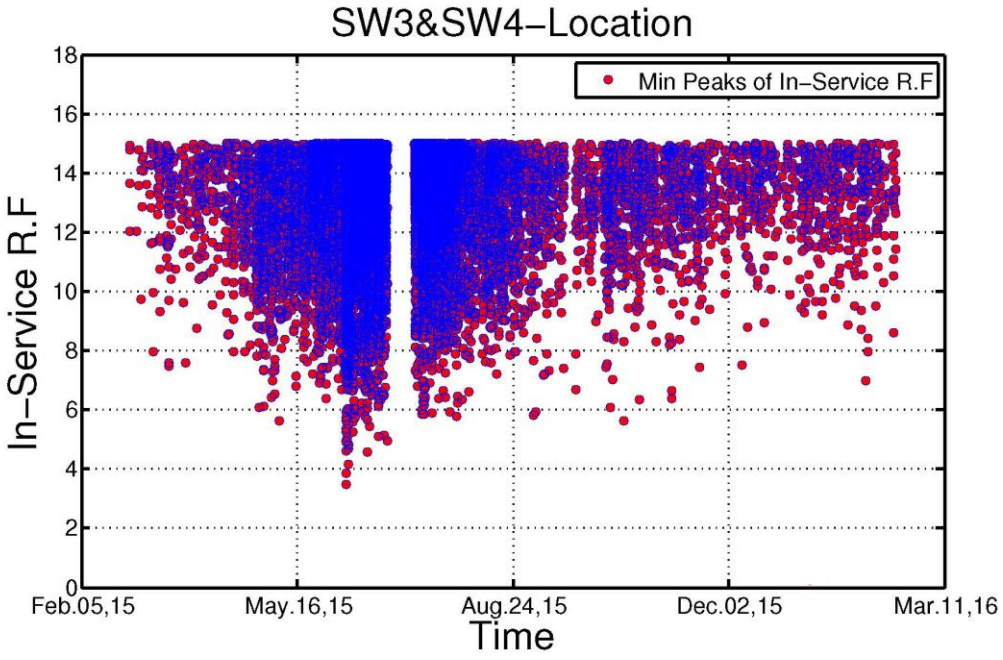
SW3&SW4–Location
Min Peaks of In–Service R.F
In–Service R.F
0
2
4
6
8
10
12
14
16
18
Feb.05,15
May.16,15
Aug.24,15
Dec.02,15
Mar.11,16
Time

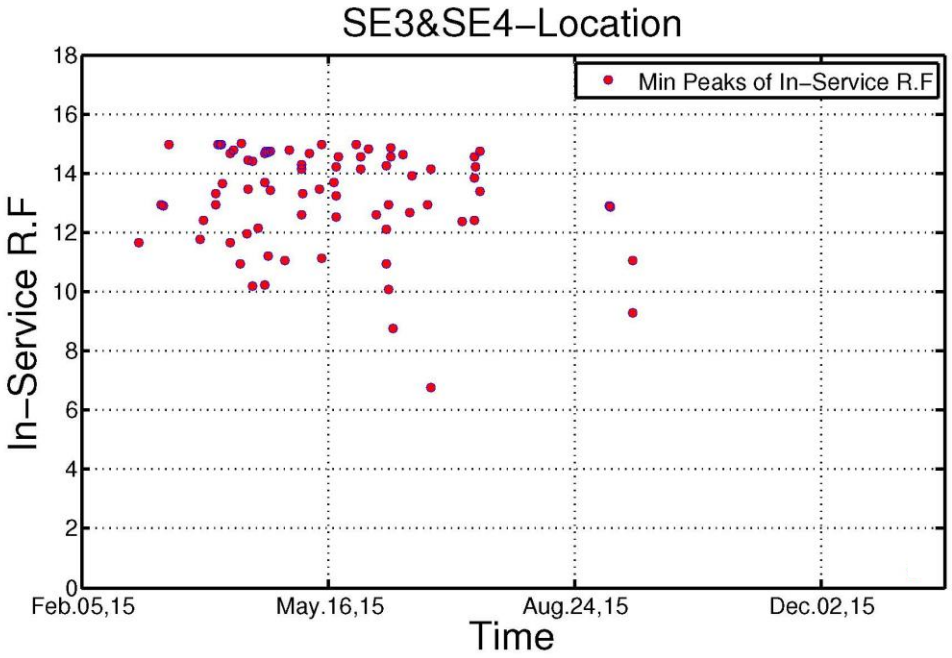
SE3&SE4–Location
Min Peaks of In–Service R.F
In–Service R.F
0
2
4
6
8
10
12
14
16
18
Feb.05,15
May.16,15
Aug.24,15
Dec.02,15
Time

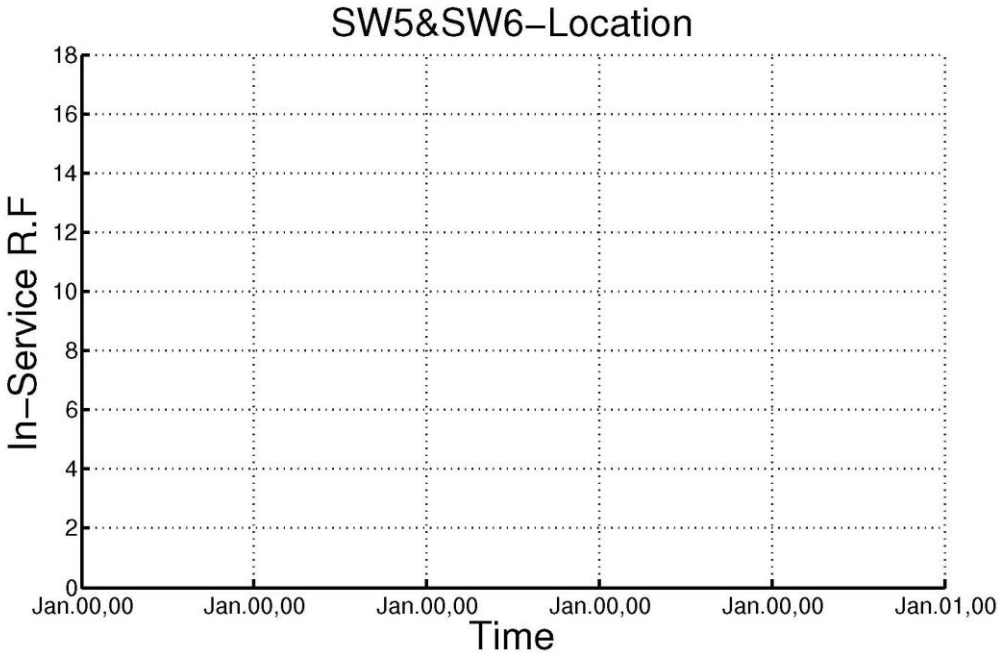
SW5&SW6–Location
In–Service R.F
0
2
4
6
8
10
12
14
16
18
Jan.00,00
Jan.00,00
Jan.00,00
Jan.00,00
Jan.00,00
Jan.01,00
Time

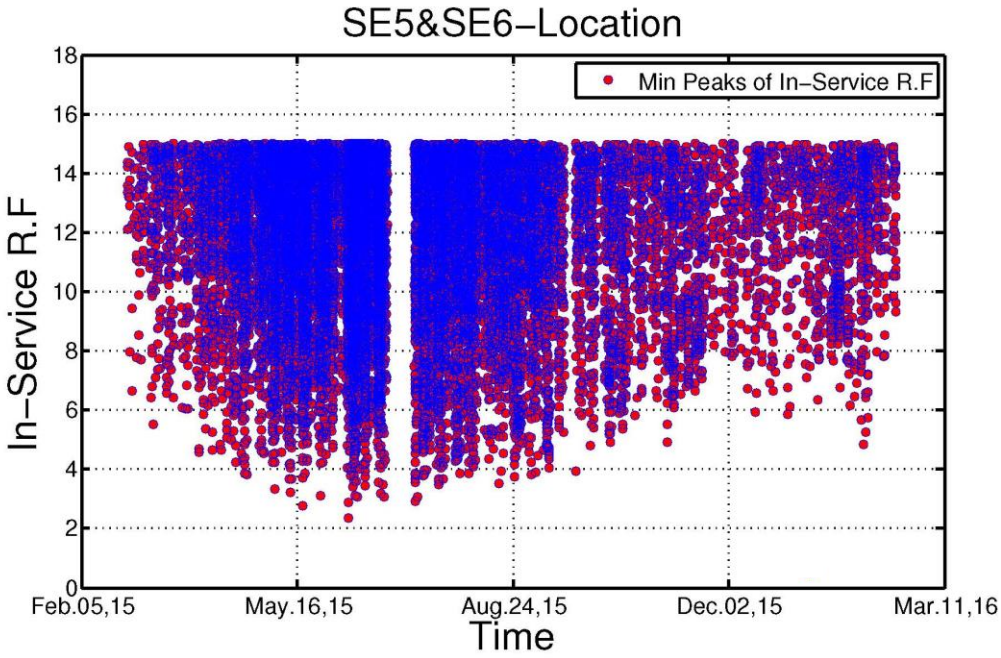
SE5&SE6–Location
Min Peaks of In–Service R.F
In–Service R.F
0
2
4
6
8
10
12
14
16
18
Feb.05,15
May.16,15
Aug.24,15
Dec.02,15
Mar.11,16
Time

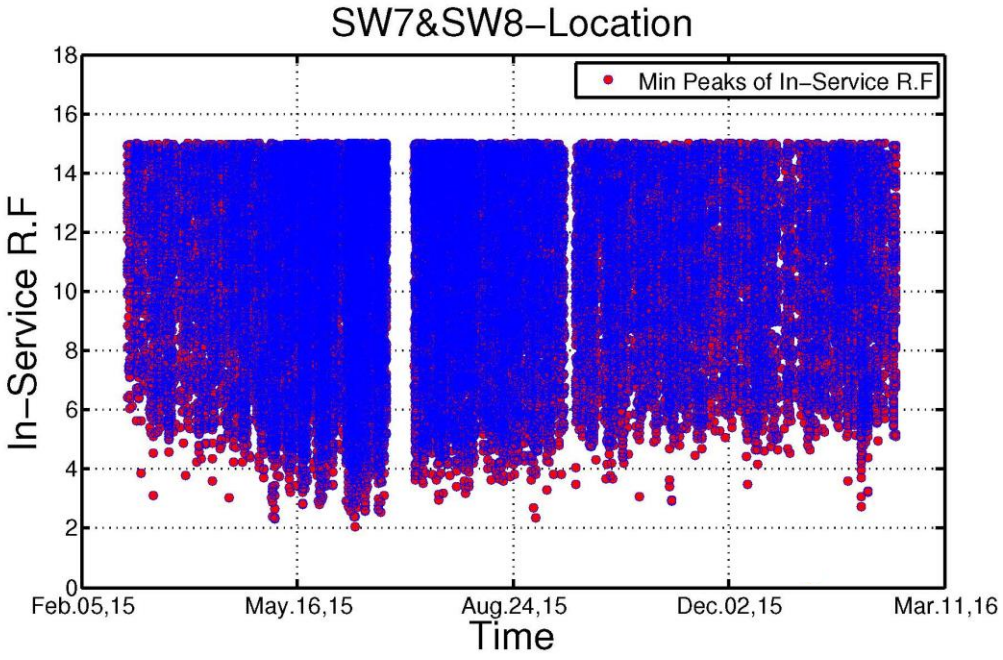
SW7&SW8–Location
Min Peaks of In–Service R.F
In–Service R.F
0
2
4
6
8
10
12
14
16
18
Feb.05,15
May.16,15
Aug.24,15
Dec.02,15
Mar.11,16
Time

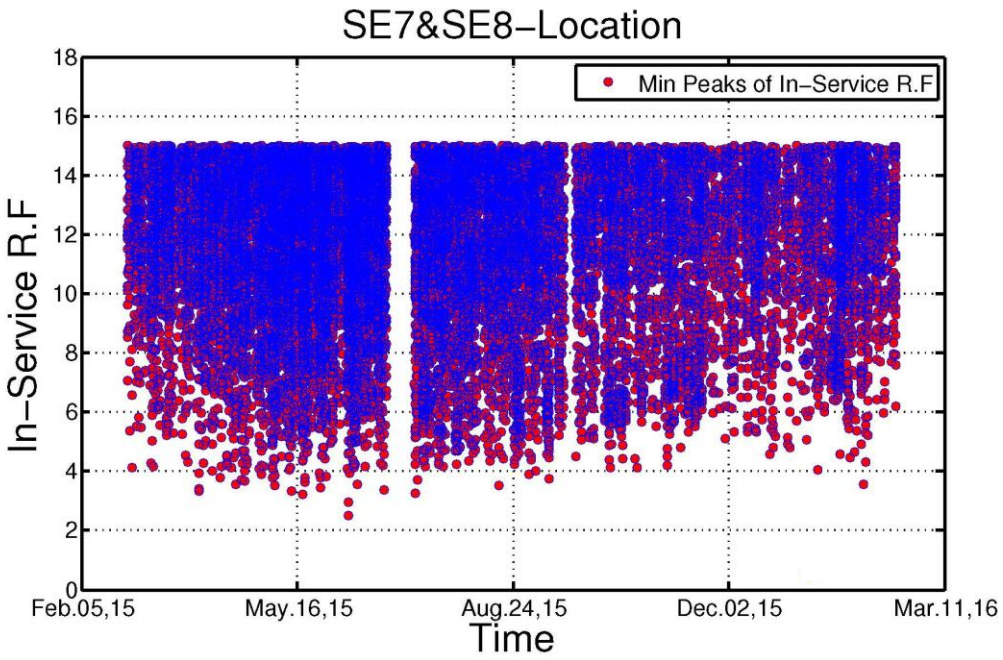
SE7&SE8–Location
Min Peaks of In–Service R.F
In–Service R.F
0
2
4
6
8
10
12
14
16
18
Feb.05,15
May.16,15
Aug.24,15
Dec.02,15
Mar.11,16
Time

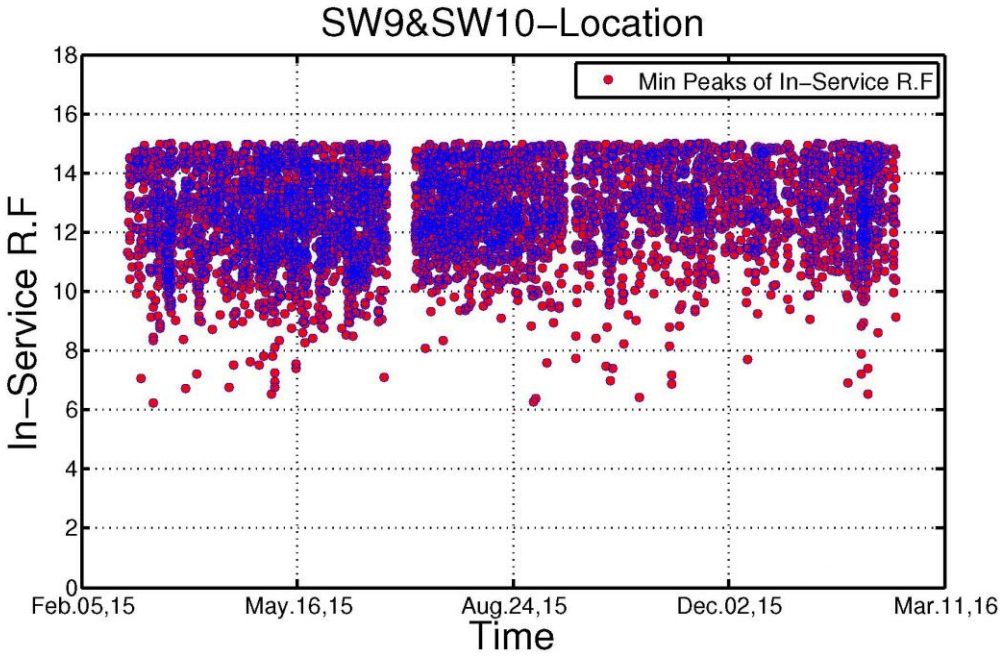
SW9&SW10−Location
Min Peaks of In−Service R.F
In−Service R.F
0
2
4
6
8
10
12
14
16
18
Feb.05,15
May.16,15
Aug.24,15
Dec.02,15
Mar.11,16
Time

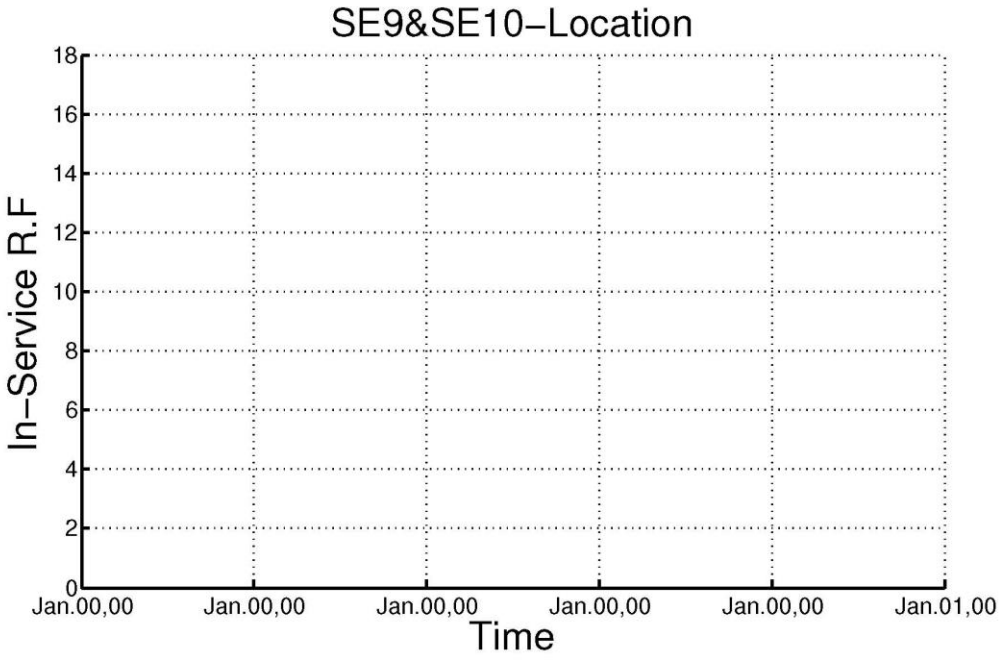
SE9&SE10−Location
In−Service R.F
0
2
4
6
8
10
12
14
16
18
Jan.00,00
Jan.00,00
Jan.00,00
Jan.00,00
Jan.00,00
Jan.01,00
Time

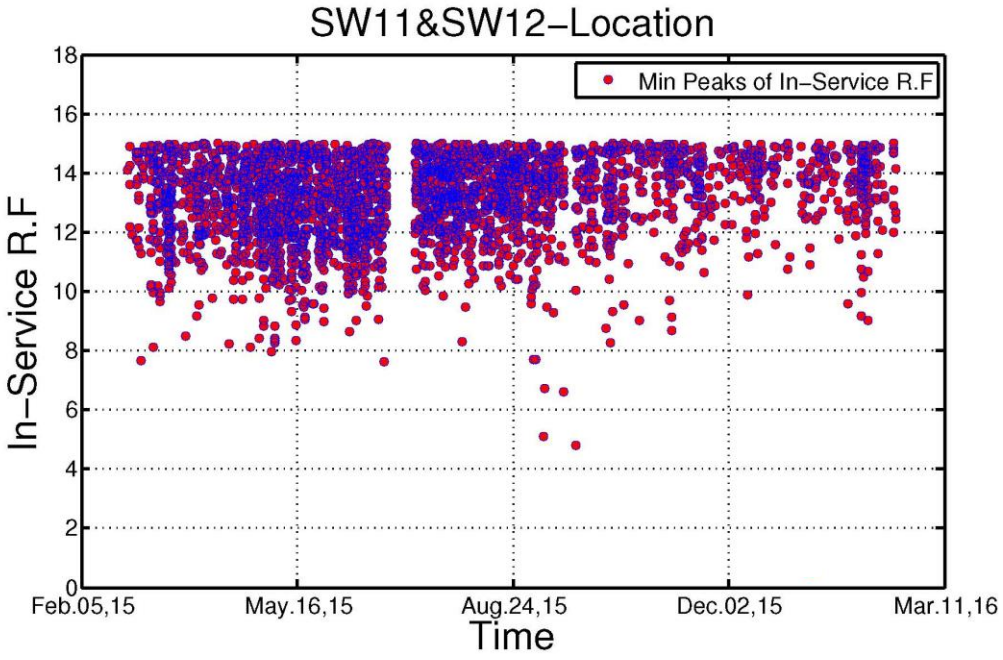
SW11&SW12−Location
Min Peaks of In−Service R.F
In−Service R.F
0
2
4
6
8
10
12
14
16
18
Feb.05,15
May.16,15
Aug.24,15
Dec.02,15
Mar.11,16
Time

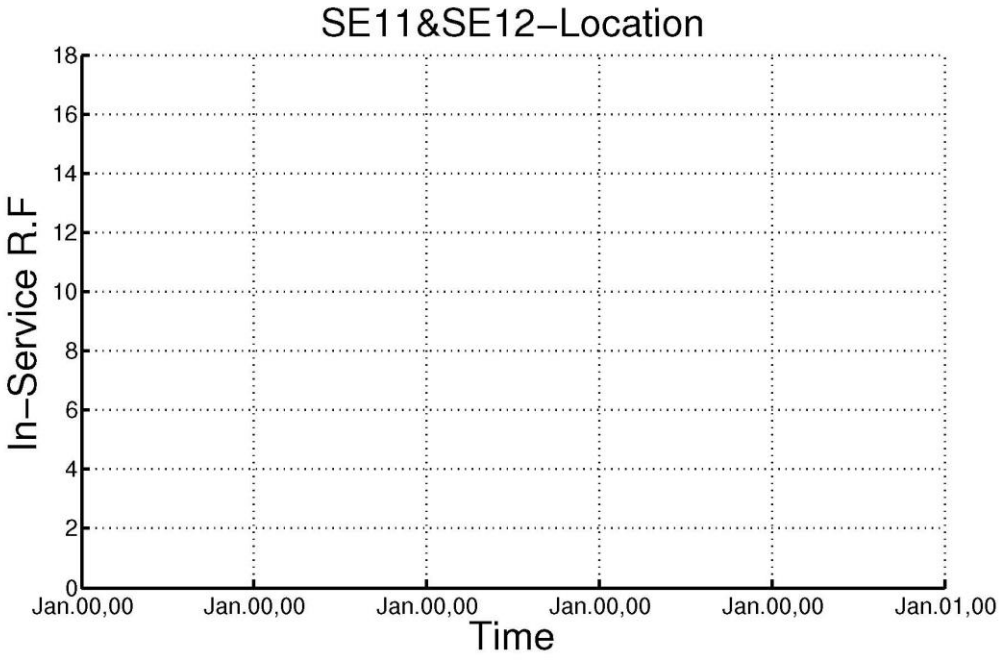
SE11&SE12−Location
In−Service R.F
0
2
4
6
8
10
12
14
16
18
Jan.00,00
Jan.00,00
Jan.00,00
Jan.00,00
Jan.00,00
Jan.01,00
Time

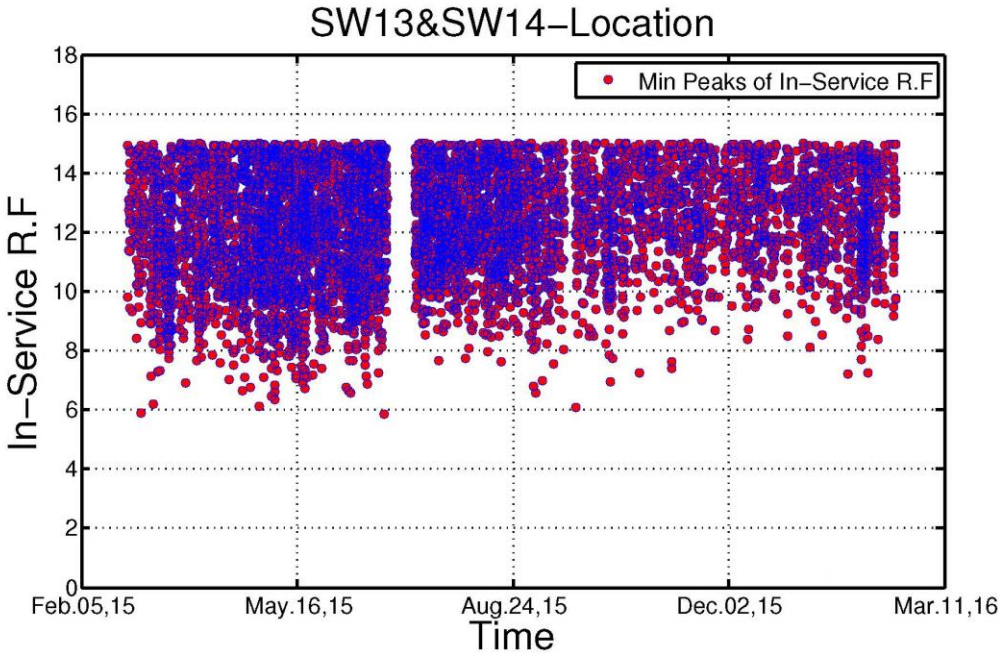
SW13&SW14−Location
Min Peaks of In−Service R.F
In−Service R.F
0
2
4
6
8
10
12
14
16
18
Feb.05,15
May.16,15
Aug.24,15
Dec.02,15
Mar.11,16
Time

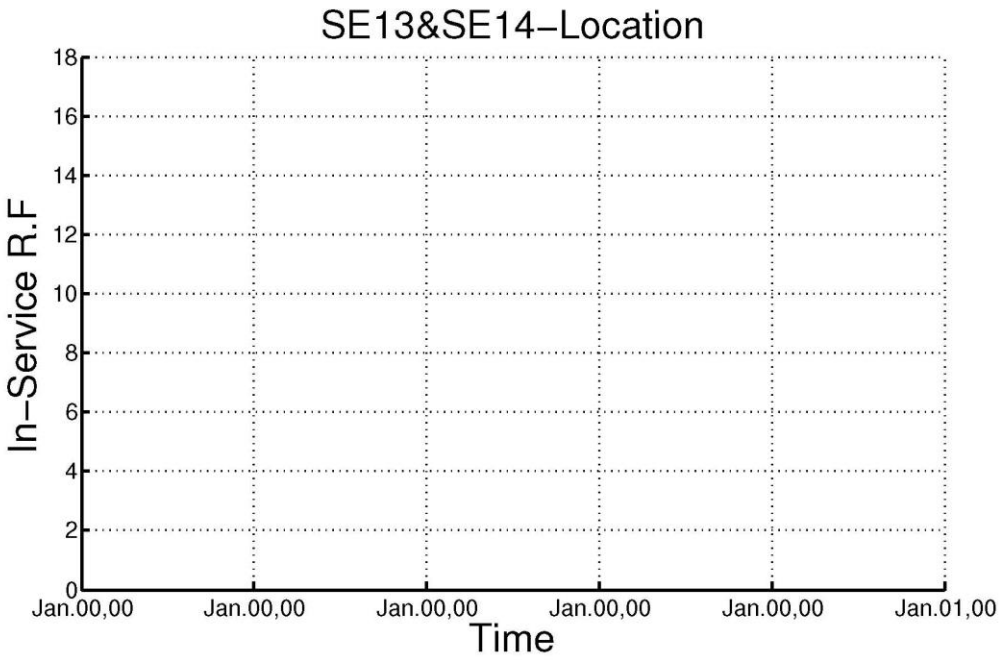
SE13&SE14−Location
In−Service R.F
0
2
4
6
8
10
12
14
16
18
Jan.00,00
Jan.00,00
Jan.00,00
Jan.00,00
Jan.00,00
Jan.01,00
Time

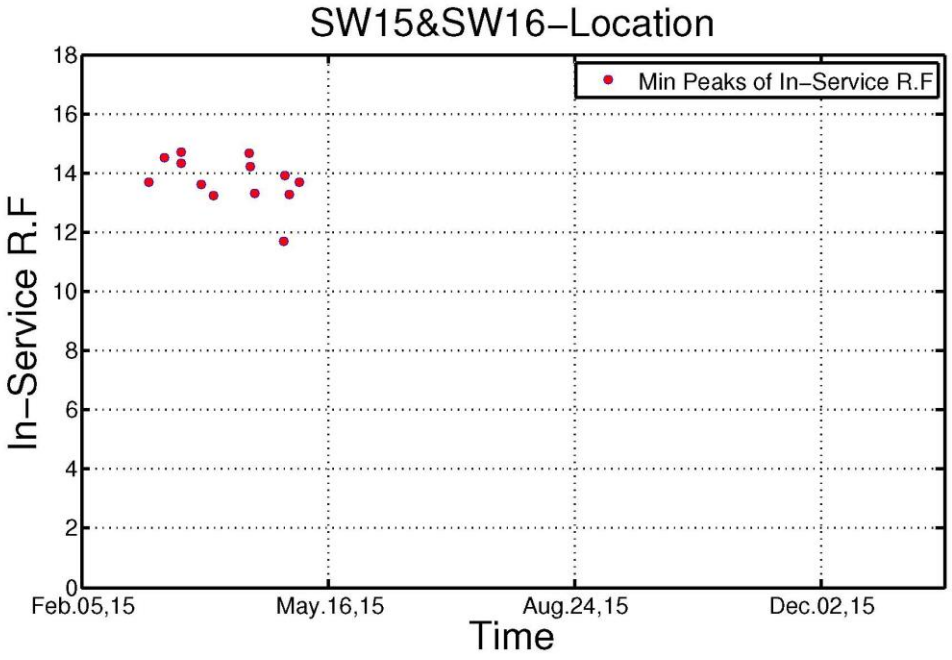
SW15&SW16−Location
Min Peaks of In−Service R.F
In−Service R.F
0
2
4
6
8
10
12
14
16
18
Feb.05,15
May.16,15
Aug.24,15
Dec.02,15
Time

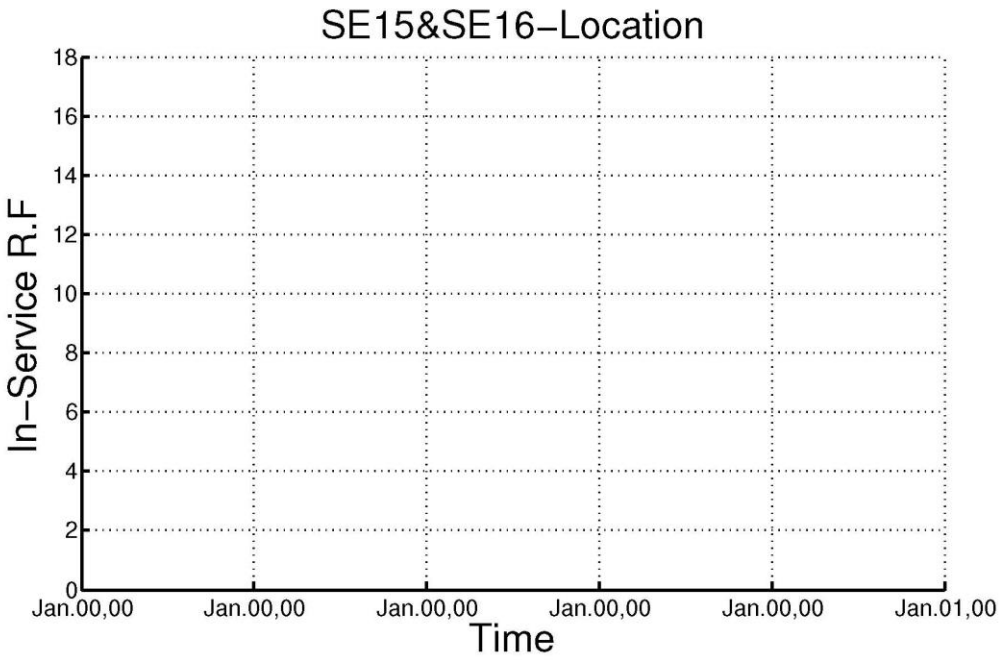
SE15&SE16−Location
In−Service R.F
0
2
4
6
8
10
12
14
16
18
Jan.00,00
Jan.00,00
Jan.00,00
Jan.00,00
Jan.00,00
Jan.01,00
Time

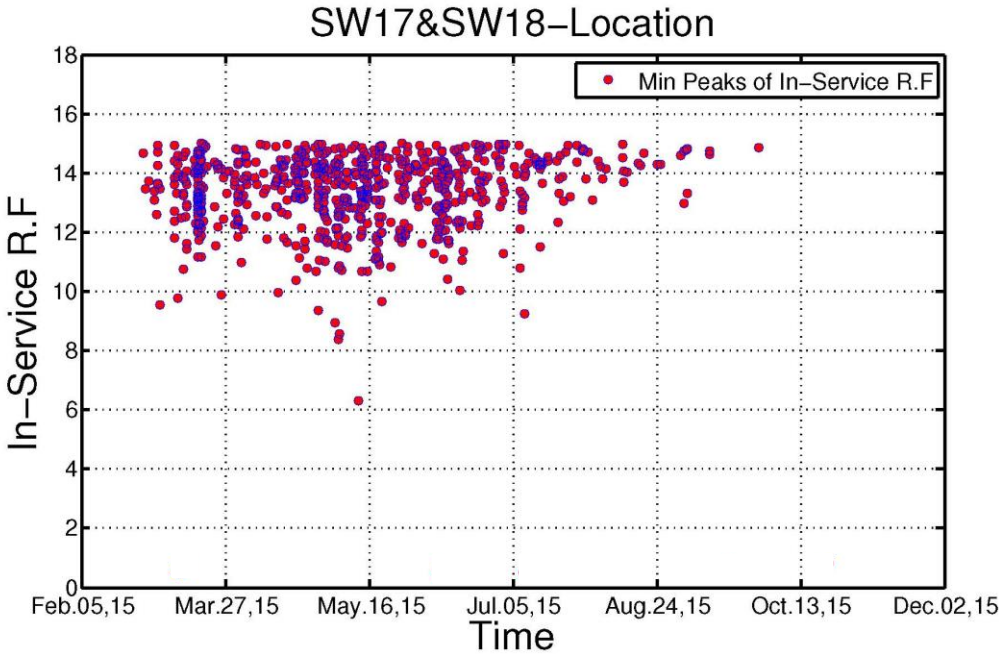
SW17&SW18−Location
Min Peaks of In−Service R.F
In−Service R.F
0
2
4
6
8
10
12
14
16
18
Feb.05,15
Mar.27,15
May.16,15
Jul.05,15
Aug.24,15
Oct.13,15
Dec.02,15
Time

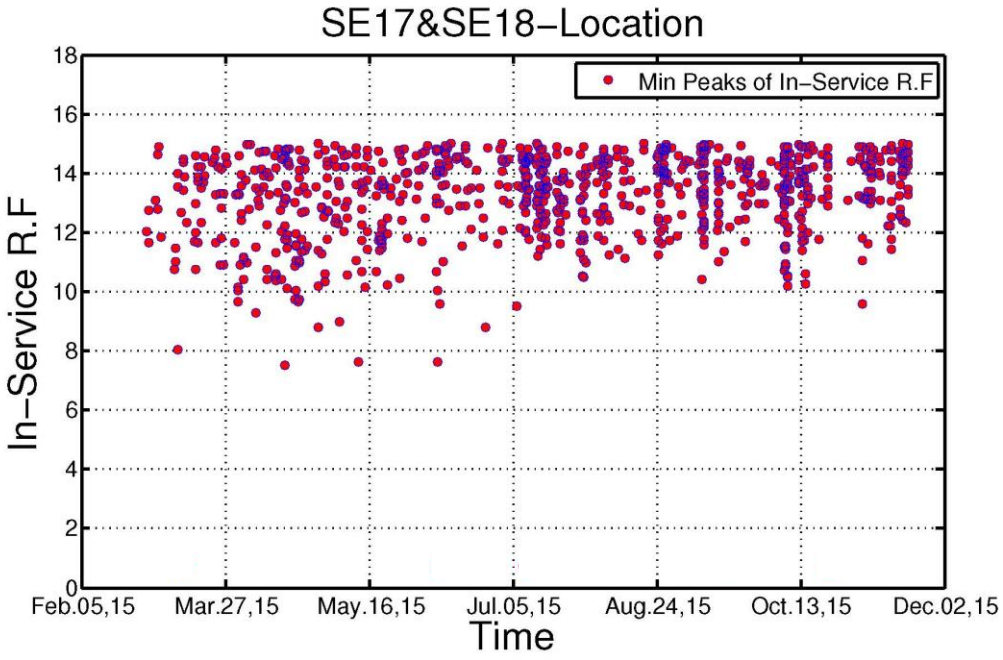
SE17&SE18−Location
Min Peaks of In−Service R.F
In−Service R.F
0
2
4
6
8
10
12
14
16
18
Feb.05,15
Mar.27,15
May.16,15
Jul.05,15
Aug.24,15
Oct.13,15
Dec.02,15
Time

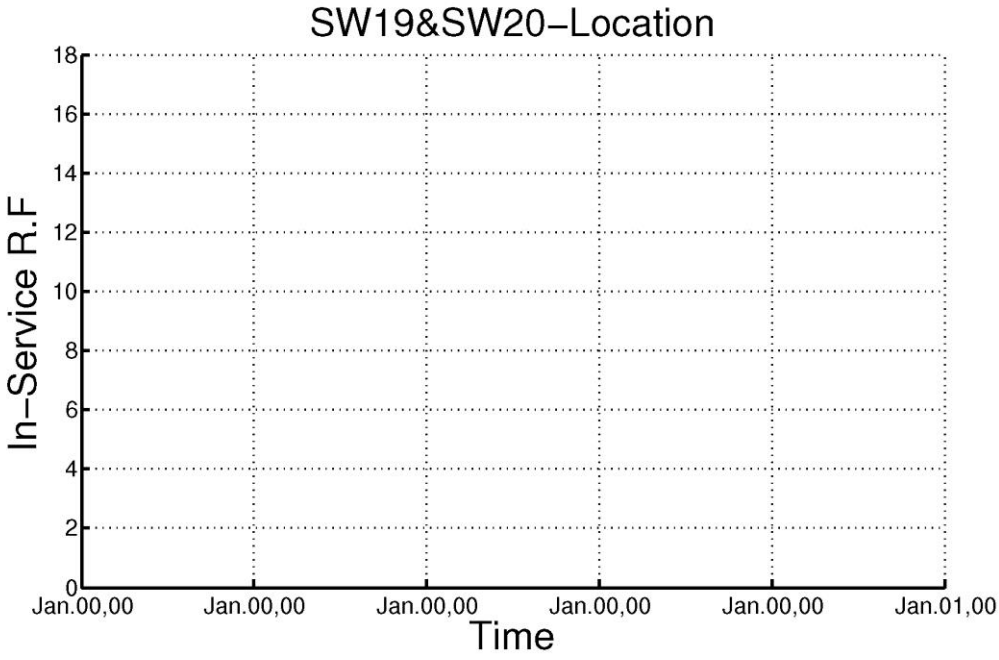
SW19&SW20−Location
In−Service R.F
0
2
4
6
8
10
12
14
16
18
Jan.00,00
Jan.00,00
Jan.00,00
Jan.00,00
Jan.00,00
Jan.01,00
Time

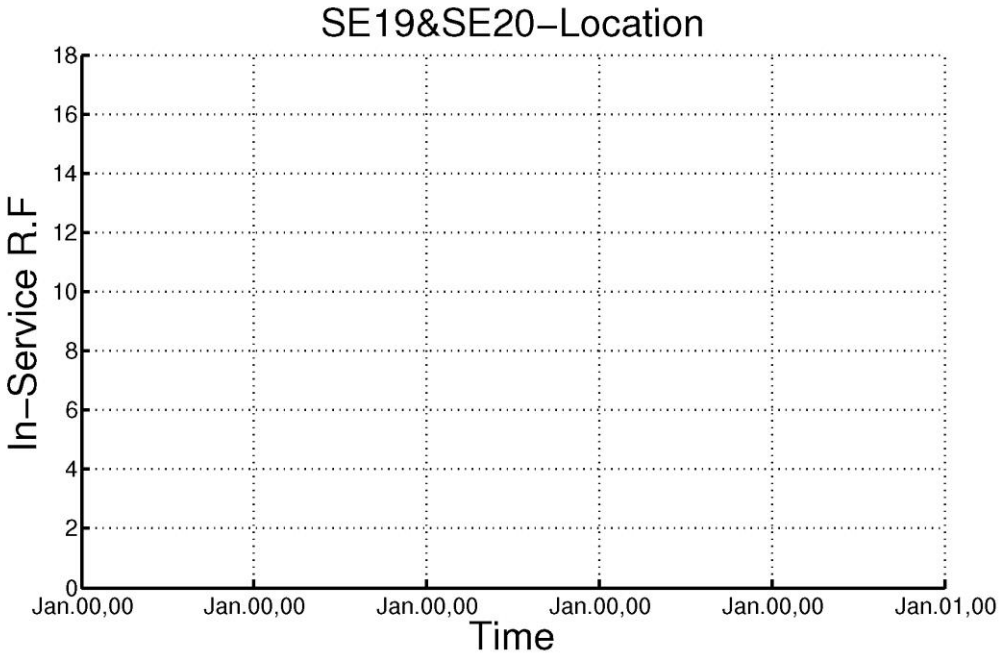
SE19&SE20−Location
In−Service R.F
0
2
4
6
8
10
12
14
16
18
Jan.00,00
Jan.00,00
Jan.00,00
Jan.00,00
Jan.00,00
Jan.01,00
Time

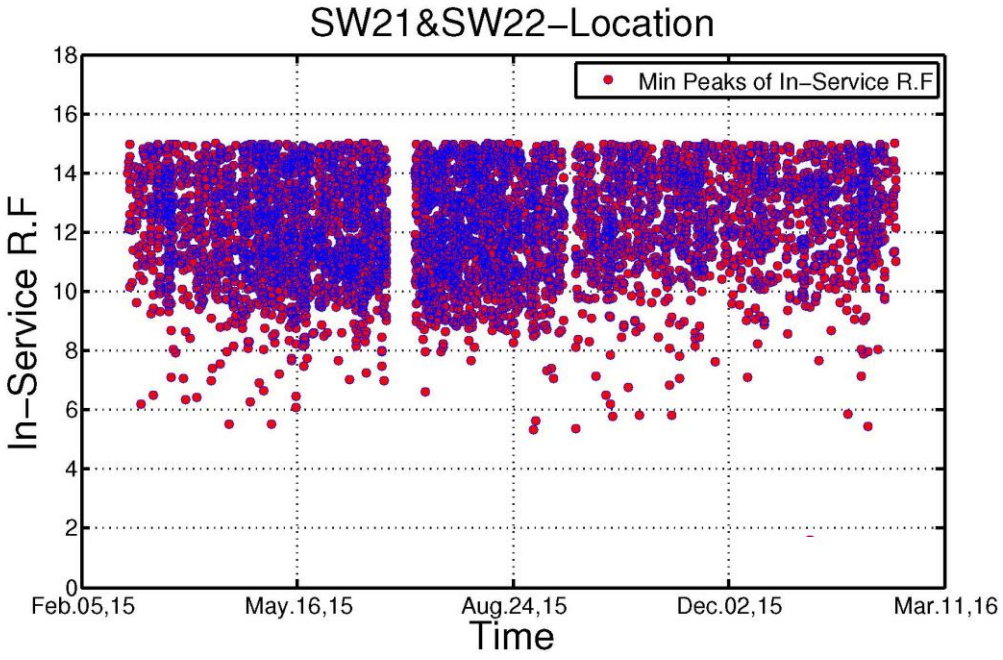
SW21&SW22−Location
Min Peaks of In−Service R.F
In−Service R.F
0
2
4
6
8
10
12
14
16
18
Feb.05,15
May.16,15
Aug.24,15
Dec.02,15
Mar.11,16
Time

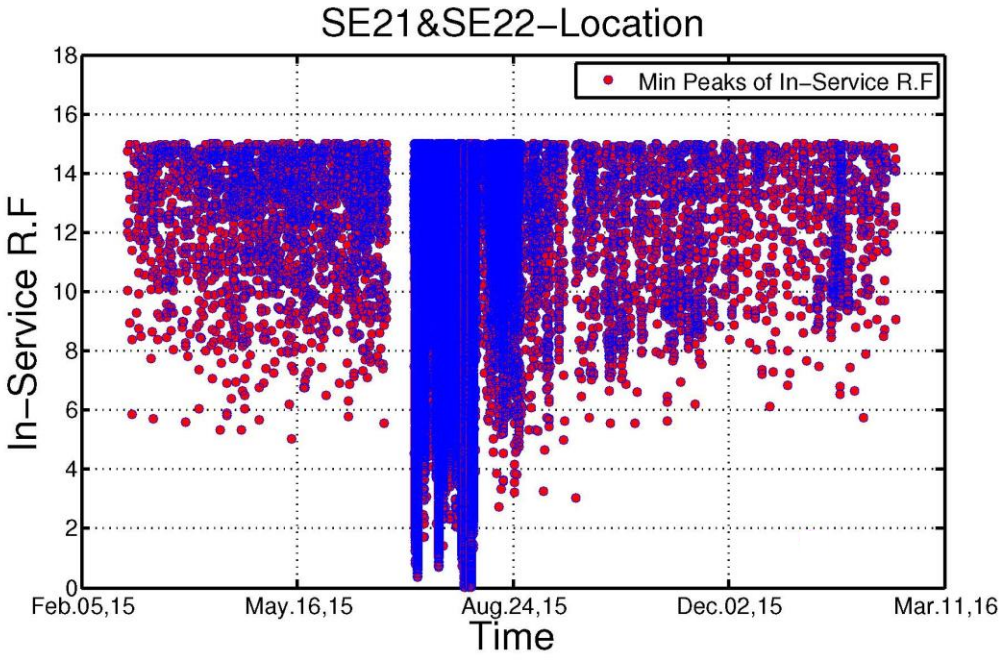
SE21&SE22−Location
Min Peaks of In−Service R.F
In−Service R.F
0
2
4
6
8
10
12
14
16
18
Feb.05,15
May.16,15
Aug.24,15
Dec.02,15
Mar.11,16
Time

D.3 Combined Rating Factor Report

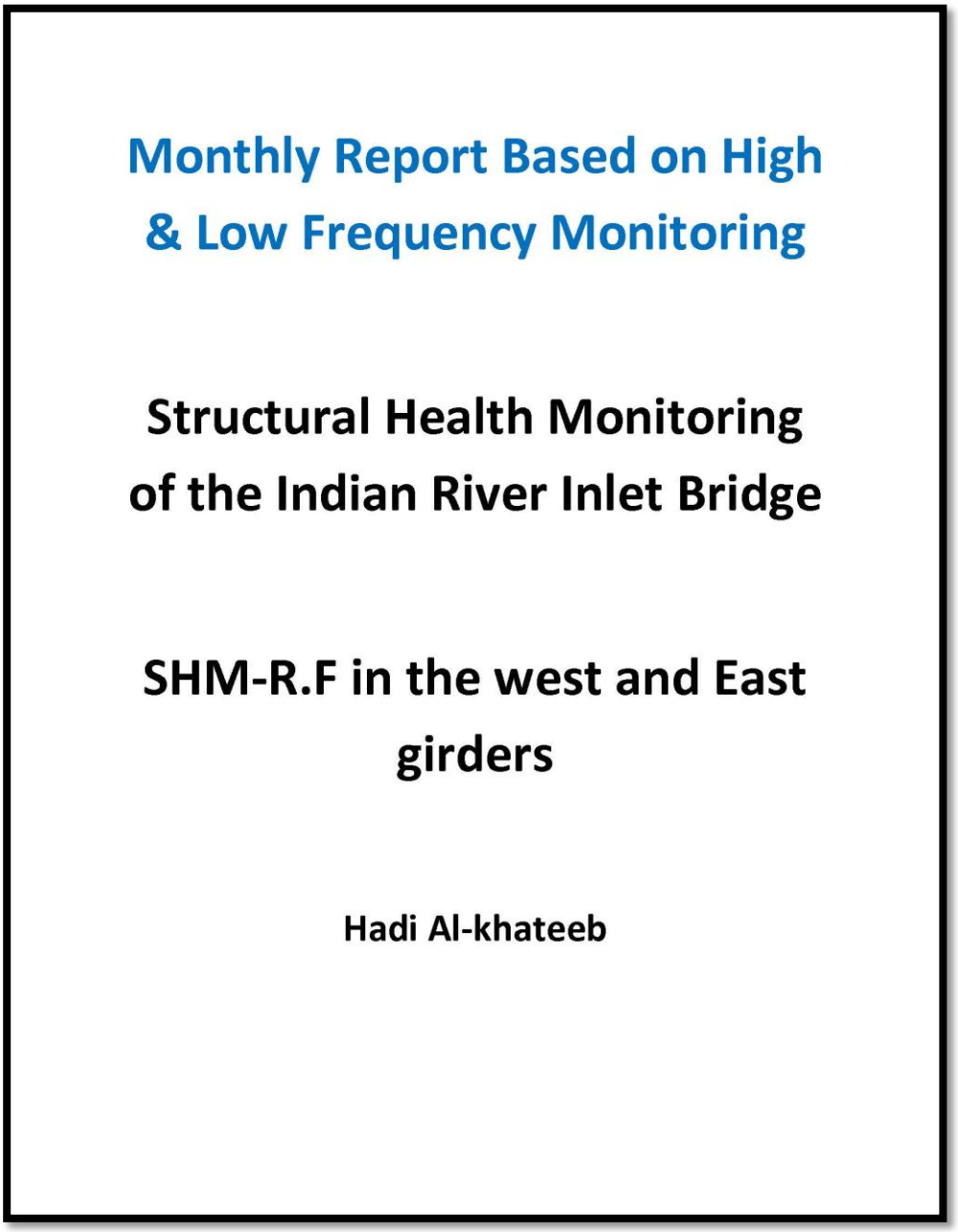

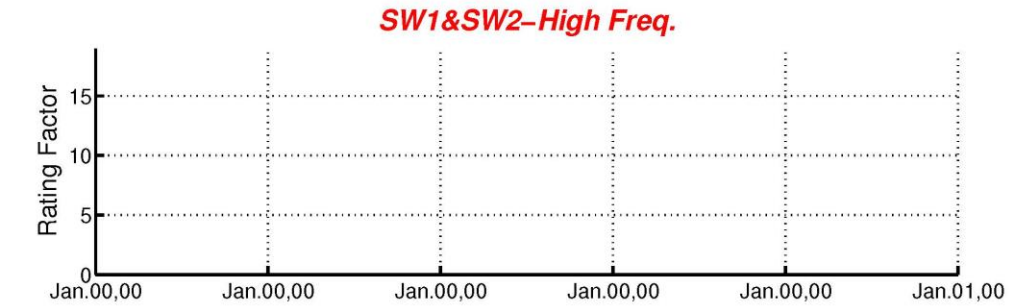
SW1&SW2–High Freq.
Rating Factor
15
10
5
0
Jan.00,00
Jan.00,00
Jan.00,00
Jan.00,00
Jan.00,00
Jan.01,00

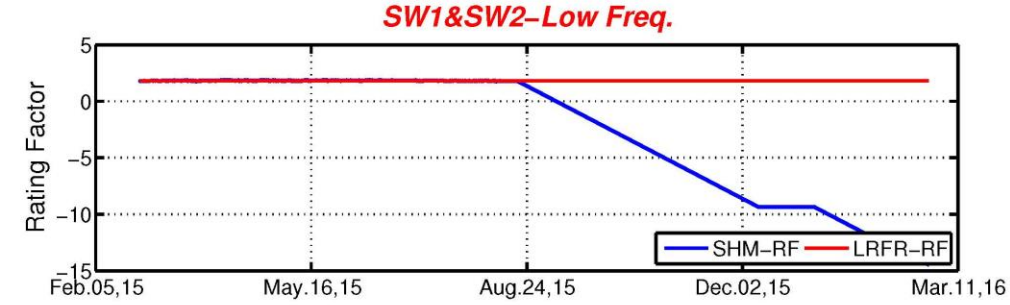
SW1&SW2–Low Freq.
Rating Factor
5
0
−5
−10
−15
SHM–RF
LRFR–RF
Feb.05,15
May.16,15
Aug.24,15
Dec.02,15
Mar.11,16

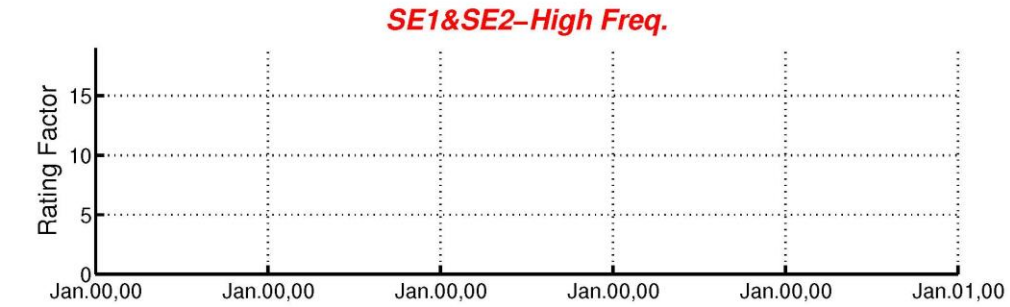
SE1&SE2–High Freq.
Rating Factor
15
10
5
0
Jan.00,00
Jan.00,00
Jan.00,00
Jan.00,00
Jan.00,00
Jan.01,00

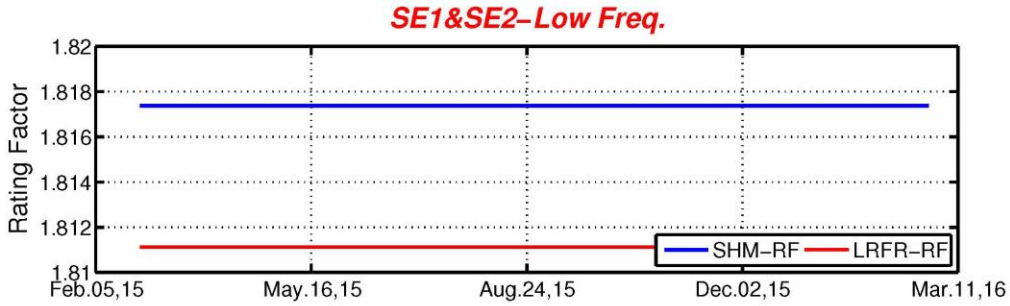
SE1&SE2–Low Freq.
Rating Factor
1.82
1.818
1.816
1.814
1.812
1.81
SHM–RF
LRFR–RF
Feb.05,15
May.16,15
Aug.24,15
Dec.02,15
Mar.11,16

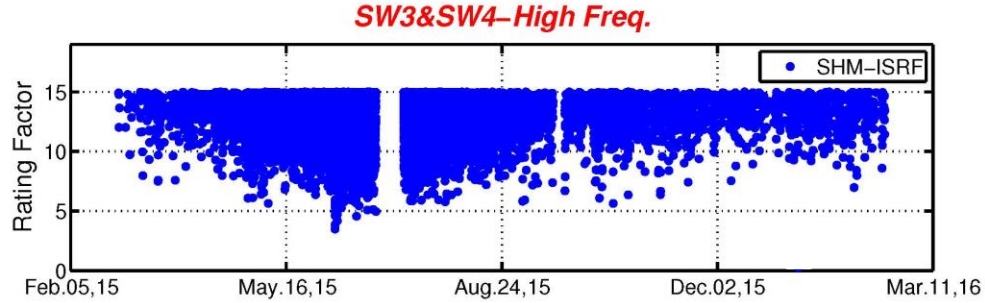
SW3&SW4–High Freq.
SHM–ISRF
Rating Factor
0
5
10
15
Feb.05,15
May.16,15
Aug.24,15
Dec.02,15
Mar.11,16

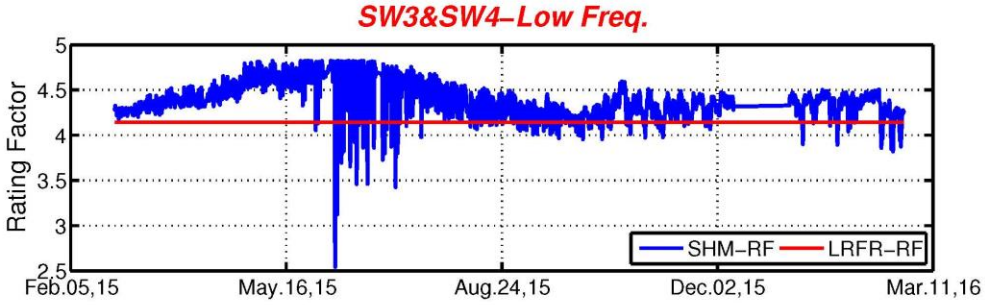
SW3&SW4–Low Freq.
SHM–RF
LRFR–RF
Rating Factor
2.5
3
3.5
4
4.5
5
Feb.05,15
May.16,15
Aug.24,15
Dec.02,15
Mar.11,16

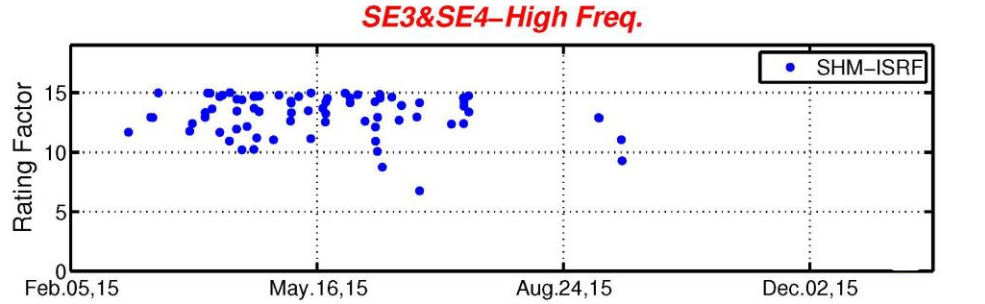
SE3&SE4–High Freq.
SHM–ISRF
Rating Factor
0
5
10
15
Feb.05,15
May.16,15
Aug.24,15
Dec.02,15

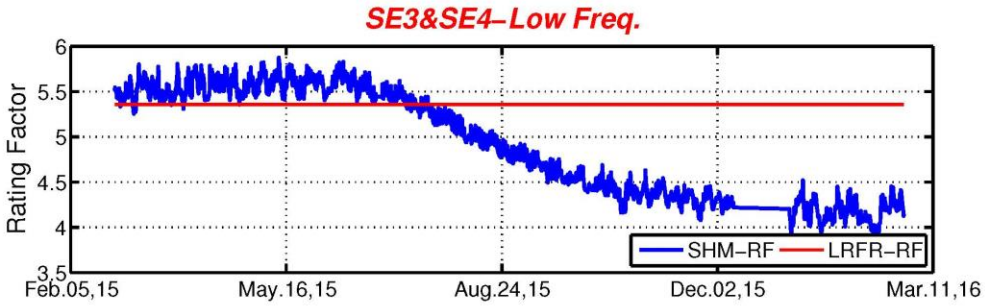
SE3&SE4–Low Freq.
SHM–RF
LRFR–RF
Rating Factor
3.5
4
4.5
5
5.5
6
Feb.05,15
May.16,15
Aug.24,15
Dec.02,15
Mar.11,16

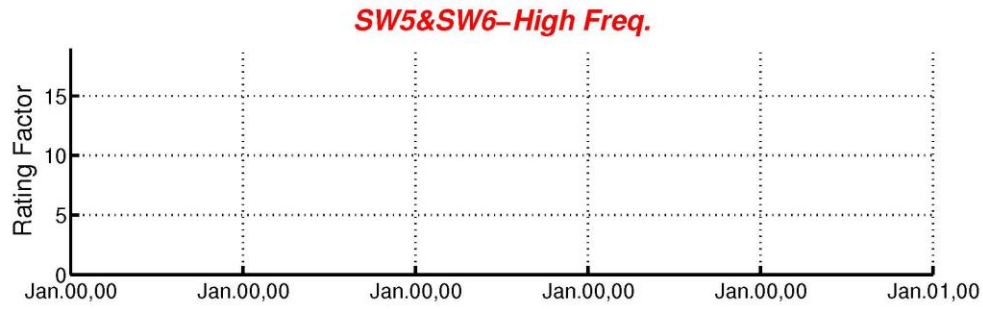
SW5&SW6–High Freq.
Rating Factor
15
10
5
0
Jan.00,00
Jan.00,00
Jan.00,00
Jan.00,00
Jan.00,00
Jan.01,00

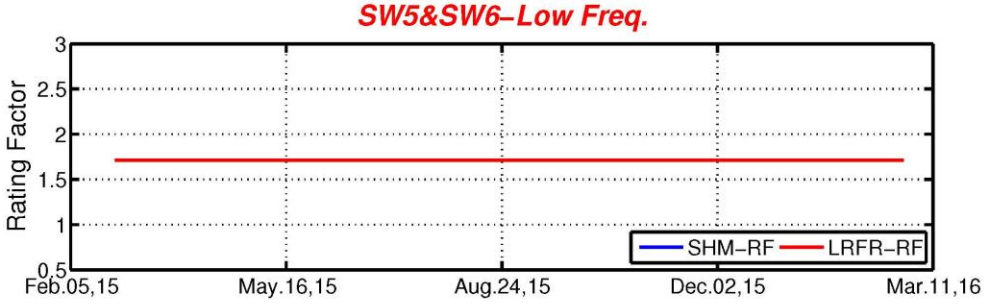
SW5&SW6–Low Freq.
Rating Factor
3
2.5
2
1.5
1
0.5
SHM–RF
LRFR–RF
Feb.05,15
May.16,15
Aug.24,15
Dec.02,15
Mar.11,16

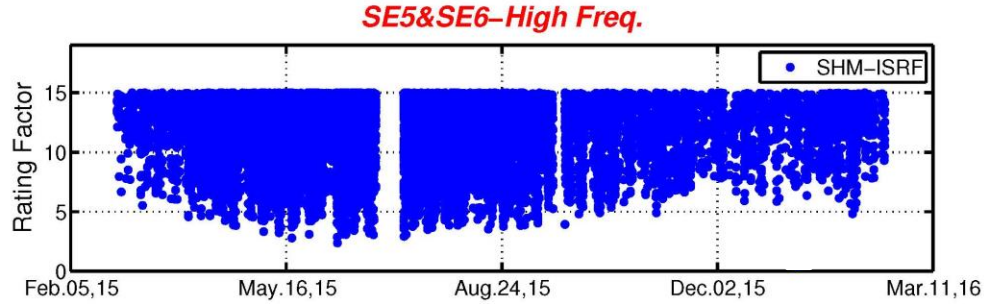
SE5&SE6–High Freq.
SHM–ISRF
Rating Factor
15
10
5
0
Feb.05,15
May.16,15
Aug.24,15
Dec.02,15
Mar.11,16

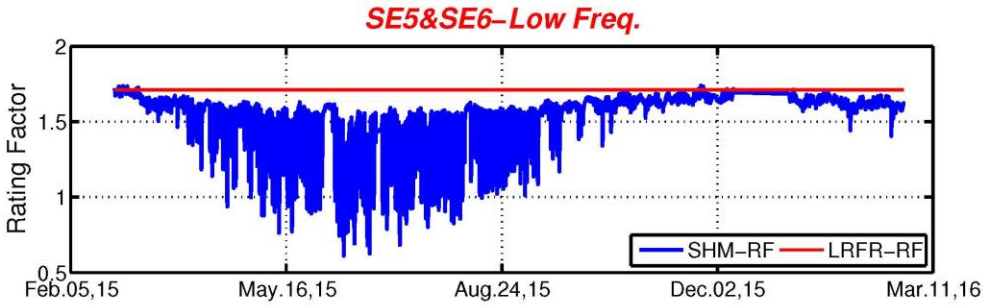
SE5&SE6–Low Freq.
Rating Factor
2
1.5
1
0.5
SHM–RF
LRFR–RF
Feb.05,15
May.16,15
Aug.24,15
Dec.02,15
Mar.11,16

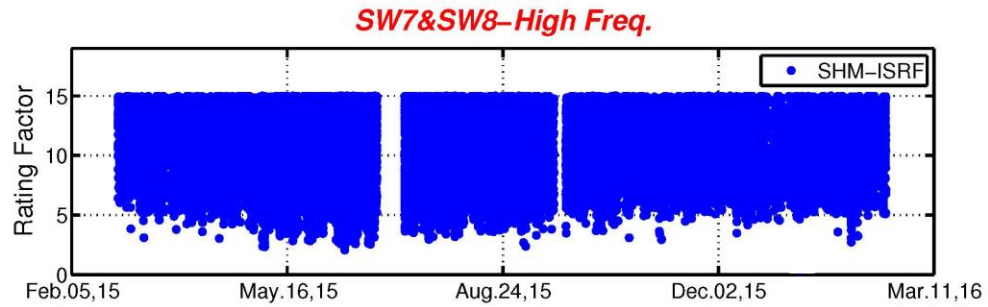
SW7&SW8–High Freq.
SHM–ISRF
Rating Factor
0
5
10
15
Feb.05,15
May.16,15
Aug.24,15
Dec.02,15
Mar.11,16

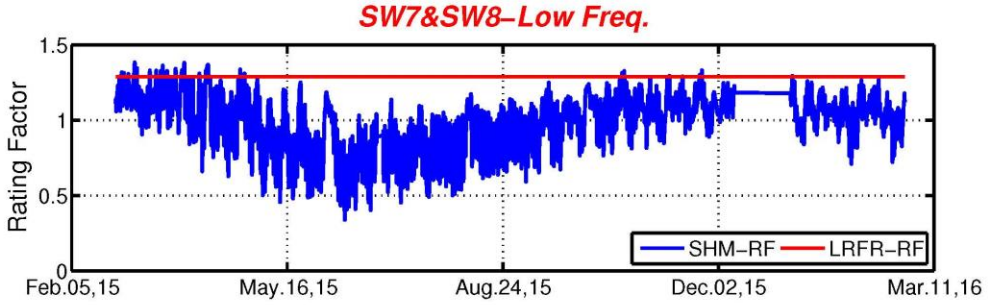
SW7&SW8–Low Freq.
SHM–RF
LRFR–RF
Rating Factor
0
0.5
1
1.5
Feb.05,15
May.16,15
Aug.24,15
Dec.02,15
Mar.11,16

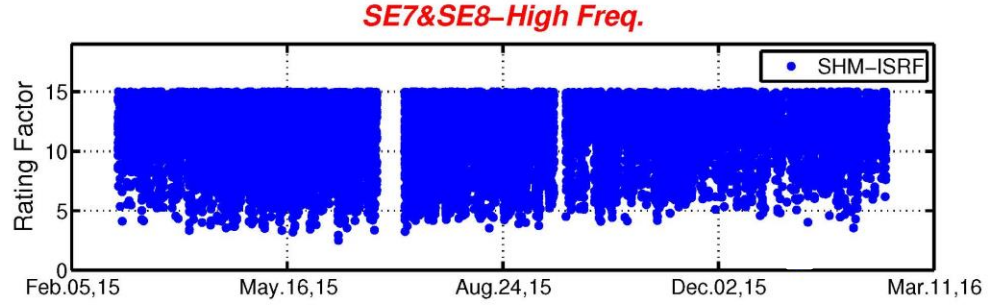
SE7&SE8–High Freq.
SHM–ISRF
Rating Factor
0
5
10
15
Feb.05,15
May.16,15
Aug.24,15
Dec.02,15
Mar.11,16

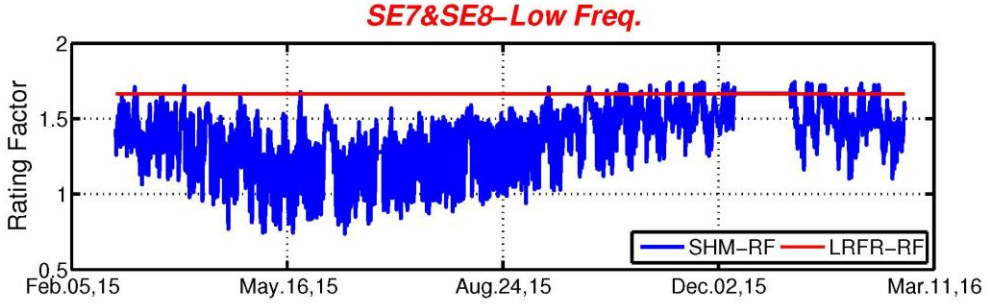
SE7&SE8–Low Freq.
SHM–RF
LRFR–RF
Rating Factor
0.5
1
1.5
2
Feb.05,15
May.16,15
Aug.24,15
Dec.02,15
Mar.11,16

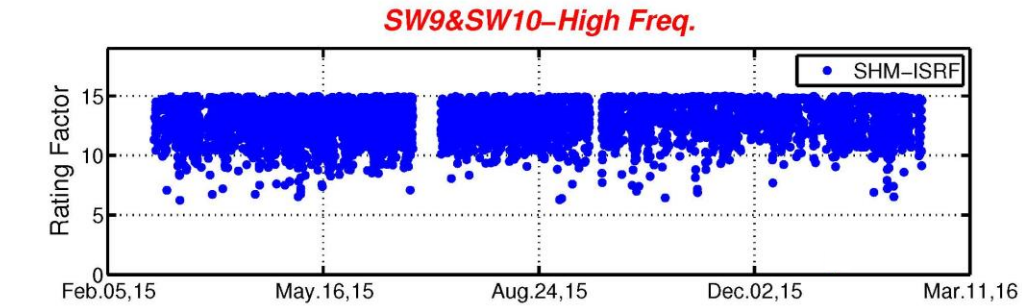
SW9&SW10–High Freq.
SHM–ISRF
Rating Factor
0
5
10
15
Feb.05,15
May.16,15
Aug.24,15
Dec.02,15
Mar.11,16

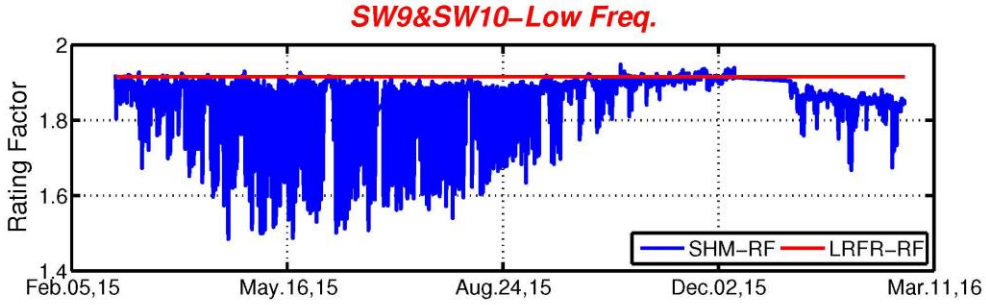
SW9&SW10–Low Freq.
SHM–RF
LRFR–RF
Rating Factor
1.4
1.6
1.8
2
Feb.05,15
May.16,15
Aug.24,15
Dec.02,15
Mar.11,16

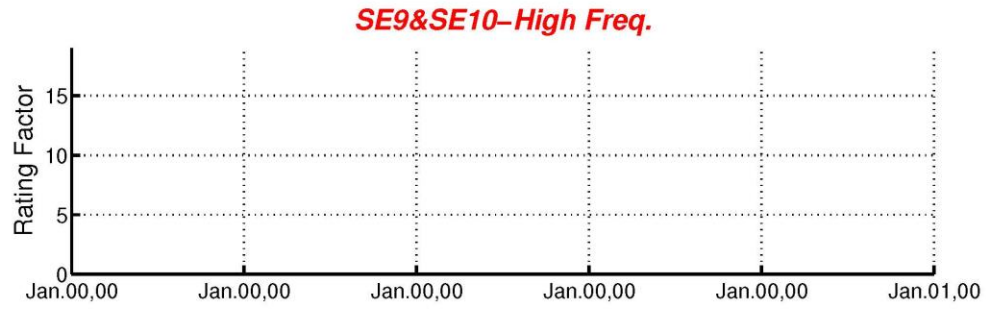
SE9&SE10–High Freq.
Rating Factor
0
5
10
15
Jan.00,00
Jan.00,00
Jan.00,00
Jan.00,00
Jan.00,00
Jan.01,00

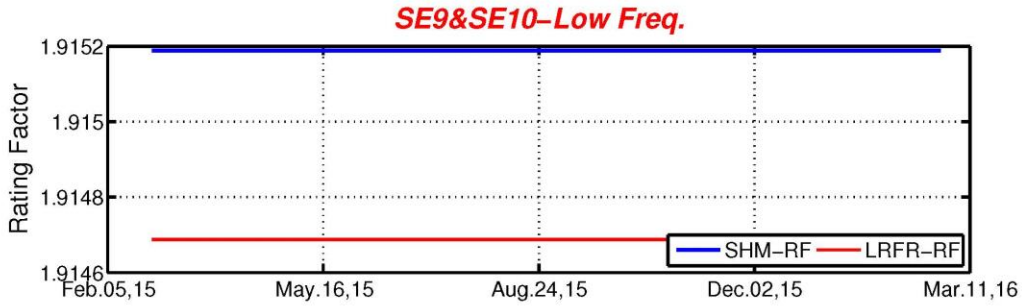
SE9&SE10–Low Freq.
SHM–RF
LRFR–RF
Rating Factor
1.9146
1.9148
1.915
1.9152
Feb.05,15
May.16,15
Aug.24,15
Dec.02,15
Mar.11,16

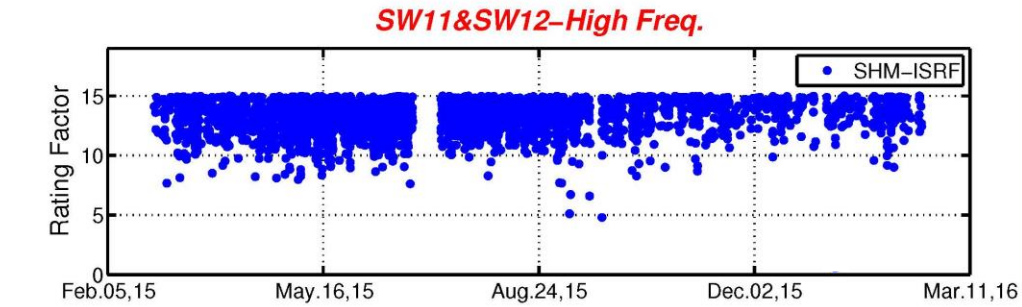
SW11&SW12–High Freq.
SHM–ISRF
Rating Factor
0
5
10
15
Feb.05,15
May.16,15
Aug.24,15
Dec.02,15
Mar.11,16

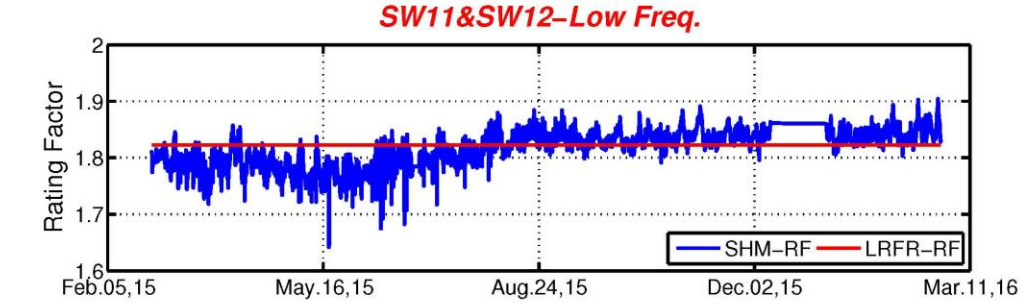
SW11&SW12–Low Freq.
SHM–RF
LRFR–RF
Rating Factor
1.6
1.7
1.8
1.9
2
Feb.05,15
May.16,15
Aug.24,15
Dec.02,15
Mar.11,16

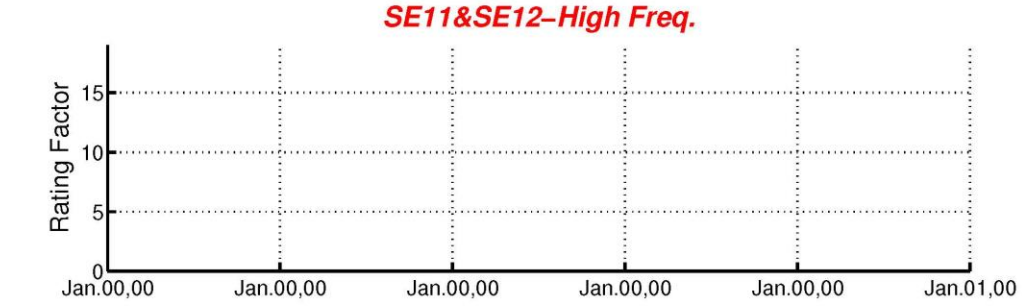
SE11&SE12–High Freq.
Rating Factor
0
5
10
15
Jan.00,00
Jan.00,00
Jan.00,00
Jan.00,00
Jan.00,00
Jan.01,00

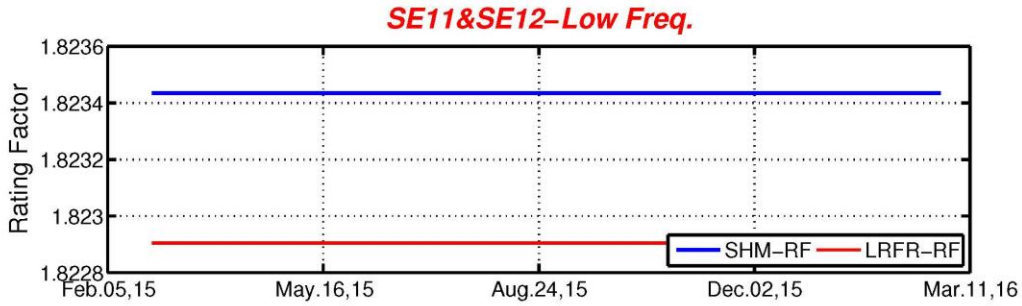
SE11&SE12–Low Freq.
SHM–RF
LRFR–RF
Rating Factor
1.8228
1.823
1.8232
1.8234
1.8236
Feb.05,15
May.16,15
Aug.24,15
Dec.02,15
Mar.11,16

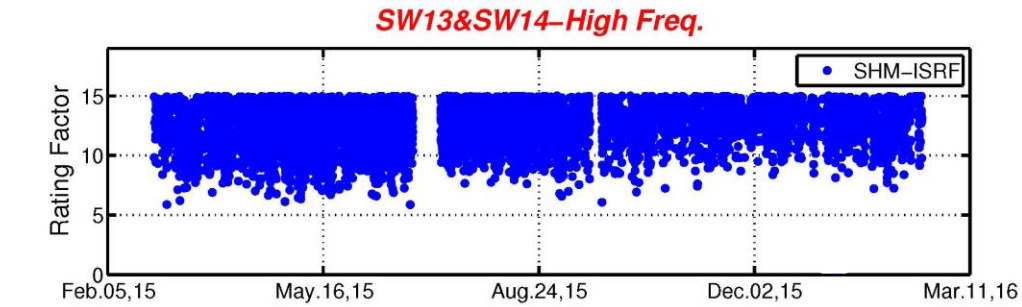
SW13&SW14–High Freq.
SHM–ISRF
Rating Factor
0
5
10
15
Feb.05,15
May.16,15
Aug.24,15
Dec.02,15
Mar.11,16

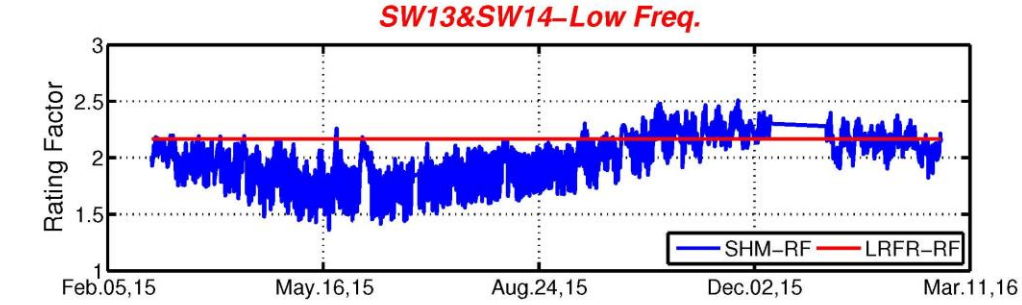
SW13&SW14–Low Freq.
SHM–RF
LRFR–RF
Rating Factor
1
1.5
2
2.5
3
Feb.05,15
May.16,15
Aug.24,15
Dec.02,15
Mar.11,16

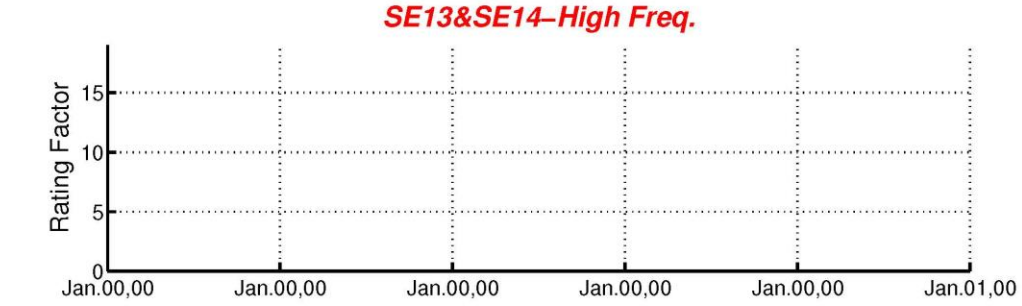
SE13&SE14–High Freq.
Rating Factor
0
5
10
15
Jan.00,00
Jan.00,00
Jan.00,00
Jan.00,00
Jan.00,00
Jan.01,00

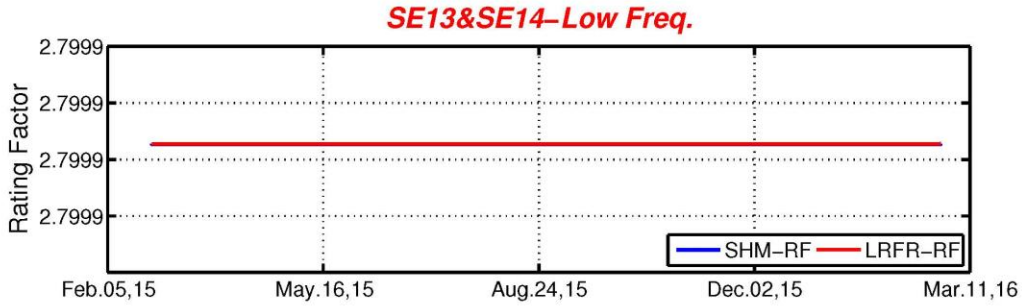
SE13&SE14–Low Freq.
SHM–RF
LRFR–RF
Rating Factor
2.7999
2.7999
2.7999
2.7999
Feb.05,15
May.16,15
Aug.24,15
Dec.02,15
Mar.11,16

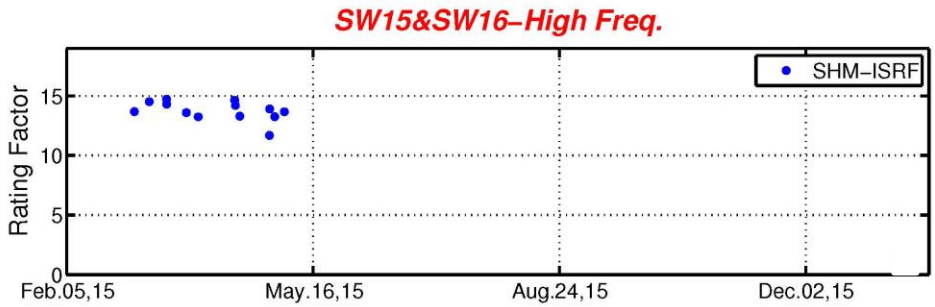
SW15&SW16–High Freq.
SHM–ISRF
Rating Factor
15
10
5
0
Feb.05,15
May.16,15
Aug.24,15
Dec.02,15

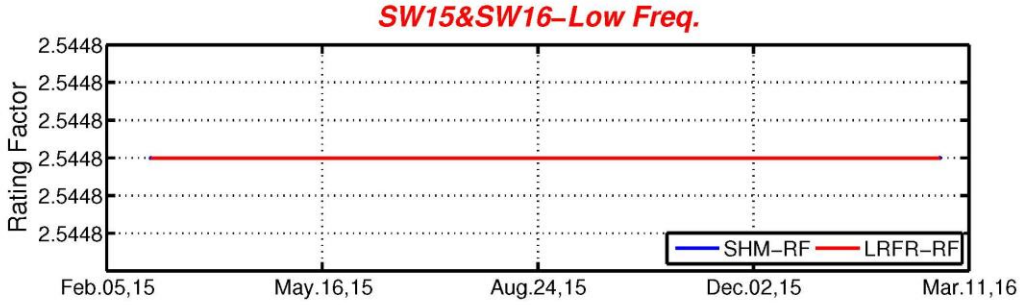
SW15&SW16–Low Freq.
Rating Factor
2.5448
2.5448
2.5448
2.5448
2.5448
2.5448
SHM–RF
LRFR–RF
Feb.05,15
May.16,15
Aug.24,15
Dec.02,15
Mar.11,16

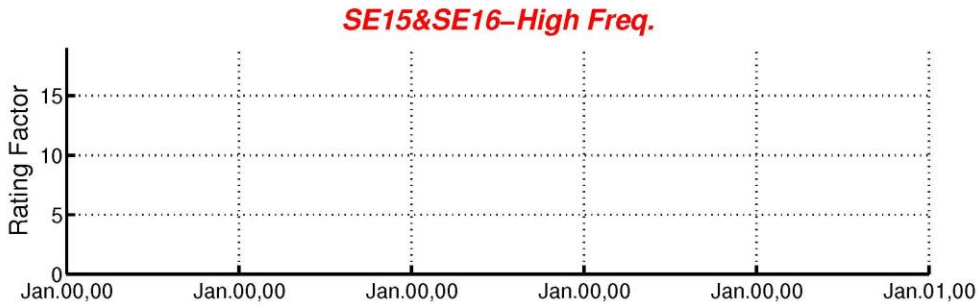
SE15&SE16–High Freq.
Rating Factor
15
10
5
0
Jan.00,00
Jan.00,00
Jan.00,00
Jan.00,00
Jan.00,00
Jan.01,00

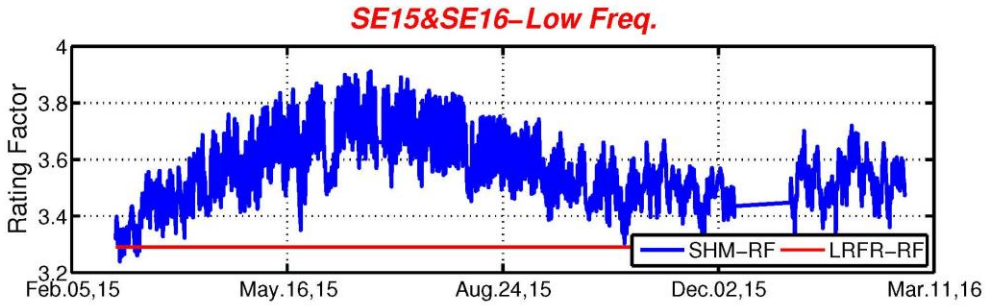
SE15&SE16–Low Freq.
Rating Factor
4
3.8
3.6
3.4
3.2
SHM–RF
LRFR–RF
Feb.05,15
May.16,15
Aug.24,15
Dec.02,15
Mar.11,16

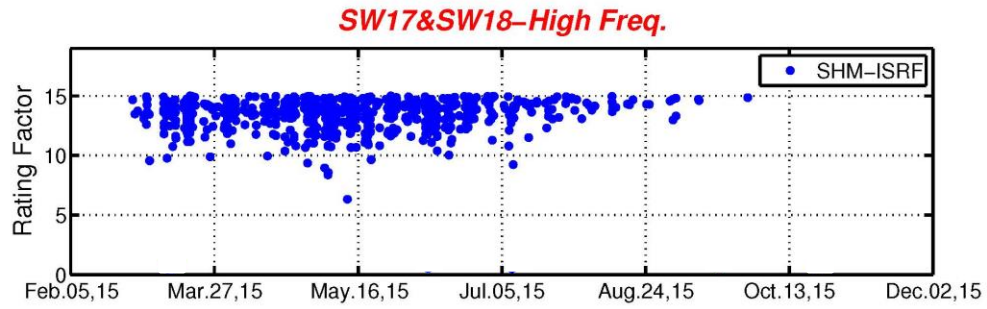
SW17&SW18–High Freq.
SHM–ISRF
Rating Factor
0
5
10
15
Feb.05,15
Mar.27,15
May.16,15
Jul.05,15
Aug.24,15
Oct.13,15
Dec.02,15

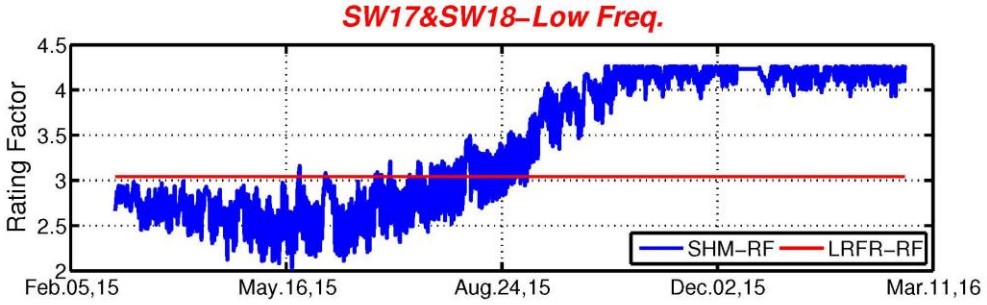
SW17&SW18–Low Freq.
SHM–RF
LRFR–RF
Rating Factor
2
2.5
3
3.5
4
4.5
Feb.05,15
May.16,15
Aug.24,15
Dec.02,15
Mar.11,16

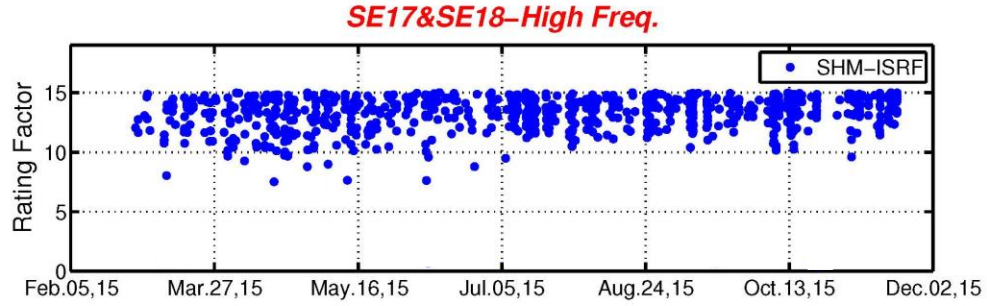
SE17&SE18–High Freq.
SHM–ISRF
Rating Factor
0
5
10
15
Feb.05,15
Mar.27,15
May.16,15
Jul.05,15
Aug.24,15
Oct.13,15
Dec.02,15

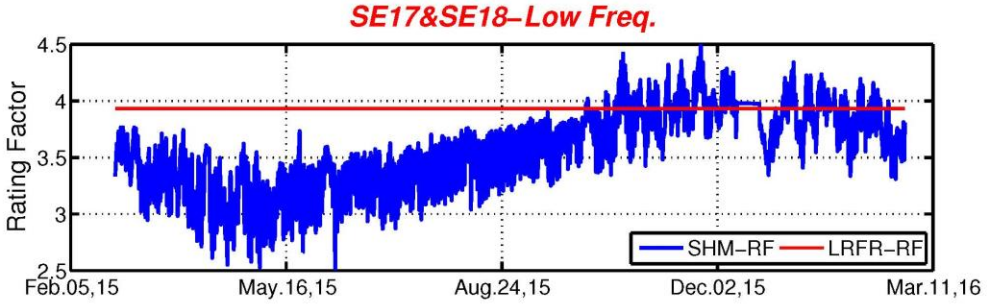
SE17&SE18–Low Freq.
SHM–RF
LRFR–RF
Rating Factor
2.5
3
3.5
4
4.5
Feb.05,15
May.16,15
Aug.24,15
Dec.02,15
Mar.11,16

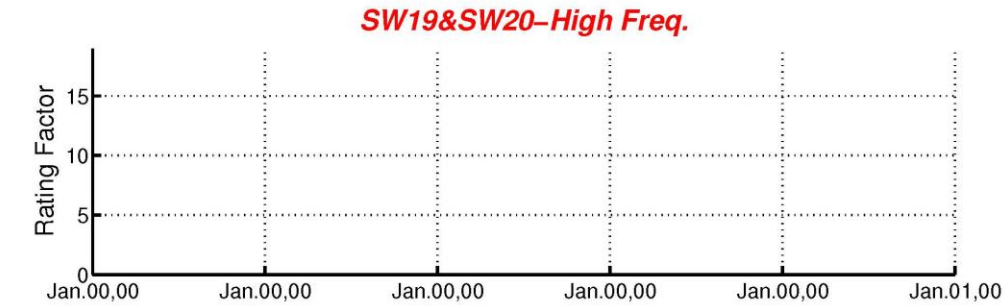
SW19&SW20–High Freq.
Rating Factor
15
10
5
0
Jan.00,00
Jan.00,00
Jan.00,00
Jan.00,00
Jan.00,00
Jan.01,00

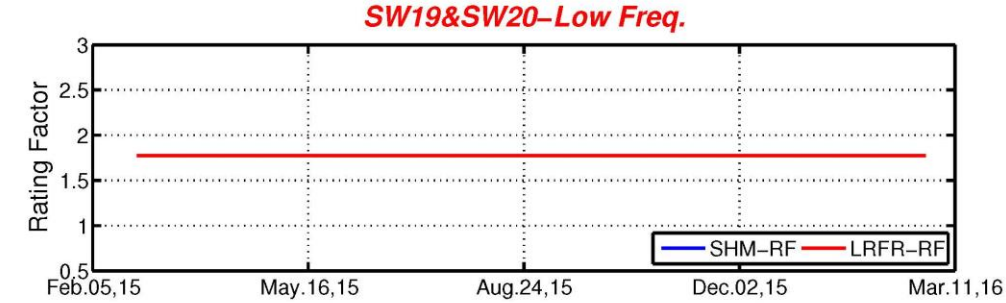
SW19&SW20–Low Freq.
Rating Factor
3
2.5
2
1.5
1
0.5
SHM–RF
LRFR–RF
Feb.05,15
May.16,15
Aug.24,15
Dec.02,15
Mar.11,16

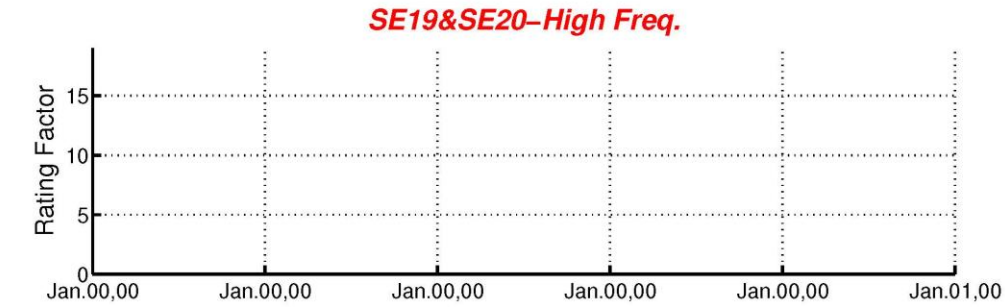
SE19&SE20–High Freq.
Rating Factor
15
10
5
0
Jan.00,00
Jan.00,00
Jan.00,00
Jan.00,00
Jan.00,00
Jan.01,00

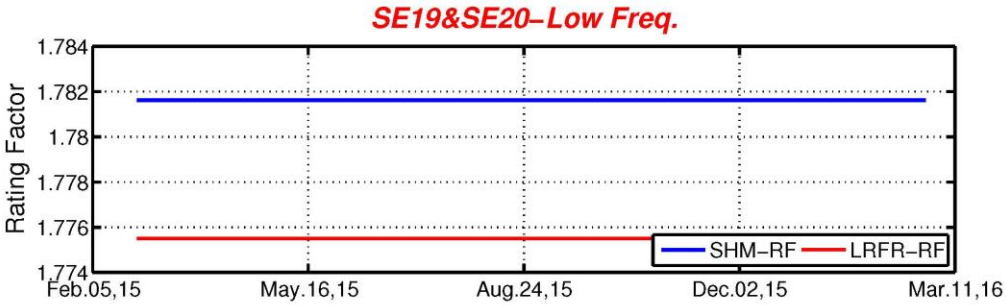
SE19&SE20–Low Freq.
Rating Factor
1.784
1.782
1.78
1.778
1.776
1.774
SHM–RF
LRFR–RF
Feb.05,15
May.16,15
Aug.24,15
Dec.02,15
Mar.11,16

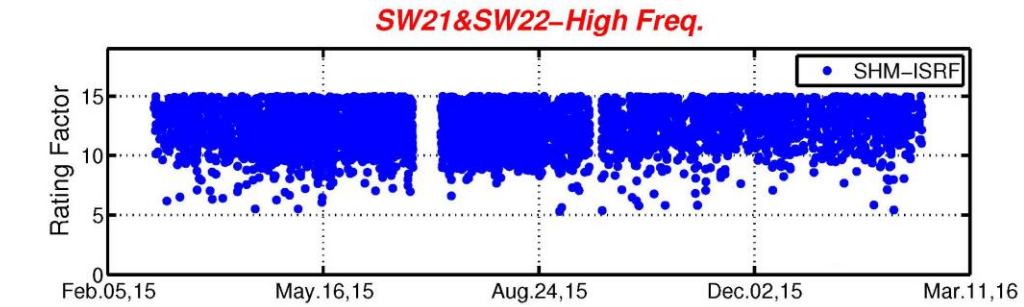
SW21&SW22–High Freq.
SHM–ISRF
Rating Factor
15
10
5
0
Feb.05,15
May.16,15
Aug.24,15
Dec.02,15
Mar.11,16

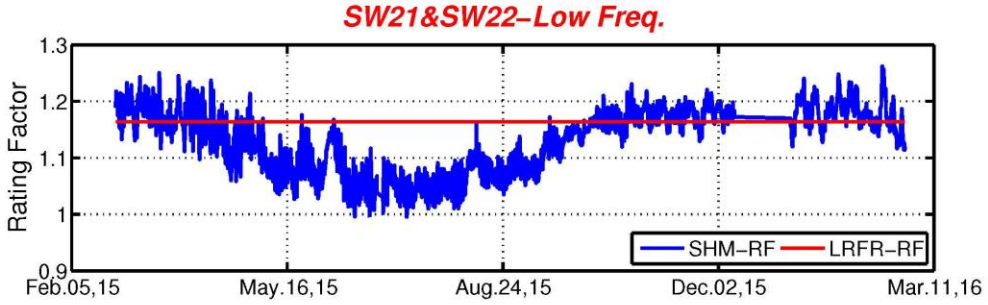
SW21&SW22–Low Freq.
Rating Factor
1.3
1.2
1.1
1
0.9
SHM–RF
LRFR–RF
Feb.05,15
May.16,15
Aug.24,15
Dec.02,15
Mar.11,16

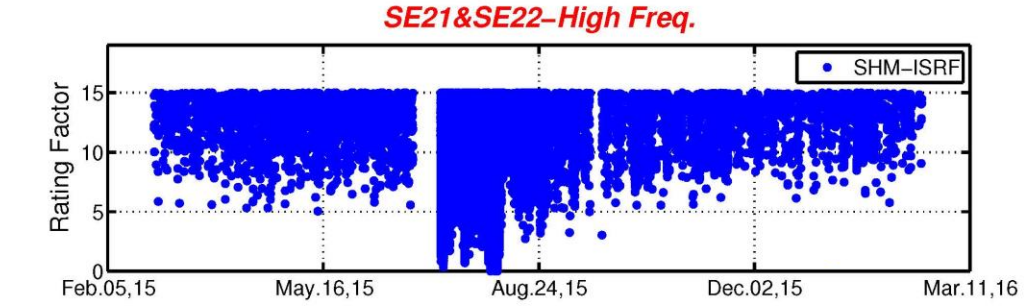
SE21&SE22–High Freq.
SHM–ISRF
Rating Factor
15
10
5
0
Feb.05,15
May.16,15
Aug.24,15
Dec.02,15
Mar.11,16

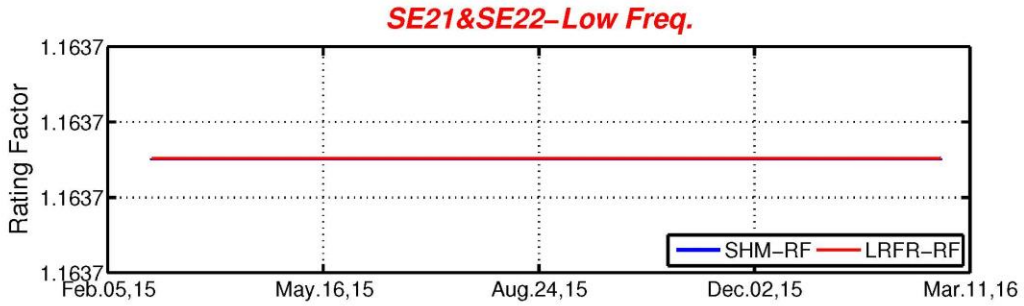
SE21&SE22–Low Freq.
Rating Factor
1.1637
1.1637
1.1637
1.1637
SHM–RF
LRFR–RF
Feb.05,15
May.16,15
Aug.24,15
Dec.02,15
Mar.11,16

Appendix E

RELIABILITY ANALYSIS BASED ON STRUCTURAL HEALTH MONITORING DATA

E.1 Matlab Code for Reliability Analysis Using SHM Data Applied on Service III Limit State

```
clear all
clc
close all
tic

%% Load files
DLM=load('mean_sigma_DL.txt');        %%%%%% Note that all of these
test files contains Strains they are already converted to strains
from stresses
LLM=load('mean_sigma_LL.txt');        %%%%% think later about multiple
presence factor
RM=load('mean_sigma_R.txt');
EM=load('temp_fluc_model.txt');       %%% The environmental model is a
combination between the two EM' and the slopes..remeber this file has
1000001 cycle..if you want more go to the 2 years stuff and create
more cycles and then copy it to the temperature fluctuation file and
then run the analysis after you change n the number of cycles
slopes=load('slopes.txt');

tic

%%
n=1000001;  %%%%%% number of trials it is essential number and you
should be aware of time effect with the number

%%% Determine the cummulative distribution vector based on what you
have
%%% (n=1000001)  for Beta_3

for i=1:n;
p(i,1)=i/(n+1);
z(i,1)=norminv(p(i,1));
end

%% Beta 4 depends on iterarions
```

```
%%% g(R,D,L,T)=R-D-L-T

DLM=load('mean_sigma_DL.txt');        %%%%%% Note that all of these
test files contains Strains they are already converted to strains
from stresses
LLM_old=load('mean_sigma_LL.txt');        %%%%% think later about
multiple presence factor
RM=load('mean_sigma_R.txt');

slopes=load('slopes.txt');


%%% to transfer the vaiables saved in log format to variable in
normal
%%% distribution
for j=1:length(LLM_old);
[M,V]=lognstat(LLM_old(j,1),LLM_old(j,2));
LLM(j,1)=M;
LLM(j,2)=V;
clearvars M V
end


for j=1:length(DLM)


%%%Step 1

mu_R=RM(j,1);
sigma_R=RM(j,2);

mu_D=DLM(j,1);
sigma_D=DLM(j,2);

mu_L=LLM(j,1);
sigma_L=LLM(j,2);

%%%Steps 2
r_star=mu_R;
d_star=mu_D;
l_star=mu_L;
t_star=r_star-d_star-l_star;


%%% This loop will do the trials for ten times. the results will be
%%% reported in Beta vector, the last value will be the final beta
needed
for n=1:1:10;
```

```
%%%Step 3
sigma_ln_R=sqrt(log(1+(sigma_R/mu_R)^2));
mu_ln_R=log(mu_R);
sigma_R_Equiv=r_star*sigma_ln_R;
mu_R_Equiv=r_star*(1-log(r_star)+mu_ln_R);

mu_D_Equiv= mu_D;
sigma_D_Equiv=sigma_D;

sigma_ln_L=sqrt(log(1+(sigma_L/mu_L)^2));
mu_ln_L=log(mu_L);
sigma_L_Equiv=l_star*sigma_ln_L;
mu_L_Equiv=l_star*(1-log(l_star)+mu_ln_L);


a=slopes(j,1);  %%%coming from slopes multiplied by constants
f_t_star=.549*normpdf(t_star,a*-
6.234,a*5.4558)+.451*normpdf(t_star,a*7.59,a*3.689);
F_t_star=.549*normcdf(t_star,a*-
6.234,a*5.458)+.451*normcdf(t_star,a*7.59,a*3.689);

sigma_T_Equiv=(1/f_t_star)*normpdf(norminv(F_t_star));
mu_T_Equiv=t_star-(sigma_T_Equiv*norminv(F_t_star));

%%%Step 4
z_star(1,1)=(r_star-mu_R_Equiv)/sigma_R_Equiv;
z_star(2,1)=(d_star-mu_D_Equiv)/sigma_D_Equiv;
z_star(3,1)=(l_star-mu_L_Equiv)/sigma_L_Equiv;
z_star(4,1)=(t_star-mu_T_Equiv)/sigma_T_Equiv;

%%%Step5
G(1,1)=-sigma_R_Equiv;
G(2,1)=sigma_D_Equiv;
G(3,1)=sigma_L_Equiv;
G(4,1)=sigma_T_Equiv;

%%%Step 6
Beta_4_iteration(n,j)=(G'*z_star)/sqrt(G'*G);

%%%Step 7
Alpha=G/sqrt(G'*G);

%%%Step 8
z_star(1,1)=Alpha(1,1)*Beta_4_iteration(n,j);
z_star(2,1)=Alpha(2,1)*Beta_4_iteration(n,j);
z_star(3,1)=Alpha(3,1)*Beta_4_iteration(n,j);

%%%Step 9
r_star=mu_R_Equiv+(z_star(1,1)*sigma_R_Equiv);
d_star=mu_D_Equiv+(z_star(2,1)*sigma_D_Equiv);
```

```
l_star=mu_L_Equiv+(z_star(3,1)*sigma_L_Equiv);

%%%Step 10
t_star=r_star-d_star-l_star;

%%%Save the design point values
t_star_design_point(n,j)=t_star;

end

end

Beta_4=Beta_4_iteration(n,:)';
clearvars -except keepVariables Beta_1 Beta_2 Beta_3 Beta_4 station
Beta_4_iteration

%%
%%%%%%%%%%%% For final Plot
%%%%%%%%%%%%%%%%%%%%%%%%%%%%%%%%%%
%%%%%%%%%%%%%%%%%%%%%%%%%%%%%%%%%%%%%%%%%%%%%%%%%%%

load('ratingfactors.txt');
load('station.txt');


figure(1)
plot(station,Beta_4,'Marker','o','MarkerSize',6,'MarkerEdgeColor','b'
,'MarkerFaceColor',[1 0 0]);
ylabel('Reliability Index (Beta)','FontSize',20);
xlabel('Station (ft)','FontSize',20);
xlim([0 1750]);
ylim([0 8])

set(gca,'XTick',[0 100 200 300 400 500 600 700 875 1050 1150 1250
1350 1450 1550 1650 1750]);
set(gca,'YTick',[1 2 3 4 5 6 7 8]);
grid on
set(gca,'FontSize',14);
% set(AX(1),'FontSize',10);
% set(AX(1),'FontSize',15);

legend('Reliability Index');
title('Service III- Tension');
savefig('A_Beta_Iteration');

toc
```